## *a critical review of the phenomenon of bond-stretch and distortional isomerism in oxo and sulphido complexes of transition metals*

Oliver B Robinson

# A Critical Review of the Phenomenon of Bond-Stretch and Distortional Isomerism in Oxo and Sulphido Complexes of Transition Metals

by

Oliver B. Robinson, B.Sc.

University of Durham



A thesis submitted in part fulfillment of the requirements for the degree of Doctor of Philosophy at the University of Durham.

July 1993

## Statement of Copyright



## Declaration

The work described in this thesis was carried out in the Department of Chemistry at the University of Durham between October 1989 and December 1992. All the work is my own, unless stated to the contrary, and it has not been submitted previously for a degree at this or any other University.

For my Mother and my dear Father

## Acknowledgements

Foremost I would like to express my gratitude to my supervisor, Dr. Vernon C. Gibson for his input and direction during my years of research at the university.

I am particularly appreciative of the work done by Prof. Mary McPartlin and co-workers (Annie Bligh, Iain Scowen and Subashini Balakvmar) of the University of North London for solving the crystal structures reported in this thesis.

I would like to thank the members of the laboratory: Pete, Dave, Jon, Ulrich, Jens, Kayumars, Tina, Phil, Matt, Ed, Leela, Martyn, Mikey and Brenda for providing the industrious and humorous atmosphere in which to work.

Finally, the financial support from Courtaulds Plc. and S.E.R.C. studentship is gratefully acknowledged.

## Abstract

### A Critical Review of the Phenomenon of Bond-Stretch and Distortional Isomerism in Oxo and Sulphido Complexes of Transition Metals

This thesis describes studies directed towards the preparation of oxo compounds of the early transition metals with a view to assessing their potentials for exhibiting distortional and bond-stretch isomerism. Analogous sulphido complexes in the case of the $M(E)X_3(PMe_3)_3$ system (M= Nb, Ta; X= Cl; E= S) have also been investigated in detail to provide a contrast with another chalcogenide element and further aid an understanding of the phenomenon of bond-stretch isomerism.

Chapter 1 reviews the body of evidence to date on the phenomena of distortional and bond-stretch isomerism, and considers possible theoretical origins for the phenomena.

Chapter 2 describes the detailed study of distortional isomerism in the six coordinate series of complexes $Mo(O)X_2(PMe_2Ph)_3$ (X= Cl, Br, I) and confirms the existence of two pure blue forms for the chloro and bromo cases.

Chapter 3 assesses the evidence for further examples of distortional isomerism in the complexes $W(O)Cl_2(PMe_2Ph)_3$, $Mo(O)(NCS)_2(PMe_2Ph)_3$ and $Mo(O)Cl_2(PEt_2Ph)_3$. Structural characterisation by X-ray crystallography has indicated the existence of a link between the orientation of the alkyl and aryl substituents on the phosphine ligands and the general features observed in their infrared spectra.

Chapters 4 and 5 describe the seven coordinate oxo and sulphido-halide derivatives of niobium and tantalum which exhibit the phenomenon of bond-stretch isomerism. Compounds studied include $M(E)X_3(PMe_3)_3$ (M= Nb, E= O, S, X=Cl, Br; M= Ta, E= S, X=Cl). The structures of these compounds have been re-investigated by X-ray crystallography in order to assess the significance of the co-crystallised isostructural $NbCl_4(PMe_3)_3$ contaminant.

Chapter 6 summaries the evidence for and against distortional and bond-stretch isomerism.

Chapter 7 gives experimental details for chapters 2-5.

Oliver B. Robinson (July 1993)

## Abbreviations

| | |
|---|---|
| L | General 2-electron donor ligand |
| X | General 1-electron donor ligand |
| **bipy** | Bipyridine |
| **bpte** | 1,2-Bis(phenylthio)ethane ($PhSCH_2CH_2SPh$) |
| COSY | Homonuclear Correlation |
| **Cp** | Cyclopentadienyl ($C_5H_5$) |
| **Cp'** | Pentamethylcyclopentadienyl ($C_5Me_5$) |
| **diars** | o-Phenylenebisdimethylarsine (o-$C_6H_4(AsMe_2)_2$) |
| DME | Dimethoxyethane |
| **dms** | Dimethylsulphide ($Me_2S$) |
| EPR | Electron Paramagnetic Resonance |
| **e.s.d.** | Estimated Standard Deviation ($\sigma$) |
| **hmpa** | Hexamethylphosphoric triamide ($OP(NMe_2)_3$) |
| HOMO | Highest Occupied Molecular Orbital |
| IR | Infrared |
| LUMO | Lowest Unoccupied Molecular Orbital |
| MO | Molecular Orbital |
| NMR | Nuclear Magnetic Resonance |
| $O_h$ | Octahedral |
| ORTEP | Oak Ridge Thermal Ellipsoid Plots |
| **tacn** | 1,4,7-triazacyclononane |
| THF | Tetrahydrofuran ($C_4H_4O$) |
| THT | Tetrahydrothiophene ($C_4H_4S$) |
| UV | Ultra violet |
| XPS | X-Ray Photoelectron Spectroscopy |
| ZPE | Zero Point Energy |

## CHAPTER ONE

## BOND-STRETCH AND DISTORTIONAL ISOMERISM: A REVIEW



## CHAPTER TWO

## A RE-EVALUATION OF DISTORTIONAL ISOMERISM IN OXOMOLYBDENUM COMPLEXES

## CHAPTER THREE

## ADDITIONAL INSTANCES OF DISTORTIONAL ISOMERISM IN OXOMOLYBDENUM AND OXOTUNGSTEN SYSTEMS

## CHAPTER FOUR

## SEVEN COORDINATE OXO-HALIDES OF NIOBIUM

## CHAPTER FIVE

## SEVEN COORDINATE SULPHIDO-HALIDES OF NIOBIUM AND TANTALUM

## CHAPTER SIX

## DISTORTIONAL AND BOND-STRETCH ISOMERISM: FACT OR ARTIFACT?



## CHAPTER SEVEN EXPERIMENTAL DETAILS

Appendix 4

## FIGURES AND TABLES LIST

### CHAPTER ONE

## CHAPTER TWO

## CHAPTER THREE

## CHAPTER FOUR

## CHAPTER FIVE

## CHAPTER SIX

# CHAPTER ONE

## Bond-Stretch and Distortional Isomerism: A Review

## 1.1 Introduction

The phenomenon of isomerism in all its varied forms, which include structural, geometrical, optical and conformational, transcends all disciplines of chemistry. It relates to the concept that two or more molecules may differ only in the arrangement of their constitutional atoms in space. The identification of a molecule's structural representation, and so its isomeric relation to its counterpart can be established by a variety of techniques. One such compelling technique is X-ray crystallography, which precisely determines the arrangement of the atoms in space within a molecule. However, the ability of X-ray crystallography to determine accurate bond lengths and angles within molecules can sometimes be called into question. It was the inability of X-ray crystallography to ascertain which particular atoms were present at one particular point in space that led to the controversy surrounding a new type of isomerism, namely, bond-stretch isomerism where the constitution of the molecules differed not in geometric arrangements or rotation of substituent groups, but merely in the length of one or more bonds. This thesis is concerned with the concept of bond-stretch isomerism, and in this introductory chapter its historical origin will be retraced. It will consider the evidence for and against it, and show how even if one is reluctant to believe in it that it is still difficult to disprove.

## 1.2 Historical Development

The concept of bond-stretch isomerism was first proposed by Strohrer and Hoffmann[1] in 1972 in a theoretical study on a series of hypothetical molecules of the type $(CH)_5^+$ and $(CH)_4CO$.[2] In the interaction of two atoms as a function of their separation the bond length is represented by a minimum point on a potential energy surface (figure 1.1). This work, however, required the presence of a double minimum, separated by a substantial energy barrier, for the existence of isomers which differ only in the length of one or more bonds to be possible. This energy barrier has important practical consequences since two molecules require an energy barrier in excess of 25 kcal

$mol^{-1}$ to exist in discrete forms in solution at room temperature, whereas the smaller energy barriers characteristic of conformers will ensure their rapid interconversion in solution at room temperature.

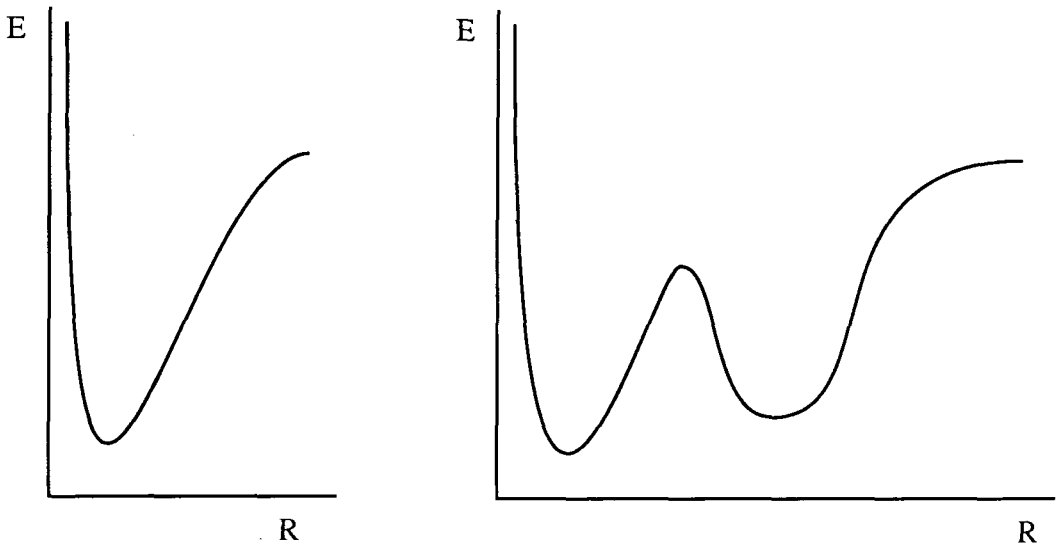


**Figure 1.1:** Plot of potential energy versus atomic separation for (left) a normal bond and (right) the double minimum representing a bond-stretch isomer pair

The presence of a double minimum on the potential energy surface necessitates the crossing of an antisymmetric level (A) with a symmetric one (S). In the

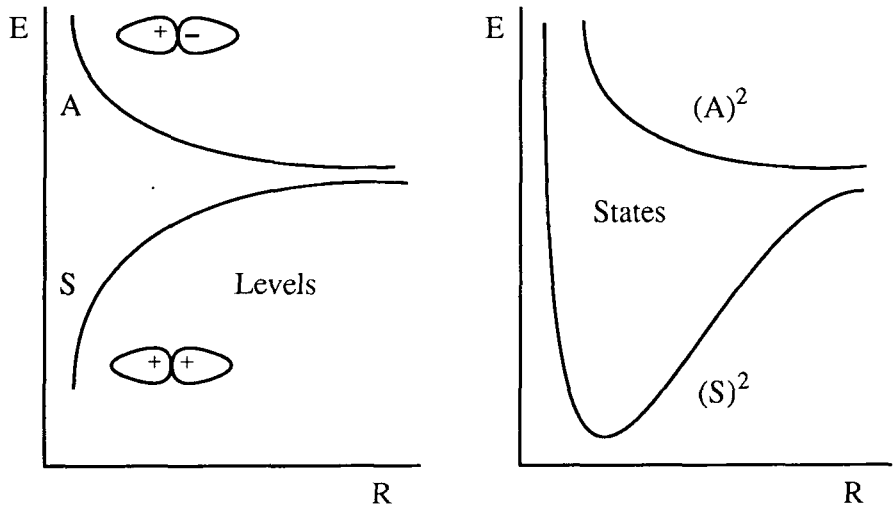


**Figure 1.2:** A plot of potential energy versus atomic separation for the antisymmetric (A) and symmetric (S) levels where crossing is forbidden, to give the normal single minimum associated with a bond length

case of a normal bond these levels do not cross, but approach each other as the interatomic separation increases (figure 1.2). However, if the two are allowed to cross,

the situation arises where a double minimum is obtained (figure 1.3). Hoffmann showed in the case of $(CH)_5^+$, that the antisymmetric combination of $C_1$ and $C_5$ p orbitals could be stabilised, if the separation of these two atoms was large, by a favourable interaction with the $C_3$ p orbital (figure 1.4). As the $C_1$-$C_5$ bond is stretched the antisymmetric component is caused to substantially mix with the p orbital of the $C_3$ atom, such that the

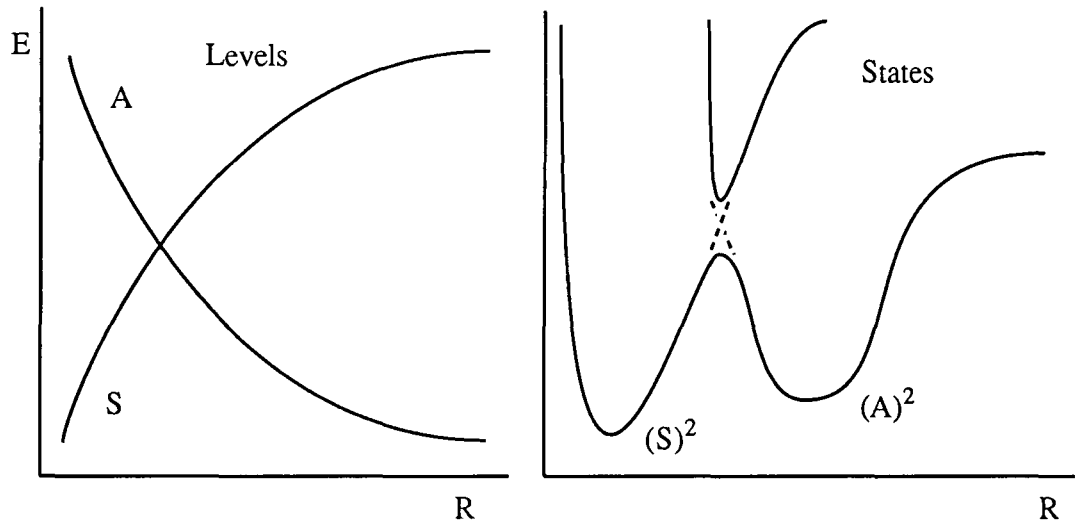


**Figure 1.3:** A plot of potential energy versus atomic separation for the antisymmetric (A) and symmetric (S) levels where crossing is allowed, giving rise to a double minimum

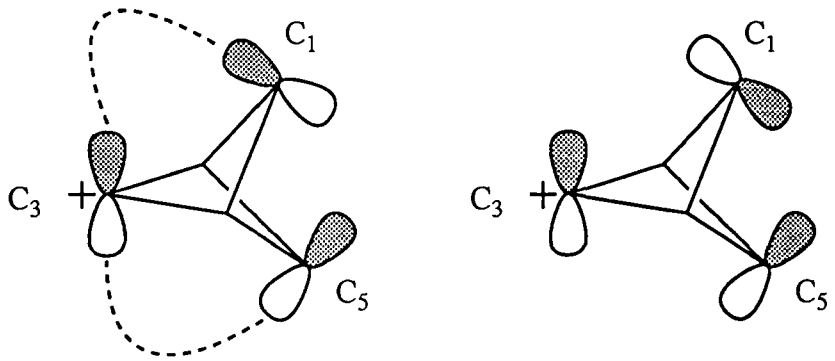


**Figure 1.4:** Stabilisation of the antisymmetric combination of p orbitals on $C_1$ and $C_5$ by an acceptor orbital at $C_3$ in $(CH)_5^+$ where a double minimum is proposed

antisymmetric component falls below the symmetric level (figure 1.5), allowing the development of a double minimum. This study was soon followed by further theoretical evaluations on heteroatom systems ($B(CH_2CH_2)_3N$[4], $Si_4H_6$, $CSi_3H_6$, $C_2Si_2H_6$[5], $Li_2B_2H_4$[6], $C_2Si_2$[7], $B_2Be_2$[8] and $C_3X$ (X=Be, BH and Si)[9]).

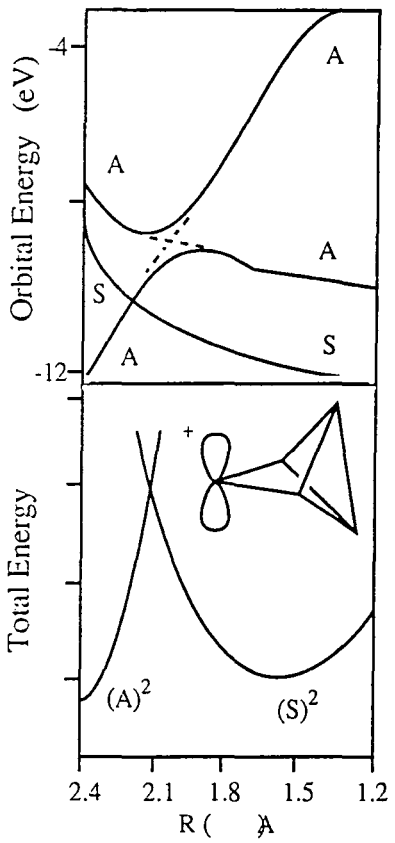


**Figure 1.5:** Highest occupied and two lower unoccupied MOs (top) and configuration energies (bottom) for stretching the $C_1$-$C_5$ bond in $(CH)_5^+$, where R is the $C_1$-$C_5$ bond distance. The total energy scale is 1.0 eV.

## 1.3 Original Experimental Evidence

Experimentally, the origins of bond-stretch isomerism lie in a study of transition metal complexes by Butcher and Chatt[3] in 1970, two years before the term bond-stretch isomerism was proposed. In this publication Chatt reported a series of octahedral oxomolybdenum complexes exhibiting a meridional arrangement of phosphine ligands, *mer*-$Mo(O)Cl_2(PR_3)_3$ (X=Cl, Br, NCO, NCS; $PR_3$=$PMe_2Ph$, $PEt_2Ph$, $P^nPr_2Ph$, $P^nBu_2Ph$, $PMePh_2$, $PEtPh_2$, $P^nPrPh_2$, $MeC[CH_2PPh_2]_3$), which were either blue or green. Particular attention was focused on the dimethylphenylphosphine derivative *mer*-$Mo(O)Cl_2(PMe_2Ph)_3$, which could be isolated in both blue and green forms. From IR spectroscopic data they concluded that the blue and green forms were geometric isomers, namely *cis-mer*-$Mo(O)Cl_2(PMe_2Ph)_3$ and *trans-mer*-$Mo(O)Cl_2(PMe_2Ph)_3$, differing in whether the two chloride ligands were cis or trans, and

having slightly different ν(Mo=O) stretching frequencies (blue 954 $cm^{-1}$ and green 943 $cm^{-1}$). Since it had been established by X-ray structure determination[10a] that the blue form showed a *cis-mer* configuration, it was concluded that the green form, and hence all green forms, should exhibit a *trans-mer* dichloro configuration (figure 1.6).

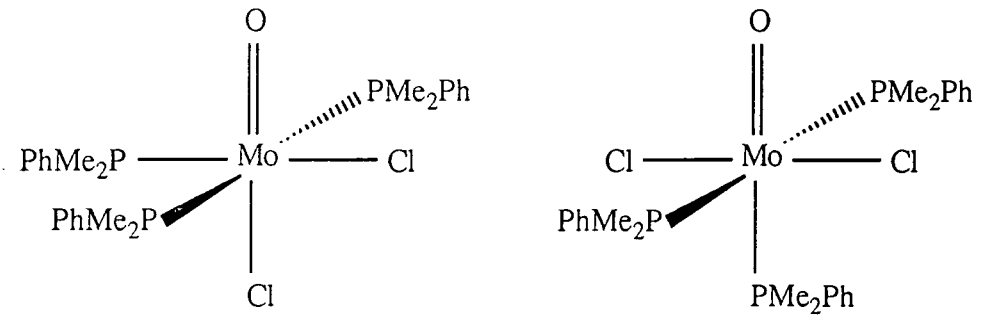


**Blue cis** **Green trans**

**Figure 1.6**: The original structure proposals for blue and green *mer*-$Mo(O)Cl_2(PMe_2Ph)_3$

At this time it was the infrared data that was being used to support the conclusion that related blue and green forms were simply geometric isomers of each other. It was of considerable surprise then when Manojlovic-Muir and co-workers[10b] showed that the analogous oxo complex *mer*-$Mo(O)Cl_2(PEt_2Ph)_3$, only isolable in the green form with the characteristically low ν(Mo=O) stretch at 940 $cm^{-1}$, possessed a *cis*-dichloro configuration and not the expected *trans*-dichloro configuration originally proposed for the green forms. That it had the same configuration as reported earlier for the blue (ν(Mo=O) 954 $cm^{-1}$) *cis-mer*-$Mo(O)Cl_2(PMe_2Ph)_3$ complex, meant the original conjecture that the blue and green forms were *cis-mer* and *trans-mer* geometric isomer was incorrect.

However, X-ray structure determination of the dimethylphenyl- and diethylphenylphosphine complexes did bring to light two significant differences in the structures of the molecules. Firstly, a substantial difference was observed in the lengths of the Mo=O bonds for the two molecules. The Mo=O bond distance of 1.803(11)Å[10b] in the green *cis-mer*-$Mo(O)Cl_2(PEt_2Ph)_3$ was significantly longer than that of 1.676(7)Å[21] observed in blue *cis-mer*-$Mo(O)Cl_2(PMe_2Ph)_3$. A similar reverse relationship was observed, to a lesser but equally significant degree, in the bond length

(a)

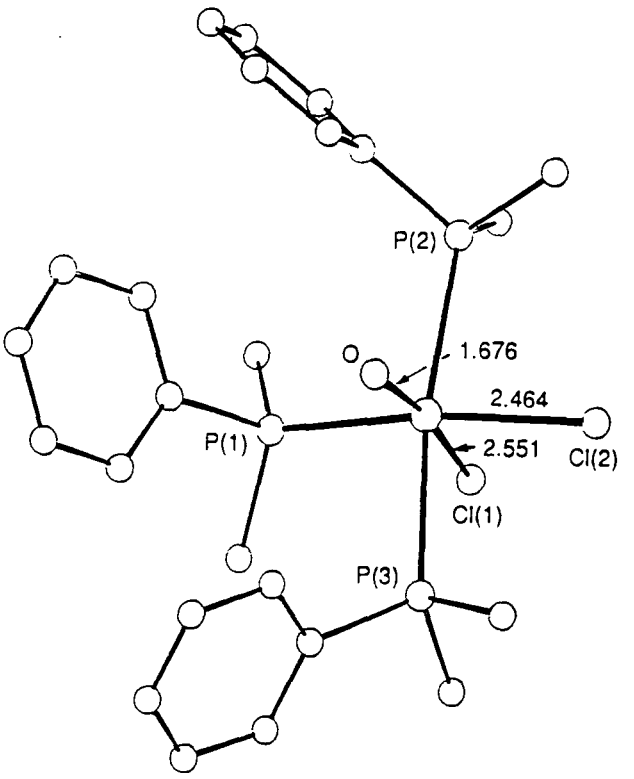


(b)

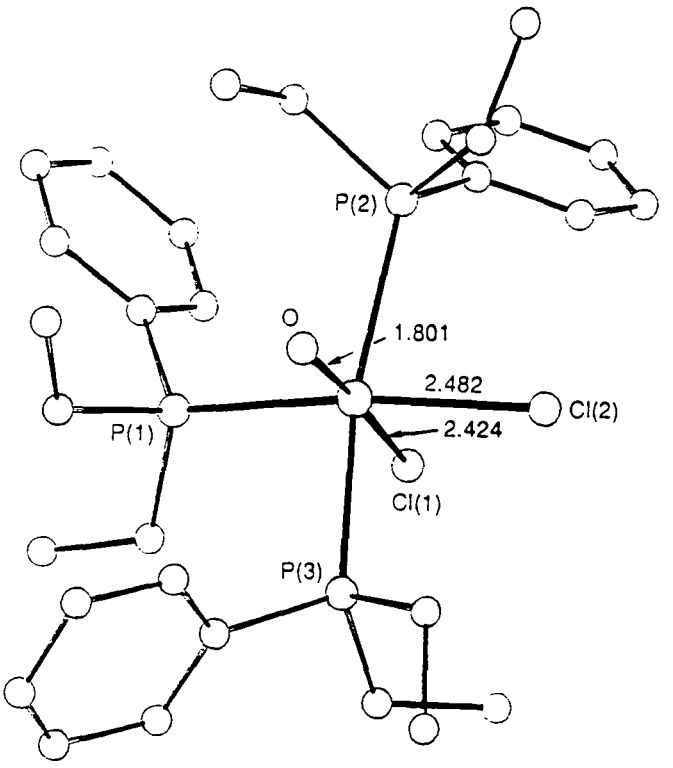


**Figure 1.7:** The crystal structures for the original 'distortional isomer pair' of *cis-mer*-$Mo(O)Cl_2(PR_2Ph)_3$ (R=Me, Et).

for the Mo-Cl bonds trans to the Mo=O moiety; being 2.426(6)Å in the case of the green species and 2.551(3)Å in the blue. Secondly, the organophosphine substituents adopt different conformations (figure 1.7) with respect to the molybdenum co-ordinate polyhedron.

This prompted Chatt to question his original conclusion that the green form of $Mo(O)Cl_2(PMe_2Ph)_3$, with $\nu$(Mo=O) at 943 $cm^{-1}$, was the *trans*-dichloro geometric isomer of the blue form, with $\nu$(Mo=O) at 954 $cm^{-1}$. Since the IR spectra of the green forms of $Mo(O)Cl_2(PMe_2Ph)_3$ and $Mo(O)Cl_2(PEt_2Ph)_3$ were remarkably similar, showing $\nu$(Mo=O)'s at 943 $cm^{-1}$ and 940 $cm^{-1}$ respectively, Chatt, now having determined by X-ray structure determination that the green *mer*-$Mo(O)Cl_2(PEt_2Ph)_3$ had a cis configuration, was compelled to conclude that the difference between the blue and green forms of *mer*-$Mo(O)Cl_2(PMe_2Ph)_3$ was centred not on the geometric argument of cis versus trans configuration of the chloride ligands, but that they had a similar cis configuration. Furthermore, the difference in the $\nu$(Mo=O) stretching frequencies for the two forms of *mer*-$Mo(O)Cl_2(PMe_2Ph)_3$ implies an inequivalence in the Mo=O bond length in each form. Knowing the blue form ($\nu$(Mo=O) 954 $cm^{-1}$) of $Mo(O)Cl_2(PMe_2Ph)_3$ to have a Mo=O bond length of 1.676(7)Å, Chatt et al.[10a] surmised that the green form should have a significantly longer Mo=O bond, similar in length (1.801(9)Å) to that of the green diethylphenyl analogue. Chatt proposed the term distortional isomerism to delineate complexes which differ in the phosphine conformations in the highly strained co-ordination polyhedra of molybdenum.

Haymore et al.[11] has since been able to report the structural characterisation of the green form of *mer*-$Mo(O)Cl_2(PMe_2Ph)_3$. It has a cis configuration of the dichloride ligands, and a Mo=O bond length of 1.80(2)Å consistent with this proposal, but unresolvable disorder between two Mo positions precluded full publication of these results. It is important at this point to stress that it is the green isomer with a long Mo=O bond distance of 1.80(2)Å, that is abnormal, the average length for a terminal Mo=O bond in a mono-oxo molybdenum complex being 1.678Å, as reported by Mayer.[12]

## 1.4 Subsequent Developments

Cotton et al.[13] have recently reported structures for two closely related compounds, originally synthesised by Butcher and Chatt.[3] Namely, green $Mo(O)Cl_2(PMePh_2)_3$ ($\nu$(Mo=O) 945 $cm^{-1}$) and blue $Mo(O)(NCO)_2(PEt_2Ph)_3$ ($\nu$(Mo=O) 941 $cm^{-1}$). The blue diethylphenyl compound was found to crystallise with two independent molecules in the asymmetric unit, showing Mo=O bond lengths of 1.678(8) and 1.690(8)Å, as expected from the colour. The coordination environment about the molybdenum is similar in both molecules, but the orientation of the aryl and alkyl groups vary considerably. Cotton was surprised that he had not observed the anticipated long Mo=O bond distance for the green complex *cis-mer*-$Mo(O)Cl_2(PMePh_2)_3$, but a short Mo=O length of 1.667(4)Å close to the value obtained for blue *cis-mer*-$Mo(O)Cl_2(PMe_2Ph)_3$ ($\nu$(Mo=O) 954 $cm^{-1}$). A comparison of Mo=O and Mo-$Cl_{trans\text{-}to\text{-}O}$ distances in related $Mo(O)X_2L_3$ complexes showed that the green $Mo(O)Cl_2(PMePh_2)_3$ resembled the blue isomers of $Mo(O)Cl_2(PMe_2Ph)_3$ and $Mo(O)(NCO)_2(PEt_2Ph)_3$, rather than green $Mo(O)Cl_2(PEt_2Ph)_3$. Interestingly, he discusses the possibility that the isolation of a second green isomer with a long Mo=O bond, could go undetected under normal laboratory conditions, when one considers the general colour trend is towards green with increasing bond length.

Carmona and Wilkinson have reported blue and green forms of the trimethylphosphine analogue *cis-mer*-$Mo(O)Cl_2(PMe_3)_3$.[14] The two forms possessed identical IR and $^1H$ NMR spectra, but unlike the dimethylphenylphosphine *cis-mer*-$Mo(O)Cl_2(PMe_2Ph)_3$ system where the green isomer (with a long Mo=O bond) irreversibly converts to the blue form (short Mo=O bond), the $PMe_3$ analogue exhibits the opposite behaviour. This system was re-investigated by Parkin and co-workers.[15] They found that crystals of the green form contained two crystallographically independent molecules per asymmetric unit with Mo=O bond lengths of 1.698(8) and 1.866(7)Å. However, only one $\nu$(Mo=O) stretching frequency at 950 $cm^{-1}$ was observed in the solid-state IR spectra, rather than the two expected absorptions corresponding to long and short isomers. This observation was inconsistent with two molecules being present in the

asymmetric unit with substantially different Mo=O bond lengths. Re-determination of the crystal structure of *cis-mer*-$Mo(O)Cl_2(PMe_3)_3$ on a new batch led surprisingly to two new Mo=O bond lengths of 1.772(12) and 2.154(8)Å. The inconsistency in the values obtained for the Mo=O bond lengths suggests that the differences were not a revelation of bond-stretch isomerism, since such a situation would require a quadruple minimum on the potential energy surface as a function of the distance between the atoms. The earlier observation[16] by our group that the green $Nb(O)Cl_3(PMe_3)_3$ is contaminated by ca. 20% of the isomorphous tetrachloride $NbCl_4(PMe_3)_3$ prompted an explanation for these differences between the two sets of Mo=O bond lengths, being due to co-crystallisation of small quantities of the isostructural trichloride $MoCl_3(PMe_3)_3$ with the oxo complex $Mo(O)Cl_2(PMe_3)_3$.

The presence of the contaminant *mer*-$MoCl_3(PMe_3)_3$ was confirmed by Parkin and co-workers[15], by examination of the $^1H$ NMR spectrum. *cis-mer*-$Mo(O)Cl_2(PMe_3)_3$ is diamagnetic and affords triplet (δ 1.38 ppm) and doublet (δ 1.26 ppm) resonances attributable to the *trans* phosphorus methyls and the methyl groups attached to the unique phosphine. In contrast *mer*-$MoCl_3(PMe_3)_3$ is paramagnetic and so under normal circumstances (δ 0-10 ppm) escapes detection. However, its presence was readily revealed by the observation of two broad resonances at δ -16 and -33 ppm. Co-crystallisation of *mer*-$MoCl_3(PMe_3)_3$ with *cis-mer*-$Mo(O)Cl_2(PMe_3)_3$ results in the incorporation of small quantities of chloride into the oxo site and thereby results in an artificial lengthening of the Mo=O bond; chloride is located at ca. 2.45Å for *mer*-$MoCl_3(PMe_3)_3$ as opposed to ca. 1.68Å for a Mo=O bond.

## 1.5 Other Instances of Bond-Stretch Isomerism

Since the original observation of distortional isomerism by Chatt[3], chemists appear not to have been too interested in this striking new kind of isomerism. Wieghardt et al.[17] were next to report a case of apparent bond-stretch isomerism in an oxo-tungsten system, in which compounds were isolated in green and blue forms, and where in each pair the blue form showed a higher ν(M=O) stretching frequency than the green form.

The blue (W=O bond length 1.72(2)Å) and green (W=O bond length 1.89(2)Å) forms of the cationic complex of the tridentate ligand N,N',N''-trimethyl-1,4,7-triazacyclononane (L), $[W(O)Cl_2L]^+$ represent an important example of bond-stretch isomerism, since the isomers are reportedly stable in acetonitrile solution for several days with no sign of change of colour, as determined by UV-visible spectroscopy (figure 1.8).

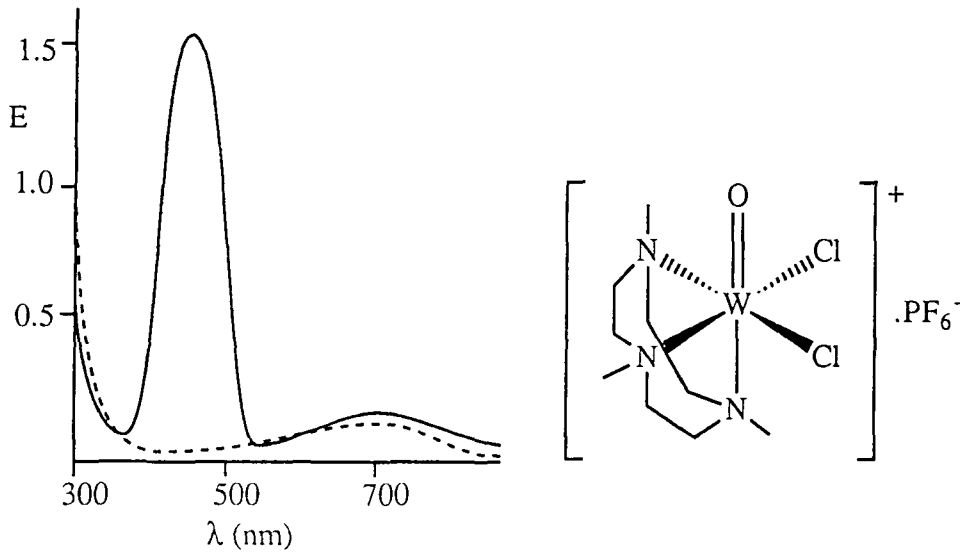


**Figure 1.8:** Electronic absorption spectra of blue $[(Me_3tacn)W(O)Cl_2][PF_6]$ (---) ($3.5x10^{-3}M$) and green $[(Me_3tacn)W(O)Cl_2][PF_6]$ (—) ($2.0x10^{-3}M$) in dry MeCN

The isomers show ν(W=O)'s at 980 (blue) and 960 (green) $cm^{-1}$, and are thermally stable to ca. 180°C, showing no interconversion. Their independent stability in the solid-state and in solution means that a packing effect is excluded to explain the difference in the W=O bond lengths, a barrier of at least 20 kcal $mol^{-1}$ having to be cleared to transform one isomer to the other.

## 1.6 A Theoretical Rationalisation for the Origin of Bond-Stretch Isomerism in Transition Metals

The theoretical evidence for bond-stretch isomerism is quite compelling, indicating that under the right conditions two energy minima can exist along a bond stretch. In the absence of more well characterised bond stretch isomer pairs, it is difficult to surmise as to the origin of the phenomenon. There are, however, several

distinguishing features found in bond stretch isomerism. First, there is usually a colour difference, presumably due to L→M charge transfer. In cases of charge-transfer processes the energy of the d-d transitions are high and thus usually lie at the extreme blue end of the visible spectrum. Nearly all charge-transfer transitions are fully allowed, hence the bands are strong. This transition is expected when the metal possesses low lying empty dπ* orbitals and the ligand has filled orbitals lying higher than the highest filled metal orbitals. Secondly, there is a marked difference in the metal-oxygen bond length, typically 0.05[22] to 0.31Å[23], and the concomitant difference in the metal-oxo stretching frequencies. The marked M-O change is accompanied by less apparent, but equally significant variations of the other metal-ligand bond lengths. Lastly, all the complexes are found in relatively high oxidation states, and are therefore electron deficient. This is not surprising when one considers the fact that for terminal oxo and sulphido moieties (where the instances of bond-stretch isomerism have so far been reported) to exist, the metal centre must be electron deficient, otherwise with oxidation states less than +4, or electronic configurations above $d^2$, the oxo or sulphido ligand usually bridges two or more metal centres.[12b] The relative paucity of electrons, coupled with the availability of orbitals and variety of ligands to tune the energy of these orbitals, will eventually turn out to be important.

Metal-ligand multiple bonds are usually considered to consist of a σ bond plus one or two π bonds, as formulated in figure 1.9. The π interactions involve the overlap of metal d orbitals with the p orbitals on the ligand. With the z-axis coincident with the metal-ligand multiple bond overlap occurs between the $d_{xz}$ and $p_x$ and/or $d_{yz}$ and $p_y$ orbitals (figure 1.10).

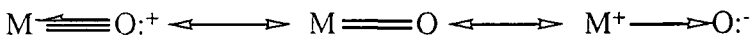

**Figure 1.9:** M=O bond order formalisation

The p orbitals of the oxo ligand are lower in energy than the metal d orbitals, due to the high electronegativity of oxygen. In an oxidation state formalism the oxo ligand is described as the closed shell anion, $O^{2-}$, implying that the $p_x$, $p_y$ and $p_z$ orbitals are filled (hence theoretically here the oxo moiety is a six electron donor ligand).

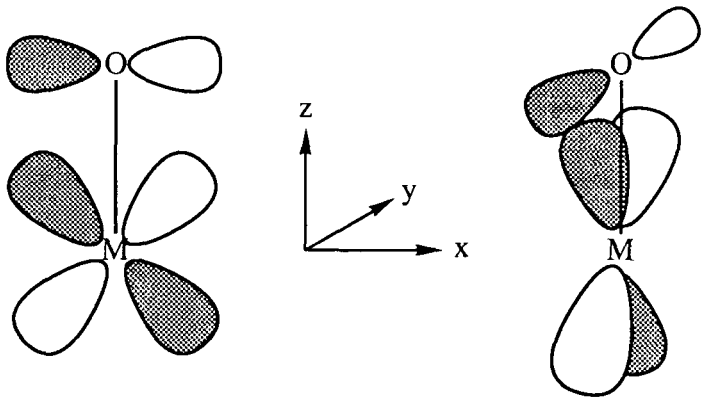


**Figure 1.10:** Diagram showing the overlap of the oxygen $p_x/p_y$ orbitals with the metal $d_{xz}/d_{yz}$ orbitals giving rise to the π-bonding interactions

Productive π bonding, in other words π interactions that stabilise the metal-oxo bond, requires that the metal dπ orbitals are empty and so the metal centre be in a high oxidation state with a low electron count. In transition metal compounds the π component is best regarded as arising from Opπ→Mdπ electron flow. Since this is the opposite of electron flow in π bonding ligands of the CO type (weak σ-donor, strong π acceptor ie., π-acidic), this accounts for the prevalence of $d^n$ configurations (where n= 0,1 and 2).

The importance of the electronic configuration is revealed on examination of the d orbital splitting pattern for octahedral mono-oxo complexes (figure 1.11). The majority of complexes containing the multiply bonded oxo ligand are six-coordinate (with the exception of the seven co-ordinate $Nb(E)X_3(PMe_3)_3$ systems where E=O, S; X=Cl, Br; which can best be described as a mono-capped distorted octahedron), and adopt a geometry best described as octahedral. All octahedral complexes have essentially the same σ-bonding framework, regardless of the π interactions. In a molecule assumed to have full $O_h$ symmetry, the five metal d orbitals split into a degenerate $e_g$ set ($d_{x^2-y^2}$, $d_{z^2}$) of σ* character and a non-bonding $t_{2g}$ set ($d_{xy}$, $d_{xz}$ and $d_{yz}$). Introduction of a cylindrically symmetric π-bonding oxo ligand (that is capable of forming a triple bond) lowers the symmetry to $C_{4v}$ and splits the degeneracy of both the $e_g$ and $t_{2g}$ orbitals. Qualitatively the $e_g$ set changes little due to both orbitals remaining σ*, but the $t_{2g}$ orbitals become substantially split because two are now involved in π-bonding ($d_{xz}$ and $d_{yz}$). The ligand field portion of the MO diagram (figure 1.11) thus consists of a non-bonding $d_{xy}$ orbital, a π* e set and two σ* levels. The two π-bonding orbitals are degenerate and the

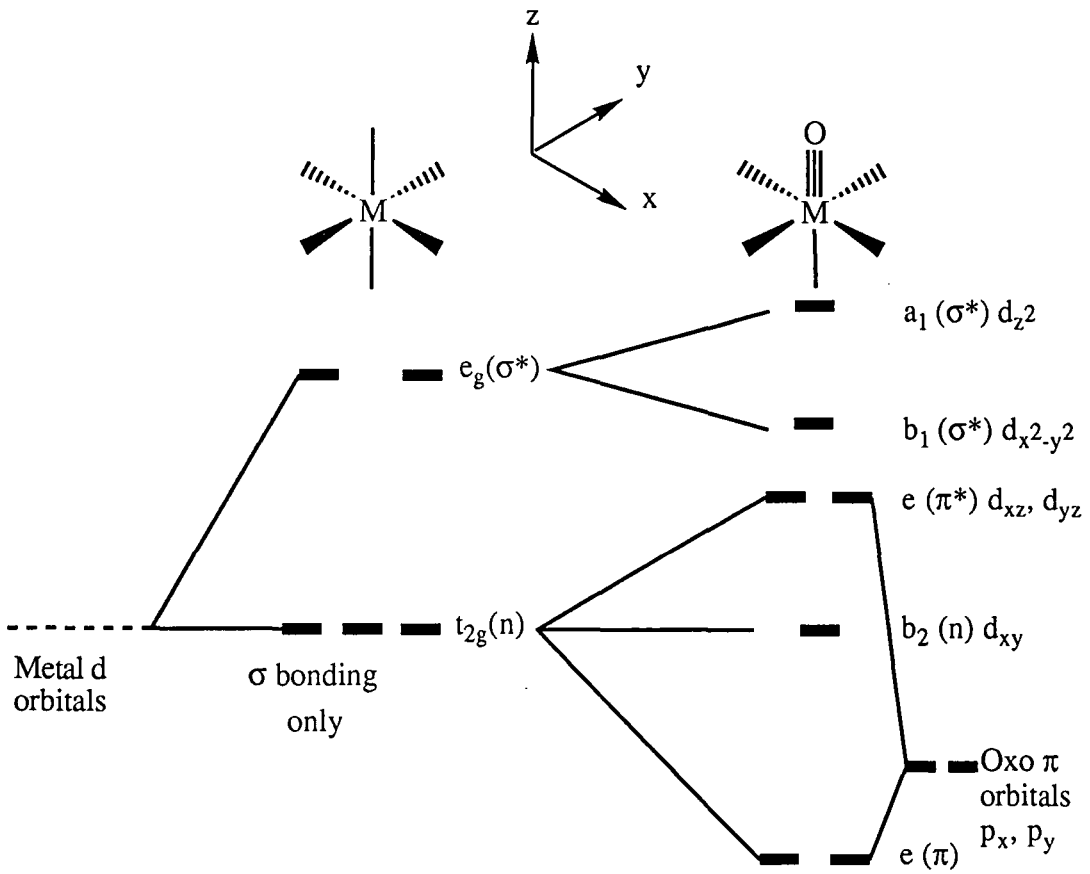


**Figure 1.11:** The ligand field MO diagram for an octahedral mono-oxo complex

multiple bond must be considered as a triple bond unless the $\pi^*$ orbitals are occupied. Thus up to two d electrons can be accommodated in the non-bonding $d_{xy}$ b orbital and so in $d^0$, $d^1$ and $d^2$ complexes the M-O interaction is best described as a triple bond. It must be remembered that the term used here for metal-oxygen bond order is quite different from the bond valence or Pauling bond strength used in the discussion of solid-state structures. The bond order described here refers to orbital occupancy in a molecular orbital sense, and is derived from a ligand field description.[18] The Pauling bond strength is an apportionment of bond valence among the bonds to a central atom and is empirically determined from the observed bond distances.[19]

Hoffmann et al.[20] have forwarded explanations of bond stretch isomerism in terms of frontier orbital crossing of (M-L) and (M-O) antibonding molecular orbitals or a second order Jahn-Teller effect (SOJT), in order to rationalise the presence of two discrete minima.

### 1.6.1 An Electronic Crossing of Filled and Empty Orbitals

The first possibility involves the crossing of two electronic states[20] with different bonding properties as the M-O linkage is stretched. Figure 1.12 shows the energy diagram for the $d^1$ species $[W(O)H_5]^{2-}$, the basis of a model for the complex $[(Me_3tacn)W(O)Cl_2]^+$, and the effect of stretching the W-O bond. It can be seen that π-bonding interactions with the oxygen induce a splitting of the $t_{2g}$ block. The purely non-bonding $d_{xy}$ orbital is unaffected, while the $d_{xz}$ and $d_{yz}$ orbitals are destabilised by

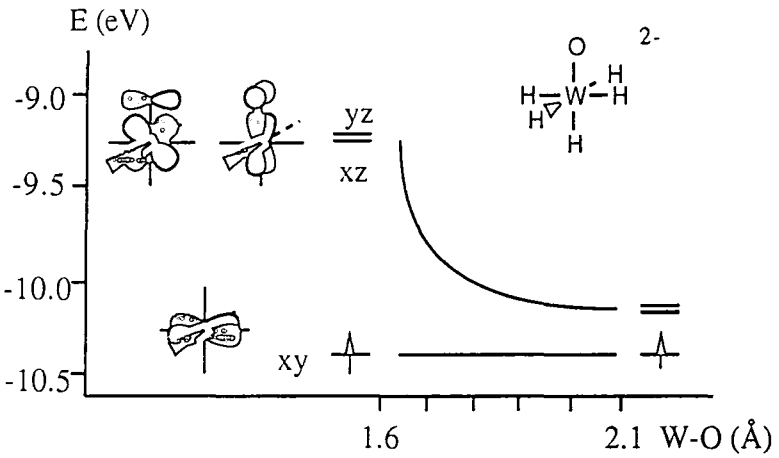


**Figure 1.12:** The energy diagram for the low-lying d orbitals in the $d^1$ model complex $[W(O)H_5]^{2-}$ as a function of the W-O stretching

antibonding mixing with the filled p-orbitals of the oxygen lone pairs. Upon stretching the W-O bond, the $d_{xz}$ and $d_{yz}$ orbitals are stabilised since antibonding interactions with the lone pairs of oxygen decrease, while the $d_{xy}$ orbital is unaffected. At infinite separation the three orbitals would become degenerate, and so, as such, no crossing in the d block would be expected. However, examples of bond-stretch isomerism carry π-acceptor and π-donor ligands capable of interacting with the metal d-orbitals. Locating a π-donor chloride ligand cis to the oxo moiety results in destabilisation of the $d_{xy}$ and $d_{xz}$ orbitals, leaving the $d_{yz}$ orbital unaffected. As the W-O bond is lengthened crossing may now occur (figure 1.13).

On stretching the W-O bond the HOMO transforms from an orbital that is originally W-O non-bonding, $d_{xy}$, to one that is W-O antibonding after crossing, $d_{yz}$. This change also corresponds to depopulation of the originally occupied antibonding W-Cl orbital, transforming to a M-Cl non-bonding orbital after crossing. This means that

lengthening the W-O bond should be accompanied by a shortening, hence strengthening, of the cis W-Cl interaction. In fact, this bond formally has multiple bond character. In other words, the crossing results in reduced bonding between W and O, and stronger bonding between W and Cl.

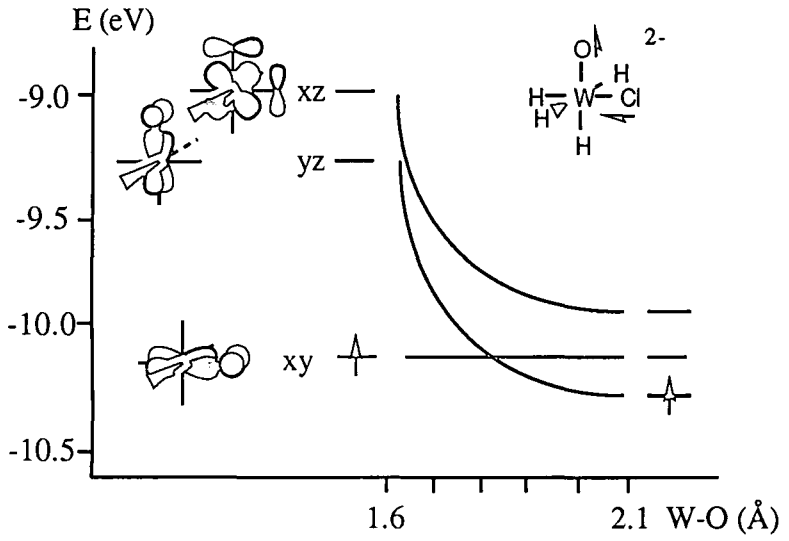


**Figure 1.13:** The energy diagram for the low-lying d orbitals in the $d^1$ model complex $[W(O)ClH_4]^{2-}$, with the chlorine cis to the oxygen, as a function of the W-O stretching

Since the xy orbitals involved in π-interactions with the ligands is cis to oxygen, π-donor ligands in this cis position favour an orbital crossing by reducing the HOMO-LUMO separation. Conversely, π-acceptor ligands at these sites would disfavour crossing. A similar treatment showed that crossing is discouraged when a π-donor ligand is located trans to the oxo ligand. In fact, since the $d_{yz}$ and $d_{xz}$ orbitals are destabilised by both an interaction with a chlorine and oxygen lone pair, while the $d_{xy}$ orbital remains non-bonding, such an interaction actually mitigates against an orbital crossing (figure 1.14). Application of these conclusions suggest that $[(Me_3tacn)W(O)Cl_2]^+$ is a good candidate for orbital crossing, since it possesses two cis chloride, π-donor ligands. Calculations by Hoffmann et al.[20] on $W(O)Cl_2(NH_3)_3^+$ confirm a crossing occurs for M-O at ca. 1.90Å. Therefore, lengthening of the W-O bond is a forbidden reaction and thus may explain the stability of both isomers, even in solution. The complexes *cis-mer*-$Mo(O)Cl_2(PR_3)_3$ and *trans*-$Mo(O)(OH_2)(CN)_4^{2-}$

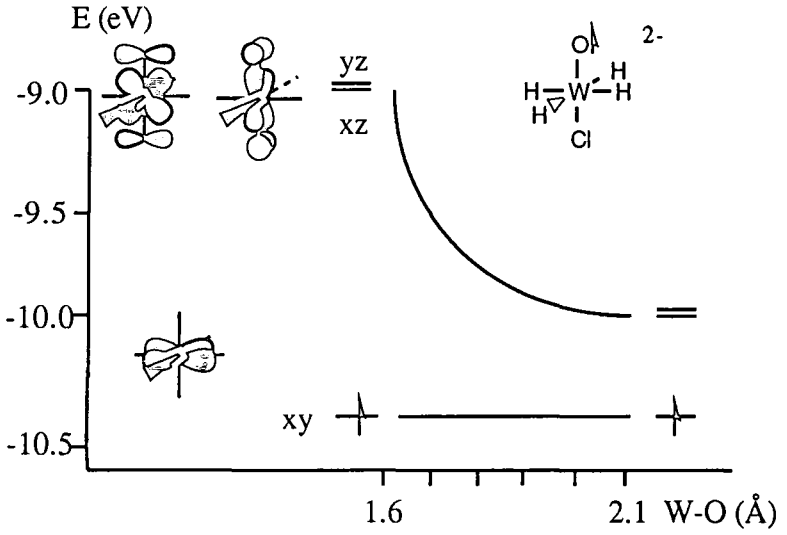


**Figure 1.14:** The energy diagram for the low-lying d orbitals in the $d^1$ model complex $[W(O)ClH_4]^{2-}$, with the chlorine trans to the oxygen, as a function of the W-O stretching

possess ligands which inhibit orbital crossing and so are bad candidates for this mechanism.

### 1.6.2 Reorganisation of the d-π Bonding

In the Chatt blue complex (ν(M=O) 954 $cm^{-1}$), structurally determined by Muir[21], the distortion that converts this Chatt blue to the Enemark blue form (ν(M=O) 941 $cm^{-1}$), is an antisymmetric motion of the Mo-O and Mo-$Cl_{trans}$ bonds (figure 1.15). That is, stretching of the Mo-O bond is accompanied by a shortening of the trans Mo-Cl bond. According to this scheme, a double minimum could also result from the reorganisation of the d-π bonding, developed mainly within the Mo-O interaction in the Chatt blue form, and mainly within the Mo-$Cl_t$ interaction of the d-π bond in the Enemark form.

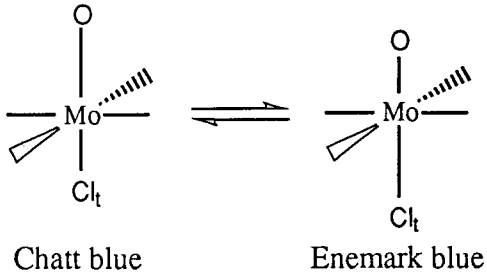


Chatt blue Enemark blue

**Figure 1.15:** Diagram showing the proposed antisymmetric stretching motion of the Mo-O and Mo-$Cl_{trans}$ bonds associated with bond lengthening and shortening on conversion from one form to the other

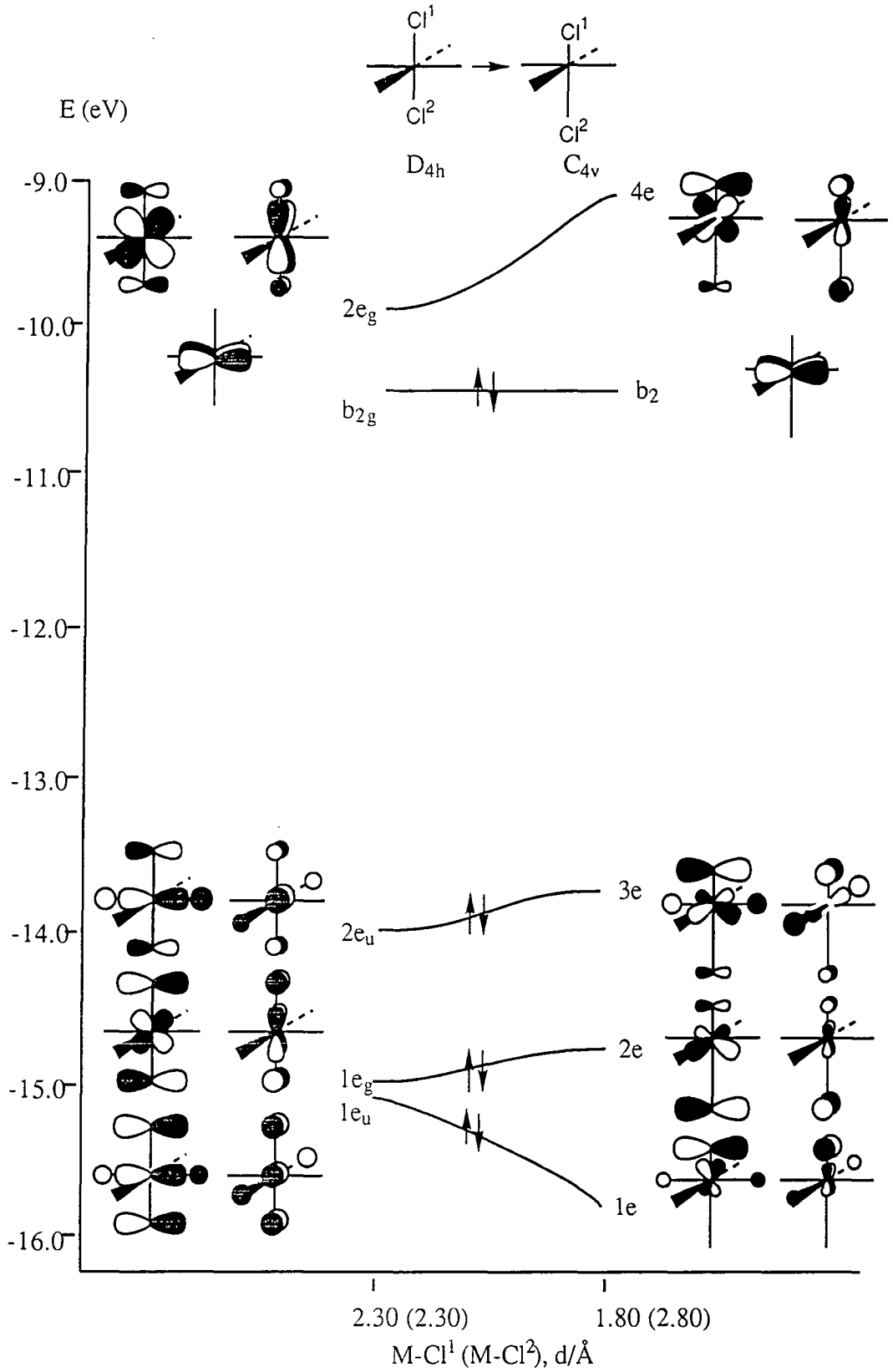


**Figure 1.16:** Orbital diagram for the asymmetric distortion of the two Mo-Cl bonds in the model complex *trans*-$[MoCl_2H_4]^{2-}$

Figure 1.16 shows that introducing asymmetry in the Mo-Cl bonds of *trans*-$MoCl_2H_4^{2-}$ (a $d^2$ species, with two identical π-donor Cl ligands trans to each other), the

$1e_u$ orbital is strongly stabilised by mixing with the $2e_g$, so prompting the distortion on π-grounds. In addition, there is a competing σ-component, with a minimum at the symmetric geometry, which is in superpostion of the π-effect, where there exists a double minimum Cl—M-Cl and Cl-M—Cl. If the π-effect dominates the σ-component, as is calculated in the model complex *trans*-$MoCl_2H_4^{2-}$, then two minima result (figure 1.17, left). If the σ-component dominates, only one minimum would be found (e.g. $CO_2$; figure 1.17, right). This mechanism could thus furnish an explanation for the observed distortion in *cis-mer*-$Mo(O)Cl_2(PMe_2Ph)_3$.

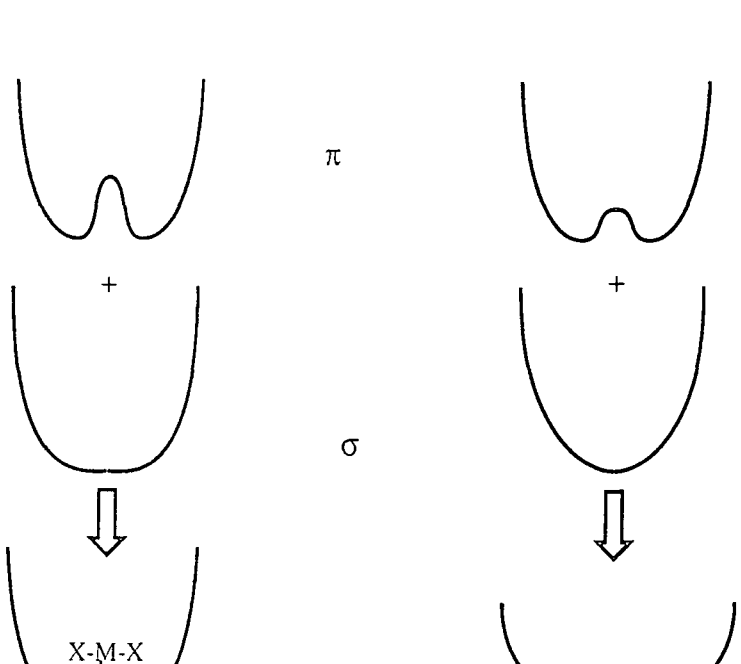


**Figure 1.17:** The total energy as a function of distance is a result of opposite trends for $E_\sigma$ (single minimum) and $E_\pi$ (double minimum). Left where $E_\pi$ dominates and right where $E_\sigma$ dominates.

## 1.7 Structural Differences in Forms Involving a Difference of Spin States

Examples of isomerism, possibly related to bond-stretch and distortional isomerism, but which are accompanied by additional changes within a molecule than just a single bond length, are known. It has been well documented that transition metal

complexes that exhibit different spin states (high/low spin equilibria) can show significant structural changes.[24] The principal structural changes centre on either a variation in their bond lengths or a difference in their geometrical shapes. For example, $Ni[PPh_2(CH_2Ph)]_2Br_2$ exists as both square-planar and tetrahedral isomers.[25]

A recent report by Kölle[26] established the existence of two forms of $[(\eta^5\text{-}C_5Me_5)RuCl_2]_2$ where the differences lie in their Ru-Ru separations (2.930(1) and 3.753(1)Å) and the Ru-μCl-Ru bond angles (76.50(4)° and 100.24(5)°), and also in their terminal Ru-Cl bond lengths (2.366(1) and 2.418(2)Å versus 2.445(1) and 2.365(2)Å correspondingly). Magnetic susceptibility and solution NMR studies suggested that the isomers differ in their magnetic properties such that one form is a singlet with a Ru-Ru bond (2.930(1)Å), whereas the other form is a triplet without a significant Ru-Ru bonding interaction (Ru···Ru 3.753(1)Å). Extended-Hückel calculations have provided a qualitative explanation for the observed geometries and spin states of the two isomers.[27] The term 'deformational isomers' was used by Kölle to delineate them from bond-stretch and distortional isomers. A related example is $[Rh_2(\mu\text{-}Cl)_2(\mu\text{-}AuPPh_3)(CNC_8H_9)_4]_2[PF_6]_2$ which exists as red and green forms with different conformations and Rh-Rh bond lengths.[28]

## 1.8 Aims and Objectives

Following the discovery of the existence of possible bond-stretch isomer pairs in the $Nb(O)Cl_3(PMe_3)_3$ system there was renewed interest in the viability of synthesising more such matched isomer pairs in analogous Group V oxo and sulphido complexes ($M(E)X_3(PMe_3)_3$: E= O, S; X= Cl, Br) where the phosphine ligand was restricted to trimethylphosphine in order to keep a degree of control on the stereochemistry. By restricting the studies to a set series of analogous compounds it was hoped that the results would shed some light as to the origin of the phenomenon of bond-stretch isomerism.

It was also deemed worthwhile to re-investigate the original findings of Chatt[3] in order to establish the possible existence of two blue forms of *cis-mer-*

$Mo(O)Cl_2(PMe_2Ph)_3$ (and related complexes) exhibiting two different Mo=O stretching frequencies. Using X-ray crystallographic studies it was hoped to establish whether this difference was reflected in the Mo=O bond lengths and so indicate the existence or otherwise of distortional or bond-stretch isomerism.

## 1.9 References


1. W.-D. Stohrer, R. Hoffmann, *J.Amer. Chem. Soc.*, 1972, **94**, 1661.
2. W.-D. Stohrer, R. Hoffmann, *J.Amer. Chem. Soc.*, 1972, **94**, 779.
3. A.V. Butcher, J. Chatt, *J. Chem. Soc (A)*, **1970**, 2652.
4. M.N. Paddon-Row, L. Radom, A.R. Gregory, *J. Chem. Soc. Chem. Commun.*, **1976**, 427.
5. (a) P.v.R. Schleyer, A.F. Sax, J. Kalcher, R. Janoschek, *Angew. Chem. Int. Ed. Engl.*, 1987, **26**, 364; (b) J.A. Boatz, M.S. Gordon, *J. Phys. Chem.*, 1989, **93**, 2888; (c) S. Nagasse, T. Kudo, *J. Chem. Soc. Chem. Commun.*, **1988**, 54; (d) S. Collins, W.W. Schoeller, T. Dabisch, T. Busch, *Inorg. Chem.*, 1987, **26**, 4283.
6. E. Kaufmann, P.v.R. Schleyer, *Inorg. Cmem.*, 1988, **27**, 3987.
7. (a) P.V. Sudhakar, K. Lammertsma, *J. Phys. Chem.*, 1989, **93**, 7289; (b) K. Lammertsma, O.F. Guner, *J. Amer. Chem. Soc.*, 1988, **110**, 5239.
8. O.F. Guner, K. Lammertsma, *J. Amer. Chem. Soc.*, 1990, **112**, 508.
9. P.V. Sudhakar, K. Lammertsma *J. Phys. Chem.*, 1992, **96**, 4830.
10. (a) J. Chatt, Lj. Manojlovic-Muir, K.W. Muir, *Chem. Commun.*, **1971**, 655; (b) Lj. Manojlovic-Muir, K.W. Muir, *J. Chem. Soc. Dalton Trans.*, **1972**, 686.
11. B.L. Haymore, W.A. Goddard III, J.N. Allison, *Proc. Int. Conf. Coord. Chem.*, 23rd, **1984**, 535.
12. (a) J.M. Mayer, *Inorg. Chem.*, 1988, **27**, 3899; (b) W.A. Nugent, J.M. Mayer, *'Metal-Ligand Multiple Bonds'*, Wiley, New York (1988).
13. F.A. Cotton, M.P. Diebold, W.J. Roth, *Inorg. Chem.*, 1987, **26**, 2848.
14. E. Carmona, A. Galindo, L. Sanchez, A.J. Nielson, G. Wilkinson, *Polyhedron*, 1984, **3**, 347.

15. K. Yoon, G. Parkin, A.L. Rheingold, *J.Amer. Chem. Soc.*, 1991, **113**, 1437.

16. A.P. Bashall, M. McPartlin, poster presented at 15th IUC International Conference of Crystallography, Bordeaux 19th-28th July 1990.

17. K. Wieghardt, G. Baches-Dahmann, B. Nuber, J. Weiss, *Angew. Chem. Int. Ed. Engl.*, 1985, **24**, 777.

18. D.C. Brower, J.L. Templeton, D.M.P. Mingos, *J.Amer. Chem. Soc.*, 1987, **109**, 5203.

19. I. D. Brown, K.K. Wu, *Acta. Crystallogr., Sect. B: Struct. Crystallogr. Cryst. Chem.*, 1976, **B32**, 1957.

20. Y. Jean, A. Lledos, J.K. Burdett, R. Hoffmann, *J.Amer. Chem. Soc.*, 1988, **110**, 4506; *J. Chem. Soc. Chem. Commun.*, **1988**, 140.

21. Lj. Manojlovic-Muir, K.W. Muir, *J. Chem. Soc. (A)*, **1971**, 2796.

22. M.G. B. Drew, D.A. Rice, D.M. Williams, *J. Chem. Soc. Dalton Trans.*, **1985**, 1821.

23. K. Gebreyes, J. Zubieta, T.A. George, L.M. Koczon, *Inorg. Chem.*, 1986, **25**, 405.

24. E. König, *Prog. Inorg. Chem.*, 1987, **35**, 527.

25. F.A. Cotton, G. Wilkinson, *'Advanced Inorganic Chemistry'*, 5th ed.; Wiley: New York, 1988.

26. U. Kölle, J. Kossakowaski, N. Klaff, L. Wesemann, U. Englert, G.E. Heberich, *Angew. Chem. Int. Ed. Engl.*, 1991, **30**, 690.

27. U. Köelle, H. Lueken, K. Handrick, J.K. Burdett, S. Balleza, *Inorg. Chem.*, in press.

28. K.L. Bray, H.G. Drickamer, D.M.P. Mingos, M.J. Watson, J.R. Shapley, *Inorg. Chem.*, 1991, **30**, 864.

# CHAPTER TWO

## A Re-evaluation of Distortional Isomerism in Oxomolybdenum Systems

## 2.1 Introduction

This chapter draws together data relating to the observation of distortional isomerism in oxomolybdenum systems.

It has now been established that there exists independently two blue forms of $Mo(O)Cl_2(PMe_2Ph)_3$ exhibiting ν(Mo=O) stretches at 955 and 943 $cm^{-1}$ in their infrared spectra. Along with these two forms are their associated green forms, which represent the co-crystallisation of the blue species with yellow *mer*-$MoCl_3(PMe_2Ph)_3$. It will be seen that the level of this contaminant reflects the nature of which form preferentially crystallises out of solution. A brief look at analogous oxyhalide species is then considered.

## 2.2 Synthesis of the Blue and Green $Mo(O)Cl_2(PMe_2Ph)_3$ Species

Discrepancies between the infrared data reported by Chatt[3] and later by Enemark[4] on blue $Mo(O)Cl_2(PMe_2Ph)_3$, not only in the Mo=O stretching region but also in the Mo-Cl stretching vibration region of their IR spectra, led to the inescapable conclusion that two blue forms existed. A piece of evidence that supported this explanation was the fact that the Mo-Cl bond lengths reported by Parkin[1] are significantly different from those reported by Manojlovic-Muir[2] in their original X-ray structure determination of blue *cis-mer*-$Mo(O)Cl_2(PMe_2Ph)_3$.

The original preparative report by Butcher and Chatt[3] described the reaction of molybdenum pentachloride with the dropwise addition of ethanol to give a 'brown' oil. This was subsequently treated with $PMe_2Ph$ and refluxed in ethanol to give a high yield of the blue isomer exhibiting a ν(Mo=O) stretch at 954 $cm^{-1}$. Attempts to reproduce this synthesis invariably led to a green oil, which upon subsequent crystallisation from hot ethanol, afforded blue crystals that displayed a ν(Mo=O) stretch at 943 $cm^{-1}$, corresponding to the compound reported by Enemark.[4]

This temporarily proved to be a dilemma, until it was established that the green oil, reported earlier by Webb and Wardlaw[5] to be molybdenyl chloride

([$Mo(O)Cl_3$]), was found to turn brown on addition of water. This led on identical work-up to the Chatt blue isomer with a ν(Mo=O) stretch at 955 $cm^{-1}$ (scheme 2.1).

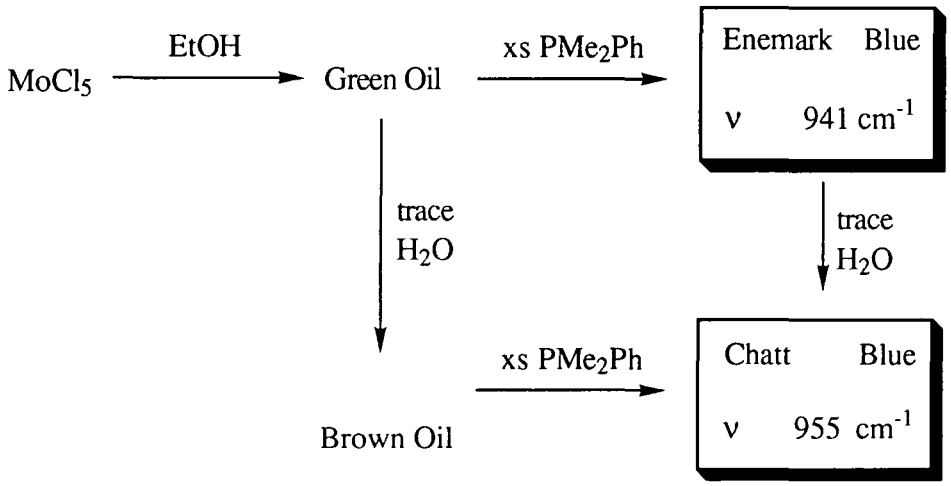


**Scheme 2.1**: Synthesis of Chatt and Enemark Blues

Butcher/Enemark green $Mo(O)Cl_2(PMe_2Ph)_3$ was similarly prepared according to the literature method[3], whereby $MoCl_4(MeCN)_2$ (in place of $MoCl_4(EtCN)_2$) reacts with $PMe_2Ph$ in ethanol to crystallise out green needles from a refluxed solution. This green form exhibits a ν(Mo=O) stretch at 941 $cm^{-1}$, with additional features at higher frequencies.

A green form of the Chatt blue $Mo(O)Cl_2(PMe_2Ph)_3$ can be prepared when slightly wet solvent is used to prepare the Chatt blue form. The presence of excess water (more than trace amounts) leads to the crystallisation of a green form exhibiting a ν(Mo=O) stretch at 955 $cm^{-1}$. Several additional routes have now been established to the Chatt blue isomer. These are outlined in scheme 2.2, along with routes to the Enemark blue and green forms. When $MoCl_4L_2$ (L=MeCN or THF) is treated with five equivalents of $PMe_2Ph$ and one equivalent of de-oxygenated water at room temperature a green solid is produced, which can be recrystallised from methanol to give the Chatt blue form. This is similar to the route to Butcher/Enemark green whereby $MoCl_4L_2$ (L=MeCN or THF) when treated with excess $PMe_2Ph$ in refluxing dry ethanol, deposits green crystals leading to the speculation that water plays a significant role in the outcome of which form is crystallised. An interesting route to the Chatt blue form involves the use of the dioxo species $Mo(O)_2Cl_2$, which when treated with four equivalents of $PMe_2Ph$

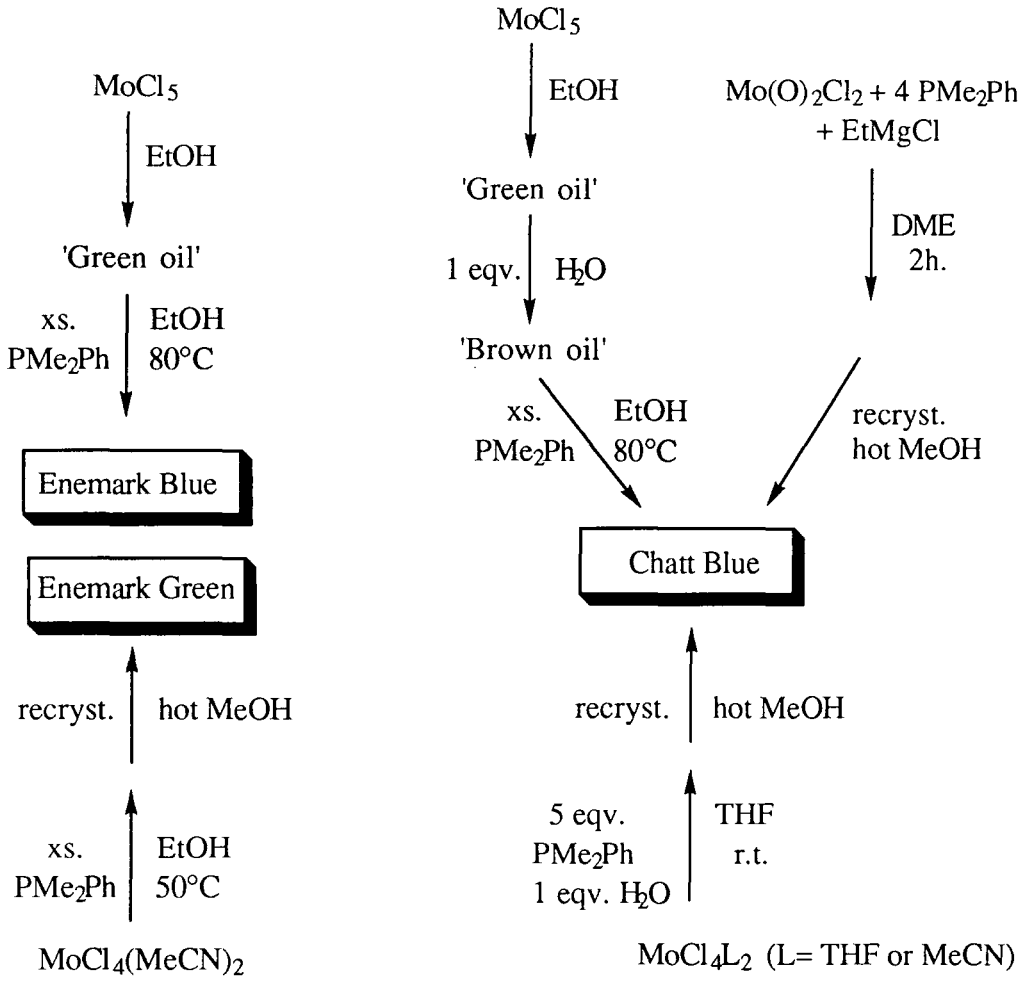


**Scheme 2.2:** Synthetic routes to *cis-mer*-$Mo(O)Cl_2(PMe_2Ph)$ species

and one equivalent of EtMgCl (presumably acting as a reducing agent) in DME, produces on work-up a green solid that recrystallises from methanol to give blue cubic crystals of Chatt blue.

## 2.3 Vibrational Studies: Infrared and Raman Spectroscopy

In an infrared *absorption* spectrum the gross selection rule for infrared activity is that the motion corresponding to a normal mode should be accompanied by a change of dipole moment, and so transforms the same as the translation components in a character table. In Raman *scattering* spectra the normal modes of vibration of molecules are Raman active if they are accompanied by a changing polarisability. This is difficult to do by inspection alone. It is left to group theory to provide an explicit recipe for judging Raman activity of a normal mode. The quadratic terms in character tables transform in the same

way as polarisability and are thus used to determine Raman activity. It can be seen from figure 2.1 that *cis-mer*-$Mo(O)Cl_2(PMe_2Ph)_3$ has symmetry elements that mean the molecule belongs to the $C_s$ point group. Using the internal coordinates along the Mo=O bond length and along each of the Mo-Cl bonds (ignoring the internal bond angles which give rise to bending deformations), the symmetries of the ν(Mo=O) and ν(Mo-Cl) *stretching* vibrations can be determined. In the case of the ν(Mo=O) stretch, reduction of the $\chi_{stretch}$ (1 1) representation gives $\Gamma_{stretch}$(Mo=O), the irreducible representation of the stretching vibration, which transforms as A'. Inspection of the character table shows that this vibration is both infrared and Raman active. Similarly, for the ν(Mo-Cl) vibrations, reduction of the $\chi_{stretch}$ (2 2) representation gives $\Gamma_{stretch}$(Mo-Cl), which is found to transform as 2A'. Therefore, two ν(Mo-Cl) stretches are expected to be infrared and Raman active. Where co-crystallisation with yellow *mer*-$MoCl_3(PMe_2Ph)_3$ occurs to give a green species, X-ray structure determination shows the apparent crystal that forms to have a $C_1$ space group. However, the symmetry of the blue form in the mixture is unaffected and so one ν(Mo=O) and two ν(Mo-Cl) infrared and Raman active stretches are expected to be observed in the spectra.

In the case of *mer*-$MoCl_3(PMe_2Ph)_3$ which belongs to the $C_{2v}$ point group

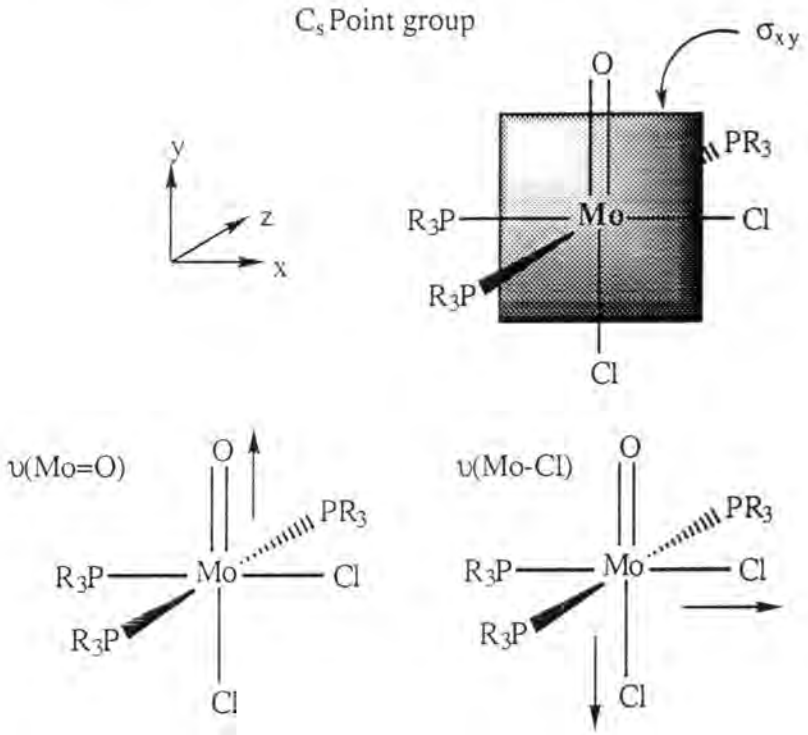


**Figure 2.1:** $Mo(O)Cl_2(PMe_2Ph)_3$ symmetry and stretching vibrations

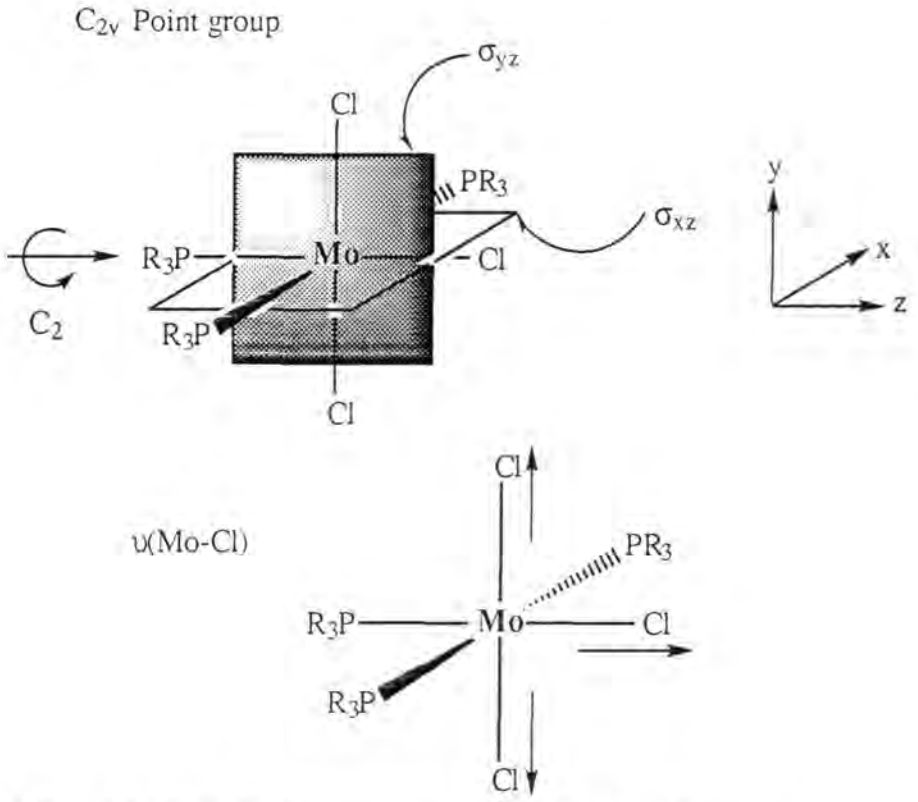


**Figure 2.2:** $MoCl_3(PMe_2Ph)_3$ symmetry and ν(Mo-Cl) vibrations

(figure 2.2) the ν(Mo-Cl) stretches ($\chi_{stretch}$(3 1 1 3)) are found to transform as $2A_1+B_2$. Thus, three IR and Raman active ν(Mo-Cl) stretches are expected.

### 2.3.1 Mo=O Infrared Fingerprint Region

In their original observation Butcher and Chatt[3] reported a blue and green species of $Mo(O)Cl_2(PMe_2Ph)_3$ each showing a strong band in the region 940-955 $cm^{-1}$ attributable to the ν(Mo=O) stretch.[6] A preliminary X-ray structure determination of the blue isomer[7b] had shown it to have a *cis-mer* configuration, and from this, together with the spectroscopic data, they concluded that the green form must be the trans-dichloro geometric isomer[7] (later proved to be wrong). They were thus convinced, even before further X-ray evidence of the existence of two isomers. The infrared spectra were particularly important in determining the existence of two forms, the blue isomer being readily distinguished from the green form in having a ν(Mo=O) stretching frequency at 954 $cm^{-1}$ as opposed to 943 $cm^{-1}$ for the latter (both values as reported in the original report).

Unknown to each other two other groups were re-examining the original Chatt $Mo(O)Cl_2(PMe_2Ph)_3$ system. Enemark and co-workers[4], who paid the Chatt observation particular attention, concluded from their observations that the original assignment of a ν(Mo=O) stretch at 954 $cm^{-1}$ in the IR spectrum of the blue form was incorrect. For their blue compound they showed that a band at 944 $cm^{-1}$ was undoubtedly due to the Mo=O stretch as it was also found at 943 $cm^{-1}$ in the Raman spectrum, and the same stretch is present in the Butcher/Enemark green form. This is in direct contrast to Chatt who found a peak in the IR spectrum at 954 $cm^{-1}$ for the blue form. Parkin and co-workers[1] were similarly unable to reproduce Chatt's original observation of a blue isomer of $Mo(O)Cl_2(PMe_2Ph)_3$ showing a ν(Mo=O) stretching frequency at 954 $cm^{-1}$.

We still, however, remained puzzled by the discrepancies between the IR data reported by Chatt and Enemark on their respective blue forms. Not only were there discernible differences in the Mo=O stretching region, but also in the Mo-Cl stretching region of the IR spectrum. Could it be that the blue form of $Mo(O)Cl_2(PMe_2Ph)_3$ (ν(Mo=O) 943 $cm^{-1}$) obtained by Enemark and Parkin, both by direct synthesis and by purification of the green Butcher/Enemark form, was not the same as the blue form reported by Chatt (ν(Mo=O) 954 $cm^{-1}$).

Here we report, as a result of following as closely as possible the original methods of Chatt and Butcher[3], the successful isolation of the two blue forms of $Mo(O)Cl_2(PMe_2Ph)_3$, one exhibiting a ν(Mo=O) stretch at 941 $cm^{-1}$ (corresponding to the Enemark blue form) and the other at the elusive 955 $cm^{-1}$ of the Chatt blue form.

Unique infrared assignment of the ν(Mo=O) bands in the series of blue and green forms of $Mo(O)Cl_2(PMe_2Ph)_3$ is complicated by the presence of intense ligand ν(P-C) bands[8] in the 1000-900 $cm^{-1}$ region (figure 2.3, table 2.1). The IR spectra of this region for all four forms show an intense peak in the range 905-911 $cm^{-1}$, including the yellow $MoCl_3(PMe_2Ph)_3$ contaminant of the two green forms. Each $Mo(O)Cl_2(PMe_2Ph)_3$ species has additionally a strong peak at 915 $cm^{-1}$, the Enemark forms also showing a shoulder/peak at ca. 928 $cm^{-1}$; yellow $MoCl_3(PMe_2Ph)_3$ shows a band at 919 $cm^{-1}$ exhibiting a shoulder at 929 $cm^{-1}$. Additionally, the spectrum of

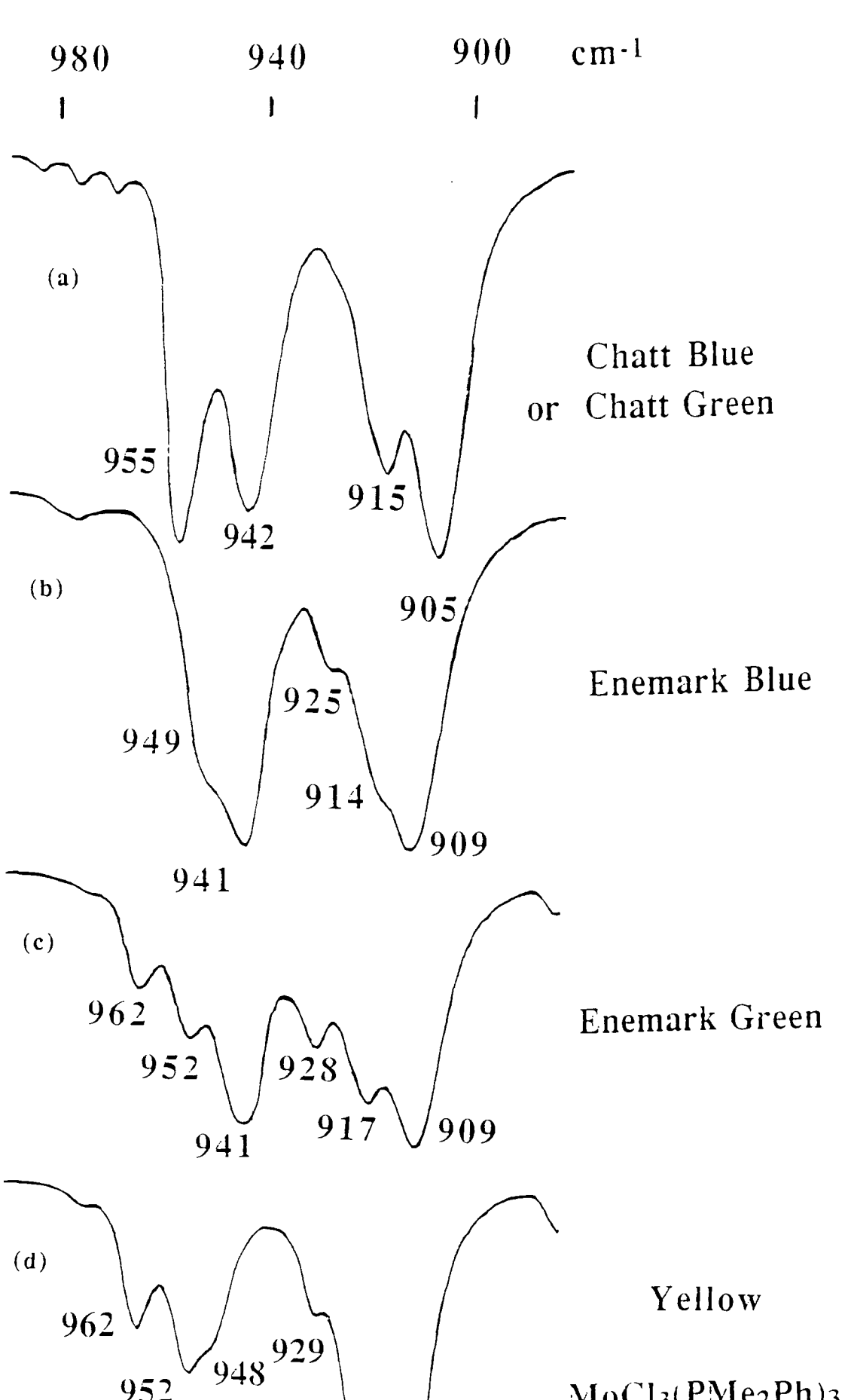


**Figure 2.3:** Solid-state infrared spectra of the ν(Mo=O) stretch 'fingerprint' region.

| Enemark Blue | Enemark Green | Chatt Blue | Chatt Green | $MoCl_3(PMe_2Ph)_3$ |
|---|---|---|---|---|
| | 962 m | | | 962 m |
| | 952 s | 955 vs [a] | 955 vs [a] | 952 s |
| 949 vs,sh | | | | 948 s,sh |
| 941 vs [a] | 941 vs [a] | 942 vs | 942 vs | |
| 925 m,sh | 928 s | | | 929 m,sh |
| 914 s,sh | 917 vs | 915 s | 915 s | 919 s,sh |
| 909 vs [b] | 909 vs [b] | 905 vs [b] | 905 vs [b] | 911 vs [b] |
| 839 m | | 834 m | 834 m | |
| | | 828 w | 828 w | |
| | | 757 s | 757 s | |
| 754 s | 754 s,sh | | | 754 s |
| 749 s | 748 s | 752 s | 752 s | 749 s |
| 740 s [c] | 740 s [c] | 740 s [c] | 740 s [c] | 740 s [c] |
| | 731 m | 728 w | 728 w | 731 m |
| | 715 m | | | 714 m |
| 712 m | | 712 m | 712 m | |
| | 708 m | | | 708 m |
| 698 s [c] | 698 s [c] | 698 s,sh [c] | 698 s,sh [c] | 698 s [c] |
| 695 s [c] | 695 s [c] | 696 s [c] | 696 s [c] | 694 s [c] |
| 677 m [c] | 677 m [c] | 677 m [c] | 676 m [c] | 678 m [c] |

**Table 2.1**: Infrared Data (1000-600 $cm^{-1}$): [a]ν(Mo=O); [b]ν(P-$CH_3$); [c]Phenyl ring bending

Enemark blue has a single very strong peak at 941 $cm^{-1}$ with a shoulder at 949 $cm^{-1}$; Chatt blue and green an intense pair of peaks at 942 and 955 $cm^{-1}$; yellow $MoCl_3(PMe_2Ph)_3$ has a medium/strong pair at 952 and 962 $cm^{-1}$, the lower frequency band showing a shoulder at 948 $cm^{-1}$; and Enemark/Butcher green an intense peak at 941 $cm^{-1}$ with additional higher frequency peaks at 952 and 962 $cm^{-1}$ of lower intensity. Over the same region free $PMe_2Ph$ has two very strong peaks at 940 and 895 $cm^{-1}$. Thus, it is difficult to assign the ν(Mo=O) stretching bands in the IR spectra with any degree of certainty without recourse to other information. This information can be gleaned from Raman spectroscopy and isotopic $^{18}O$ labelling.

### 2.3.2 Raman Spectroscopy

Two methods of investigation were used to elucidate the identification of the ν(Mo=O) stretching frequency and further validate the existence of two blue forms and support the conclusion that both green forms are made up of individual contributions

| Enemark Blue | Enemark Green | Chatt Blue | Chatt Green | $MoCl_3(PMe_2Ph)_3$ |
|---|---|---|---|---|
| 1588 s | 1588 s | 1588 s | 1588 s | 1588 s |
| 1575 vw | 1575 vw | 1575 vw | 1575 vw | 1575 vw |
| 1420 m | 1420 m | | | |
| | | 1414 m | 1414 m | |
| 1196 vw | 1196 vw | 1196 vw | 1196 vw | 1197 vw |
| 1184 vw | 1184 vw | 1184 vw | 1184 vw | |
| 1164 vw | 1164 vw | 1164 w | 1167 w | 1164 w |
| 1106 m[b] | 1106 m[b] | 1104 m[b] | 1106 m[b] | 1103 m[b] |
| 1031 m | 1031 m | 1029 m | 1029 m | 1031 m |
| 1002 vs[b] | 1002 vs[b] | 1002 vs[b] | 1002 vs[b] | 1001 vs[b] |
| | | **954** m[a] | **954** m[a] | |
| **941** m[a] | **942** m[a] | | | |
| 754 w | 754 w | 754 w | 754 w | 750 vw |
| | 735 w | | 735 w | 735 vw |
| 711 w | 711 w | 719 w | 719 w | 715 vw |
| 677 s | 677 s | 677 s | 677 s | 677 s |
| 619 w | 619 w | 623 w | 623 w | 620 w |
| 486 vw | 487 w | 490 vw | 490 vw | |
| 420 vw | 423 w | | | 420 w |
| | | 416 w | 416 w | |
| | | | | 411 w |
| | 390 vw | | | |
| | 380 vw | | | |
| 353 m | 351 w | | | 351 w |
| | | 345 m | 345 m | |
| 338 m | 339 w | | | |
| | 317 w | | | 314 m,sh[c] |
| | | 310 m | 310 m | |
| 307 m | | | | |
| | 304 w | | | |
| | 295 w[c] | | | 295 m[c] |
| 282 m[c] | 283 w[c] | | | |
| 266 m | 265 w | 263 m | 263 m | 263 m,sh |
| 254 w[d] | | 250 w[d] | 250 w[d] | |
| 244 m | | | | |
| | | | | 234 w |
| | | | 225 vw | |
| 203 m | 205 vw | 207 m | 207 m | 203 m |

**Table 2.2**: Raman Data (1600-200 $cm^{-1}$): [a]ν(Mo=O); [b]ν(P-Ph); [c]ν(Mo-Cl); δ(Mo-O)

from its respective blue form and yellow $MoCl_3(PMe_2Ph)_3$. The first of these is solid-state Raman spectroscopy (figure 2.4, table 2.2). We have seen in section 2.3 that *cis-mer*-$Mo(O)Cl_2(PMe_2Ph)_3$ can crystallise out in two forms which belong to $C_s$ and $C_1$ point groups (see section 2.7) and that *mer*-$MoCl_3(PMe_2Ph)_3$ belongs to $C_{2v}$. The number of ν(Mo=O) and ν(Mo-Cl) stretches, and their Raman activity can thus be determined, and hence solid-state Raman spectroscopy can be used to allow the

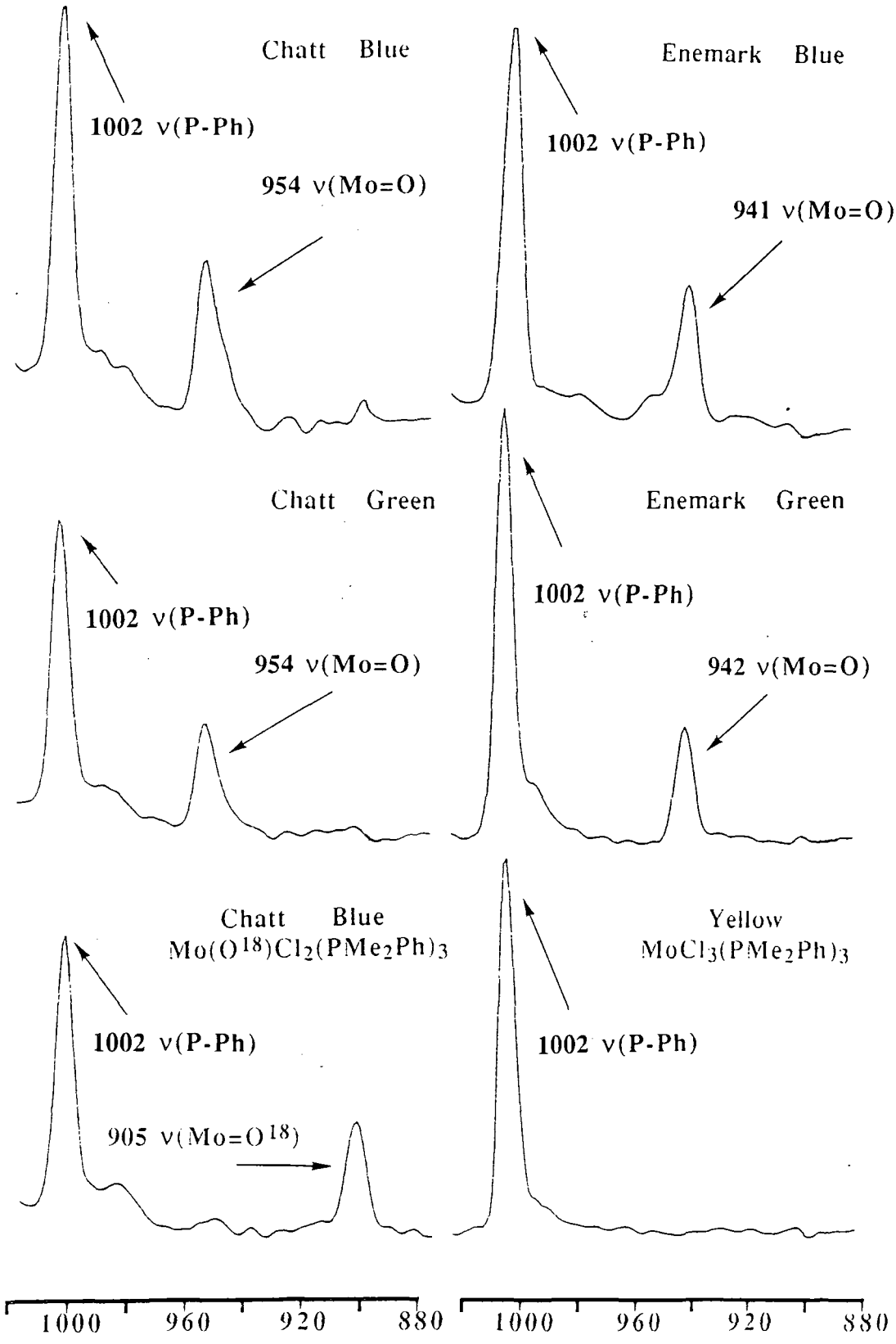


**Figure 2.4:** Raman spectra of the ν(Mo=O) stretch 'fingerprint' region for the $Mo(O)Cl_2(PMe_2Ph)_3$ species and $MoCl_3(PMe_2Ph)_3$.

identification of the ν(Mo=O) stretching frequency and so support the evidence, for both the existence of two blue forms of *cis-mer*-$Mo(O)Cl_2(PMe_2Ph)_3$, and that each form can be contaminated by yellow *mer*-$MoCl_3(PMe_2Ph)_3$ to produce a corresponding green form. The absence of the strong bands at 941 and 942 $cm^{-1}$ (present in the Enemark blue and green forms respectively), and at 954 $cm^{-1}$ (present in the Chatt forms), in the spectrum of yellow *mer*-$MoCl_3(PMe_2Ph)_3$ and the free $PMe_2Ph$ IR spectrum, means that these bands may be confidently assigned to a ν(Mo=O) stretching frequency. In the original report by Chatt et al.[3] the ν(Mo=O) stretching frequencies of the blue and green forms of *cis-mer*-$Mo(O)Cl_2(PMe_2Ph)_3$ were assigned to bands at 954 and 943 $cm^{-1}$ respectively. Our Raman data shows the existence of two blue forms of *cis-mer*-$Mo(O)Cl_2(PMe_2Ph)_3$ showing ν(Mo=O) stretching frequencies at 941 and 954 $cm^{-1}$, and so are in accord with the original findings of Chatt, unlike Parkin[1,9] and Enemark[4], who failed to recognise the existence of two blue forms in their separate and independent re-investigations.

The bands at 941 and 954 $cm^{-1}$ are also present in the respective green forms, along with peaks at 735, 317 and 295 $cm^{-1}$ which are characteristic of contributions due to the presence of yellow *mer*-$MoCl_3(PMe_2Ph)_3$. It is also interesting to note that relative to the constant intensity of the invariant peak at 1002 $cm^{-1}$ present in each species, the intensity of the ν(Mo=O) band in Enemark green (ν(Mo=O) 941 $cm^{-1}$) is 21% weaker compared to that of the ν(Mo=O) peak in the Enemark blue form. This decreased intensity endorses the green form being an 81:19 (blue:yellow) mixture, as found by elemental analysis. Similarly, in the Chatt green form the intensity of the ν(Mo=O) at 954 $cm^{-1}$ is reduced in intensity by 7%, in line with the finding that the Chatt green form is contaminated to a significantly reduced extent compared to the Enemark green form.

Raman studies have also been used to confirm the assignment of the ν(Mo=$^{18}$O) peak in *cis-mer*-$Mo(^{18}O)Cl_2(PMe_2Ph)_3$, as being a strongly absorbing shoulder at 902 $cm^{-1}$, on an intense ν(P-C) band at 905 $cm^{-1}$ in the IR spectrum which is only weakly active in the Raman spectrum, whereas the ν(Mo=O) band is strongly active in the Raman spectrum (figure 2.4).

### 2.3.3 $^{18}O$ Isotopic Substitution Studies

Confirmation of the correct assignment of the ν(Mo=O) absorption in each species of $Mo(O)Cl_2(PMe_2Ph)_3$ is found in observing the isotopic shift produced on introducing an oxygen-18 label. Calculations using equation 4 (appendix 3) show that the ν(Mo=O) peaks in the 955 and 941 $cm^{-1}$ forms should be shifted to the lower frequencies of 901.9 and 888.7 $cm^{-1}$ respectively, when substituting $M_X$=M[$MoCl_2(PMe_2Ph)_3$]=581.2681. This was experimentally carried out according to equation 2.1, whereby $MoCl_4(THF)_2$ was treated with 5 equivalents of $PMe_2Ph$ and 1 equivalent of de-oxygenated 95% atom oxygen-18 water and stirred overnight at room temperature in THF. Work-up and recrystallisation from methanol led to an observed ν(Mo=$^{18}O$) at 902 $cm^{-1}$ for blue $Mo(^{18}O)Cl_2(PMe_2Ph)_3$, as a strong shoulder on the 905 $cm^{-1}$ absorption (figure 2.5, a). This peak can be highlighted by subtracting the peaks due the $Mo(^{16}O)Cl_2(PMe_2Ph)_3$ species (figure 2.5, a). In addition the peak at 955 $cm^{-1}$ is observed to be significantly reduced in intensity, in keeping with a reduced contribution due to $Mo(^{16}O)Cl_2(PMe_2Ph)_3$.

The ν(Mo=$^{18}O$) absorption at 902 $cm^{-1}$ corresponds to the isotopically shifted ν(Mo=$^{16}O$) 955 $cm^{-1}$ peak of the Chatt blue form. The assignment of this shoulder as a ν(Mo=$^{18}O$) stretch was confirmed by Raman spectroscopy (see section 2.3.2). There was no evidence of a peak at 888.7 $cm^{-1}$ in accordance with the formation of an Enemark oxygen-18 enriched blue form. The isolation of the Chatt oxygen-18 enriched form is consistent with reactivity studies (section 2.8) on Enemark blue, which shows conversion to the Chatt blue form in the presence of water.

$$MoCl_4(THF)_2 + 5PMe_2Ph + H_2{}^{18}O \xrightarrow[\text{r.t.}]{\text{THF}} Mo(^{18}O)Cl_2(PMe_2Ph)_3 \qquad \textbf{(2.1)}$$

Parkin et al.[9] report an observed isotopic shift for the oxygen-18 labelled derivative (prepared by the same procedure) of ν(Mo=$^{18}O$) at 897 $cm^{-1}$ and concludes

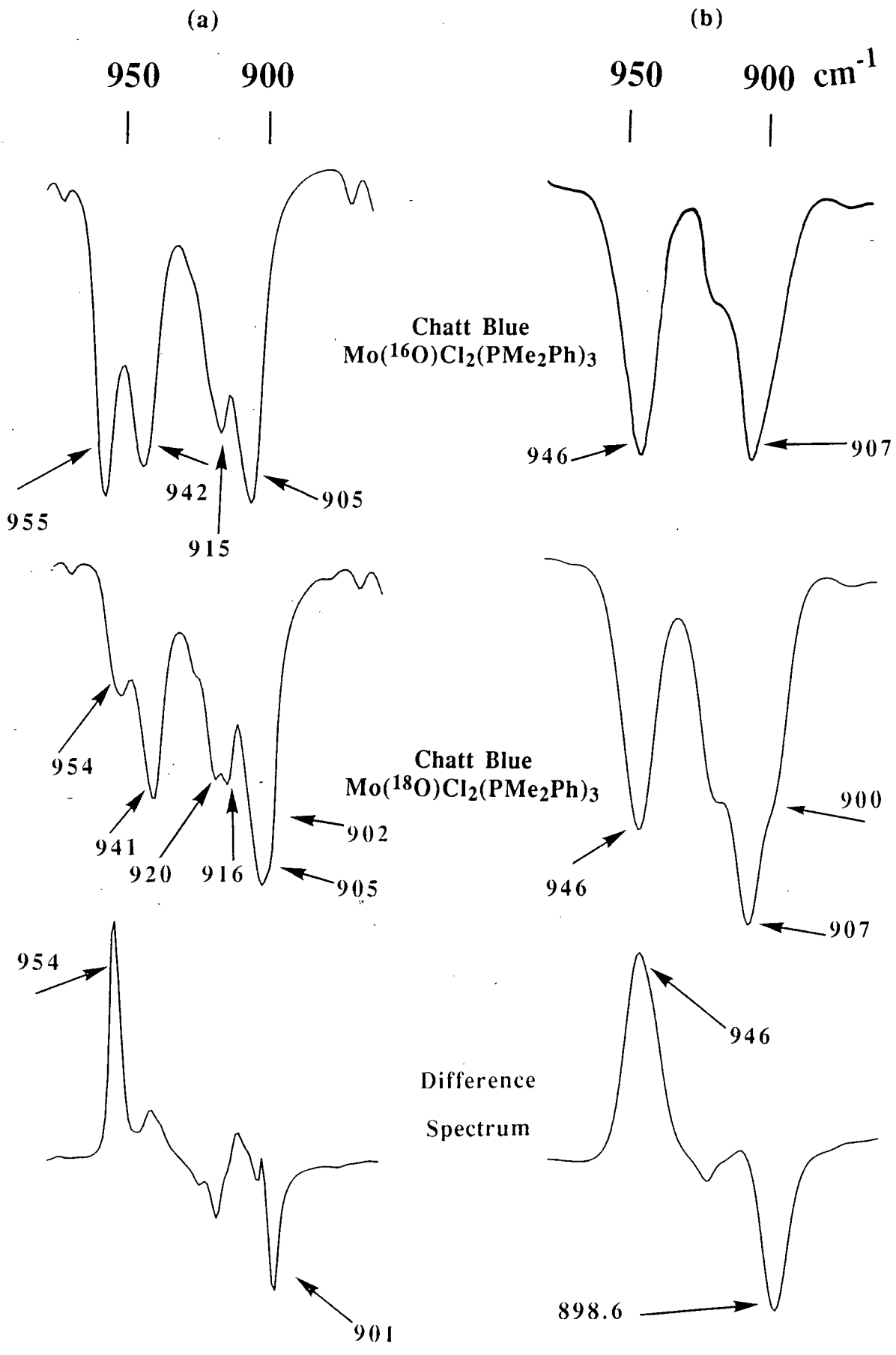


**Figure 2.5:** Chatt blue *cis-mer*-Mo(*O)$Cl_2(PMe_2Ph)_3$ (*=16, 18) (a) solid-state and (b) solution ($CH_2Br_2$) infrared spectra.

that this corresponds to the $\nu(Mo=^{16}O)$ stretching frequency at 943 $cm^{-1}$ of the Enemark blue form. However, this seems unlikely, since even substituting 943 for 941 into equation 3.4 would lead to an isotopically shifted value of 890.6 $cm^{-1}$. Clearly a question mark must remain concerning Parkin's assignment of a $\nu(Mo=^{18}O)$ stretching frequency at 897 $cm^{-1}$ as being due to the Enemark oxygen-18 form, since his reported value lies in between the two theoretically expected positions.

### 2.3.4 Low Frequency Infrared Stretching Region

The low-energy IR spectra (figure 2.6, table 2.3) clearly show both the existence of two blue forms and that the green forms are attributable to being a mixture of their corresponding blue form and yellow $MoCl_3(PMe_2Ph)_3$. The most striking difference of this region between the two blue forms is that the Enemark blue shows medium intensity bands at 486 and 288 $cm^{-1}$, whereas the Chatt blue shows strong peaks at 490 and 297 $cm^{-1}$ with a shoulder at 285 $cm^{-1}$.

The Enemark/Butcher green shows three strong bands at 322, 306 and 287 $cm^{-1}$, which are an exact replication of the two bands of yellow $MoCl_3(PMe_2Ph)_3$ at 323 and 307 $cm^{-1}$ with the single intense band of Enemark blue at 288 $cm^{-1}$. Analogous peaks occurring at 324, 304 and 285 $cm^{-1}$ were reported by Chatt in their original characterisation of the Butcher/Enemark green form.[3]

In the case of the Chatt green form this region does not elucidate the presence of yellow $MoCl_3(PMe_2Ph)_3$, primarily because the level of contamination (as shown by elemental analysis (section 2.7)) is only 0.69%.

The presence of yellow $MoCl_3(PMe_2Ph)_3$ can also be seen in the bands near 480 and 420 $cm^{-1}$. For instance the 491 and 483 $cm^{-1}$ peaks of Enemark green result from the summation of a 486 $cm^{-1}$ peak from Enemark blue and the 493 (shoulder), 487 and 482 $cm^{-1}$ peaks from yellow $MoCl_3(PMe_2Ph)_3$. Similarly the bands at 420 and 413 (shoulder) $cm^{-1}$ comprise the 419 $cm^{-1}$ from Enemark blue and the 420 and 412 $cm^{-1}$ peaks from the yellow $MoCl_3(PMe_2Ph)_3$.

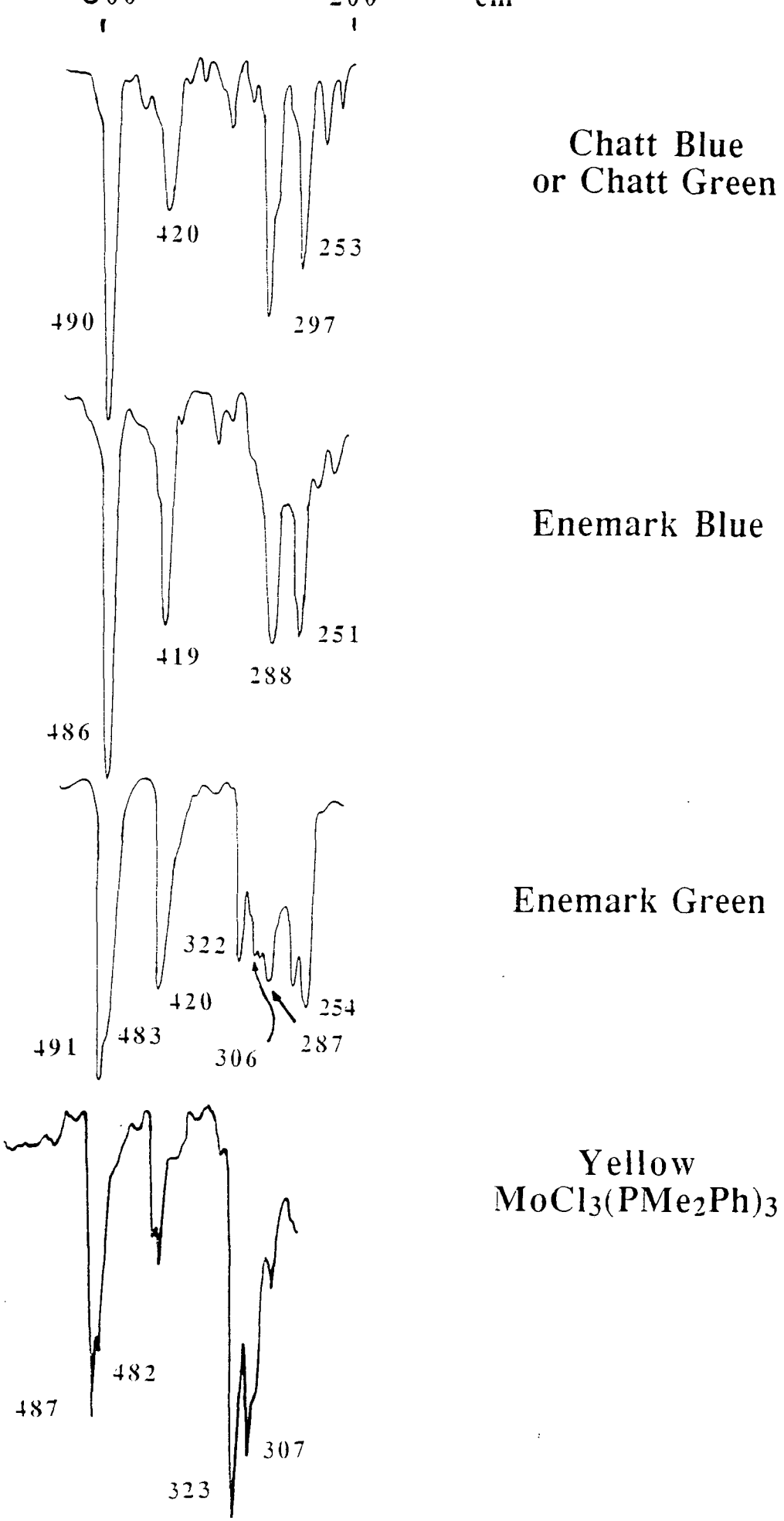


**Figure 2.6:** Low frequency solid-state infrared spectra of the blue and green forms of $Mo(O)Cl_2(PMe_2Ph)_3$ and yellow $MoCl_3(PMe_2Ph)_3$.

| Enemark Blue | Enemark Green | Chatt Blue | Chatt Green | $MoCl_3(PMe_2Ph)_3$ |
|---|---|---|---|---|
| | 491 m | 490 m | 490 m | 493 m,sh |
| 486 m | | | | 487 m |
| | 483 m | | | 482 m |
| 419 m | 420 m | 420 m | 420 m | 420 m |
| | 413 m,sh | 413 m,sh | 413 m,sh | 412 m |
| 355 w | | 345 w | 345 w | |
| 340 vw | | | | |
| | 322 m | | | 323 m |
| 313 w,sh | | 315 w | 315 w,sh | |
| | 310 m,sh | | | |
| | 306 m | | | 307 m |
| | | | | 300 m,sh |
| | 298 m,sh | 297 s [a] | 297 s [a] | |
| 288 m [a] | 287 m [a] | 285 m,sh | 285 m,sh | 282 w |
| | 274 m | | | |
| 251 m [b] | 254 m [b] | 253 m [b] | 253 m [b] | 250 w |
| 230 w | | | | 235 vw |
| | | 223 w | 223 w | |
| | | 214 vw | 214 vw | |
| 210 w | | | | |

**Table 2.3**: Low energy infrared data (600-200 $cm^{-1}$): [a]ν(Mo-Cl); [b]δ(Mo-O)

## 2.4 Solution Infrared Spectroscopy

The solution infrared spectra of the Enemark and Chatt blue forms of *cis-mer*-$Mo(O)Cl_2(PMe_2Ph)_3$ in dibromomethane at room temperature were found to be identical (figure 2.7, c) and show a ν(Mo=O) stretching frequency at 946 $cm^{-1}$ that is intermediate between the values exhibited in the solid-state infrared spectra. This suggests that in solution the phosphine ligands, which influence the Mo=O bond's stretching frequency are unconstrained and free to adopt any orientation. It therefore seems that the orientation adopted upon crystallisation depends on the nature of the nucleation sites, the amount of trichloride that might be present in the solution, and possibly on the presence of trace amounts of water (as shown by reactivity studies, section 2.8).

A study of the low frequency region of the spectra (figure 2.8) also indicates that the presence of the trichloride *mer*-$MoCl_3(PMe_2Ph)_3$ as shown by a weakly absorbing peak at 325 $cm^{-1}$, is observed only in the spectrum of Enemark green where the level of contamination is sufficiently high (19%) for the impurity to be detected.

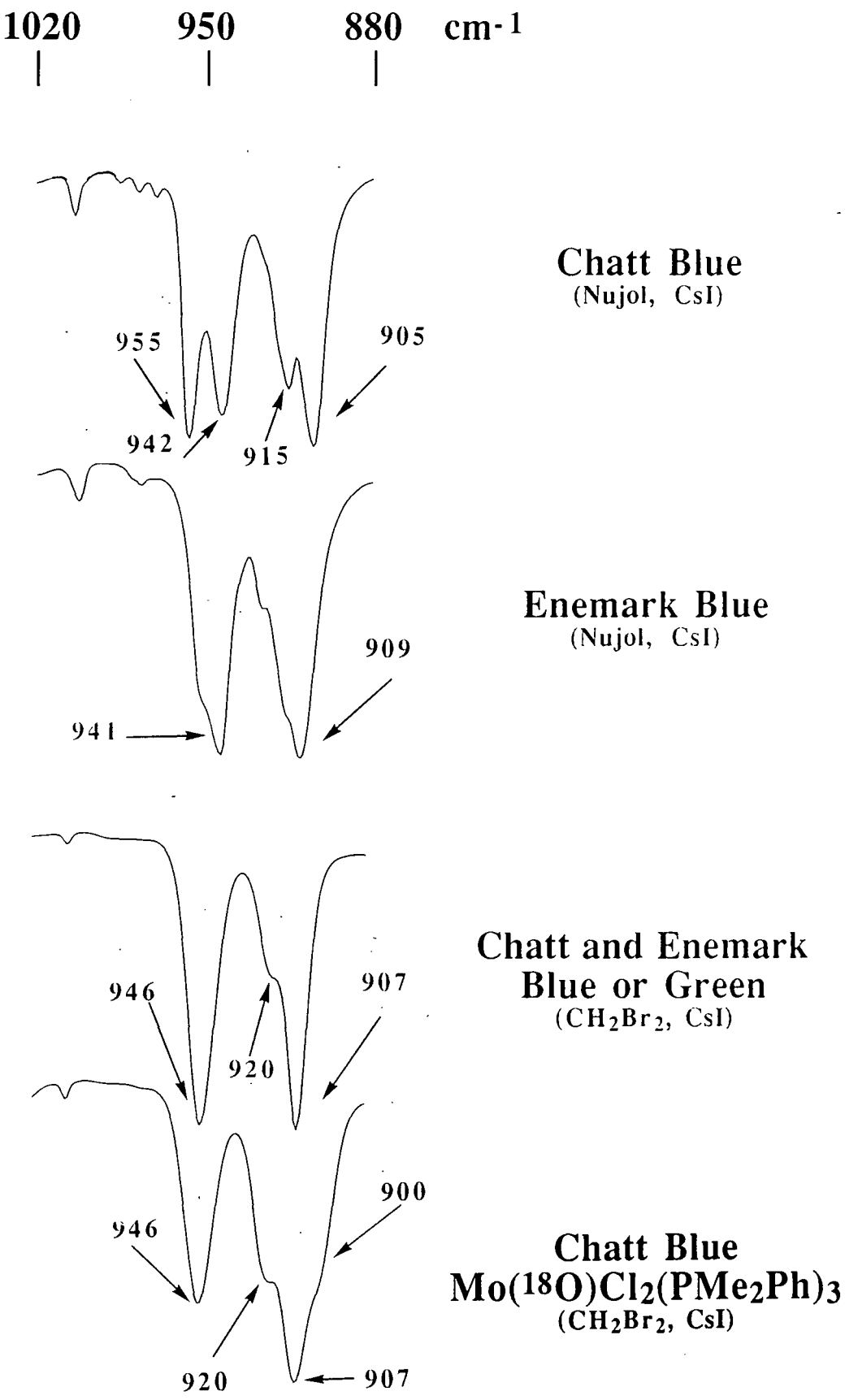


**Figure 2.7:** Comparison of the (a,b) solid-state and (c,d) solution infrared spectra of Chatt and Enemark blue and green forms of $Mo(O)Cl_2(PMe_2Ph)_3$.

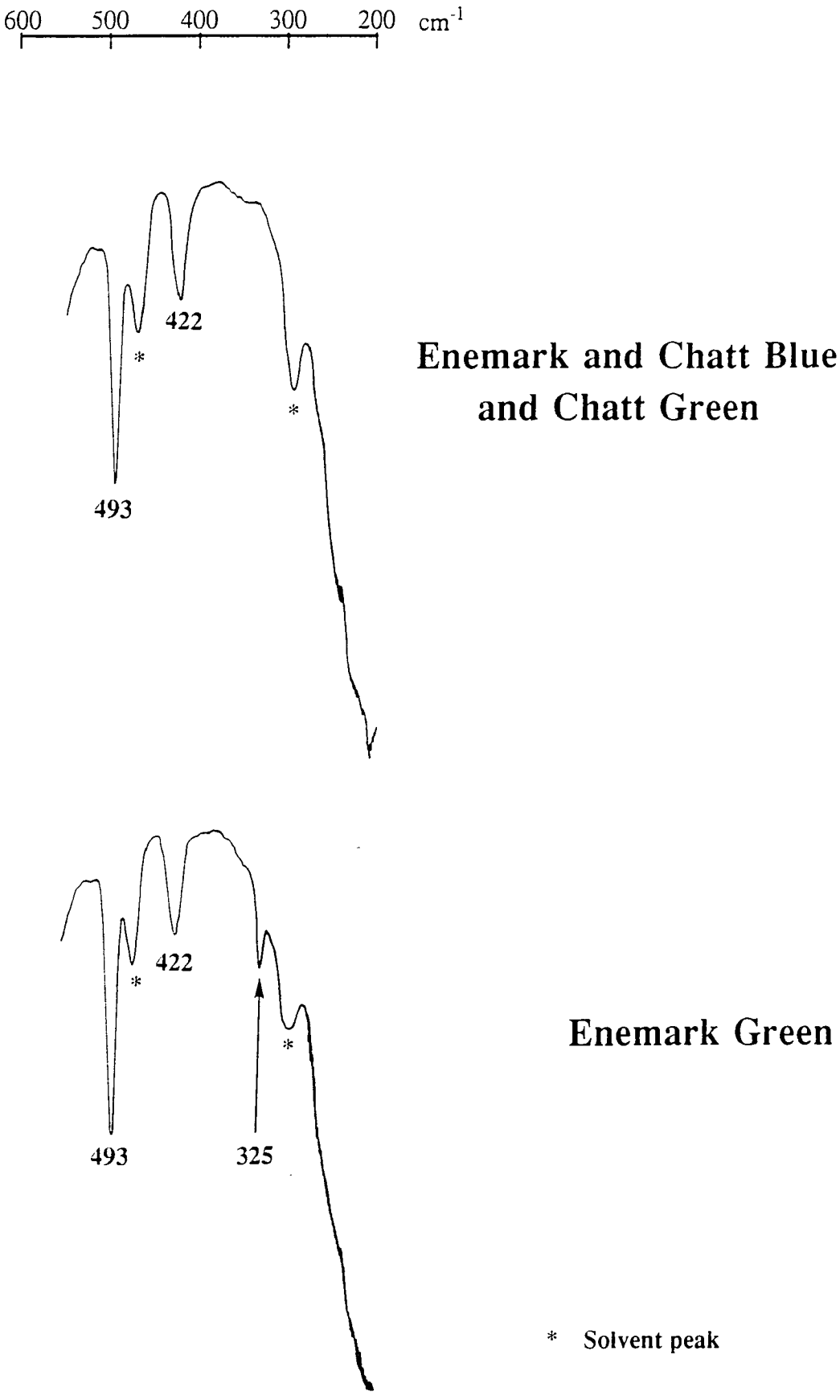


**Figure 2.8:** Low frequency solution infrared spectra in $CH_2Br_2$ of Chatt and Enemark blue and green forms of *cis-mer*-$Mo(O)Cl_2(PMe_2Ph)_3$.

Each of the oxo species possess two very strong bands between 300 and 240 $cm^{-1}$, at 288 and 251 $cm^{-1}$ for the Enemark blue, and at 297 and 253 $cm^{-1}$ for the Chatt blue. Comparison with the bromide analogues shows that the higher frequency may be assigned to ν(Mo-Cl), but that at the lower frequency is probably due to a metal-oxygen deformation[3], despite group theory predicting two active ν(Mo-Cl) vibrations.

## 2.5 UV-Visible Spectroscopy

A reliable means of providing a quick way of examining the green mixtures is to use UV-visible electronic spectra. Both blue and green species show a weak absorption at ca. 600 nm with extinction coefficients in the range typical of spin-forbidden octahedral d→d transitions. Typical of a $d^2$ system, Mo(IV) complexes show two additional absorptions, one of which is observable in the range 235-500 nm. For the Chatt and Enemark blue species this band occurs at 393 (ε=1911 $mol^{-1}$ $cm^2$) and 395 nm (ε=1688 $mol^{-1}$ $cm^2$) respectively (figure 2.9, b), whereas in the green species the band occurs at a slightly higher wavelength; 397 nm (ε=1585 $mol^{-1}$ $cm^2$) for the Chatt green and 409 nm (ε=1752 $mol^{-1}$ $cm^2$) for the Enemark green (figure 2.9, a). Enemark suggested that this band could be used to invoke the presence of the intensely coloured yellow species, which showed absorptions at 415 nm (ε=3138 $mol^{-1}$ $cm^2$) and 355 nm (ε=3719 $mol^{-1}$ $cm^2$). He was able to discern that this band in the green forms was much more intense relative to its band at ca. 600 nm than was the corresponding band of the synonymous blue. This fact is also apparent in our data. The increased intensity of this peak, especially in the Enemark green form (which is additionally shifted to a higher wavelength due to its near proximity with the yellow 415 nm absorbance), suggests that the green forms contain yellow $MoCl_3(PMe_2Ph)_3$. The fact that in the Chatt green the relative intensity of the band compared to the Chatt blue is not significantly different in intensity, in comparison to the Enemark green with the Enemark blue, demonstrates additionally that the level of yellow $MoCl_3(PMe_2Ph)_3$ in the Enemark green is appreciably higher than in the Chatt green. Enemark[4] has shown that the spectrum of Enemark green is consistent with a 0.35 mole fraction of yellow $MoCl_3(PMe_2Ph)_3$. In fact the

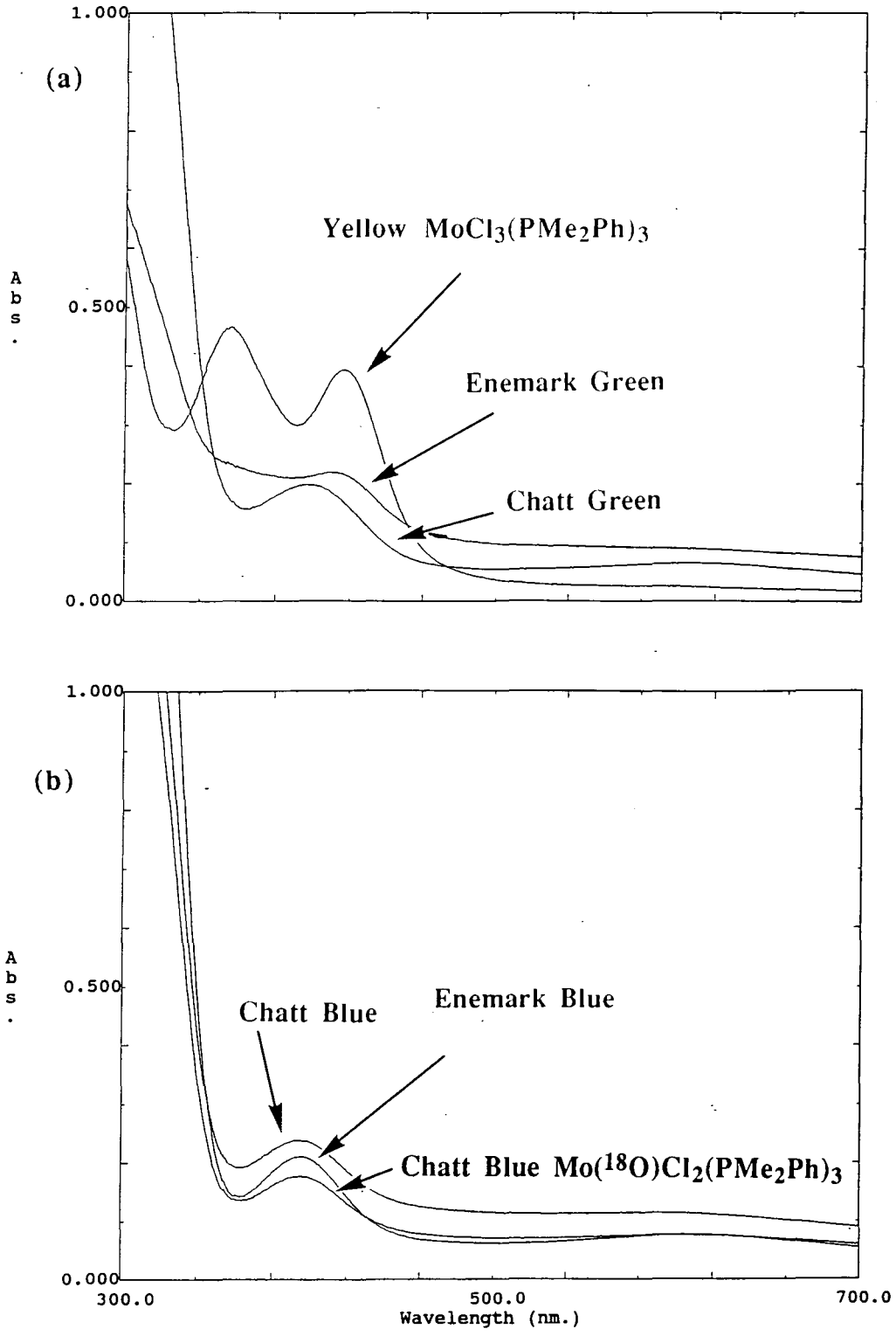


**Figure 2.9:** UV-visible spectra of Chatt and Enemark *cis-mer*-$Mo(O)Cl_2(PMe_2Ph)_3$ species and yellow *mer*-$MoCl_3(PMe_2Ph)_3$.

spectrum of the green compound can be independently reproduced by mixing this proportion of yellow $MoCl_3(PMe_2Ph)_3$ with Enemark blue.

## 2.6 NMR Studies

Previous reports on the $^1H$ NMR spectra of *cis-mer*-$Mo(O)Cl_2(PMe_2Ph)_3$ had been carried out by Chatt in his original communication.[3] This was collected at 60 MHz on his authentic samples: blue ($\nu$(Mo=O)=954 $cm^{-1}$) and green ($\nu$(Mo=O)=943 $cm^{-1}$). This report indicated that in deuterochloroform the $^1H$ NMR spectra of the Chatt blue form and the Butcher/Enemark green were identical, showing a doublet ($\delta$ 1.23 ppm) and two virtually coupled triplets ($\delta$ 1.73 and 1.83 ppm). Since no sign of two forms or an equilibrium mix was observed, it was surmised that the spectra were those of the blue isomer, since in addition it had been observed that the green form readily isomerised to that of the blue form in solution.

Although reasonable, this is not the full picture, since it has been established in these studies that there exist two blue forms, each of which can be contaminated by yellow $MoCl_3(PMe_2Ph)_3$. Figure 2.10 shows the 400 MHz $^1H$ NMR spectrum of Enemark green ($\nu$(Mo=O)=941 $cm^{-1}$) in $CDCl_3$ in the normal range $\delta$ 0$\rightarrow$10 ppm, consisting of two virtually coupled triplets due to the two trans-$PMe_2Ph$ ligands and a doublet due to the single cis-$PMe_2Ph$ ligand. As presented the spectrum furnishes little enlightenment as to the nature of the difference in $\nu$(Mo=O) stretching frequencies between the 'originally' reported forms. However, the $^1H$ NMR spectrum of the same sample in the range $\delta$ -45$\rightarrow$+10 ppm (figure 2.11) shows two broad resonances at $\delta$ -22.5 and -40.6 ppm in the ratio 1:2 (corresponding to the methyl protons of cis- and trans-$PMe_2Ph$ ligands respectively). In addition, five peaks could be observed in the region $\delta$ +7.5 to +12 ppm. The two broad resonances upfield could quite easily not be noted in a sample assumed to be diamagnetic.

Yellow $MoCl_3(PMe_2Ph)_3$, however, is not diamagnetic. Mo(III) is a $d^3$ system and as such is paramagnetic. It is possible that the problem of observing small amounts of the paramagnetic *mer*-$MoCl_3(PMe_2Ph)_3$ under normal $^1H$ NMR limits

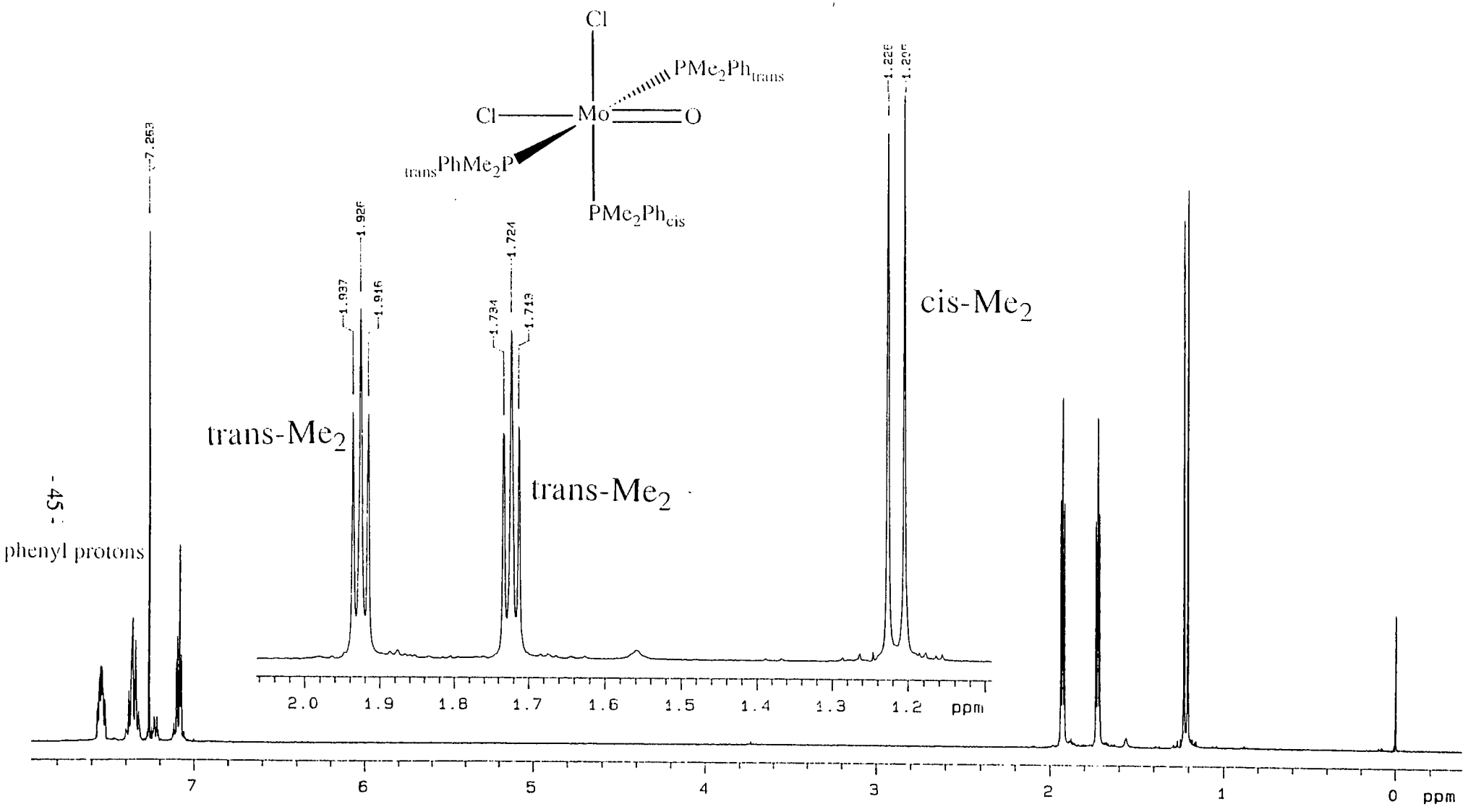


**Figure 2.10:** 400 MHz $^1$H NMR spectrum of Enemark green *cis-mer*-$Mo(O)Cl_2(PMe_2Ph)_3$ in $CDCl_3$ over the range $\delta$ 0 to +8 ppm.

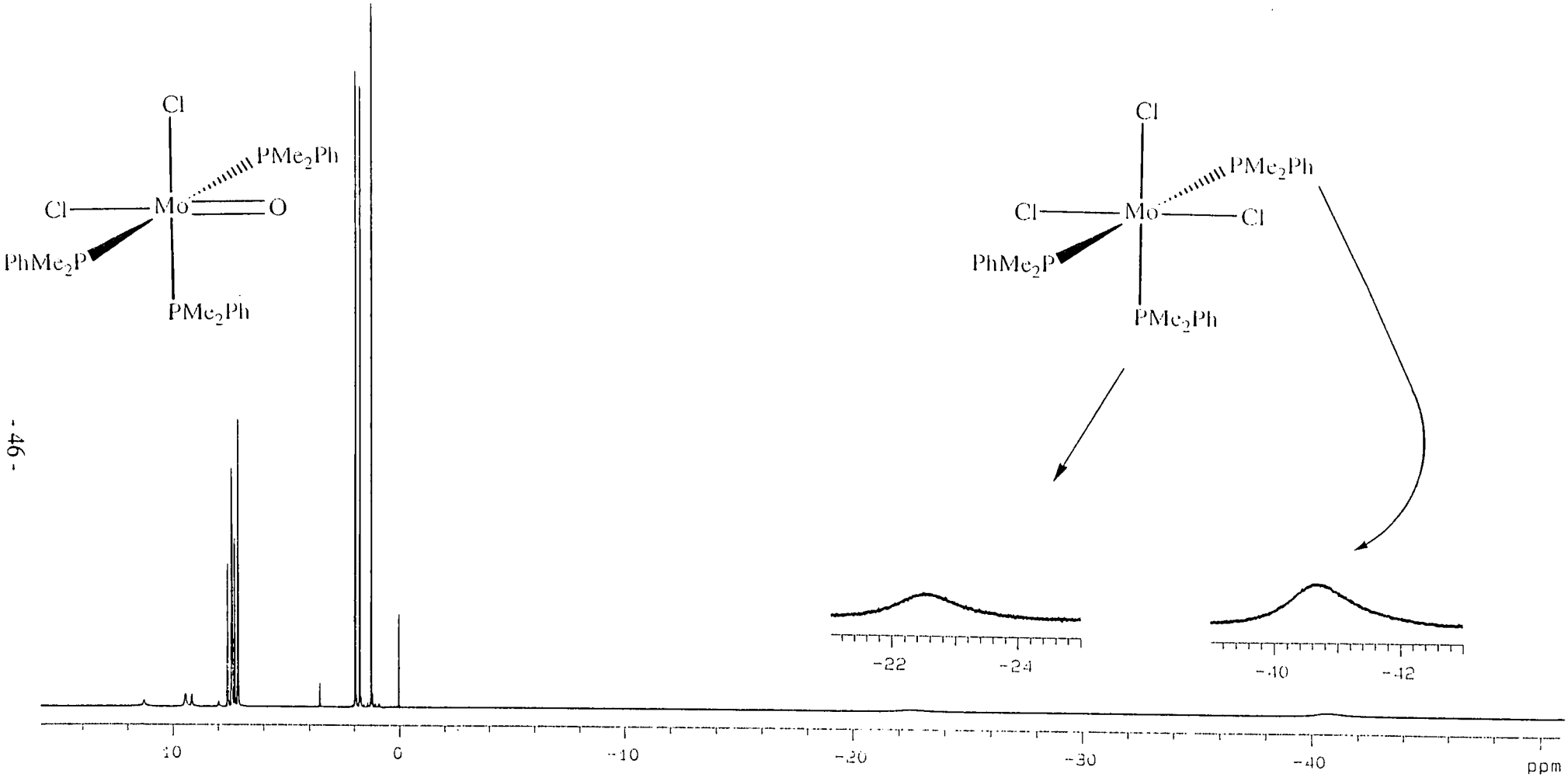




**Figure 2.11:** 400 MHz $^1$H NMR spectrum of Enemark green *cis-mer*-$Mo(O)Cl_2(PMe_2Ph)_3$ in $CDCl_3$ over the range $\delta$ +15 to -50 ppm.

prevented earlier workers from discovering its existence. The 400 MHz $^1$H NMR spectrum (figure 2.12) of $MoCl_3(PMe_2Ph)_3$ in $CDCl_3$ shows two broad upfield resonances at $\delta$ –22.5 and –40.5 ppm due likely to the methyl protons. This is consistent with NMR spectra of the paramagnetic complexes *trans*-$WCl_4(PMe_2Ph)_2$ [10] and *mer*-$MCl_3(PMe_2Ph)_3$ (M=Tc[11], Re[12]). The greater intensity of the resonance at -40.5 ppm suggests that it is due to the trans methyl protons, and that at -22.5 ppm due to the cis methyl protons. Studies on an extensive variety of *mer*-$ReX_3(ER_2Ph)_3$ (E=P,As; R=Me, Et, $^n$Pr, $^n$Bu)[12] and trans-$MCl_4(ER_{3-n}Ph_n)_3$ (M=W[10], Os[12,13]; R=Me, Et, $^n$Pr, $^n$Bu, $^i$Bu (M=Os); n=1, E=P,As; n=2, E=P) complexes show that the ortho phenyl protons are consistently downfield of their para and meta phenyl protons. The broadened resonance at ca. 12 ppm is attributed to the combined signals of the unresolved cis and trans ortho phenyl protons of yellow $MoCl_3(PMe_2Ph)_3$. The remaining four resonances have been assigned by Enemark[4] to cis meta (11.28 ppm), trans meta (9.47 ppm), trans para (9.17 ppm) and cis para (7.97 ppm) phenyl protons. This assignment is backed-up by the evidence that the half-height line widths of the 11.28 and 9.47 ppm peaks are similar (50.5 Hz and 42.1 Hz respectively); the half-height line widths of the 9.17 and 7.97 ppm resonances are also comparable (20.2 Hz and 21.1 Hz respectively). The 2:1 intensities of the 9.47/11.28 ppm peak pair and 9.17/7.97 ppm peak pair, together with the information gleaned from the line width series ortho>meta>para (consistent with the proximity of each proton to the Mo(III) centre), are in agreement with the assignments. This leads to the conclusion, first stated by Enemark[4], that the green form ($\nu$(Mo=O) at 943 cm$^{-1}$) of $Mo(O)Cl_2(PMe_2Ph)_3$ reported originally by Chatt is a mixture of a blue form and yellow $MoCl_3(PMe_2Ph)_3$. The same conclusion was independently obtained by Parkin and co-workers.[1]

Two blue isomers have now been reported by this group[14] showing $\nu$(Mo=O) stretches at 941 and 955 cm$^{-1}$. The question arises whether these two forms can be observed independently in solution, and whether any evidence for an equilibrium between the two is observed. The 400 MHz $^1$H NMR spectra in both $CDCl_3$ (figures 2.13 to 2.15) and $CD_2Cl_2$ of the two blue forms are identical at room temperature. Both forms show a doublet ($\delta$ 1.22 ppm) due to the methyl protons of the single cis-$PMe_2Ph$

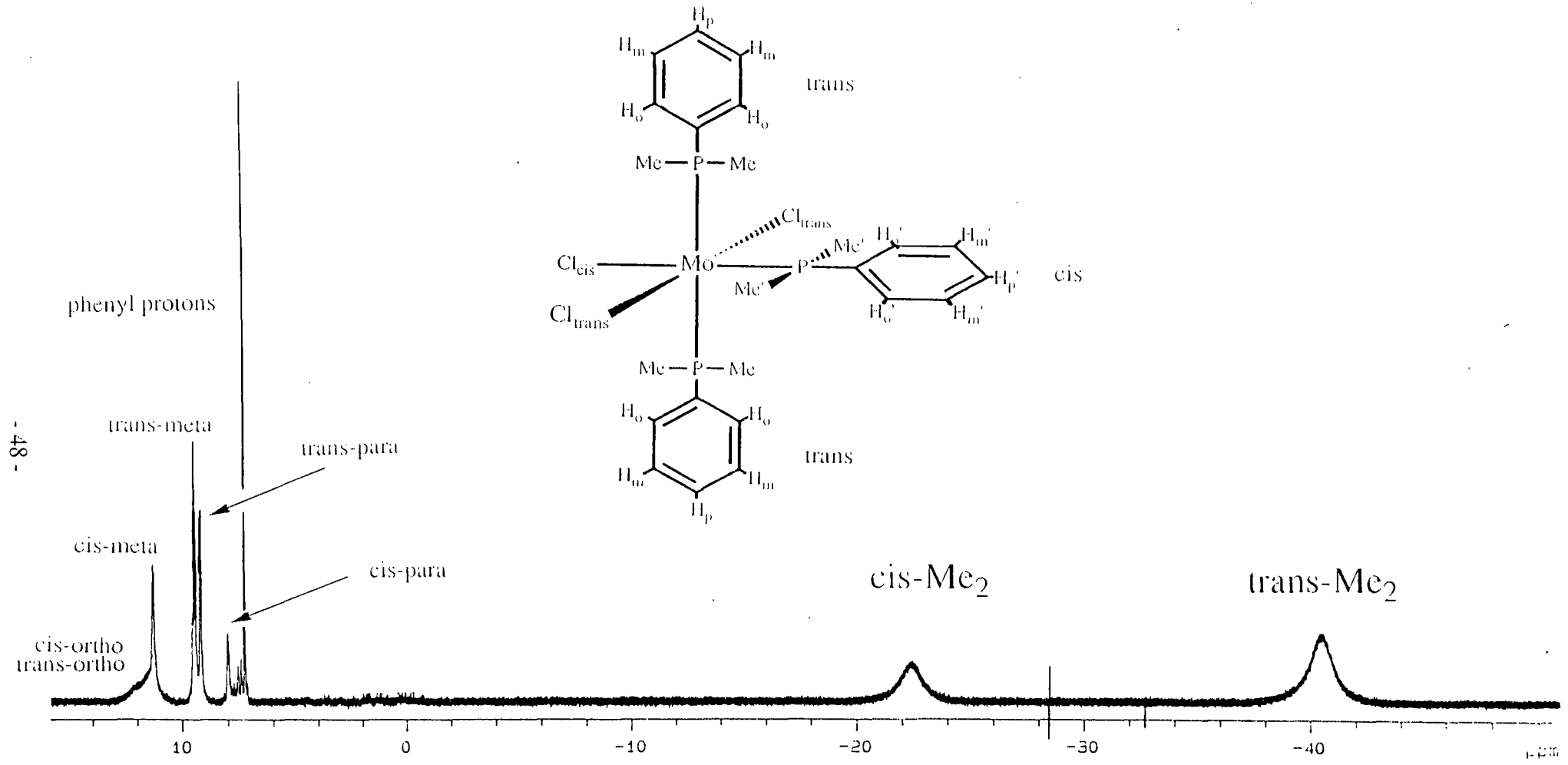




**Figure 2.12:** 400 MHz $^1$H NMR spectrum of yellow *mer*-$MoCl_3(PMe_2Ph)_3$ in $CDCl_3$ over the range δ +15 to -50 ppm.

ligand, and two virtually coupled triplets (δ 1.72 and 1.93 ppm) due to the methyl protons of the two trans-$PMe_2Ph$ ligands (figure 2.14). Downfield, four sets of multiplets are observed and are tentively assigned, by the use of $^1H$-$^1H$ COSY NMR, to trans meta (δ 7.57 ppm), unresolved trans-ortho/para (δ 7.40 ppm), cis-para (δ 7.28 ppm) and unresolved cis-meta/ortho phenyl protons.

Important stereochemical information about the $PMe_2Ph$ environments can be obtained from the $^1H$ NMR. If two such phosphines are cis, they behave independently, and we see a doublet for the methyl groups, due to coupling to its own $I=^1/_2$ $^{31}P$ nucleus ($^2J_{PH}$). If the two are trans, the phosphorus-phosphorus coupling becomes so large that the $^1H$ NMR of the methyl substituents is affected. Instead of a doublet, a distorted triplet with a broad central peak is observed. This behaviour is called virtual coupling[16] ($^2J_{PP}$) and means that the methyl group appears to be coupled both to its own and to the trans-phosphorus nucleus about equally, giving rise to the virtual triplet (figure 2.14).

Variable temperature $^1H$ NMR in $CD_2Cl_2$ over the range -80°C to 25°C shows that both sets of virtual triplets and the doublet are shifted upfield as the temperature is lowered and at the same time the signals broaden as the freezing point of the $CD_2Cl_2$ is approached. No resolving of the signals into components due to two blue forms is observed. This implies that in solution the $PMe_2Ph$ ligands are free to rotate about the Mo-P bond causing an averaged signal to be observed. This observation concurs with that found in the solution IR spectra of the two blue forms at room temperature.

The 400 MHz $^1H$ NMR spectrum of Chatt green (ν(Mo=O) at 955 $cm^{-1}$) is similar to that of Enemark green (figure 2.15) with the exception that the integrated peak areas for the paramagnetic $MoCl_3(PMe_2Ph)_3$ contaminant show that it is much lower in the former.

As to using NMR to assess the degree of contaminant in the green forms due to $MoCl_3(PMe_2Ph)_3$, several complications arise due to its paramagnetism compared to $Mo(O)Cl_2(PMe_2Ph)_3$ being diamagnetic. The fact that metal complexes can be paramagnetic which leads to large shifts in the NMR resonances is often overlooked, and these can be broadened to such an extent that they effectively become unobservable. In addition, the integral values obtained for a mixed diamagnetic/paramagnetic sample can

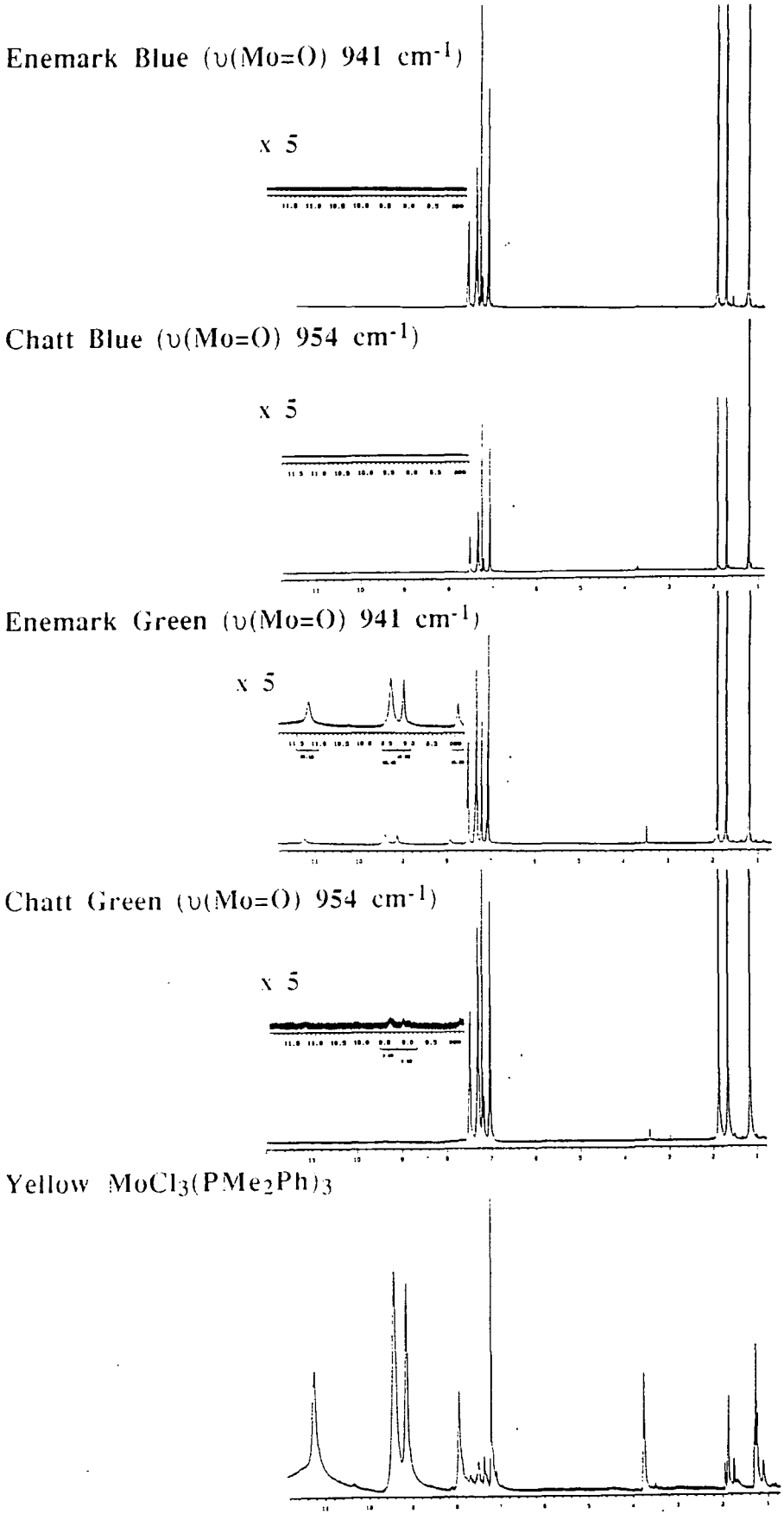


**Figure 2.13:** 400 MHz $^1$H NMR spectrum of *cis-mer*-$Mo(O)Cl_2(PMe_2Ph)_3$ species and yellow *mer*-$MoCl_3(PMe_2Ph)_3$ in $CDCl_3$ over the range δ +12 to +1 ppm.

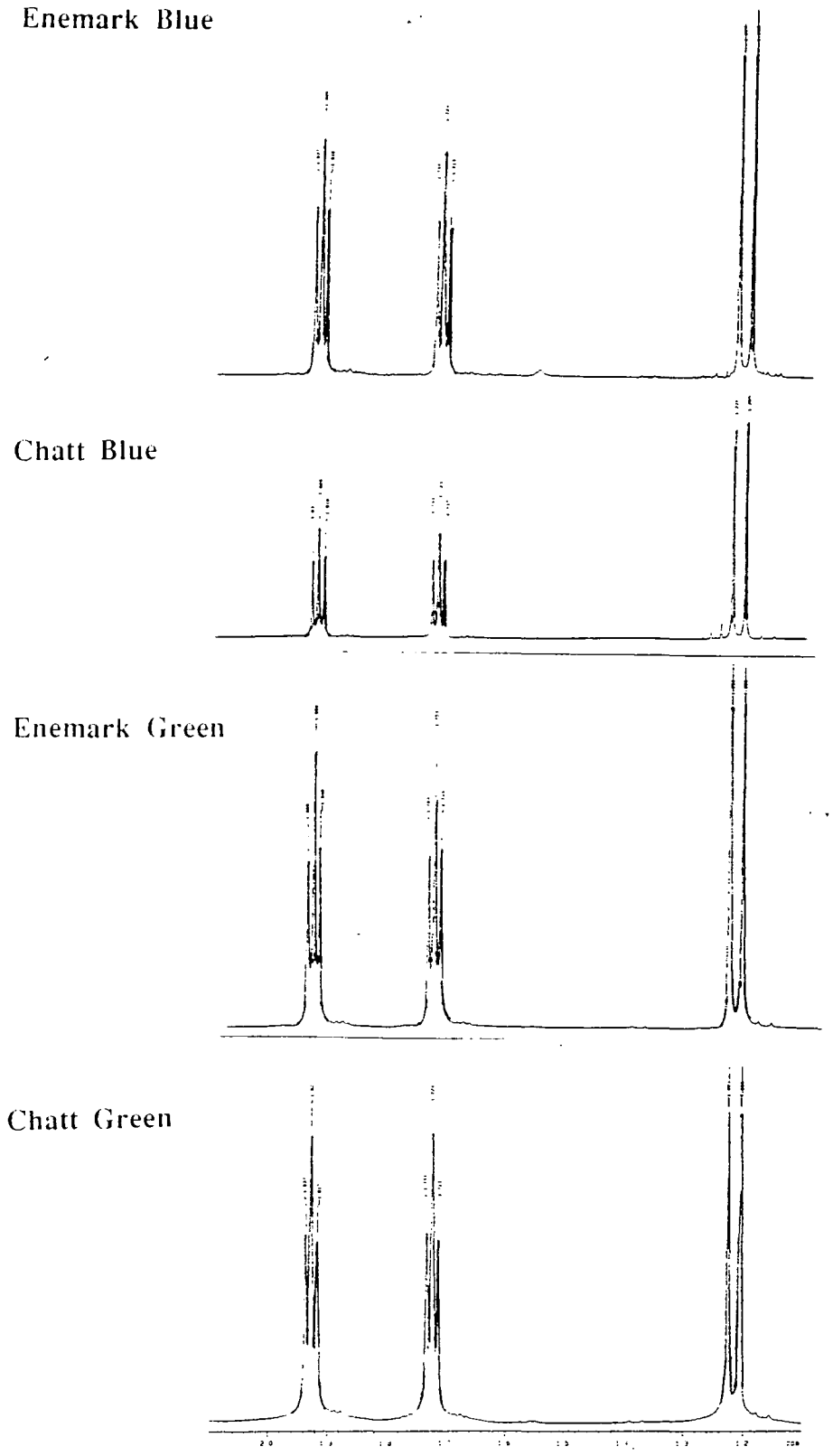


**Figure 2.14:** 400 MHz $^1$H NMR spectrum of *cis-mer*-$Mo(O)Cl_2(PMe_2Ph)_3$ species in $CDCl_3$ over the range $\delta$ +2.1 to 1.1 ppm showing the two virtual triplets and one doublet (1:1:1 relative intensity) of the methyl proton region.

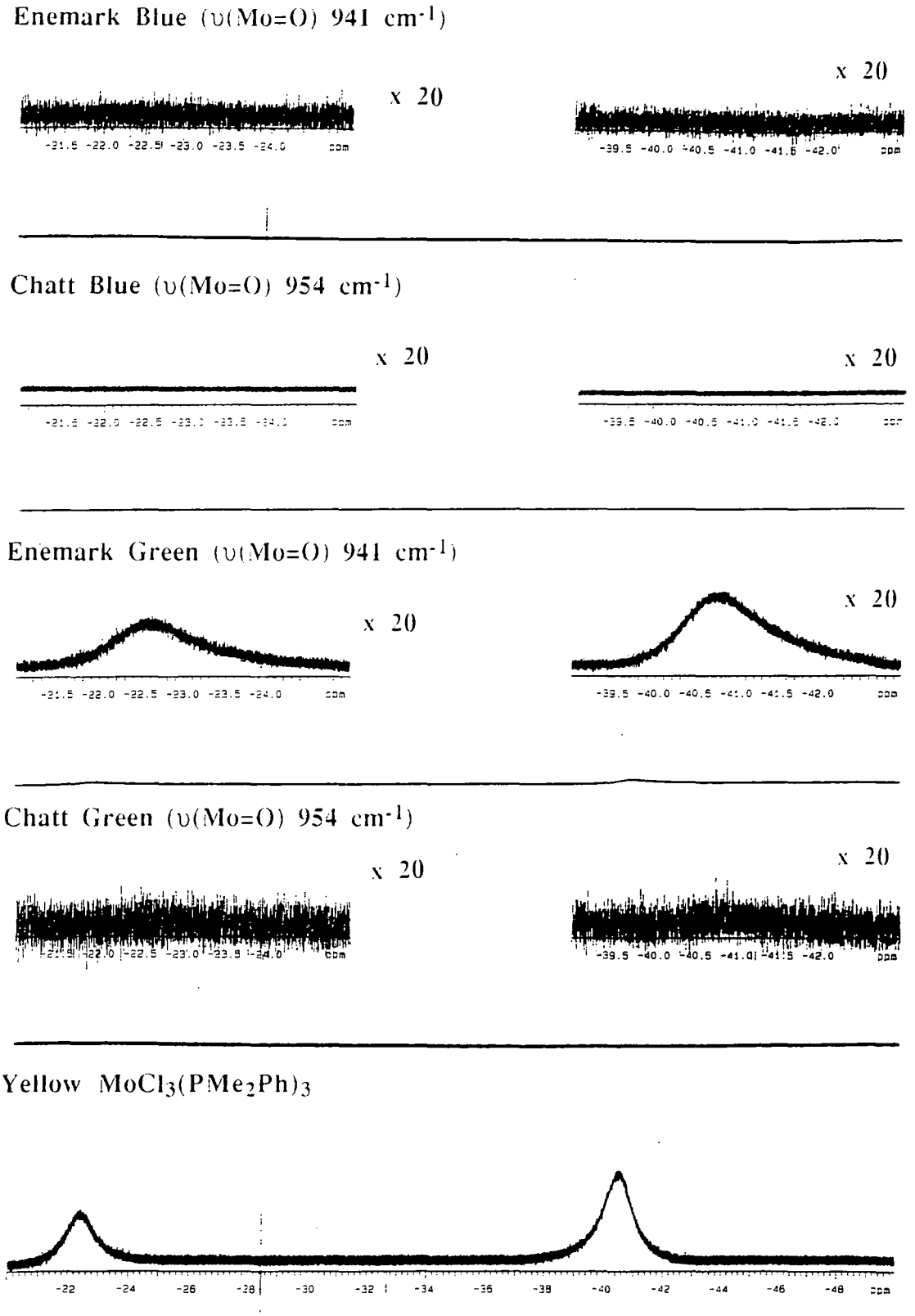


**Figure 2.15:** 400 MHz $^1$H NMR spectrum of *cis-mer*-$Mo(O)Cl_2(PMe_2Ph)_3$ species and yellow *mer*-$MoCl_3(PMe_2Ph)_3$ in $CDCl_3$ over the range δ -20 to -50 ppm showing their levels of contamination due to the trichloride.

not be related independently. When nuclei absorb radiation they make transitions to their upper spin states. Relaxation to the lower states causes the widths of spectral lines to increase. In a saturated sample the population difference disappears and the life-time of the spin-states are maximised. In a paramagnetic sample the mechanism for relaxation is different than that in a diamagnetic sample, and this leads to reduced life-times of the excited states and hence broadening. As the domains are affected differently when an external magnetic field is applied to a paramagnetic sample compared to a diamagnetic one, this leads to an unreconcilable difference in the meaning associated with integrated peak areas. However, for ease of considering the level of contamination we shall say that no such complication exists. This means we can say that the mole fraction of $MoCl_3(PMe_2Ph)_3$ by $^1H$ NMR in Enemark green is gauged to be 0.267 and in Chatt green to be 0.017. This compares favourably with the values 0.190 and 0.006 respectively, obtained by elemental analysis determination.

The 400 MHz $^1H$ NMR spectra in $CDCl_3$ of the high and low frequency forms of blue *cis-mer*-$Mo(O)Br_2(PMe_2Ph)_3$ are identical and show evidence of solvent exchange. The $Mo(O)Br_2(PMe_2Ph)_3$ species give rise to a doublet at $\delta$ 1.20 ppm ($^2J(PH)$= 8.8Hz) and two virtually coupled triplets at $\delta$ 1.81 ($^2J(PH)$= 4.2Hz) and 2.01 ppm ($^2J(PH)$= 4.2Hz) consistent with a meridional configuration. Neither forms show evidence in the upfield region of any broad resonances associated with the presence of a paramagnetic $MoBr_3(PMe_2Ph)_3$ contaminant.

Solvent exchange is evident from the fact that after two days in solution only resonances due to $Mo(O)Cl_2(PMe_2Ph)_3$ are observed, the interim spectra showing evidence of two isomeric mixed chloro-bromo species, $Mo(O)(Cl)Br(PMe_2Ph)_3$, where the bromo ligand is either trans or cis to the oxo moiety.

In the case of green $Mo(O)I_2(PMe_2Ph)_3$ two sets of signals are observed, one due to $Mo(O)I_2(PMe_2Ph)_3$ and the other to $Mo(O)I(Cl)(PMe_2Ph)_3$. The di-iodo species gives rise to resonances at $\delta$ 1.34 (doublet, $^2J(PH)$= 8.6Hz), 2.06 (virtual triplet, $^2J(PH)$= 4.0Hz) and 2.24 ppm (virtual triplet, $^2J(PH)$= 4.0Hz). The other set of resonances are assigned to the mixed chloro-iodo species where the chlorine trans to the

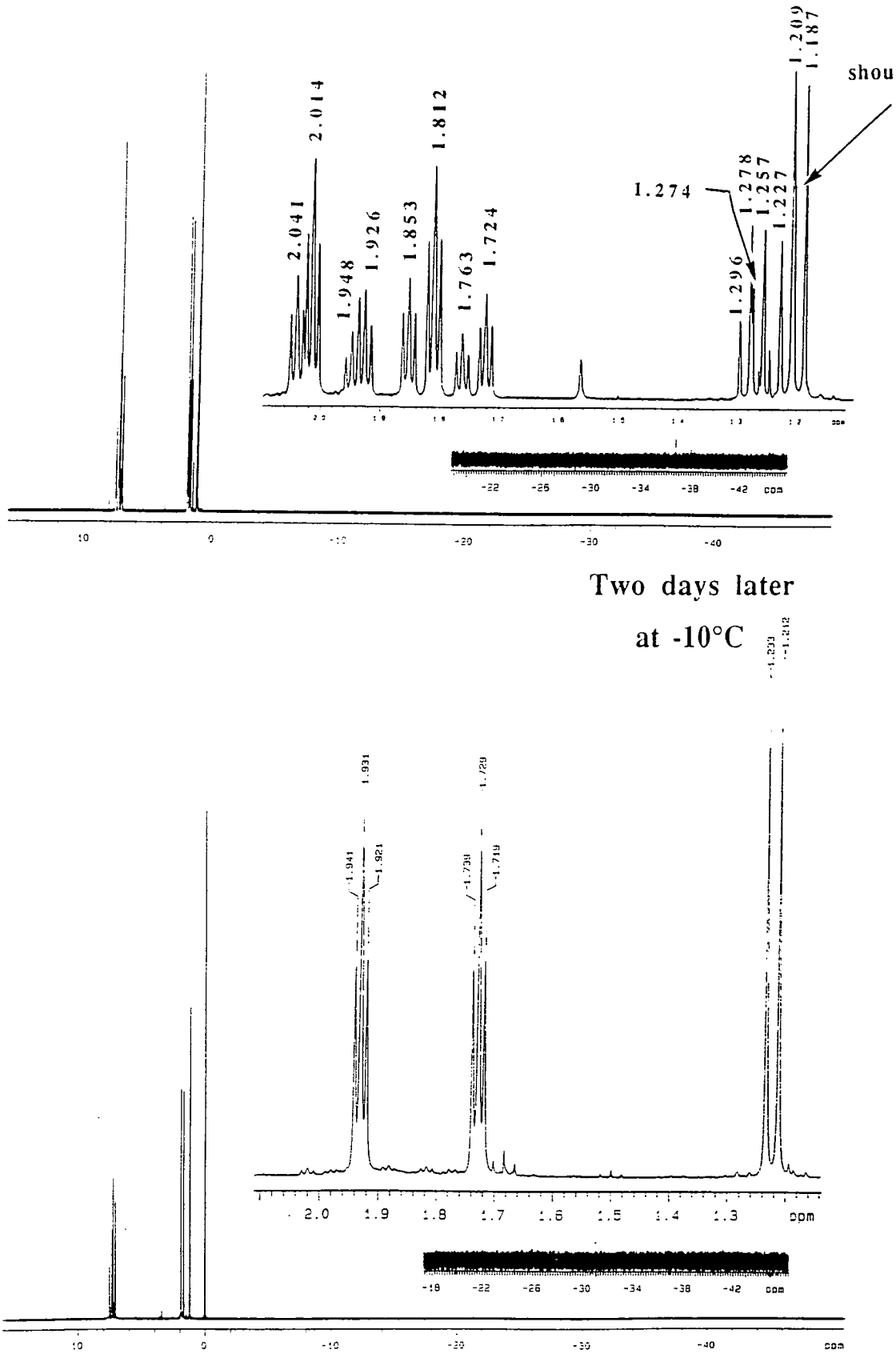


**Figure 2.16:** 400 MHz $^1$H NMR spectrum of blue *cis-mer*-Mo(O)Br$_2$(PMe$_2$Ph)$_3$ in $CDCl_3$ over the range $\delta$ +15 to -50 ppm.

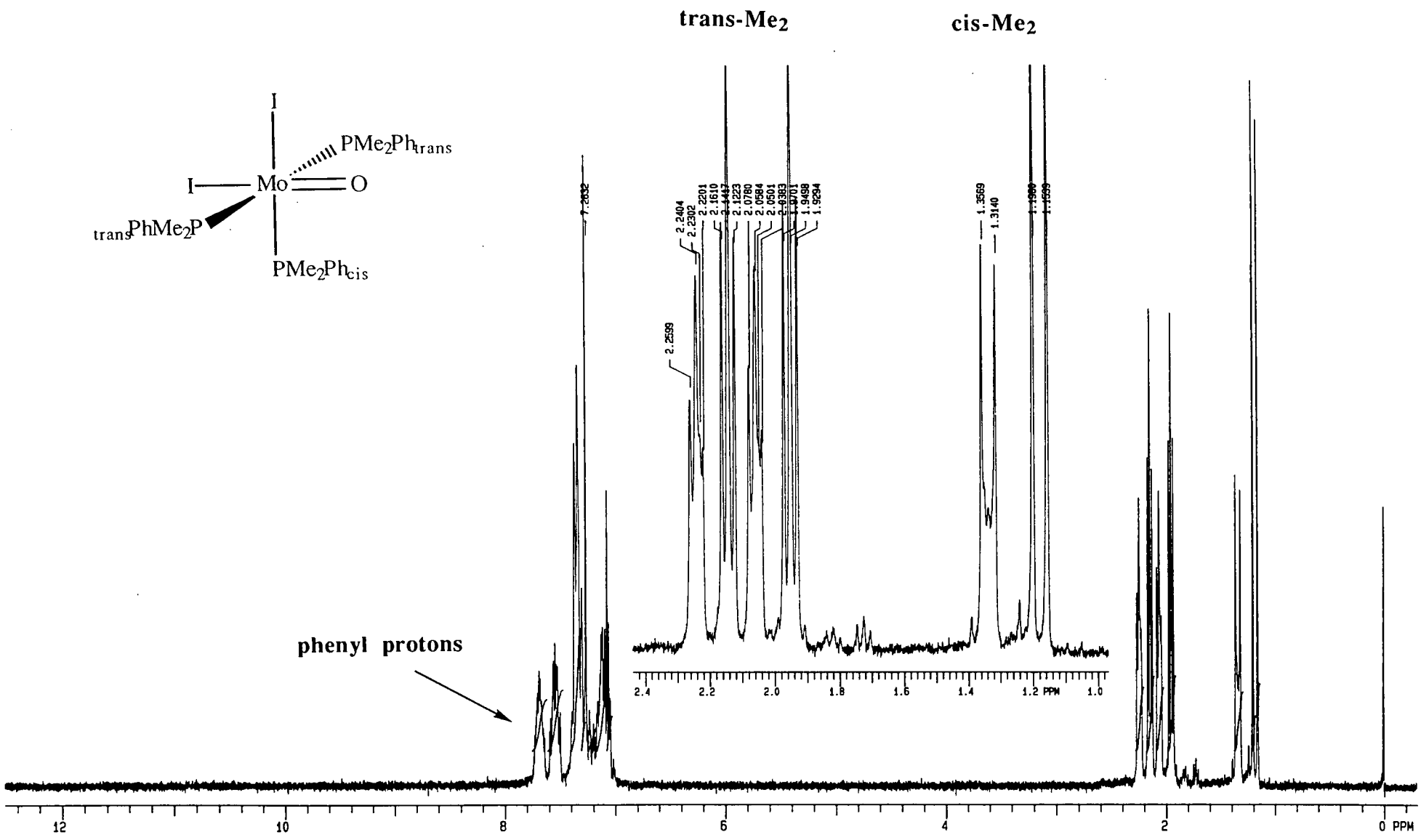


**Figure 2.17:** 200 MHz $^1$H NMR spectrum of green *cis-mer*-$Mo(O)I_2(PMe_2Ph)_3$ in $CDCl_3$ over the range $\delta$ +15 to 0 ppm.

oxo group is replaced by the iodo group, by analogy with the oxorhenium series of complexes.[3,26]

## 2.7 Elemental Analysis: Determination of Level of $MoCl_3(PMe_2Ph)_3$

Authentic samples of both blue forms (ν(Mo=O) at 941 and 955 $cm^{-1}$) along with their respective green forms have been prepared. Their elemental analyses, $^1H$ NMR and IR spectra were consistent with those originally reported.[3,4] However, each of the former characterisation procedures supports the conclusion that the green forms are a mixture of their associated blue form and yellow $MoCl_3(PMe_2Ph)_3$. Elemental analysis can be used to quantify the level of yellow contaminant $MoCl_3(PMe_2Ph)_3$ present in each of the green forms.

It was originally proposed by Chatt et al.[15] that the blue (954 $cm^{-1}$) and green (943 $cm^{-1}$) forms were distortional isomers, and as such should have identical molecular formulae and thus give the same elemental analyses. Yet Enemark green (ν(Mo=O) at 941 $cm^{-1}$) shows a percentage of chlorine higher compared to that observed in the Chatt blue (ν(Mo=O) at 955 $cm^{-1}$) or predicted by theory (table 2.4). It is also noticed that a similar discrepancy exists in the original analysis of the green form.[3] In association with the finding that the level of percentage chlorine is higher, is the fact that the observed percentages for carbon and hydrogen are lower than the theoretical values. Using a mathematical approach, the values obtained for a series of determinations of the %Cl in a sample can be used to calculate the mole fraction of $MoCl_3(PMe_2Ph)_3$ present in that sample.

Letting x represent the mole fraction of $MoCl_3(PMe_2Ph)_3$, then the reported % Cl in the sample is given by the expression:-

$$\frac{\%Cl}{100} = \frac{x.M_{Cl}[MoCl_3(PMe_2Ph)_3] + (1-x).M_{Cl}[Mo(O)Cl_2(PMe_2Ph)_3]}{x.RMM[MoCl_3(PMe_2Ph)_3] + (1-x).RMM[Mo(O)Cl_2(PMe_2Ph)_3]}$$

$$= \frac{3x.RMM[Cl] + 2(1-x).RMM[Cl]}{x.(RMM[MoCl_2(PMe_2Ph)_3] + RMM[Cl]) + (1-x).(RMM[MoCl_2(PMe_2Ph)_3] + RMM[Cl])}$$

$$= \frac{2RMM[Cl] + x.RMM[Cl]}{RMM[Mo(O)Cl_2(PMe_2Ph)_3] + x.RMM[Cl\text{-}O]}$$

Rearrangement leads to:-

$$100.x.RMM[Cl] - x.\%Cl.RMM[(Cl)-(O)] = \%Cl.RMM[Mo(O)Cl_2(PMe_2Ph)_3 - 200.RMM[Cl]$$

$$\Longrightarrow$$

$$x = \frac{\%Cl.RMM[Mo(O)Cl_2(PMe_2Ph)_3] - 200.RMM[Cl]}{100.RMM[Cl] - \%Cl.RMM[(Cl) - (O)]}$$

$$= \frac{597.2671\ \%Cl - 7090.6}{3545.3 - 19.454\ \%Cl} \qquad (2.2)$$

| | %C | %H | %Cl | Mean %Cl | $\%MoCl_3(PMe_2Ph)_3$ |
|---|---|---|---|---|---|
| Calculated | 48.26 | 5.57 | 11.87 | | |
| Chatt Blue | 48.30 | 5.59 | 11.50 | 11.89 | 0.33 |
| | 48.22 | 5.55 | 11.59 | | |
| | 47.97 | 5.72 | 11.77 | | |
| | 47.83 | 5.64 | 12.07 | | |
| | 47.75 | 5.57 | 12.13 | | |
| | 47.33 | 5.58 | 12.28 | | |
| Chatt Green | 48.16 | 5.58 | 11.64 | 11.91 | 0.63 |
| | 47.95 | 5.72 | 11.81 | | |
| | 47.84 | 5.56 | 11.81 | | |
| | 47.33 | 5.58 | 11.93 | | |
| | | | 12.00 | | |
| | | | 12.25 | | |
| Enemark Blue | 48.72 | 5.68 | 11.78 | 12.13 | 4.62 |
| | 48.62 | 5.68 | 11.97 | | |
| | 48.30 | 5.57 | 12.35 | | |
| | 47.85 | 5.48 | 12.41 | | |
| | 47.75 | 5.56 | | | |
| Enemark Green | 48.31 | 5.66 | 12.28 | 12.92 | 19.03 |
| | 48.16 | 5.67 | 12.72 | | |
| | 48.08 | 5.61 | 13.33 | | |
| | 47.02 | 5.41 | 13.35 | | |

**Table 2.4**: Elemental analysis data for $Mo(O)Cl_2(PMe_2Ph)_3$

Using equation 2.2 the results of repeated elemental analyses can be tabulated (table 2.4) to give an indication of the level of $MoCl_3(PMe_2Ph)_3$ in each form. From this table it can be seen that in the sample of Enemark/Butcher green ($\nu$(Mo=O) 941 $cm^{-1}$) the estimated mole fraction of yellow *mer*-$MoCl_3(PMe_2Ph)_3$ is 0.190. This level is significantly lower in the Chatt green ($\nu$(Mo=O) 954 $cm^{-1}$), where the mole fraction is

0.006. These levels of yellow *mer*-$MoCl_3(PMe_2Ph)_3$ are also reflected in the other forms of analysis; namely $^1H$ NMR, which shows the levels to be 27% and 1.7% respectively; Raman spectroscopy, where the level of contamination are determined to be 21% and 7% respectively; and IR spectroscopy, where solid-state mixing studies show that the level of yellow *mer*-$MoCl_3(PMe_2Ph)_3$ in Enemark green is estimated to be 25±5% and in the Chatt green form the level of contaminant is indiscernible.

## 2.8 Reactivity Studies

From elemental analysis, IR and UV-visible spectroscopic studies it has already been observed that the level of $MoCl_3(PMe_2Ph)_3$ is critical in determining whether the Chatt ($\nu$(Mo=O) 955 $cm^{-1}$) or Enemark ($\nu$(Mo=O) 941 $cm^{-1}$) form of *cis-mer*-$Mo(O)Cl_2(PMe_2Ph)_3$ preferentially crystallises, and with what degree of purity.

Synthesis studies by ourselves and Enemark[4] have shown that the Enemark blue form can be prepared by re-crystallisation of the trichloride contaminated green form by using 'super-dry' methanol. Similarly Chatt blue can be recrystallised from Chatt green.

Crystals of Enemark green ($\nu$(Mo=O) 941 $cm^{-1}$) left standing in air are found to convert to the Chatt green form, the IR spectrum now showing a $\nu$(Mo=O) stretch at 955 $cm^{-1}$. Elemental analysis reveals that the chlorine content is reduced, in accord with the lower level of $MoCl_3(PMe_2Ph)_3$ contamination associated with this form. This indicates that a solid-state conversion is occurring to the Chatt form, the process being found to be irreversible. No change is observed when the study is carried out under an inert atmosphere of nitrogen. The conversion must thus involve oxidation of the $MoCl_3(PMe_2Ph)_3$ via incorporation of water into the crystal lattice ($^1H$ NMR studies having shown that $MoCl_3(PMe_2Ph)_3$ is unaffected by oxygen), in order to explain its reduced level.

Thermal studies, similarly show that melting either sets of pure blue crystals at ca.155°C results in the 're-crystallisation' of the Chatt form, indicating that it is the

trichloride's nucleation properties in solution which leads to the preferential crystallisation of the 'constrained' Enemark blue form.

The independent application of UV photolysis or trace amounts of de-oxygenated water is found to led to the conversion of the Enemark blue form to the Chatt blue form. In the presence of stoichiometric amounts of water the Chatt form is found to co-crystallise with $MoCl_3(PMe_2Ph)_3$ giving rise to green crystals. These findings are summarised in scheme 2.3.

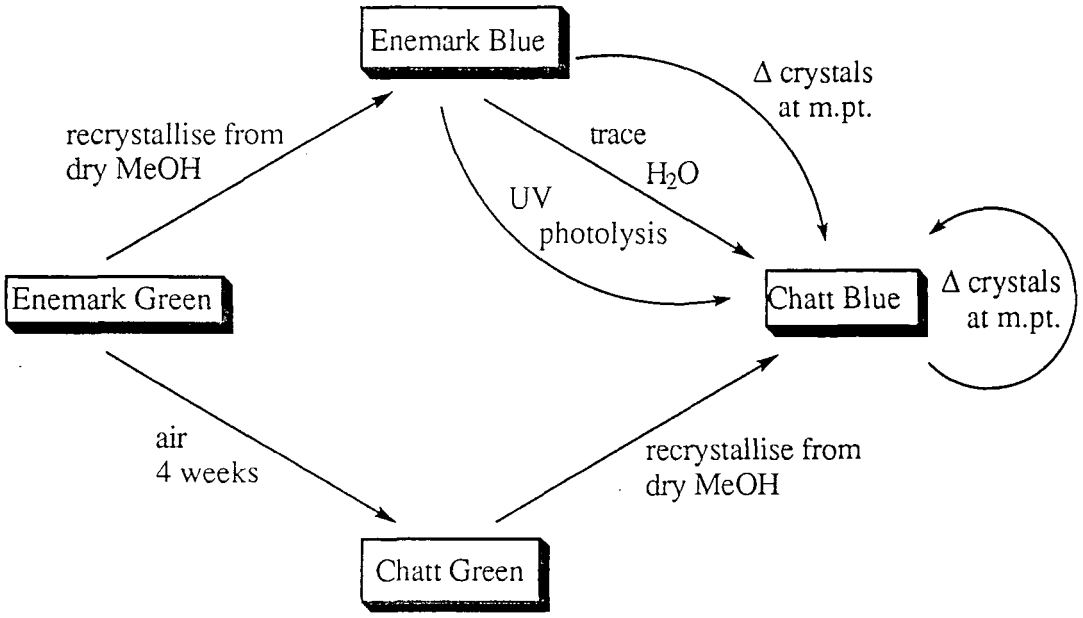


**Scheme 2.3:** Scheme outlining reactivity studies

## 2.9 X-Ray Crystallography: Disorder

In 1970 Chatt reported that the complex *mer*-$Mo(O)Cl_2(PMe_2Ph)_3$ could be isolated in two apparently different coloured forms, namely blue and green.[3] He originally proposed that they were cis-dichloro (blue) and trans-dichloro geometric isomers[15] on the basis of IR spectroscopic evidence, and that the blue form ($\nu$(Mo=O) 954 $cm^{-1}$ as reported by Chatt) had an established X-ray structurally determined *cis-mer* configuration.[7] However, in 1971, Muir established that the related complex, green *mer*-$Mo(O)Cl_2(PEt_2Ph)_3$ had a cis arrangement of the chloride ligands.[15b] The original crystal structure of the blue and green forms of the $Mo(O)Cl_2(PR_2Ph)_3$ complexes (R=Me and Et respectively) indicated that the most noticeable differences were in the

Mo=O bond lengths and the phosphine conformations. Both forms apparently refined satisfactorily for room-temperature structures, the blue *cis-mer*-$Mo(O)Cl_2(PMe_2Ph)_3$ having a Mo=O bond length of 1.676(7)Å and the green *cis-mer*-$Mo(O)Cl_2(PEt_2Ph)_3$ a Mo=O bond distance of 1.801(9)Å. Haymore[17] later established that the green *mer*-$Mo(O)Cl_2(PMe_2Ph)_3$ had a cis configuration and a bond length of 1.80(2)Å (unpublished result due to disorder between two Mo centres), consistent with the finding for the green diethylphenylphosphine complex.

It has now been established by our group and independently by Parkin[1] and Enemark[4] that the green *cis-mer*-$Mo(O)Cl_2(PMe_2Ph)_3$ ($\nu$(Mo=O) 943 $cm^{-1}$) is a mixture of blue *cis-mer*-$Mo(O)Cl_2(PMe_2Ph)_3$ and yellow *mer*-$MoCl_3(PMe_2Ph)_3$, and it is the presence of this trichloride that leads to the apparent lengthening of the Mo=O bond. That is, the 0.13Å bond lengthening is the manifestation of intramolecular disorder between an oxo group and a chloride ligand, which cannot normally be resolved crystallographically because the apparent separation between the fractional O and Cl atoms will only be about 0.4-0.7Å.[1,18]

Work reported in this thesis has now shown the existence of two blue forms of *cis-mer*-$Mo(O)Cl_2(PMe_2Ph)_3$, showing $\nu$(Mo=O) stretches at 941 $cm^{-1}$, as reported by Enemark[4] (hence our terminology Enemark blue), and at 955 $cm^{-1}$ as originally reported by Chatt.[3] The bromide analogues (*cis-mer*-$Mo(O)Br_2(PMe_2Ph)_3$), namely $\nu$(Mo=O) 956 $cm^{-1}$ reported by Butcher and Chatt[3] (and whose structure is reported in this thesis in table 2.6, appendix 1K), and the previously unknown form with $\nu$(Mo=O) at 943 $cm^{-1}$ have also been synthesized.[25]

The corresponding chloride and bromide blue forms with $\nu$(Mo=O) stretches of 955 and 956 $cm^{-1}$ respectively, show by X-ray determination to have dimethylphenylphosphine ligands with highly symmetrical orientations, in molecules which show almost exact $C_s$ symmetry (figure 2.18). These findings are similar to those established for the original structural determination by Muir of Chatt's blue *cis-mer*-$Mo(O)Cl_2(PMe_2Ph)_3$. The two analogous blue forms showing the lower stretching frequency at $\nu$(Mo=O) 943 $cm^{-1}$, have virtually identical asymmetric dimethylphenylphosphine conformations exhibiting $C_1$ symmetry (figure 2.19). The

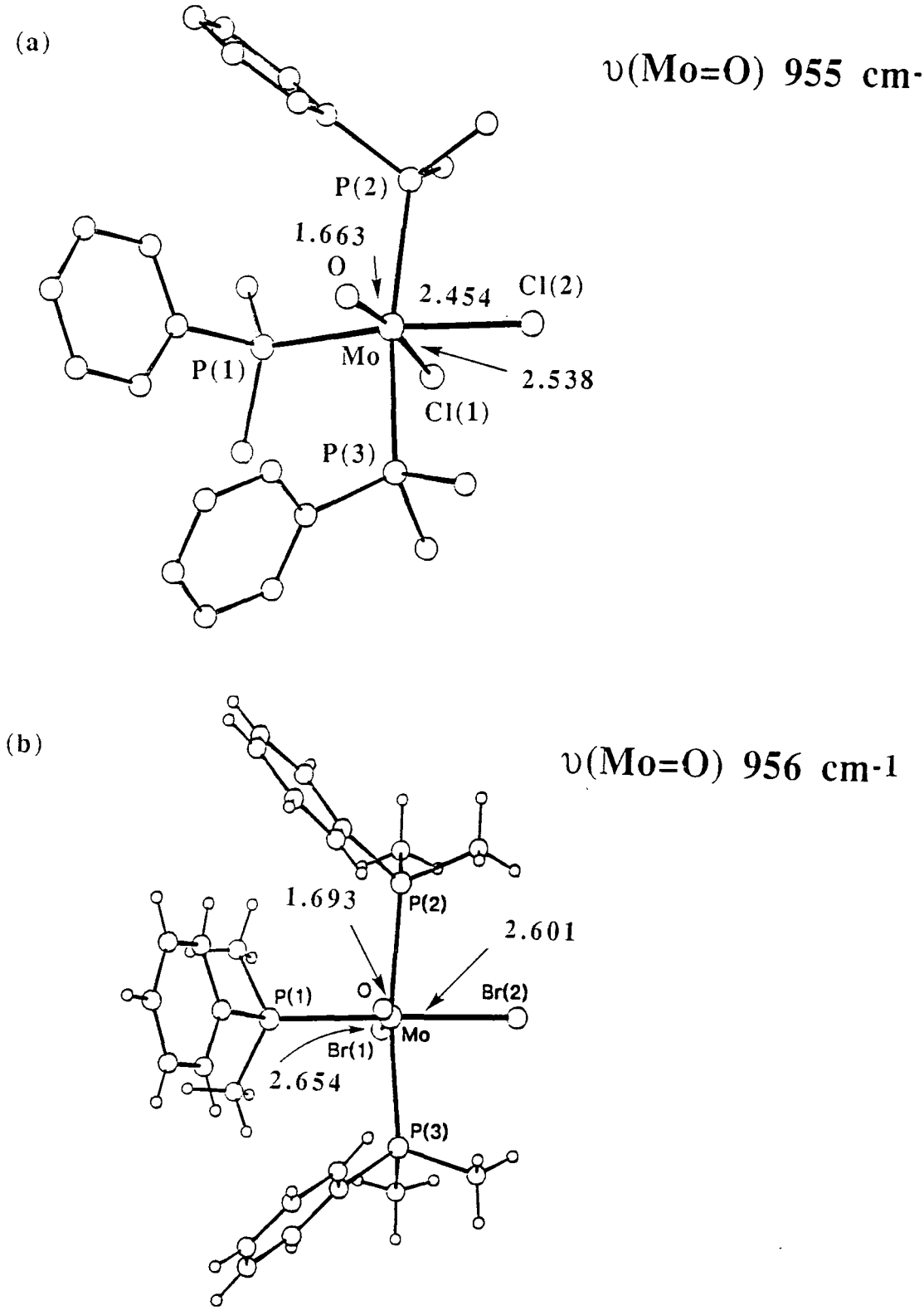


**Figure 2.18:** The *cis-mer* structures observed in the X-ray structure analysis of the high frequency forms of $Mo(O)X_2(PMe_2Ph)_3$ (X=Cl, Br) which show $C_s$ symmetry.

(a)

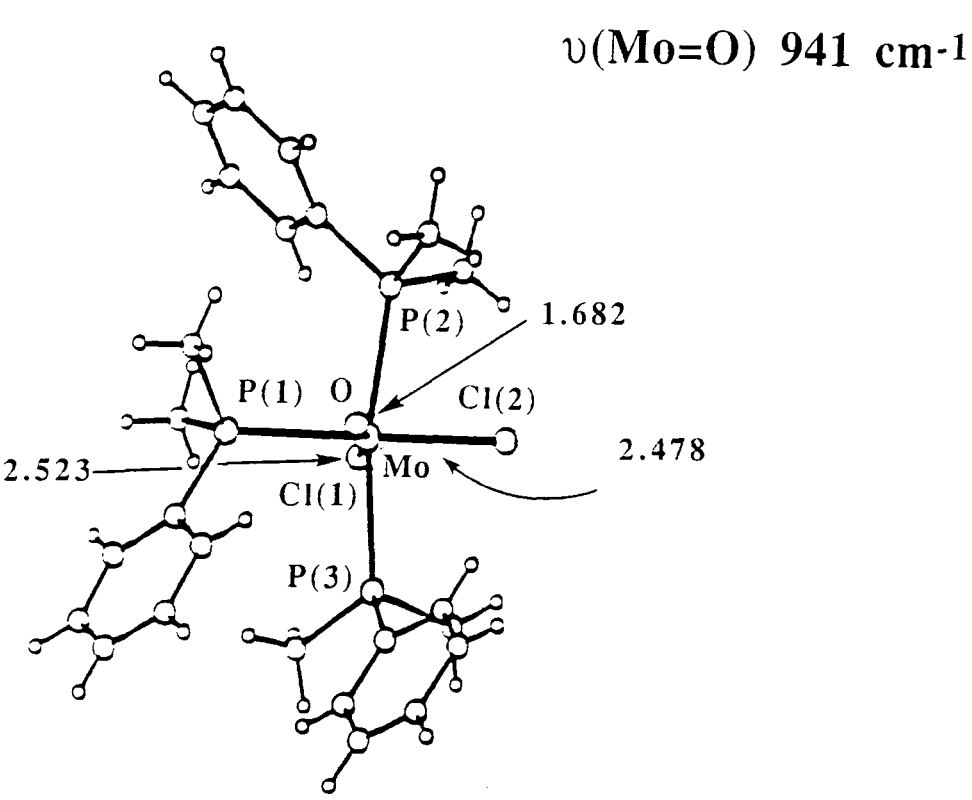


(b)

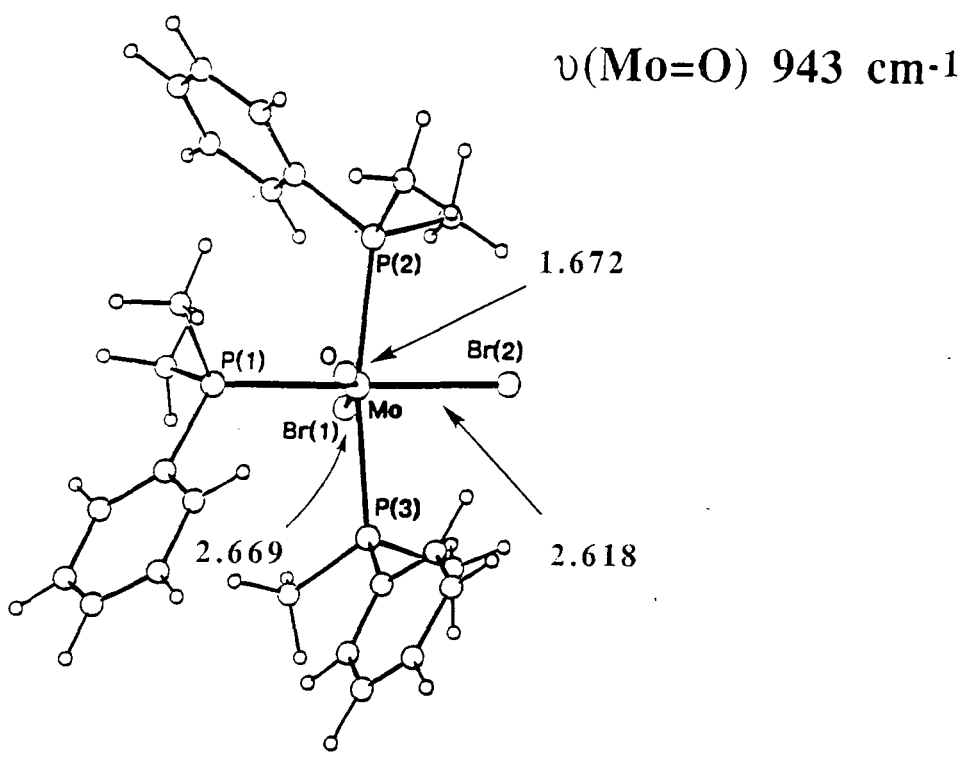


**Figure 2.19:** The *cis-mer* structures observed in the X-ray structure analysis of the low frequency forms of $Mo(O)X_2(PMe_2Ph)_3$ (X=Cl, Br) which show $C_1$ symmetry.

discovery of blue forms with different space groups, clearly establishes the existence of two blue forms of *cis-mer*-$Mo(O)X_2(PMe_2Ph)_3$ (X=Cl, Br), as is exemplified by the observation of two independent ν(Mo=O) stretching frequencies.

Examination of table 2.5 shows that the two isomers within the pair differ most dramatically in large variations between equivalent bond angles at the molybdenum centre due to different distortions from ideal octahedral geometry. They are most dramatic in the plane defined by the atoms O, X(1), X(2) and P(1). For example, the X(2)-Mo-P(1) and O-Mo-X(2) angles are transformed from values of 177.8(1)° (178.5(1)°) and 98.0(1)° (97.2(3)°) respectively, in the ν(Mo=O) 943 $cm^{-1}$ forms, to 162.4(1)° (162.2(2)°) and 105.7(3)° (104.0(5)°) respectively, in the ν(Mo=O) ca. 955 $cm^{-1}$ forms (the values for the bromide analogues being given in parenthesis). These angular distortions are reflected in significant changes in many of the metal-ligand bond lengths. The Mo=O bond length of 1.663(2)Å (appendix 1G) in the ν(Mo=O) 955 $cm^{-1}$ form of *cis-mer*-$Mo(O)Cl_2(PMe_2Ph)_3$ is significantly shorter than 1.682(3)Å (appendix 1H) observed in the corresponding ν(Mo=O) 941 $cm^{-1}$ form. As the frequency of a bond's vibration is inversely related to the atom separation, then assuming the force constant is not significantly different, this observed change in bond length (0.019(1)Å) is in line with the 14 $cm^{-1}$ difference seen in their Mo=O stretching frequencies. Substituting $k=-F/x^2$ (Hooke's law), where x represents the bond's deformation from equilibrium, into equation 1 (appendix 3), then it can been seen that the frequency of a bond's oscillation is inversely related to its deformation. A change of 0.025Å is thus predicted from the 14 $cm^{-1}$ difference in the Mo=O stretching frequencies. The difference in the Mo=O bond length observed in the chloro and bromo analogues of *cis-mer*-$Mo(O)X_2(PMe_2Ph)_3$, together with the variation in other bonds to the metal are undoubtedly related to the distortions of the highly strained co-ordination polyhedron of the metal, and so Chatt's original description of the system as being distortional isomerism would seem quite appropriate. This is one of the few examples to date, where the different orientation of bulky organophosphine ligands in metal complexes gives rise to a marked effect on the IR spectrum, as well as significant differences in bond lengths and angles. For example cis-$[PtCl_2(PMePh_2)_2]$ crystallises in two forms, differing

markedly in phosphine orientation.[19] Very accurate X-ray structure analysis showed small but significant differences in the Pt-Cl lengths related to marked differences in the angles at the Pt atom.

In his study Chatt found many differences between blue *cis-mer*-$Mo(O)Cl_2(PMe_2Ph)_3$ ($\nu$(Mo=O) 954 $cm^{-1}$) and green *cis-mer*-$Mo(O)Cl_2(PEt_2Ph)_3$ ($\nu$(Mo=O) 943 $cm^{-1}$). At the time he divided these differences into two categories. The first included those differences that are caused by the different steric and electronic requirements of the ligands. These would include differences in L-Mo-L bond angles and slight differences in Mo-L bond distances. The second type includes those differences that are the manifestation of distortional isomerism. These differences are limited mainly to the Mo-O and Mo-$L_{trans\text{-}to\text{-}O}$ distances. Changes in the orientation of the organic groups on the phosphine ligand may cause minor changes in some bond distances and angles (like those described in the first case), but that those changes need not necessarily lead to distortional isomers.

| | X=Cl[a] | | X=Cl[b] | | X=Br[c] | |
|---|---|---|---|---|---|---|
| $\nu$(Mo=O) | 955 | 954 | 941 | 943 | 956 | 943 |
| Mo-O | 1.663(2) | [1.676(7)] | 1.682(3) | [1.675(3)] | 1.693(13) | 1.672(10) |
| Mo-X(1) | 2.538(1) | [2.551(3)] | 2.523(1) | [2.528(1)] | 2.654(4) | 2.669(3) |
| Mo-X(2) | 2.454(1) | [2.464(3)] | 2.478(3) | [2.482(1)] | 2.601(3) | 2.618(2) |
| Mo-P(1) | 2.491(1) | [2.500(3)] | 2.484(3) | [2.489(1)] | 2.506(6) | 2.500(5) |
| Mo-P(2) | 2.542(1) | [2.541(3)] | 2.519(3) | [2.529(1)] | 2.557(6) | 2.527(5) |
| Mo-P(3) | 2.539(1) | [2.558(3)] | 2.530(3) | [2.533(1)] | 2.559(6) | 2.545(5) |
| O-Mo-X(1) | 169.3(1) | [168.8(3)] | 170.0(3) | [169.8(1)] | 170.6(5) | 168.5(3) |
| O-Mo-X(2) | 105.2(1) | [105.7(3)] | 97.6(3) | [98.0(1)] | 104.0(5) | 97.2(3) |
| P(1)-Mo-X(2) | 162.4(1) | [162.4(1)] | 177.8(1) | [177.6(1)] | 162.2(2) | 178.5(1) |
| P(2)-Mo-P(3) | 171.2(1) | [171.2(1)] | 160.4(1) | [160.5(1)] | 171.2(2) | 160.4(2) |

**Table 2.5**: Selected bond lengths (Å) and angles (°) for *cis-mer*-$Mo(O)X_2(PMe_2Ph)_3$: X=Cl, Br; [a]Values published by Chatt in parenthesis[7]; [b]Values published by Enemark in parenthesis[4]; [c]Appendices 1K and 1L

The phenomenon is not simple polymorphism because it has been clearly established that the differences are not merely a result of two different crystal packings. Distortional isomerism is a rather rare and poorly understood phenomenon, and is fundamentally different from ordinary steric distortions, crystal packing effects, or so

| | | | |
|---|---|---|---|
| Mo - P(1) | 2.506(6) | P(2) - Mo - P(1) | 93.9(2) |
| Mo - P(2) | 2.557(6) | P(3) - Mo - P(1) | 94.1(2) |
| Mo - P(3) | 2.559(6) | P(3) - Mo - P(2) | 171.2(2) |
| | | | |
| Mo - Br(1) | 2.654(4) | O - Mo - Br(1) | 170.6(5) |
| Mo - Br(2) | 2.601(3) | O - Mo - Br(2) | 104.0(5) |
| | | | |
| Mo - O | 1.693(13) | O - Mo - P(1) | 93.7(5) |
| | | O - Mo - P(2) | 91.3(5) |
| P(1) - C(11) | 1.835(22) | O - Mo - P(3) | 91.7(5) |
| P(1) - C(17) | 1.765(20) | | |
| P(1) - C(18) | 1.857(20) | Br(1) - Mo - P(1) | 76.8(2) |
| P(2) - C(21) | 1.836(20) | Br(1) - Mo - P(2) | 89.3(2) |
| P(2) - C(27) | 1.810(23) | Br(1) - Mo - P(3) | 89.0(2) |
| P(2) - C(28) | 1.814(21) | Br(2) - Mo - P(1) | 162.2(2) |
| P(3) - C(31) | 1.826(22) | Br(2) - Mo - P(2) | 85.5(2) |
| P(3) - C(37) | 1.835(20) | Br(2) - Mo - P(3) | 85.8(1) |
| P(3) - C(38) | 1.859(20) | | |
| | | Br(2) - Mo - Br(1) | 85.4(1) |
| C(11) - P(1) - Mo | 113.5(7) | | |
| C(17) - P(1) - Mo | 118.5(7) | C(17) - P(1) - C(11) | 103(1) |
| C(18) - P(1) - Mo | 116.3(7) | C(18) - P(1) - C(11) | 104(1) |
| C(21) - P(2) - Mo | 116.9(7) | C(18) - P(1) - C(17) | 99(1) |
| C(27) - P(2) - Mo | 115.7(8) | C(27) - P(2) - C(21) | 106(1) |
| C(28) - P(2) - Mo | 111.8(8) | C(28) - P(2) - C(21) | 101(1) |
| C(31) - P(3) - Mo | 115.5(7) | C(28) - P(2) - C(27) | 104(1) |
| C(37) - P(3) - Mo | 114.6(7) | C(37) - P(3) - C(31) | 107(1) |
| C(38) - P(3) - Mo | 112.8(7) | C(38) - P(3) - C(31) | 101(1) |
| | | C(38) - P(3) - C(37) | 105(1) |

**Table 2.6:** Selected bond lengths (Å) and angles (°) for blue *cis-mer*-$Mo(O)Br_2(PMe_2Ph)_3$ which exhibits a ν(Mo=O) stretch at 956 $cm^{-1}$

called 'polymorphism'. Distortional isomerism is not a solid-state effect. Metal-oxygen terminal bonds are quite strong, and it is seems unlikely that simple packing forces would be strong enough to distort these bonds to the extent seen. In addition, the two blue forms of *cis-mer*-$Mo(O)X_2(PMe_2Ph)_3$ (X=Cl, Br) contain different molecules readily distinguished by their characteristic (Mo=O) stretching frequencies and symmetry. Confirmation that the (Mo=O) stretching frequencies are molecular properties of the two isomers, and not just the manifestation of a particular crystalline arrangement, is provided by the stretching frequency at 943 $cm^{-1}$ being exhibited by the low symmetry isomer in both the pure orthorhombic crystalline modification and in the contaminated monoclinic polymorph studied by Enemark[4] and Parkin.[9]

Some of the reported[1,4,7,9,14] orthorhombic forms of the blue oxo complex *cis-mer*-$Mo(O)Cl_2(PMe_2Ph)_3$ are isomorphous with the monoclinic trichloride *mer*-$MoCl_3(PMe_2Ph)_3$[9], as is reflected by the slight differences in the orientations of the phosphine substituents, especially at P(3) (cf. figures 2.20(a) and 2.20(b)). Nevertheless, molecules of *cis-mer*-$Mo(O)Cl_2(PMe_2Ph)_3$ and *mer*-$MoCl_3(PMe_2Ph)_3$ co-crystallise readily, giving both orthorhombic and monoclinic modifications, depending upon composition.

It is noted, in table 2.7, that in the unpublished structure of Chatt blue-green the increase in the apparent Mo=O bond length to 1.698(6) ($\Delta$= +0.035Å) is not accompanied by a significant change in either the $Mo\text{-}Cl_{trans}$ or $Mo\text{-}Cl_{cis}$ bond lengths (+0.007 and +0.011Å respectively), which by examination of figure 2.22 suggests a trichloride composition of ca. 3%, in good agreement with the observed level of trichloride by $^1H$ NMR. This is also reflected in the fact that the other crystal parameters are similarly not significantly affected by the change in composition. However, in the case of the Chatt green there is an appreciable change in all three corresponding bond lengths, of +0.330, -0.048 and -0.003Å respectively. These reported changes indicate a trichloride contamination level of ca. 28% according to figure 2.22, which is reflected in the $O\text{-}Mo\text{-}Cl_{trans}$ and $O\text{-}Mo\text{-}Cl_{cis}$ bond angles approaching those reported for *mer*-$MoCl_3(PMe_2Ph)_3$. Additionally, it reflects the observation by Parkin[9] that the trans Mo-Cl bond is more sensitive to the level of trichloride contaminant than the cis bond.

| | Chatt $\nu$(Mo=O) 955 $cm^{-1}$ | | | Enemark $\nu$(Mo=O) 941 $cm^{-1}$ | $MoCl_3(PMe_2Ph)_3$ |
|---|---|---|---|---|---|
| | Blue[14] | Blue-Green[25] | Green[25] | Blue[14] | Yellow |
| Mo - O/Mo - $Cl_{ax}$ | 1.663(2) | 1.698(6) | 2.028(8) | 1.682(3) | 2.400(1) |
| Mo - Cl(1) | 2.538(1) | 2.545(2) | 2.490(3) | 2.523(1) | 2.427(1) |
| Mo - Cl(2) | 2.454(1) | 2.465(3) | 2.457(3) | 2.478(3) | 2.420(1) |
| Mo - P(1) | 2.491(1) | 2.503(3) | 2.524(3) | 2.484(3) | 2.572(1) |
| Mo - P(2) | 2.542(1) | 2.543(3) | 2.567(4) | 2.519(3) | 2.567(1) |
| Mo - P(3) | 2.539(1) | 2.557(3) | 2.531(4) | 2.530(3) | 2.610(1) |
| $O/Cl_{ax}$ - Mo - $Cl_{trans}(1)$ | 169.3(1) | 169.3(2) | 173.3(2) | 170.0(3) | 174.8(1) |
| $O/Cl_{ax}$ - Mo - $Cl_{cis}(2)$ | 105.2(1) | 105.1(2) | 94.5(2) | 97.6(3) | 91.1(1) |
| P(1) - Mo - Cl(2) | 162.4(1) | 162.7(1) | 177.0(1) | 177.8(1) | 177.4(1) |
| P(2) - Mo - P(3) | 171.2(1) | 171.2(1) | 162.3(1) | 160.4(1) | 167.2(1) |

**Table 2.7:** A comparison of selected bond lengths (Å) and angles (°) for the complexes Chatt blue and green, and Enemark blue *cis-mer*-$Mo(O)Cl_2(PMe_2Ph)_3$ and yellow $MoCl_3(PMe_2Ph)_3$

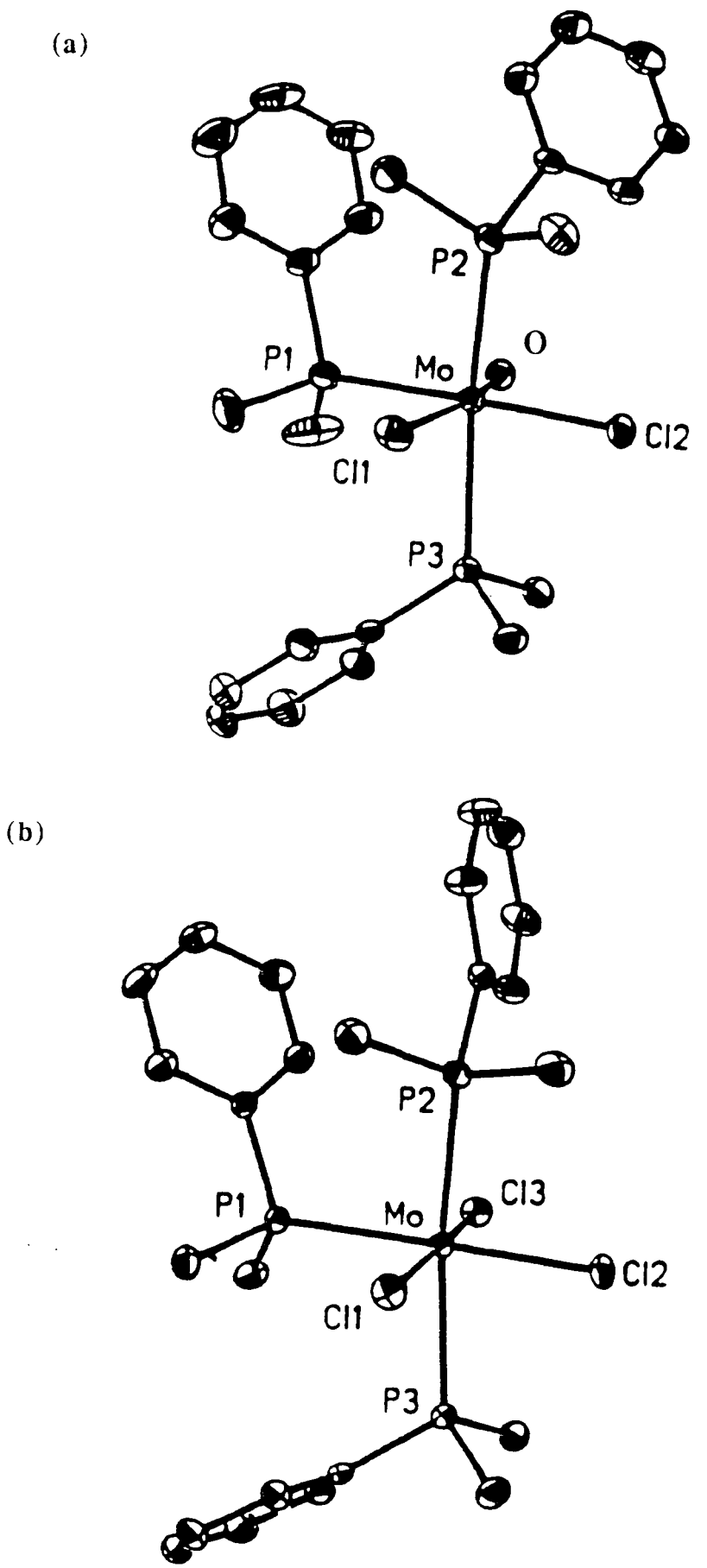


**Figure 2.20:** A comparison of the ORTEP drawings of (a) orthorhombic Enemark blue *cis-mer*-$Mo(O)Cl_2(PMe_2Ph)_3$ and (b) monoclinic yellow *mer*-$MoCl_3(PMe_2Ph)_3$.

Parkin and Enemark who re-examined Chatt's *cis-mer*-$Mo(O)Cl_2(PMe_2Ph)_3$ system, concluded that the apparent lengthening of the Mo=O bonds in the green form was due to co-crystallisation of the blue form ($\nu$(Mo=O) 943 $cm^{-1}$) with yellow *mer*-$MoCl_3(PMe_2Ph)_3$, ignoring the two different $\nu$(Mo=O) stretching values reported originally by Chatt in the blue and green forms, and concluded that the original 954 $cm^{-1}$ $\nu$(Mo=O) assignment in the IR spectrum of the blue form was incorrectly recorded as no evidence of such a stretch was observed in their spectra.

Parkin and co-workers[9] initially had investigated the structure of the trimethylphosphine analogue $Mo(O)Cl_2(PMe_3)_3$, reported by Carmona et al.[20,21] to exist in blue and green forms, but structurally uncharacterised. Their determination of the molecular structure of *cis-mer*-$Mo(O)Cl_2(PMe_3)_3$ interestingly showed that crystals of the green form (they were unable to isolate the blue form) had two independent molecules per asymmetric unit, which differed significantly only in the lengths of the Mo=O bonds. These were 1.698(8)Å, that expected of a normal Mo=O bond, and an abnormally long 1.866(7)Å. To them it thus appeared that two bond-stretch isomers of *cis-mer*-$Mo(O)Cl_2(PMe_3)_3$ were present in the same crystal, and thus they expected to observe two absorptions in the IR spectrum, corresponding to the $\nu$(Mo=O) stretches of the long and short isomers. However, only one absorption at 950 $cm^{-1}$ was observed.[22] This observation was confirmed by $^{17}O$ and $^{18}O$ isotopic substitution, which revealed $\nu(Mo=^{17}O)$ and $\nu(Mo=^{18}O)$ stretches at 920 and 900 $cm^{-1}$ respectively, indicating the presence of only one $\nu(Mo=^{16}O)$ stretch and a coincident $PMe_3$ absorption. A second crystal obtained from a new batch was re-examined in order to verify their original findings, but this through up two new values of 1.772(12) and 2.154(8)Å for the Mo=O bond lengths. This discrepancy suggested that these differences were not a manifestation of bond-stretch isomerism, but after examination of the difference electron density plots, which revealed a large excess of electron density close to the oxo position in the molecule with a long Mo=O bond, they concluded that the discrepancy was due to compositional disorder arising from co-crystallisation of *cis-mer*-$Mo(O)Cl_2(PMe_3)_3$ with a small quantity of the isostructural *mer*-$MoCl_3(PMe_3)_3$, similar to that earlier reported by McPartlin[23] in our $Nb(O)Cl_3(PMe_3)_3$ system by the isomorphous $NbCl_4(PMe_3)_3$.

The incorporation of chloride into the oxo position would be expected to lead to an artificial increase in the Mo=O bond length. Indeed evidence for co-crystallisation of *cis-mer*-$Mo(O)Cl_2(PMe_3)_3$ and *mer*-$MoCl_3(PMe_3)_3$ was readily provided by $^1H$ NMR analysis. Despite being paramagnetic, *mer*-$MoCl_3(PMe_3)_3$ was observed as two broad resonances at $\delta$ -16 and -33 ppm.

In view of the evidence of compositional disorder within the green crystals of *cis-mer*-$Mo(O)Cl_2(PMe_2Ph)_3$ Parkin and co-workers[1] were led to question the original proposal of distortional isomerism in the analogous $Mo(O)Cl_2(PMe_2Ph)_3$ system being responsible for the observation of anomalous Mo=O bond lengths. They were able to isolate crystals which varied in colour from blue, through blue-green, to emerald green, the colour change being associated with an increasing level of contamination by the paramagnetic yellow *mer*-$MoCl_3(PMe_2Ph)_3$ complex, as shown by the $^1H$ NMR spectra over the range $\delta$ +10 to -30 ppm. It was proposed that the bulk sample of the Enemark green form ($\nu$(Mo=O) 943 $cm^{-1}$) of *cis-mer*-$Mo(O)Cl_2(PMe_2Ph)_3$ was a mixture of blue *cis-mer*-$Mo(O)Cl_2(PMe_2Ph)_3$ and yellow *mer*-$MoCl_3(PMe_2Ph)_3$.

This result has been verified independently by ourselves (see sections 2.2-2.8) and by Enemark, who used an extensive series of spectroscopic studies to investigate the enigma. Their studies provided overwhelming evidence that as a result of thin-layer chromatographic separation, the green $Mo(O)Cl_2(PMe_2Ph)_3$ ($\nu$(Mo=O) 943 $cm^{-1}$) was a 65:35 mixture of their blue *cis-mer*-$Mo(O)Cl_2(PMe_2Ph)_3$, showing a $\nu$(Mo=O) stretch at 941 $cm^{-1}$, and yellow *mer*-$MoCl_3(PMe_2Ph)_3$. This was paralleled by their elemental analysis data, which showed the green mixture to have a higher percentage of chlorine than theoretically expected for pure $Mo(O)Cl_2(PMe_2Ph)_3$. They also called attention to the fact that this slight deviation was also present in Chatt's original data.[3] In addition they were able to show that UV-visible data similarly implied that the green colour was the result of the summation of absorptions from the blue form and yellow trichloride.

X-ray photoelectron spectroscopy (XPS) was also used by Enemark and co-workers[4] to show the existence of the mixture nature of the green sample. As Enemark green is a composite of blue Mo(IV) and yellow Mo(III) species, the 3d binding energies

of the two different metal centres behave independently of one another, and so resolve the Mo 3d XPS spectrum of the Enemark green into its components reflecting contributions due to each oxidation state. However, careful line shape analysis was required to provide evidence that the green form (ν(Mo=O) 943 $cm^{-1}$) was a 65:35 mixture of blue *cis-mer*-$Mo(O)Cl_2(PMe_2Ph)_3$ and yellow *mer*-$MoCl_3(PMe_2Ph)_3$. Solid-state Raman studies also implied that for their blue species the band at 941 $cm^{-1}$ was undoubtedly due to a ν(Mo=O) stretch as it was found at 943 $cm^{-1}$ in the Raman spectrum. This stretch was similarly observed in the green form (942 $cm^{-1}$ in IR and 944 $cm^{-1}$ in Raman). Moreover, the intensity of this band in the Raman spectrum was found to be reduced in intensity in accord with the level of contamination of the yellow trichloride.

Spectroscopic evidence is only able to allude to the possible source of the apparent lengthening of the Mo=O bond being compositional disorder, and is not definitive proof of the cause. It was thus necessary for Parkin to verify this proposal by proving the mixture to be homogeneous in the solid-state (i.e., a solid solution), so that single crystals consisting of *cis-mer*-$Mo(O)Cl_2(PMe_2Ph)_3$ and *mer*-$MoCl_3(PMe_2Ph)_3$ could give rise to a long apparent 'Mo=O' bond length. X-ray diffraction studies were carried out on a series of crystals, which differed in the extent of the level of trichloride contaminant, and whose composition was *mer*-$Mo(O)_xCl_{3-x}(PMe_2Ph)_3$ ($0 \leq x \leq 1$), the extremes being blue *cis-mer*-$Mo(O)Cl_2(PMe_2Ph)_3$ (x=1) and yellow *mer*-$MoCl_3(PMe_2Ph)_3$ (x=0). These crystals were obtained by co-crystallisation from mixtures of blue *cis-mer*-$Mo(O)Cl_2(PMe_2Ph)_3$ and *mer*-$MoCl_3(PMe_2Ph)_3$. It is worth noting at this point that it is the Enemark green form, with ν(Mo=O) at 943 $cm^{-1}$, and not the Chatt green form, with ν(Mo=O) at 954 $cm^{-1}$, that was selectively crystallised from this solution. This, however, is not surprising when one considers that the solutions are loaded in favour of *mer*-$MoCl_3(PMe_2Ph)_3$, and so co-crystallisation of a form which exhibits organophosphine orientations that mimic those present in *mer*-$MoCl_3(PMe_2Ph)_3$ is preferred. Interestingly, Parkin comments on the fact that the blue *cis-mer*-$Mo(O)Cl_2(PMe_2Ph)_3$ examined had a structure that was not isomorphous to that originally reported by Muir[2], $C_1$ as opposed to $C_s$, even though both crystals were orthorhombic Pbca, and in particular that the unit cell volumes were significantly different

(5630 vs 5429 $Å^3$), an observation which reflects the different orientations adopted by the phosphine substituents. Clearly, the reported structure of Chatt's blue (ν(Mo=O) 954 $cm^{-1}$), which shows a psuedomirror symmetry ($C_s$) defined by the atoms Mo, O and both Cl, is significantly different from that found by Parkin, and is confirmation of the existence of two independent ν(Mo=O) stretching frequencies as originally observed by Chatt, albeit in blue (954 $cm^{-1}$) and green (943 $cm^{-1}$) forms. However, Enemark appears to have overlooked the significance of his finding of a blue form which showed conformational differences to those originally reported, and a ν(Mo=O) stretch, at 941 $cm^{-1}$, which was previously associated with a green colouration.

Using the results of his X-ray diffraction studies, Parkin was able to draw up a graph of apparent 'Mo=O' length as a function of the estimated composition and show that a continuity of observed 'Mo=O/Mo-Cl' lengths is seen (figure 2.21, table 2.8). Parkin quotes that emerald green crystals of '*cis-mer*-$Mo(O)Cl_2(PMe_2Ph)_3$' obtained from a solution containing an approximately 10:1 molar mixture of Enemark blue *cis-mer*-$Mo(O)Cl_2(PMe_2Ph)_3$ and yellow *mer*-$MoCl_3(PMe_2Ph)_3$ gave rise to an apparent 'Mo=O' bond length of 1.789(3)Å. This molar ratio represents a 9.1% proportion of *mer*-$MoCl_3(PMe_2Ph)_3$, yet the compositional content of the green mixture as revealed by $^1H$ NMR analysis, is quoted as $Mo(O)_{0.97}Cl_{2.03}(PMe_2Ph)_3$, representing a trichloride contamination level of 3.0%. The composition of the crystal is clearly not reflected by that found in the bulk sample. Parkin states that the compositions are only approximate and were determined by analysis of the $^1H$ NMR of the bulk sample. He also comments that the composition as determined by refining site occupancy typically showed slightly higher oxo contents, that is a lower trichloride contamination level. This discrepancy could be due to X-ray crystals not being representative of the bulk sample, or an artifact of the refining model employed, or alternatively as previously discussed in section 2.6 that using $^1H$ NMR to calculate the level of a paramagnetic compound in a predominantly diamagnetic sample is not truly a one-to-one relationship due to the different relaxation mechanisms involved in paramagnetic and diamagnetic compounds in $^1H$ NMR spectroscopy.

The findings of Parkin and Enemark clearly illustrate that the apparent 'Mo=O' bond length varies as a function of the composition (and hence the degree of contamination by the trichloride), providing evidence that the observation of short and long Mo=O bond lengths in the original report by Chatt and Muir is a consequence of compositional disorder. X-ray single crystal analysis must thus be treated with a degree of caution.

| Composition | Colour | d(Mo-O), Å | d(Mo-$Cl_{trans}$), Å | d(Mo-$Cl_{cis}$), Å |
|---|---|---|---|---|
| $Mo(PMe_2Ph)_3OCl_2$ | blue | 1.675(3) | 2.528(1) | 2.481(1) |
| $Mo(PMe_2Ph)_3O_{0.99}Cl_2$ | blue | 1.683(3) | 2.528(1) | 2.479(1) |
| $Mo(PMe_2Ph)_3O_{0.98}Cl_2$ | green-blue | 1.694(5) | 2.529(1) | 2.481(2) |
| $Mo(PMe_2Ph)_3O_{0.97}Cl_2$ | green | 1.789(3) | 2.510(1) | 2.471(2) |
| $Mo(PMe_2Ph)_3O_{0.96}Cl_2$ | green | 1.871(3) | 2.510(1) | 2.465(2) |
| $Mo(PMe_2Ph)_3O_{0.72}Cl_2$ | green | 2.205(2) | 2.481(1) | 2.447(2) |
| $Mo(PMe_2Ph)_3O_{0.51}Cl_2$ | green | 2.316(2) | 2.460(1) | 2.437(2) |
| $Mo(PMe_2Ph)_3O_{0.09}Cl_2$ | yellow-green | 2.391(1) | 2.430(1) | 2.422(2) |
| $Mo(PMe_2Ph)_3Cl_3$ | yellow | 2.400(1) | 2.427(1) | 2.420(1) |

**Table 2.8:** Apparent bond lengths in *mer*-$Mo(O)_xCl_{3-x}(PMe_2Ph)_3$ as a function of composition

The shape of the graph in figure 2.21 does, however, seem to overexemplify the weight of the effect of the presence of very small amounts of trichloride impurity. The excessive steepness in the low trichloride region indicates a large lengthening in the Mo=O bond for only small quantities of co-crystallised Mo-Cl, which is unacceptable on crystallographic grounds. For example, a crystal containing ca. 66% Mo=O and 33% Mo-Cl in the trans position would be expected to have the same electron density at the oxo position as at the chloro site, so that a bond length of about 2.04Å, intermediate between the two extremes of 1.675 and 2.400Å found in the pure blue oxo and trichloride, would be expected. A length of 2.2Å obtained from the curve, demonstrates the chlorine content estimate as being too low. This is not entirely unexpected when the inherent uncertainties in attributing the same composition to a single crystal as to that calculated for the bulk sample.

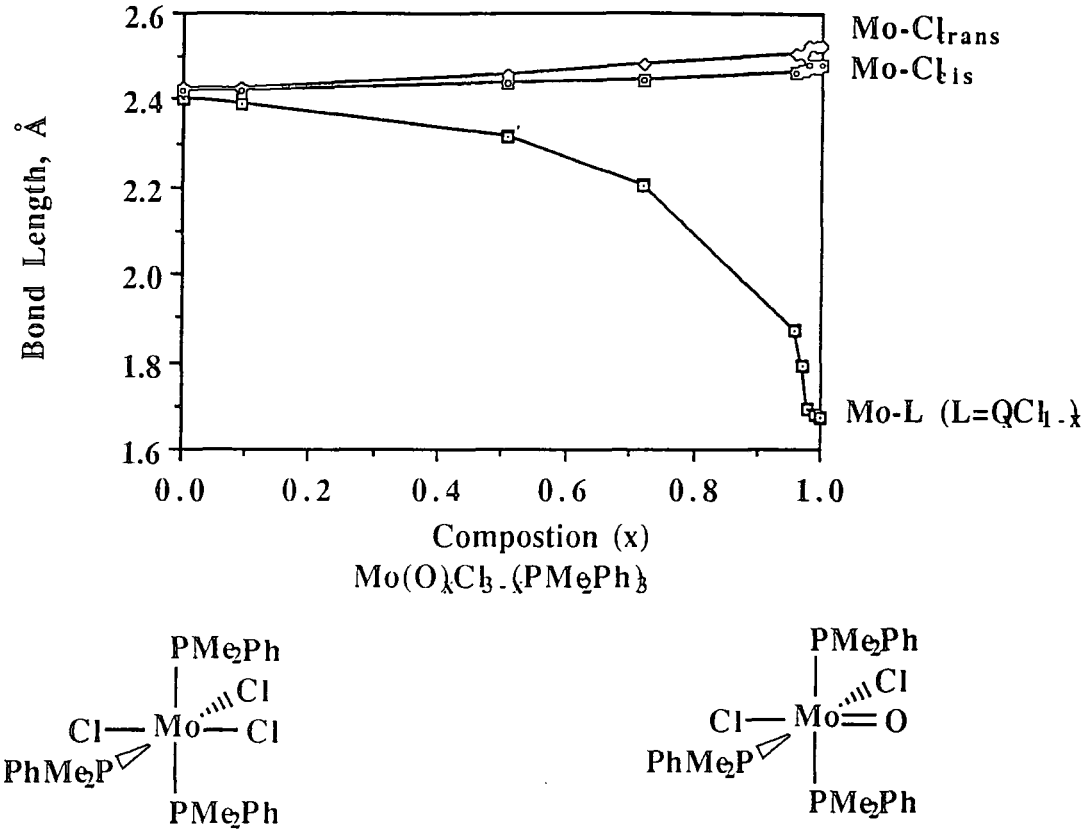


**Figure 2.21:** Apparent bond lengths as a function of composition as determined by Parkin

Therefore, in collaboration with McPartlin, Parkin's data was re-examined using internal correlation[24] in order to obtain a more representative estimate of the fraction of trichloride truly present in the crystal studied as opposed to that of the bulk sample. The trans Mo-Cl length is found to be more sensitive to composition than the cis value, changing from 2.528(1)Å to 2.427(1)Å[9] in going from the pure Enemark/Parkin blue oxo form to the trichloride (where the value represents a mean for the two mutually trans Mo-Cl lengths). These apparent changes of the trans Mo-Cl length are a consequence of the weak trans influence of the chloro versus the oxo moiety, as demonstrated by comparing the structures of the pure blue oxo and trichloride. Thus, as the chloride content increases, the long trans Mo-Cl length of the blue oxo form (2.528(1)Å) approaches that of the trichloride (2.427(1)Å). It was assumed that an approximately linear relation existed between bond length and composition between the two extremes. This is reasonable as only chloride atoms are now involved in the calculations. Three data points were omitted, the first two and the last, since the difference in trans Mo-Cl length from the adjacent extremes of the pure blue oxo and

trichloride forms, were less than three standard deviations and so of very low significance. This approach leads to a much higher estimate of the chloride content than obtained by using bulk sample estimates, and the resultant change in 'Mo=O/Mo-Cl' bond length is more gradual (figure 2.22). The greater plausibility associated with this model is demonstrated by the finding that the estimated Mo=O/Mo-Cl length of 2.04Å for the instance when there is equal electron density at the two sites, fits well onto the

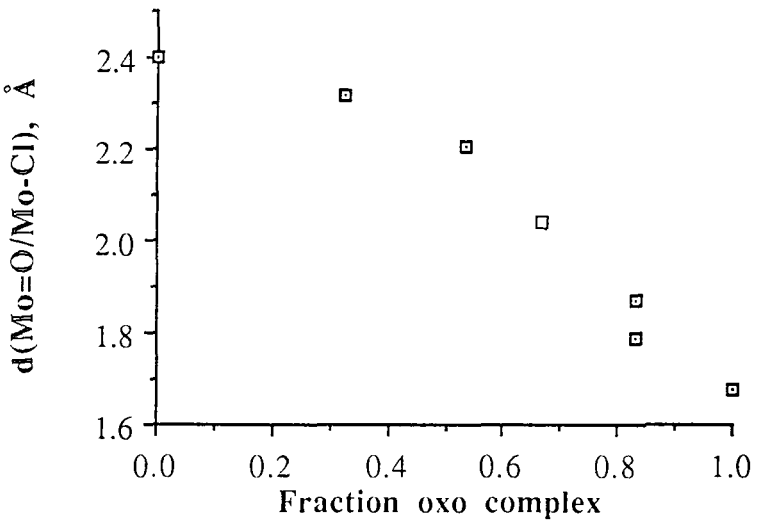


**Figure 2.22:** The variation of Mo=O/Mo-Cl lengths observed in '$Mo(O)Cl_2(PMe_2Ph)_3$' as a function of the fraction of oxo complex using internal correlation from X-ray results

re-evaluated curve (black square). Parkin's conclusion that apparent 'Mo=O' bond lengthening is a manifestation of trichloride contamination still remains indisputable, but the use of internal correlation clearly reflects a more reasonable magnitude for the effect. This is highlighted when one considers that in the original graph, co-crystallisation of 4% trichloride causes an apparent Mo=O lengthening of 0.2Å, when the point on which this is based ('Mo-Cl/Mo=O' length of 1.871Å) appears to have closer to a 20% trichloride content when the length of its trans Mo-Cl bond is taken into consideration. In fact, this ties in quite neatly with our findings of a 19% trichloride contamination level as determined by elemental analysis for the Enemark green form in the bulk sample when the co-crystallising conditions are not controlled or forced in any way, which by X-ray determination show an apparent 'Mo=O' bond length close to this value.

## 2.10 Summary

In this chapter we have seen that despite the belief of Parkin and Enemark that Chatt's original assignment of the ν(Mo=O) stretch was incorrect and not corroborated by their findings, two unique blue forms of *cis-mer*-$Mo(O)Cl_2(PMe_2Ph)_3$ have been isolated. Although the Mo=O bond lengths are comparable, significant differences in the ν(Mo=O) stretching frequencies are observed and this is reflected in the different orientations adopted by the aryl and alkyl groups on the phosphine ligands.

Additionally, it has been established that each of these pure oxo forms can be contaminated by the isostructural species $MoCl_3(PMe_2Ph)_3$. This leads to an apparent Mo=O bond lengthening (as determined by X-ray crystallography) which is actually the consequence of co-crystallisation of the $Mo\text{-}Cl_{axial}$ bond of the trichloride resulting in the chloride co-occupying the oxo site.

## 2.11 References


1. K. Yoon, G. Parkin, A.L. Rheingold, *J.Amer. Chem. Soc.*, 1991, **113**, 1437; G. Parkin, *Acc. Chem. Res.*, 1992, **25**, 455.
2. Lj. Manojlovic-Muir, *Chem. Commun.* , **1971**, 147; *J. Chem. Soc (A)*, **1971**, 686.
3. A.V. Butcher, J. Chatt, *J. Chem. Soc (A)*, **1970**, 2652.
4. P.J. Desrochers, K.W. Nebesny, M.J. LaBarre, S.E. Lincoln, T.M. Loehr, J.H. Enemark, *J.Amer. Chem. Soc.*, 1991, **113**, 9193.
5. W. Wardlaw, H.W. Webb, *J. Chem. Soc.*, **1930**, 2100.
6. M.L. Larson, F.W. Moore, *Inorg. Chem.*, 1966, **5**, 801.
7. (a) Lj. Manojlovic-Muir, *Chem. Commun.* , **1971**, 147; (b) *J. Chem. Soc (A)*, **1971**, 2796.
8. R.M. Silverstein, G.C. Bassler, T.C. Morrill, *'Spectroscopic Identification of Organic Compounds'*, 4th edition, John Wiley and Sons, New York, 1981, p170.
9. K. Yoon, G. Parkin, A.L. Rheingold, *J.Amer. Chem. Soc.*, 1992, **114**, 2210; G. Parkin, *Chem. Rev.*, 1993, **93**, 887.
10. A.V. Butcher, J. Chatt, G.J. Leigh, P.L. Richards, *J. Chem. Soc. Dalton. Trans.*, **1972**, 1064.

11. (a) U. Mazzi, G. De Paoli, G. Rizzardi, L. Magon, *Inorg. Chim. Acta.*, 1974, **10**, L2; (b) U. Mazzi, G. De Paoli, P. Di Bernardo, L. Magon, *J. Inorg. Nucl. Chem.*, 1976, **38**, 721.

12. E.W. Randall, D.J. Shaw, *J. Chem. Soc. (A)*, **1969**, 2867.

13. J. Chatt, G.J. Leigh, D.M.P. Mingos, *J. Chem. Soc. (A)*, **1969**, 1674.

14. A.P. Bashall, S.W. Annie Bligh, A.J. Edwards, V.C. Gibson, M. McPartlin, O.B. Robinson, *Angew. Chem. Int. Ed. Engl.*, 1992, **31**, 1607.

15. (a) J. Chatt, Lj. Manojlovic-Muir, K.W. Muir, *Chem. Commun.*, **1971**, 655; (b) Lj. Manojlovic-Muir, K.W. Muir, *J. Chem. Soc. Dalton Trans.*, **1972**, 686.

16. J.C. Green, M.L.H. Green, J. Bailat et al. (eds), *'Comprehensive Organometallic Chemistry'*, Pergamon, Oxford, 1973, p355.

17. B.L. Haymore, W.A. Goddard III, J.N. Allison, *Proc. Int. Conf. Coord. Chem.*, 23rd, **1984**, 535.

18. S. Lincoln, S.A. Koch, *Inorg. Chem.*, **1986**, 25, 1594; G. Ferguson, B. Kaitner, F.J. Lalor, G. Roberts, *J. Chem. Res. Synop.*, 1982, **1**, 6.

19. K.-C. Ho, G.M. McLaughlin, M. McPartlin, G.B. Robertson, *Acta. Cryst.*, **B38**, 1982, 421.

20. E. Carmona, L. Sanchez, M.L. Poseda, R.A. Jones, J.G. Hefner, *Polyhedron*, 1983, **2**, 797.

21. E. Carmona, A. Galindo, L. Sanchez, A.J. Nielson , G. Wilkinson, *Polyhedron*, 1984, **3**, 347.

22. It is noted here that the value in fact differs from that originally reported by Carmona et al. in ref. 21, who reported a strong absorption at 940 $cm^{-1}$ due to coordinated $PMe_3$, with a shoulder at ca. 960 $cm^{-1}$ possibly due to a $\nu$(Mo=O) stretch. It would seem to me that even in the *cis-mer*-$Mo(O)Cl_2(PMe_3)_3$ there still remains the possibility of finding two blue forms showing different $\nu$(Mo=O) stretches.

23. A.P. Bashall, M. McPartlin, poster presented at the 15th International Conference of Crystallography, Bordeaux, 19th-28th July, 1990.

24. V.C. Gibson, M. McPartlin, *J. Chem. Soc. Dalton Trans.*, **1992**, 947.

25. Unpublished results of this thesis (private communication with Prof. M. McPartlin).

26. J. Chatt, G.A. Rowe, *J. Chem. Soc.*, **1962**, 4019.

# CHAPTER THREE

## Additional Instances of Distortional Isomerism in Oxomolybdenum and Oxotungsten Systems

## 3.1 Introduction

In this chapter, other compounds of the general form $M(O)X_2(PR_3)_3$ are examined with a view to assessing evidence for distortional isomerism. In light of the observation of two blue species in both the chloro and bromo $Mo(O)X_2(PMe_2Ph)_3$ (X= Cl, Br) systems each exhibiting ν(Mo=O) vibrations relating to the orientations of the organic substituents on the phosphine ligands, it seemed strange that more instances of such cases had been not reported in other related molybdenum and tungsten complexes.

## 3.2 Synthesis and Characterisation of $Mo(O)(NCS)_2(PMe_2Ph)_3$

### 3.2.1 Introduction

Interestingly, Cotton had reported the existence of two oxo complexes of *cis-mer*-$Mo(O)(NCO)_2(PEt_2Ph)_3$ in the asymmetric unit differing in the orientations of their phosphine ligands, but only one stretch was reported as being assignable to a ν(Mo=O) vibration. It was envisaged that the dimethylphenylphosphine derivative $Mo(O)(NCS)_2(PMe_2Ph)_3$ would provide a good candidate for investigation, since like the cyanate complex, the thiocyanate complex ought to be free of trichloride contaminant, the presence of which has led to so much controversy about the true origin of the differences in the M=O stretching vibrations.

### 3.2.2 Solid-State Infrared and Raman Spectroscopy

The reaction of Enemark blue *cis-mer*-$Mo(O)Cl_2(PMe_2Ph)_3$ with KNCS yielded the blue crystalline metathesis product $Mo(O)(NCS)_2(PMe_2Ph)_3$ (section 7.2.9) in a similar manner to that described by Chatt.[1] A green isomer was not observed.

The NCS derivative shows several absorptions, at 949, 942, 920 (shoulder) and 910 $cm^{-1}$ in the IR Mo=O fingerprint region. The presence of intense ligand ν(P-C) bands is eliminated by the use of Raman spectroscopy, which confirms that the band at 949 $cm^{-1}$ in the IR spectrum (figure 3.1, top) is due to the Mo=O stretch, since a strong

# 'Chatt type' blue $Mo(O)(NCS)_2(PMe_2Ph)_3$

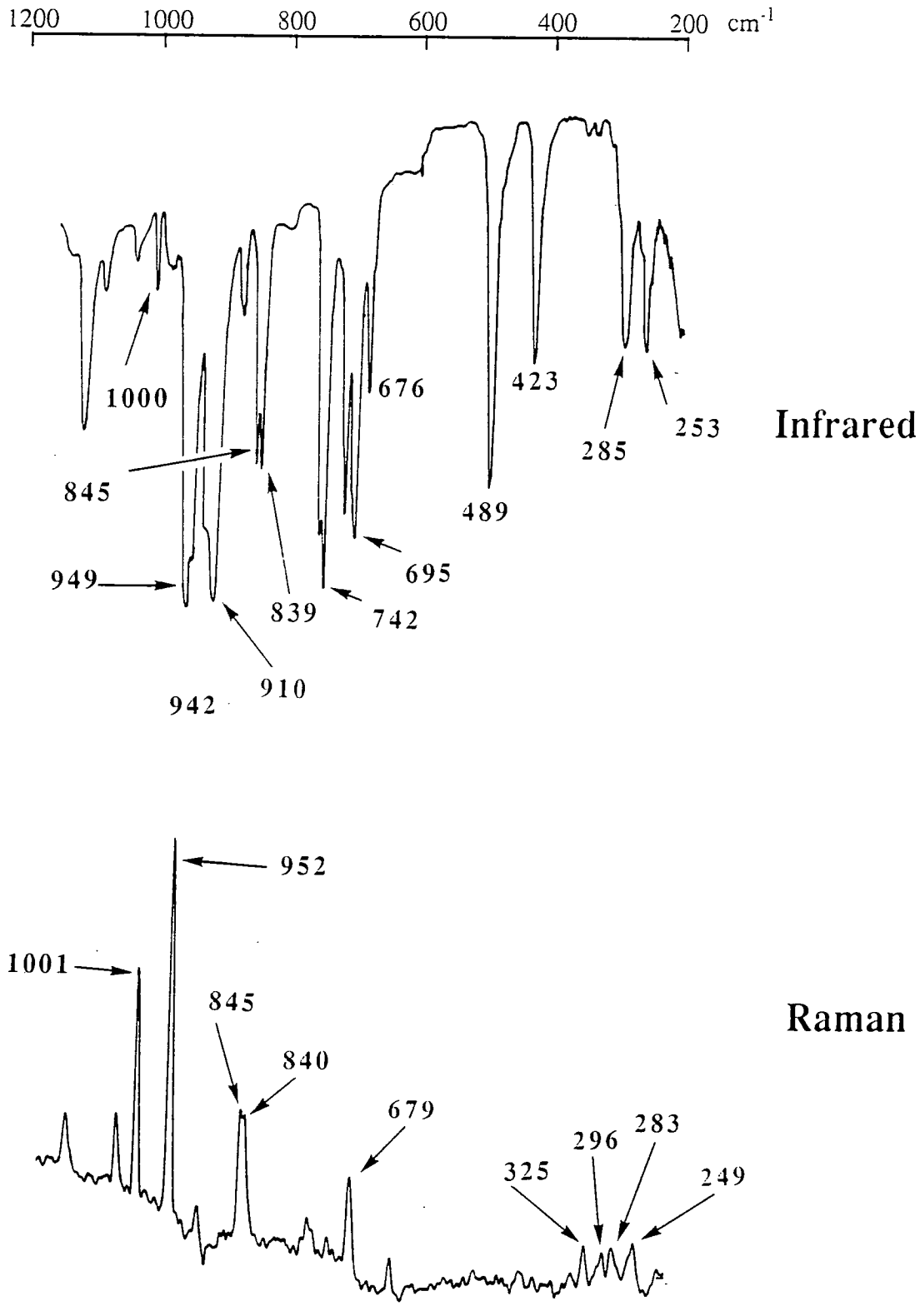


**Figure 3.1:** Solid-state infrared (top) and Raman (bottom) spectra of blue *cis-mer*-$Mo(O)(NCS)_2(PMe_2Ph)_3$ (1150 to 200 $cm^{-1}$).

absorption at 952 $cm^{-1}$ is observed in the Raman spectrum[2] (figure 3.1). As predicted by group theory for a molecule assumed to possess $C_s$ symmetry, the terminal oxo moiety is both IR and Raman active ($\Gamma_{Mo=O\ stretch}$ transforms as A'). In this chapter the terms 'Chatt-like' and 'Enemark-like' will be used to refer to those species that have ν(Mo=O) stretches in the mid 950 and low 940 $cm^{-1}$ regions respectively, and which have been established by X-ray diffraction determinations to possess similar phosphine orientations to those previously reported for the two blue forms of *cis-mer*-$Mo(O)Cl_2(PMe_2Ph)_3$ originally synthesized by Chatt[1] and Enemark.[4]

The NCS group may coordinate to a metal through either the nitrogen or the sulphur, or even both in a bridging species. Several factors, such as the oxidation state of the metal, the nature of the other ligands (electronic effects) and steric considerations

| | ν(CN) | | ν(CX) | δ(NCX) |
|---|---|---|---|---|
| | $\nu_{as}$ | $\nu_s$ | X=O or S | |
| $Mo(O)(NCO)_2(PEt_2Ph)_3$ | 2233 | 2195 | 1332 | 624, 615, 586 |
| $Mo(O)(NCO)_2(PMe_2Ph)_3$ | 2218 | 2171 | 1325 | 624, 587 |
| $Mo(O)(NCS)_2(PEt_2Ph)_3$ | 2067 | 2031 | † | † |
| $Mo(O)(NCS)_2(PMe_2Ph)_3$ | 2070 | 2040 | 845* | † |

**Table 3.1:** Table showing the IR bands characteristic of $NCX^-$ (X=O or S): † obscured by ligand absorption; * by comparison with the IR spectrum of $Mo(O)Cl_2(PMe_2Ph)_3$.

are known to influence the mode of coordination.[3] The IR data of the thiocyanate complex, along with those of the related $Mo(O)X_2(PR_2Ph)_3$ complexes (X=NCO, R=Et, Me; X=NCS, R=Et) in the ν(CN) region are shown in table 3.1.

This indicates that an N-bonded NCX group is more likely, but there is uncertainty concerning the bonding in the NCS case because both the ν(CS) and δ(NCS) regions are obscured by strong absorptions of the other ligands. However, the low values of the ν(CN) stretches (nearer 2050 $cm^{-1}$ and typical of N-bonded complexes)[3], together with an IR comparison with the Chatt or Enemark blue *cis-mer*-$Mo(O)Cl_2(PMe_2Ph)_3$ species both of which show a ligand absorption at 839 $cm^{-1}$ of medium intensity, strongly suggest that the band at 845 $cm^{-1}$ (in addition to the 839 $cm^{-1}$

ligand absorption) can be assigned to the ν(CS) stretch and so indicates N-bonding rather than S-bonding typically found between 720 to 690 $cm^{-1}$.[3]

In these phosphine complexes, there is an electronic preference for bonding through nitrogen. Considering the MOs of the ion $SCN^-$ (figure 3.2) it can be seen that the π-bonding MO is polarised toward the N atom (N is the most electronegative atom), and so the $\pi^*$ MO is polarised toward sulphur. Now all three MOs can overlap with a metal orbital of π-symmetry using either end of the $SCN^-$ ion. However, if M-N overlap occurs, the ligand would function as a stronger π-donor than π-acceptor. Conversely, for M-SCN complexes the ligand would function as a strong π-acceptor but a weak π-donor. Therefore, it is to be expected that $SCN^-$ will preferentially use the S end in binding to a metal ion having filled (or partially filled) π-symmetry orbitals. On the other

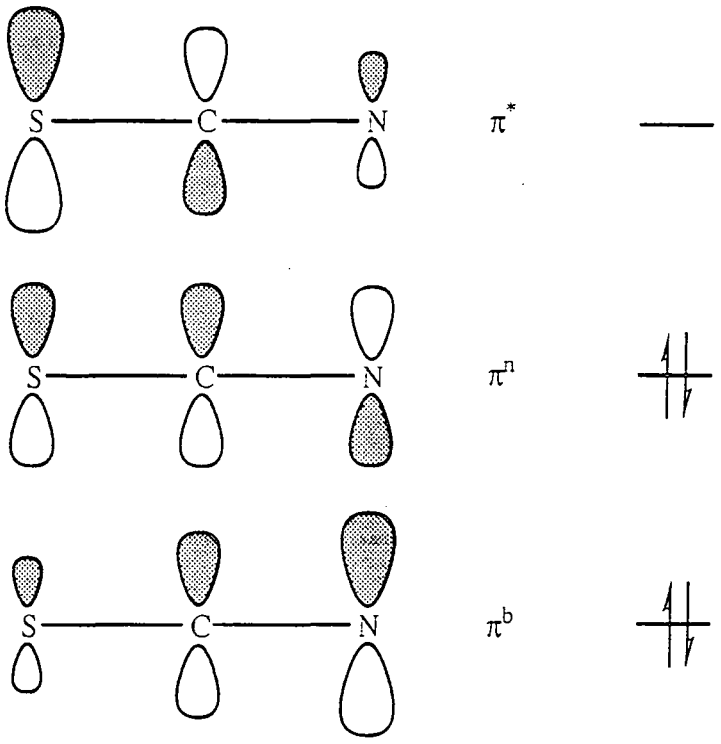


**Figure 3.2:** MO representation of the orbitals available for π-bonding to a metal centre

hand, when the metal ion has no such orbitals or another ligand competes successfully for them, then $SCN^-$ will prefer to use the π-donor N end of the ligand. The low value of the ν(CN) stretches is indicative of substantial metal-to-ligand π-back bonding. The metal-terminal oxo complex with a $d^2$ configuration is diamagnetic and so possesses two paired

electrons in an orbital that lies perpendicular to the the metal-oxygen bond ($d_{xy}$ when the z axis is taken as coincident with the M-O bond vector [figure 1.11]).[18] Back-bonding therefore occurs predominantly to the ligands cis to the oxo group and so in addition to establishing a cis configuration of the NCS group within the meridional geometry, also supports the observation of N-bonding in the thiocyanate complex, a ligand possessing π-acidic (acceptor) capabilities (figure 3.3).

The presence of two strong bands of equal intensity in the ν(CN) region, strongly suggests that the pseudohalide groups are mutually cis, since π-back bonding to the NCS group in the site cis to the oxo moiety will result in a shortening of the Mo-N bond and a lengthening of the N=C bond and hence a reduction in the frequency of ν(CN) stretch associated with this cis ligand compared to that situated trans to oxo group which experiences no π-back bonding (cf. the case of $W(O)Cl_2(CH_2{=}CH_2)(PMePh_2)_2$

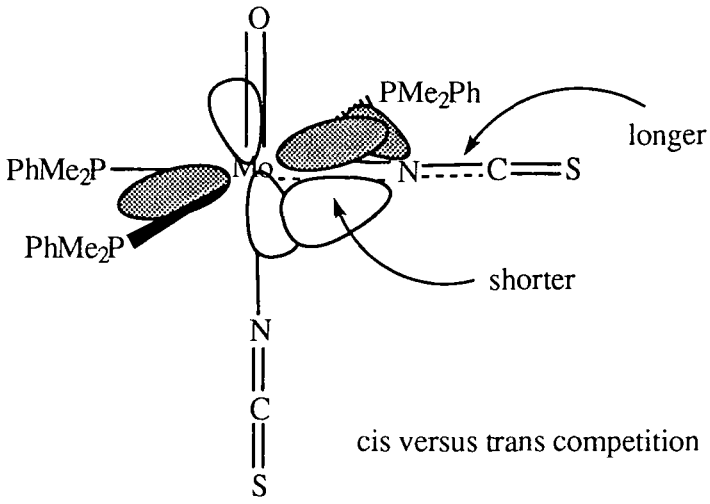


**Figure 3.3:** π-Back bonding in *cis-mer*-$Mo(O)(NCS)_2(PMe_2Ph)_3$

reported by Mayer[19]). This is backed up by the fact that group theory predicts that the symmetric and antisymmetric ν(CN) stretches in the *cis-mer* case will be strong, whereas in the *trans-mer* case one of the two allowed vibrations will only be weakly active, since the symmetric vibration involving the two *trans* groups causes little change in the dipole moment. The blue forms of *mer*-$Mo(O)Cl_2(PMe_2Ph)_3$ are known to have mutually *cis*-chlorine ligands[4,5], and the *cis-mer* nature of the thiocyanate ligands is confirmed by an X-ray structure determination (section 3.2.5).

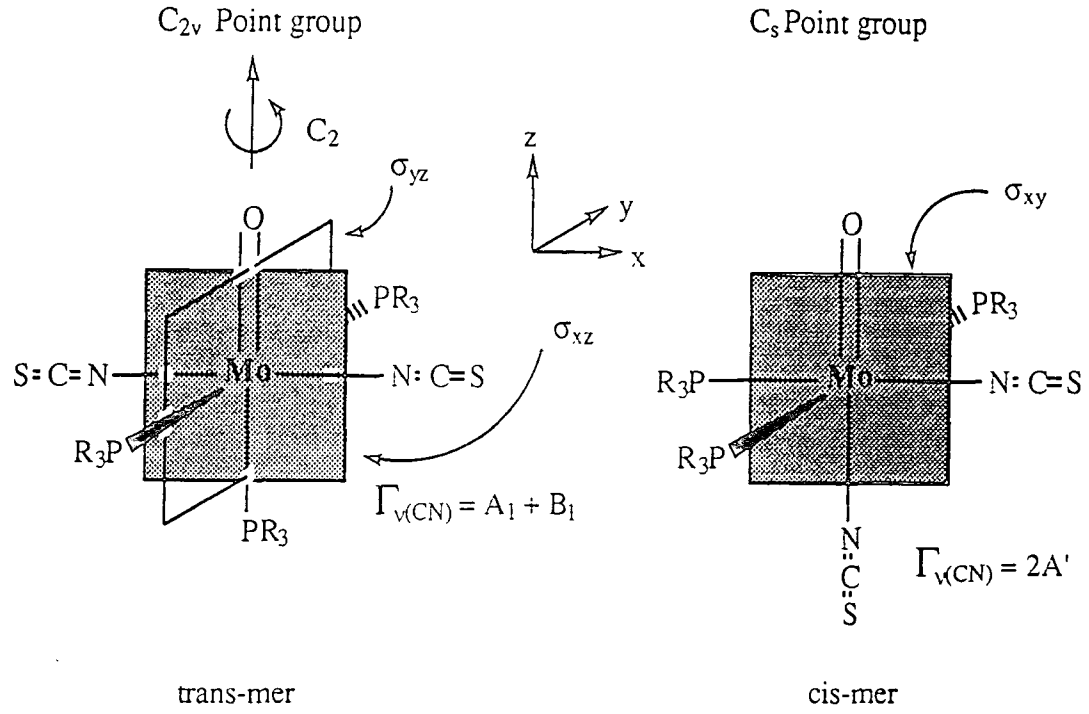


**Figure 3.4:** Group theory predictions for *cis-mer* and *trans-mer* ν(CN) stretches

### 3.2.3 $^1$H NMR Spectroscopy

The 400 MHz $^1$H NMR spectrum in $CDCl_3$ of blue $Mo(O)(NCS)_2(PMe_2Ph)_3$ (figure 3.5) shows a doublet at δ 1.22 ppm ($^2J(PH)$=8.2Hz) and two virtually coupled triplets at δ 1.65 ($^2J(PH)$=3.9Hz) and δ 1.86 ppm ($^2J(PH)$=4.0Hz), which can be explained on the basis of a meridional arrangement of the phosphine ligands and strong trans P-P coupling and weak cis P-P coupling, analogous to the spectra observed for the dichloride analogue and those of $[IrHX_2(PMe_2Ph)_3]$ (X=Cl, Br, I) and related compounds discussed by Shaw and co-workers.[6,7] This dimethylphenylphosphine complex shows a triplet to doublet relative peak intensity of 2:1, consistent with a *cis-mer* configuration in chloroform solution.

It has been shown that for many transition metal dimethylphenylphosphine complexes the methyl resonance of the two $PMe_2Ph$ ligands in mutual *trans*-positions is a relatively well-defined 'triplet' due to virtual coupling with both phosphorus nuclei, but for the two phosphines in mutual *cis*-positions a 1:1 doublet is obtained.[8] Thus for the six-coordinate meridional molybdenum complexes studied in chapters two and three, the methyl resonances are expected to consist of one or two 1:2:1 triplets of total relative

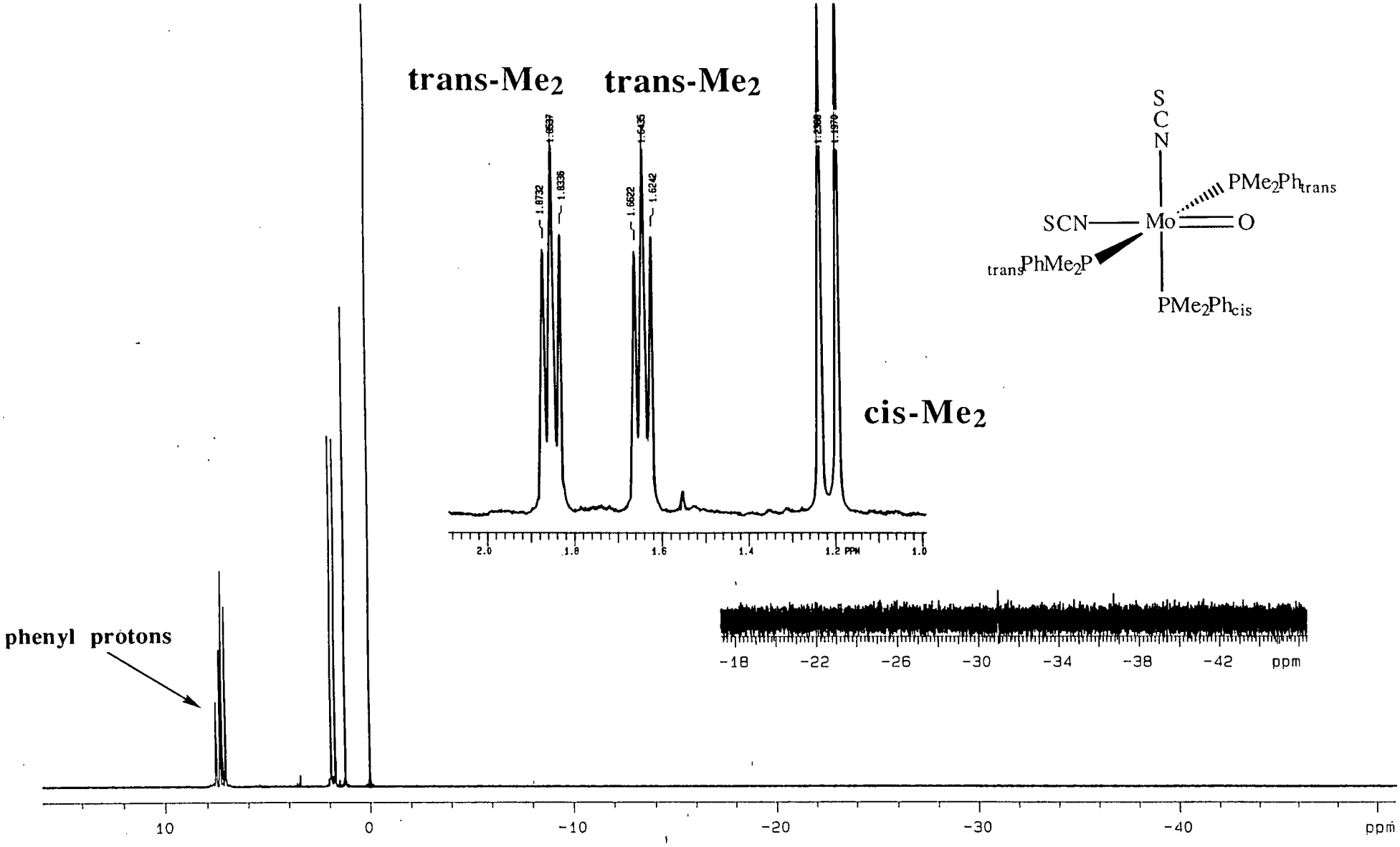


**Figure 3.5:** 400 MHz $^1$H NMR of *cis-mer*-Mo(O)(NCS)$_2$(PMe$_2$Ph)$_3$ in $CDCl_3$ over the range +15 to -50 ppm.

intensity two and a 1:1 doublet of total intensity one. In a facial complex, such as *fac*-$[IrH_3(PMe_2Ph)_3]$[7], where the phosphines are all mutually cis to each other, a single 1:1 doublet is expected (due to their chemical and magnetic equivalence). Furthermore, two configurations are possible for a *mer*-configuration (**I** and **II**) depending on the cis or trans disposition of the 'pseudohalide' ligand. In configuration **I** there is no plane of symmetry through the two *trans*-phosphorus atoms so that the shielding experienced by the two methyl groups on the same phosphine ligand may differ significantly, even without any effects due to restricted rotation about the Mo-P bond. Whereas, in configuration **II** there is such a plane of symmetry passing through the line P-Mo-P (figure 3.6) and a well-defined 1:2:1 methyl triplet resonance of total intensity two relative to the doublet would be observed. In isomers of configuration **I** (seen in the species described in chapter two), two triplet resonances (or less well-defined overlapping triplets) are expected due to the non-equivalent nature of the methyl groups.

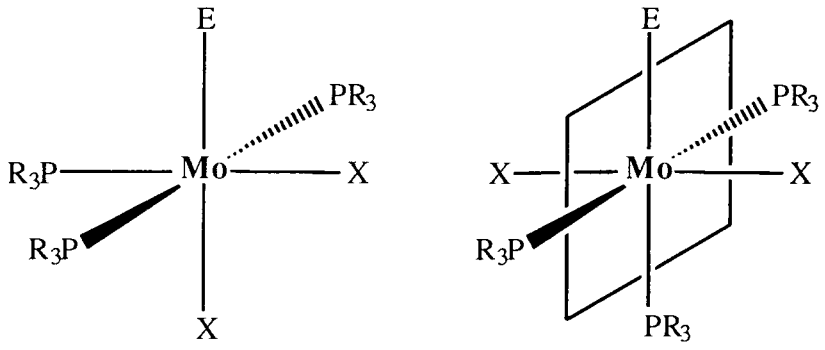


cis-mer **I** trans-mer **II**

**Figure 3.6:** Diagram explaining the origin of the inequivalence of the *trans*-phosphorus methyl groups

At this point it is worth noting that the δ values of all the resonances in the dimethylphenylphosphine complexes, tabulated in table 3.2, decrease in the order I>Br>Cl>NCS>NCO. This is in line with the order of increasing electronegativity for the halides, I<Br<Cl. One would thus expect the electrons in a σ-bond formed between phosphorus and molybdenum to lie closer to the molybdenum the more electronegative is the halide group. This would draw electrons away from the methyl groups and so increase the δ value. However, this is not what is observed, and so electronegativity can

| Complex | Doublet (δ ppm) | Triplets (δ ppm) | |
|---|---|---|---|
| $Mo(O)I_2(PMe_2Ph)_3$ | 1.33 | 2.06 | 2.24 |
| $Mo(O)Br_2(PMe_2Ph)_3$ | 1.27 | 1.85 | 2.04 |
| $Mo(O)Cl_2(PMe_2Ph)_3$ | 1.22 | 1.72 | 1.93 |
| $Mo(O)(NCS)_2(PMe_2Ph)_3$ | 1.22 | 1.65 | 1.86 |
| $Mo(O)(NCO)_2(PMe_2Ph)_3$ | 1.12 | 1.52 | 1.71 |

**Table 3.2:** Chemical shifts (δ) for the doublet and virtual triplets in the complexes $Mo(O)X_2(PMe_2Ph)_3$ (X=I, Br, Cl, NCS, NCO)

not be the factor determining the δ value of the resonances. It was tentatively suggested[7] that the dominant factor in removing electron density from the methyl groups and increasing the δ value in the order Cl<Br<I is the ability of the halide ligand to accept back-donation of electrons from the metal. This ability is believed to increase in the order Cl<Br<I.[9] This is also consistent with the even better π-accepting capacities of NCO and NCS.

### 3.2.4 Elemental Analysis

Elemental analysis of the blue $Mo(O)(NCS)_2(PMe_2Ph)_3$ (table 3.3) shows that the stoichiometry agrees with the empirical formula $C_{26}H_{33}MoN_2P_3$.

| | %C | %H | %N | %Cl |
|---|---|---|---|---|
| Required | 48.60 | 5.18 | 4.36 | ---- |
| Found | 48.13 | 5.09 | 4.21 | ---- |
| | 48.08 | 5.09 | 4.23 | ---- |

**Table 3.3:** Elemental analysis data for blue $Mo(O)(NCS)_2(PMe_2Ph)_3$

This agrees with $^1H$ NMR evidence that the sample is free of a paramagnetic contaminant, whether it be $MoCl_3(PMe_2Ph)_3$ (derived from the dichloride starting material) or $Mo(NCS)_3(PMe_2Ph)_3$.

### 3.2.5 Crystal Structure of *cis-mer*-$Mo(O)(NCS)_2(PMe_2Ph)_3$

Cotton has recently published the structure of blue *cis-mer*-$Mo(O)(NCO)_2(PEt_2Ph)_3$.[16] Selected bond lengths and angles for this complex and blue

*cis-mer*-$Mo(O)(NCS)_2(PMe_2Ph)_3$, determined as a part of this study (table 3.5), are presented in table 3.4. An ORTEP representation of each complex is shown in figure 3.7.

Both complexes have a *cis-mer* configuration of the ligands, although the cyanate (NCO) asymmetric unit contains two independent molecules. The coordination about the central metal atom in these molecules is the same, but the orientation of the organic groups on the phosphine ligands differ. In 2a there is a virtual mirror plane coincident with the plane containing the Mo, O, both N atoms, and P(1). This orientation is virtually identical with that observed in the blue *cis-mer*-$Mo(O)Cl_2(PMe_2Ph)_3$ which

| | *cis-mer*-$Mo(O)X_2(PR_2Ph)_3$ | | |
|---|---|---|---|
| | X=NCS,R=Me | X=NCO, R=Et | |
| | 1 | 2a | 2b |
| Mo-O | 1.687(8) | 1.678(8) | 1.690(8) |
| Mo-N(1) | 2.180(11) | 2.18(1) | 2.18(1) |
| Mo-N(2) | 2.079(10) | 2.10(1) | 2.09(1) |
| Mo-P(1) | 2.503(3) | 2.542(4) | 2.524(4) |
| Mo-P(2) | 2.537(4) | 2.548(4) | 2.555(4) |
| Mo-P(3) | 2.530(4) | 2.575(4) | 2.577(4) |
| O-Mo-N(1) | 168.5(4) | 170.5(4) | 167.3(4) |
| O-Mo-N(2) | 105.1(4) | 102.9(4) | 106.5(5) |
| P(1)-Mo-N(2) | 165.3(3) | 167.0(4) | 161.7(4) |
| P(2)-Mo-P(3) | 166.4(1) | 166.8(1) | 168.6(1) |

**Table 3.4:** A comparison of selected bond lengths (Å) and angles (°) for the complexes blue *cis-mer*-$Mo(O)X_2(PR_2Ph)_3$ (1, X= NCS, R= Me; 2a, 2b, X= NCO, R= Et)

exhibits a high ν(Mo=O) stretching frequency.[5b] In 1 and 2b the phosphine ligand trans to the thiocyanate or cyanate ligand has a different orientation to that in 2a (rotated through ca. 120° along the Mo-P axis). Because of this difference, molecules 1 and 2b have no virtual symmetry, and this is reflected in different steric requirements for the ligands, and so while the M-L bond distances are nearly the same in each of the three molecules, some of the L-M-L angles are significantly different (table 3.4). In each

| | | | |
|---|---|---|---|
| Mo - N(1) | 2.180(11) | P(2) - Mo - P(1) | 94.1(1) |
| Mo - N(2) | 2.079(10) | P(3) - Mo - P(1) | 95.4(1) |
| | | P(3) - Mo - P(2) | 166.4(1) |
| Mo - P(1) | 2.503(4) | | |
| Mo - P(2) | 2.537(4) | O - Mo - N(1) | 168.5(4) |
| Mo - P(3) | 2.530(4) | O - Mo -N(2) | 105.1(4) |
| Mo - O | 1.687(8) | O - Mo - P(1) | 89.6(3) |
| | | O - Mo - P(2) | 96.8(3) |
| N(2) - Mo - N(1) | 86.0(4) | O - Mo - P(3) | 93.0(3) |
| P(1) - C(16) | 1.858(12) | C(16) - P(1) - Mo | 119.4(4) |
| P(1) - C(17) | 1.810(13) | C(17) - P(1) - Mo | 117.0(5) |
| P(1) - C(18) | 1.799(12) | C(18) - P(1) - Mo | 111.5(5) |
| P(2) - C(26) | 1.852(12) | C(26) - P(2) - Mo | 113.8(4) |
| P(2) - C(27) | 1.795(12) | C(27) - P(2) - Mo | 115.3(5) |
| P(2) - C(28) | 1.796(12) | C(28) - P(2) - Mo | 114.8(4) |
| P(3) - C(36) | 1.857(13) | C(36) - P(3) - Mo | 118.1(4) |
| P(3) - C(37) | 1.823(12) | C(37) - P(3) - Mo | 110.8(4) |
| P(3) - C(38) | 1.817(12) | C(38) - P(3) - Mo | 114.5(5) |
| P(1) - Mo - N(1) | 79.2(3) | | |
| P(1) - Mo - N(2) | 165.3(3) | C(16) - P(1) - C(17) | 100.9(6) |
| P(2) - Mo - N(1) | 86.8(3) | C(16) - P(1) - C(18) | 102.9(6) |
| P(2) - Mo - N(2) | 85.0(3) | C(17) - P(1) - C(18) | 103.0(7) |
| P(3) - Mo - N(1) | 85.5(3) | C(26) - P(2) - C(27) | 106.1(7) |
| P(3) - Mo - N(2) | 83.3(3) | C(26) - P(2) - C(28) | 102.4(5) |
| | | C(27) - P(2) - C(28) | 102.8(6) |
| C(1) - N(1) - Mo | 172(1) | C(36) - P(3) - C(37) | 102.2(5) |
| C(2) - N(2) - Mo | 168(1) | C(36) - P(3) - C(38) | 107.2(7) |
| | | C(37) - P(3) - C(38) | 102.1(6) |
| S(1) - C(1) - N(1) | 177(1) | | |
| S(2) - C(2) - N(2) | 179(1) | | |

**Table 3.5:** Selected bond lengths (Å) and angles (°) for blue *cis-mer*-$Mo(O)(NCS)_2(PMe_2Ph)_3$

(2a)

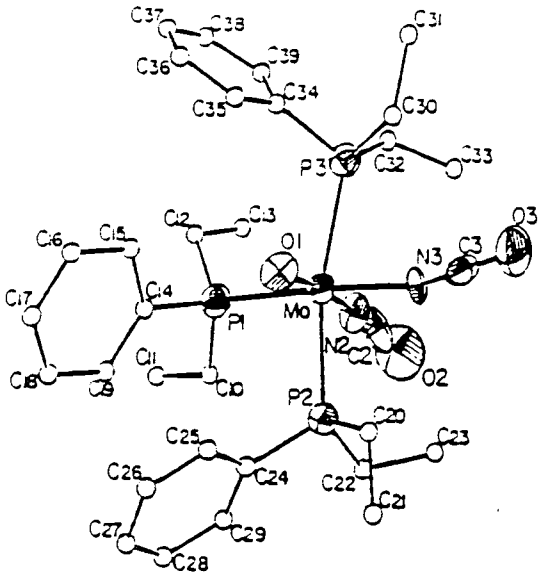


(2b)

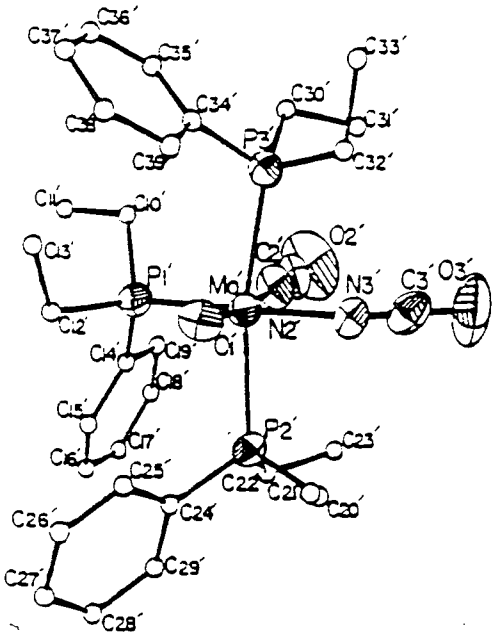


(1)

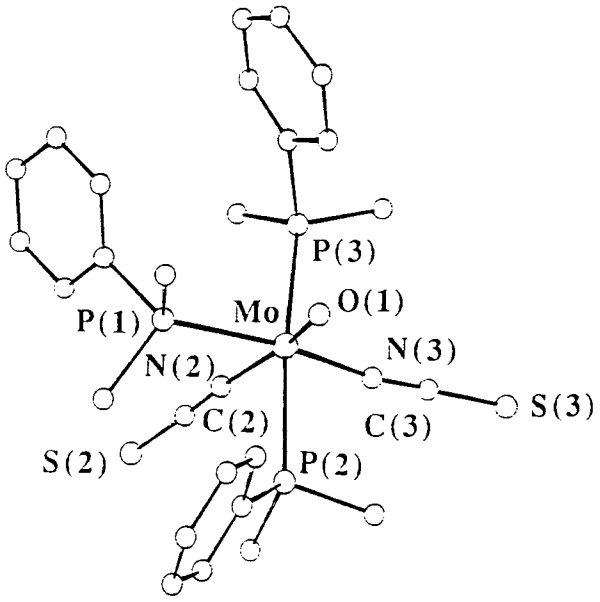


**Figure 3.7:** Molecular drawings of the complexes *cis-mer*-$Mo(O)(NCX)_2(PR_2Ph)_3$ (1: X= S, R= Me; 2: X=O, R= Et).

molecule the Mo-O bond is short (ca. 1.68Å) and the Mo-$N_{cis\text{-}to\text{-}O}$ bond is ca. 0.08Å shorter than the Mo-$N_{trans\text{-}to\text{-}O}$.

Since there is no evidence for a paramagnetic impurity, the Mo=O bond length of 1.687(8)Å reported for blue *cis-mer*-$Mo(O)(NCS)_2(PMe_2Ph)_3$ represents a true Mo=O distance, which corresponds to the 949 $cm^{-1}$ ν(Mo=O) stretch.

At this point it is interesting to comment on the fact that despite the observation of two independent molecules in the asymmetric unit for *cis-mer*-$Mo(O)(NCO)_2(PMe_2Ph)_3$, only one ν(Mo=O) stretch, at 940 $cm^{-1}$, was reported by Cotton and co-workers[16] when two would be expected. This case is different from that reported by Parkin[17] in the instance of green $Mo(O)Cl_2(PMe_3)_3$ where the second molecule in the asymmetric unit was the trichloride contaminant, and not a pure oxo form as reported by Cotton in the cyanate complex. In the light of the evidence accumulated in this thesis this observation remains to be resolved.

## 3.3 Synthesis and Characterisation of $W(O)Cl_2(PMe_2Ph)_3$

### 3.3.1 Introduction

Complexes of the the composition $W(O)Cl_2(PR)_3$ are known[10] for several monotertiary phosphines ($PR_3$=$PMe_2Ph$, $PMePh_2$, $PEt_2Ph$) and were prepared in rather poor yields (ca. 30%) by the reaction of $WCl_6$ with the phosphine in ethanol for $PR_3$=$PMe_2Ph$, and in the presence of zinc in the case of $PMePh_2$ and $PEt_2Ph$. The complexes $W(O)(NCX)_2(PMe_2Ph)_3$ (X=NCO, NCS) were also obtained, by metathesis using NaNCO and KNCS.

Carmona et al.[11] have since prepared the trimethylphosphine analogue $W(O)Cl_2(PMe_3)_3$ in 80% yield by an oxygen-atom abstraction reaction between $WCl_4(PMe_3)_x$ (x=2, 3) and stoichiometric amounts of water, in the presence of excess $PMe_3$ to accept the generated hydrogen chloride.

$$WCl_4(PMe_3)_2 + H_2O + 3\ PMe_3 \longrightarrow W(O)Cl_2(PMe_3)_3 + 2\ HCl.PMe_3 \qquad (3.1)$$

Wilkinson et al.[12] have also independently prepared this compound. Carmona's route has also been employed to synthesise the complexes $W(O)Cl_2(PR_3)_3$ ($PR_3$=$PMe_2Ph$, $PMePh_2$). Parkin[14] reports using a modification of Carmona's route to prepare the dimethylphenylphosphine complex. These air stable materials are purple and possess bands in the IR spectrum in the range 940-960 $cm^{-1}$, assignable to ν(W=O) stretches, with the exception of $W(O)Cl_2(PMe_3)_3$ where a strong absorption due to coordinated $PMe_3$ centred at 940 $cm^{-1}$ is thought to overlap with the ν(W=O) band.

Here we report a new high yield (73%) route to the dimethylphenylphosphine analogue $W(O)Cl_2(PMe_2Ph)_3$, which involves the reaction of $W(O)_2Cl_2$ with excess dimethylphenylphosphine in DME, in the presence of ethylmagnesiumchloride as a reducing agent. This yields a brown oil which on washing with n-pentane gives a solid. Crystallisation from ethanol afforded purple-blue crystals.

### 3.3.2 Solid-State Infrared and Raman Spectroscopy

In the ν(W=O) IR fingerprint region (figure 3.8, top) several strong absorptions are observed, at 957, 940, 915 and 904 $cm^{-1}$. A strong Raman absorbance at 958 $cm^{-1}$ (figure 3.8, bottom) confirms the peak at 957 $cm^{-1}$ in the IR spectrum as being assignable to the ν(W=O) stretch. The ν(W=O) stretches of known tungsten oxo complexes $W(O)X_2(PR_3)_3$ are listed in table 3.6.

Without recourse to crystal structure data (undetermined for the majority), these observations of ν(W=O) stretches fall into two categories: low 940s and high 950s. This suggests that as was observed in the $Mo(O)X_2(PR_3)_3$ systems, the ν(W=O) stretch seems dependent upon the orientation of the alkyl and/or aryl fragments on the phosphine ligands.

In the far-IR spectrum two strong absorptions are observed at 286 and 245 $cm^{-1}$. This is typical of other tungsten oxo phosphine complexes, which likewise show two strong absorptions between 290 and 240 $cm^{-1}$, and suggests that they have the same cis configurational relationship for the halide ligands, as in the molybdenum systems. The Raman spectrum in this region shows absorbances for the complex

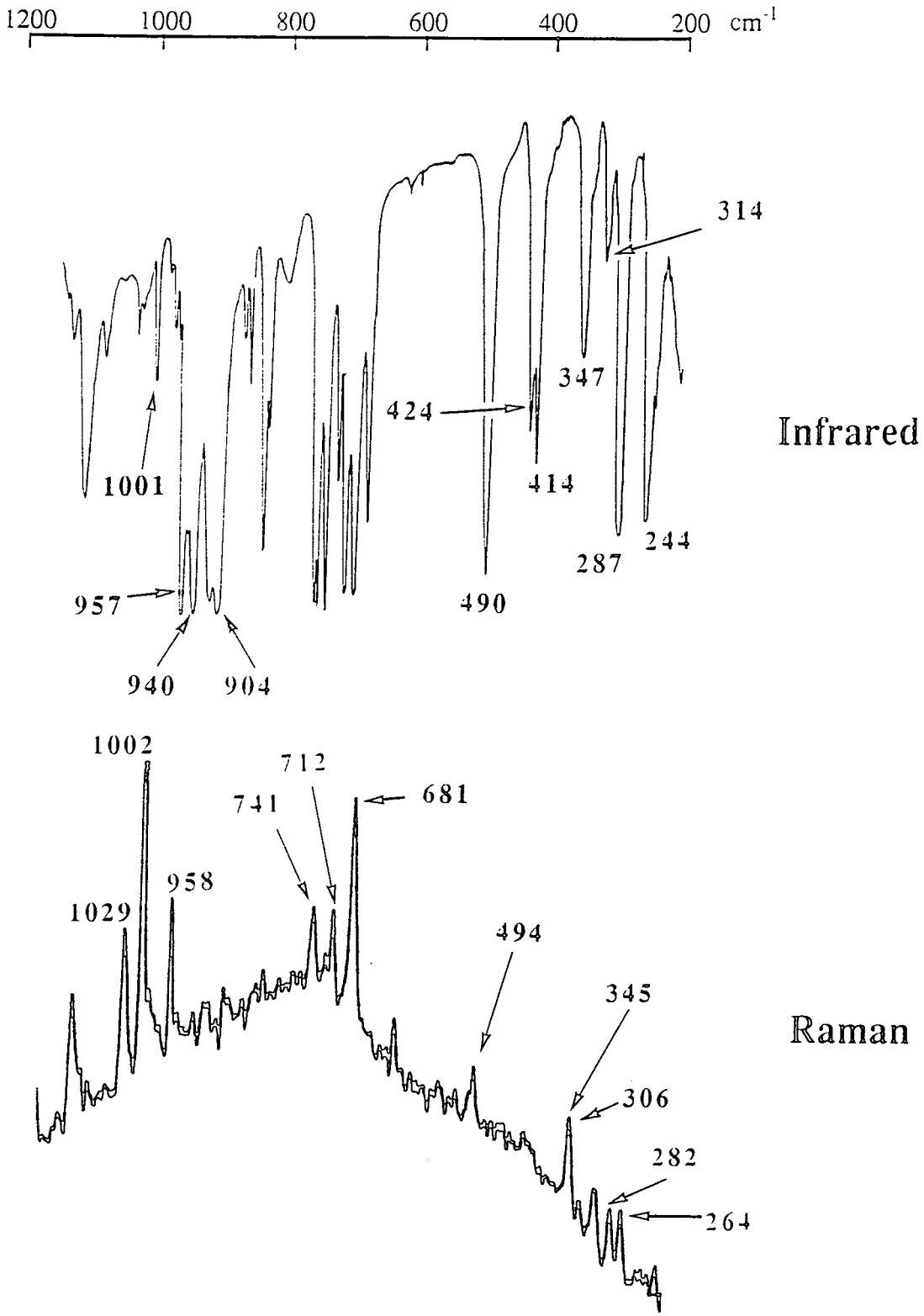


**Figure 3.8:** Solid-state infrared (top) and Raman (bottom) spectra of blue *cis-mer*-$W(O)Cl_2(PMe_2Ph)_3$ (1150 to 200 $cm^{-1}$).

| Complex | ν(W=O) $cm^{-1}$ | Ref. |
|---|---|---|
| $W(O)Cl_2(PMe_2Ph)_3$ | 957 | This work |
| | 960 | 10 |
| $W(O)Cl_2(PMePh_2)_3$ | 950 | 10 |
| $W(O)Cl_2(PEt_2Ph)_3$ | 943 | 10 |
| $W(O)Cl_2(PMe_3)_3$ | ~940† | 11 |
| | 950†* | 12 |
| $W(O)(NCO)_2(PMe_2Ph)_3$ | 945, 939(sh) | 10 |
| $W(O)(NCS)_2(PMe_2Ph)_3$ | 952, 940(sh) | 10 |
| $W(O)Cl_2(P(OMe)_3)_3$ | 955 | 11 |
| $W(O)(NCO)_2(PMe_3)_3$ | 950 | 11 |
| $W(O)(NCS)_2(PMe_3)_3$ | 965, 945 | 11 |
| $W(O)Br_2(PMe_2Ph)_3$ | | 13 |
| $W(O)Br_2(PMePh_2)_3$ | | 13 |
| $W(O)Br_2(PMe_3)_3$ | | |

**Table 3.6:** ν(W=O) stretches of known *cis-mer*-$W(O)X_2(PR_3)_3$ complexes: * very strong, broad peak; † peak obscured by M-$PMe_3$ vibration

$W(O)Cl_2(PMe_2Ph)_3$ at 279 and 264 $cm^{-1}$, suggesting that the higher frequency peak in the IR at 286 $cm^{-1}$ is the only strongly infrared active ν(W-Cl) stretch, the absorbance at 264 $cm^{-1}$ in the Raman presumably representing the symmetric ν(W-Cl) vibration which in the IR spectrum is absent due the lack of a significant change in the dipole moment caused by this vibration.

### 3.3.3 $^1H$ NMR Spectroscopy

The complex $W(O)Cl_2(PMe_2Ph)_3$ is diamagnetic and in $CDCl_3$ the 400 MHz $^1H$ NMR spectrum (figure 3.9) shows two virtually coupled triplets at δ 1.96 and 1.76 ppm with $^2J(PH)$ coupling constants of ca. 4.0Hz respectively, and a doublet at δ 1.36 ppm ($^2J(PH)$= 9.2Hz). The resonance intensity ratios are 1:1:1 and can be rationalised in terms of a meridional arrangement of the phosphine ligands with strong trans P-P coupling and without a plane of symmetry through the P-W-P axis. Hence the chloride atoms should be cis and the stereochemistry as in figure 3.10.

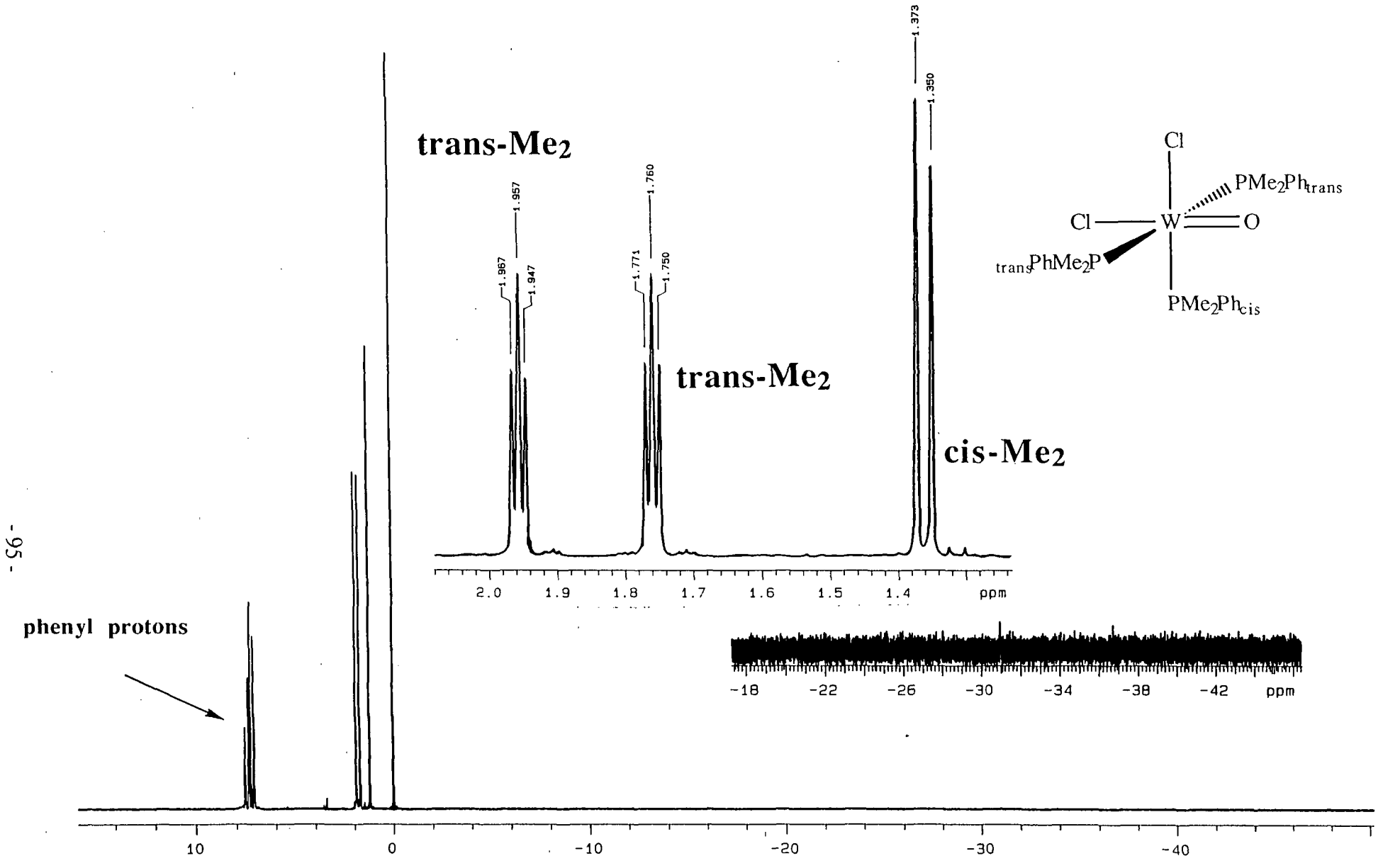


**Figure 3.9:** 400 MHz $^1$H NMR of *cis-mer*-$W(O)Cl_2(PMe_2Ph)_3$ in $CDCl_3$ over the range +15 to -50 ppm.

This arrangement of the phosphine ligands in $W(O)Cl_2(PMe_2Ph)_3$ is consistent with the $^{31}P$ NMR in $C_6D_6$, which shows two singlets, of intensity ratio 2:1 at $\delta$ -14.7 and -23.8 ppm upfield of $H_3PO_4$, respectively, corresponding to the two trans phosphorus atoms and the single cis phosphorus atom in a meridional arrangement. The facial conformation cannot, however, be excluded.

These observations are consistent with those reported by Parkin and co-workers[14] and those of Leigh et al.[15] on *mer*-$WCl_3(PMe_2Ph)_3$, whose data was subsequently found by Parkin[14] to indicate a 20% contamination by *cis-mer*-$W(O)Cl_2(PMe_2Ph)_3$ in the structure of *mer*-$WCl_3(PMe_2Ph)_3$.

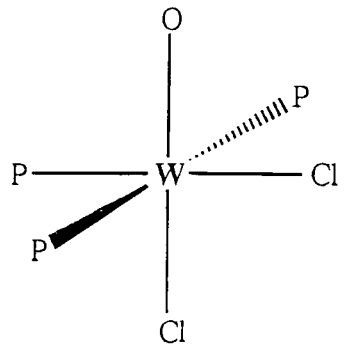


cis-mer

**Figure 3.10:** Stereochemistry in $W(O)Cl_2(PMe_2Ph)_3$ (P= $PMe_2Ph$)

$WCl_3(PMe_2Ph)_3$ was originally prepared by Leigh[15] and later by Parkin[14] by routes involving the reduction of $WCl_4(PMe_2Ph)_3$ with zinc in the absence of added phosphine. The trichloride is paramagnetic, and the most distinctive features in the $^1H$ NMR spectrum were two broad resonances at $\delta$ -24.7 and -16.4 ppm ($C_6D_6$) in the ratio 2:1, assigned to the two sets of methyl groups of the *trans*-$PMe_2Ph$ and *cis*-$PMe_2Ph$ ligands, respectively. Contamination of the trichloride by the oxo complex $W(O)Cl_2(PMe_2Ph)_3$ was revealed by the observation of two triplets at $\delta$ 1.92 and 1.67 ppm and a doublet at $\delta$ 1.31 ppm due to the methyl groups of the $PMe_2Ph$ ligands.

An examination of the upfield region down to $\delta$ -50 ppm revealed that the sample reported in this thesis contained no paramagnetic $WCl_3(PMe_2Ph)_3$[14,15] contaminant.

### 3.3.4 Crystal Structure of $W(O)Cl_2(PMe_2Ph)_3$

The synthesis of *mer*-$WCl_3(PMe_2Ph)_3$[15] represented the first neutral mononuclear tungsten (III) derivative to be structurally characterised by X-ray diffraction. Although the lengths of the three W-P bonds were similar (2.514(1), 2.536(1) and 2.555(1)Å), the three W-Cl bond lengths (2.295(2), 2.437(1) and 2.441(1)Å) were significantly different. Particularly surprising was the fact that the short W-Cl bond length corresponded to one of the chloro ligands that were mutually trans, and not the unique chloro ligand located trans to $PMe_2Ph$. This is surprising since the complex possesses a plane of symmetry meaning that supposedly chemically equivalent W-Cl bonds had substantially different bond lengths (2.437(1) and 2.295(2)Å). The cause of this inequivalence was determined by Parkin[14] to be co-crystallisation of *mer*-$WCl_3(PMe_2Ph)_3$ with ca. 20% of the isostructural *cis-mer*-$W(O)Cl_2(PMe_2Ph)_3$. This is analogous to the apparent lengthening of the Mo=O bond observed in *cis-mer*-$Mo(O)Cl_2(PMe_2Ph)_3$ due to incorporation of chlorine into the oxo site, except that in the case of *mer*-$WCl_3(PMe_2Ph)_3$ there is incorporation of oxo into one of the chloro sites resulting in an apparent shortening of the W-Cl bond.

Here we report the molecular structure of *cis-mer*-$W(O)Cl_2(PMe_2Ph)_3$ that is free of paramagnetic *mer*-$WCl_3(PMe_2Ph)_3$ (as determined by $^1H$ NMR), revealing a W=O bond length of 1.697(7)Å which is considerably shorter than that previously reported by Parkin (1.752(4)Å).[14] However, Parkin refrains from commenting on the significance that his reported W=O bond length is somewhat longer than the average of 1.70Å for monooxotungsten complexes as established by Mayer.[20] Rather he points to the problems associated with the corresponding molybdenum complexes, hesitating to attach any significance to its abnormal length, and additionally does not state whether or not this W=O bond length is associated with an observation of the paramagnetic *mer*-$WCl_3(PMe_2Ph)_3$ contaminant in the upfield region of the $^1H$ NMR spectrum. He prefers to concentrate on the fact that the trichloride itself is contaminated with ca. 20% of the oxo complex.

| | | | |
|---|---|---|---|
| W - P(1) | 2.480(3) | P(2) - W - P(1) | 95.0(1) |
| W - P(2) | 2.534(3) | P(3) - W - P(1) | 93.9(1) |
| W - P(3) | 2.541(3) | P(3) - W - P(2) | 170.7(1) |
| | | | |
| W - Cl(1) | 2.539(3) | O - W - Cl(1) | 170.6(3) |
| W - Cl(2) | 2.462(3) | O - W - Cl(2) | 104.8(3) |
| | | | |
| W - O | 1.697(7) | O - W - P(1) | 93.1(3) |
| | | O - W - P(2) | 90.8(3) |
| P(1) - C(10) | 1.807(12) | O - W - P(3) | 91.3(3) |
| P(1) - C(16) | 1.823(13) | | |
| P(1) - C(17) | 1.822(12) | Cl(1) - W - P(1) | 77.5(1) |
| P(2) - C(20) | 1.833(12) | Cl(1) - W - P(2) | 89.5(1) |
| P(2) - C(26) | 1.851(11) | Cl(1) - W - P(3) | 89.9(1) |
| P(2) - C(27) | 1.873(13) | Cl(2) - W - P(1) | 162.0(1) |
| P(3) - C(30) | 1.822(13) | Cl(2) - W - P(2) | 85.6(1) |
| P(3) - C(36) | 1.841(12) | Cl(2) - W - P(3) | 85.1(1) |
| P(3) - C(37) | 1.847(12) | | |
| | | Cl(2) - W - Cl(1) | 84.6(1) |
| C(10) - P(1) - W | 114.2(4) | | |
| C(16) - P(1) - W | 116.3(4) | C(16) - P(1) - C(10) | 103.1(6) |
| C(17) - P(1) - W | 118.3(4) | C(17) - P(1) - C(10) | 103.6(5) |
| C(20) - P(2) - W | 115.8(4) | C(17) - P(1) - C(16) | 98.9(6) |
| C(26) - P(2) - W | 116.4(4) | C(26) - P(2) - C(20) | 104.0(5) |
| C(27) - P(2) - W | 113.8(4) | C(27) - P(2) - C(20) | 101.8(6) |
| C(30) - P(3) - W | 118.0(4) | C(27) - P(2) - C(26) | 103.2(6) |
| C(36) - P(3) - W | 116.1(4) | C(36) - P(3) - C(30) | 105.5(6) |
| C(37) - P(3) - W | 113.2(5) | C(37) - P(3) - C(30) | 99.8(6) |
| | | C(37) - P(3) - C(36) | 101.9(6) |

**Table 3.7:** Selected bond lengths (Å) and angles (°) for *cis-mer*-$W(O)Cl_2(PMe_2Ph)_3$

Selected bond lengths and angles are presented in table 3.7, and a comparison with those reported by Parkin, along with the corresponding values for *mer*-$WCl_3(PMe_2Ph)_3$[15], Chatt and Enemark blue forms of *cis-mer*-$Mo(O)Cl_2(PMe_2Ph)_3$ and *mer*-$MoCl_3(PMe_2Ph)_3$, is made in table 3.8. Figures 3.11 to 3.13 represent ORTEP and 'ball and stick' drawing comparisons of the corresponding high and low frequency stretching forms of *cis-mer*-$M(O)Cl_2(PMe_2Ph)_3$, and additionally *mer*-$MCl_3(PMe_2Ph)_3$, where M= Mo and W.

It is immediately evident from both inspection of table 3.8 and the molecular drawings that the structure reported in this thesis of pure blue $W(O)Cl_2(PMe_2Ph)_3$ represents a new, different crystal modification of this complex. The structure previously reported by Parkin[14] differs dramatically from that described here, in particularly in the plane defined by the atoms O, Cl(1), Cl(2) and P(1). For example, the Cl(2)-W-P(1) and O-W-Cl(2) bond angles of 175.2° and 97.8(2)° respectively, observed in Parkin's determination correspond to values of 162.0(1)° and 104.8(3)° reported in this thesis. Yet more significant is the finding that a comparison with the structures reported for the molybdenum analogues reveals that there exists a parallel relationship between the molybdenum and tungsten systems. The conformations in the two blue forms of *cis-mer*-$Mo(O)Cl_2(PMe_2Ph)_3$ are found to resemble those in the tungsten complexes, and once again the structure reported by Parkin shows conformational similarities to those seen in the isostructural trichloride species. Moreover, the ν(W=O) stretching frequency of 957 $cm^{-1}$ observed in the blue form reported in this thesis compares favourably with the value of 955 $cm^{-1}$ seen for the ν(Mo=O) stretch in the Chatt blue form of *cis-mer*-$Mo(O)Cl_2(PMe_2Ph)_3$ which adopts a similar conformation of its alkyl and aryl fragments on the phosphine ligands The Enemark blue molybdenum complex which adopts a different phosphine conformation exhibits a ν(Mo=O) stretch at the considerably lower value of 941 $cm^{-1}$. This suggests that a link exists between the ν(M=O) stretching frequency and the orientation adopted by the organic substituents on the phosphines. Unfortunately, Parkin neglects to report the ν(W=O) stretch observed in his form, but in the light of the available evidence, it seems unlikely that he would have been able to reproduce a stretch at 960 $cm^{-1}$ corresponding to that previously reported by Chatt.[10] In

| | *mer*-$MCl_3(PMe_2Ph)_3$ | | *cis-mer*-$M(O)Cl_2(PMe_2Ph)_3$ | | | |
|---|---|---|---|---|---|---|
| | | | 'Chatt-like' | | 'Enemark-like' | |
| | M= Mo | M= W | M= Mo | M= W | M= Mo | M= W |
| W - O/W - Cl | 2.400(1) | 2.295(2) | 1.663(2) | 1.697(7) | 1.682(3) | 1.752(4) |
| W - Cl(1) | 2.427(1) | 2.437(1) | 2.538(1) | 2.539(3) | 2.523(1) | 2.493(2) |
| W - Cl(2) | 2.420(1) | 2.441(1) | 2.454(1) | 2.462(3) | 2.478(3) | 2.478(3) |
| W - P(1) | 2.572(1) | 2.514(1) | 2.491(1) | 2.480(3) | 2.484(3) | 2.483(2) |
| W - P(2) | 2.567(1) | 2.555(1) | 2.542(1) | 2.534(3) | 2.519(3) | 2.538(2) |
| W - P(3) | 2.610(1) | 2.536(1) | 2.539(1) | 2.541(3) | 2.530(3) | 2.508(2) |
| $O/Cl_{ax}$ - W - Cl(1) | 174.8(1) | 175.0(1) | 169.3(1) | 170.6(3) | 170.0(3) | 172.8(2) |
| $O/Cl_{ax}$ - W - Cl(2) | 91.1(1) | 91.4(1) | 105.2(1) | 104.8(3) | 97.6(3) | 97.8(2) |
| P(1) - W - Cl(2) | 177.4(1) | 178.2(1) | 162.4(1) | 162.0(1) | 177.8(1) | 175.2(1) |
| P(2) - W - P(3) | 167.2(1) | 165.0(1) | 171.2(1) | 170.7(1) | 160.4(1) | 160.5(1) |

**Table 3.9:** A comparison of selected bond lengths (Å) and angles (°) for the blue molybdenum and tungsten complexes *cis-mer*-$M(O)Cl_2(PMe_2Ph)_3$ and *mer*-$MCl_3(PMe_2Ph)_3$.

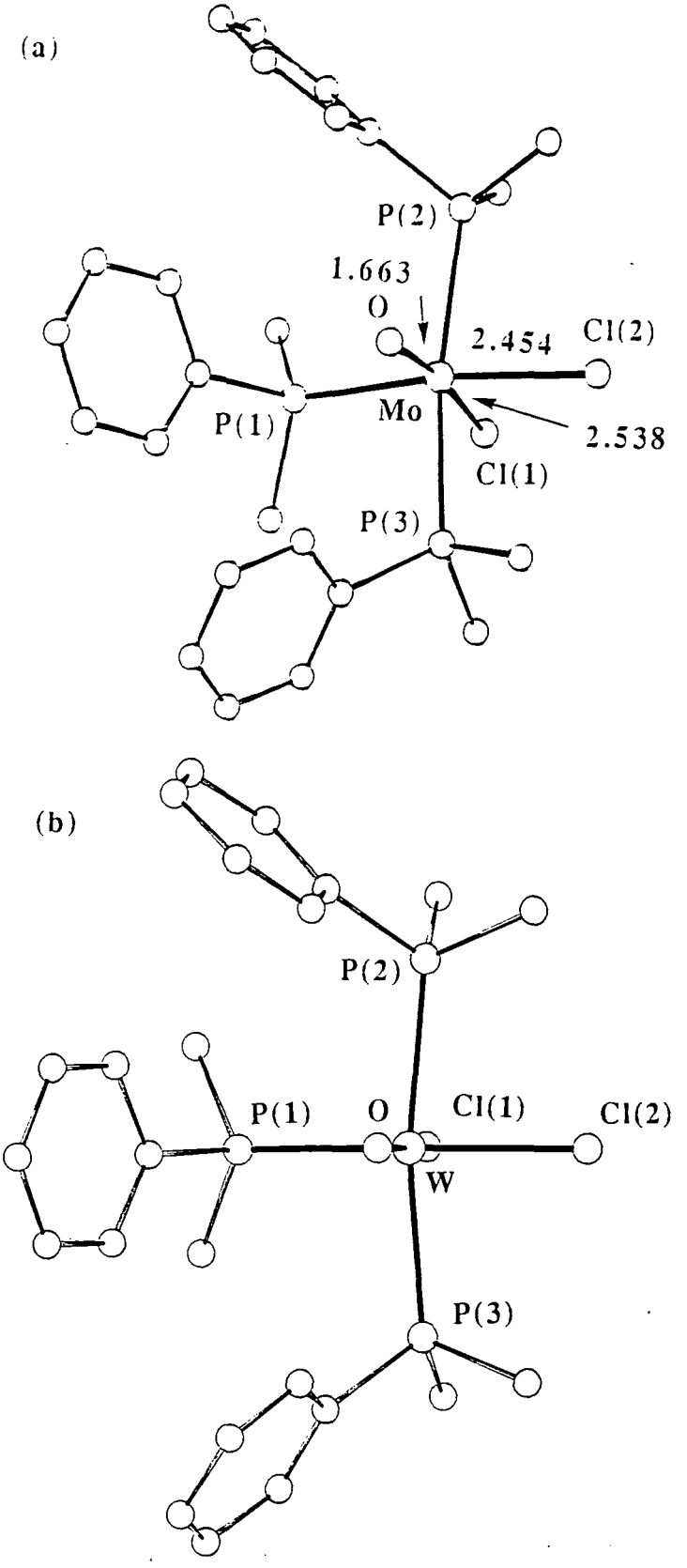


**Figure 3.11:** Molecular drawing comparisons of the 'Chatt-like' molybdenum and tungsten complexes *cis-mer*-$M(O)Cl_2(PMe_2Ph)_3$.

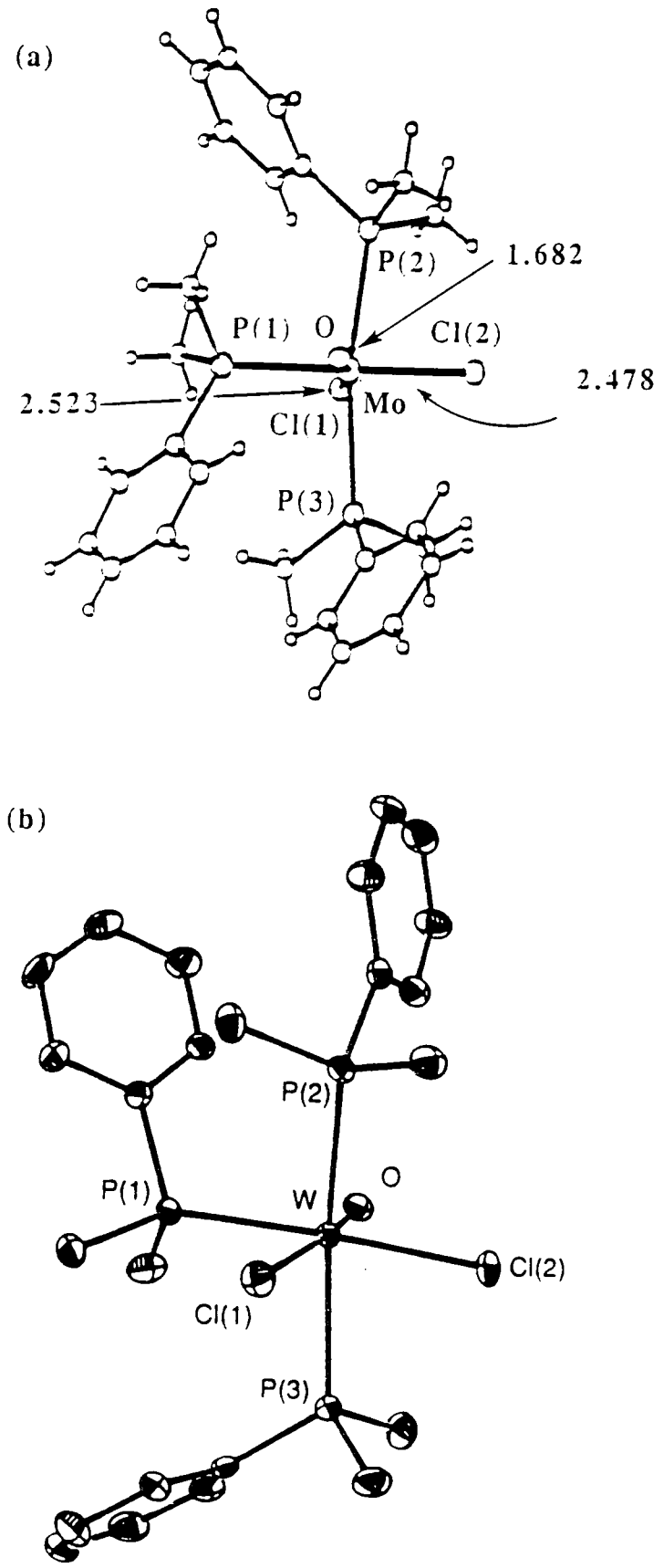


**Figure 3.12:** Molecular drawing comparisons of the 'Enemark/Parkin-like' molybdenum and tungsten complexes *cis-mer*-$W(O)Cl_2(PMe_2Ph)_3$.

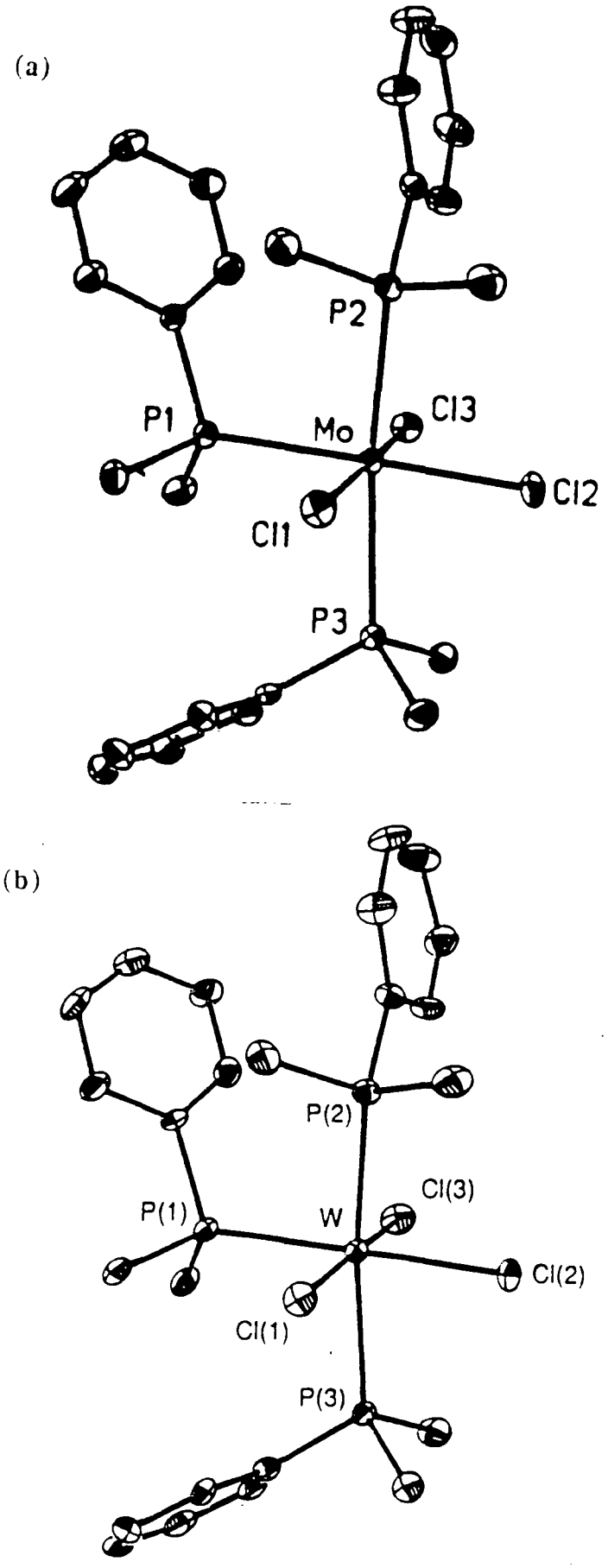


**Figure 3.13:** ORTEP drawing comparisons of the molybdenum and tungsten complexes *mer*-$MCl_3(PMe_2Ph)_3$.

view of his findings in the *cis-mer*-$Mo(O)Cl_2(PMe_2Ph)_3$ system[17] of a blue form exhibiting a ν(Mo=O) stretch at 941 $cm^{-1}$, which led to the suggestion that Chatt's original assignment of a Mo=O stretch at 955 $cm^{-1}$ was incorrect, it seems odd that he fails to report the stretching frequency observed in his form, when if, if it were to occur in the low 940s, as indicated from the available data, this should strengthen the position of his argument.

## 3.4 The Characterisation of $Mo(O)Cl_2(PEt_2Ph)_3$

### 3.4.1 Introduction: Chatt's Original Observations

In 1971 the green complex *mer*-$Mo(O)Cl_2(PEt_2Ph)_3$ was shown by X-ray diffraction to possess cis chloride ligands[21] and not trans chlorides as Chatt had originally postulated on the basis of the differences observed in the low frequency region of the IR spectrum compared to that of the already structurally determined blue *cis-mer*-$Mo(O)Cl_2(PMe_2Ph)_3$ species. A comparison of selected bond lengths and angles (table 3.9) revealed both differences in the overall coordination environments about the molybdenum centre and a substantial variation in the Mo=O bond lengths, the diethylphenyl complex having a significantly longer bond length of 1.803(11)Å compared to 1.676(7)Å in the dimethylphenyl complex.

| | Blue *cis-mer*-$Mo(O)Cl_2(PMe_2Ph)_3$[5] | Green *cis-mer*-$Mo(O)Cl_2(PEt_2Ph)_3$[21] |
|---|---|---|
| Mo-O | 1.676(7) | 1.803(11) |
| Mo-$Cl(1)_{trans}$ | 2.551(3) | 2.426(6) |
| Mo-$Cl(2)_{cis}$ | 2.464(3) | 2.479(5) |
| Mo-P(1) | 2.500(3) | 2.521(5) |
| Mo-P(2) | 2.541(3) | 2.582(6) |
| Mo-P(3) | 2.558(3) | 2.556(6) |
| O-Mo-Cl(2) | 105.7(3) | 98.8(4) |
| P(1)-Mo-Cl(2) | 162.4(1) | 167.5(2) |

**Table 3.9:** Selected bond lengths (Å) and angles (°) for blue *cis-mer*-$Mo(O)Cl_2(PMe_2Ph)_3$ and green *cis-mer*-$Mo(O)Cl_2(PEt_2Ph)_3$

### 3.4.2 Two Different Green Forms of $Mo(O)Cl_2(PEt_2Ph)_3$

Although it has been established that the abnormal Mo=O bond length in the green *cis-mer*-$Mo(O)Cl_2(PMe_2Ph)_3$ species is due to trichloride co-crystallisation, the chronicle has taken yet another turn with the recent discoveries in the case of $Mo(O)Cl_2(PEt_2Ph)_3$. Two green samples of $Mo(O)Cl_2(PEt_2Ph)_3$, synthesized according to the literature preparation[1] (equation 3.2), were supplied by S. Balakvmar of the University of North London for spectroscopic characterisation. Crystal structures performed at the University of North London have revealed two forms with different sets of orientations of the alkyl and aryl substituents on the phosphine ligands (figure 3.15). This is accompanied by a slight but significant difference in their ν(Mo=O) stretching frequencies (938 and 940 $cm^{-1}$, figure 3.14), yet both still possess abnormally long Mo=O bond lengths.

$$MoCl_5 \xrightarrow[-HCl]{EtOH} \text{'Brown oil'} \xrightarrow[EtOH]{\text{xs } PEt_2Ph} \begin{matrix}\text{Green} \\ Mo(O)Cl_2(PEt_2Ph)_3 \\ \nu(Mo{=}O)\ 938 \text{ or } 940\ cm^{-1}\end{matrix} \qquad (3.2)$$

What is particularly significant is that *both* forms *do not* possess a plane of symmetry containing the O, Cl(1), Cl(2) and P(1) atoms, and so are not simply just forms that parallel the 'Chatt-like' ($C_s$) and 'Enemark-like' ($C_1$) phosphine orientations in the two blue complexes of *cis-mer*-$Mo(O)Cl_2(PMe_2Ph)_3$.

The form that exhibits a ν(Mo=O) stretch at 940 $cm^{-1}$ corresponds to the structure originally reported by Chatt[21] for which he recorded a 940 $cm^{-1}$ stretch, and adopts phosphine orientations (figure 3.15 (b)) that are similar to those observed in the Enemark blue form of *cis-mer*-$Mo(O)Cl_2(PMe_2Ph)_3$ (ν(Mo=O) 941 $cm^{-1}$). The ν(Mo=O) 938 $cm^{-1}$ species shows a unique, and previously not observed orientation of the phosphine ligands (figure 3.15 (a)). Whereas in the 940 $cm^{-1}$ form the aryl substituents on the trans-$PEt_2Ph$ ligands are orientated such that they are disposed in an

Green $\upsilon$(Mo=O) 938 and 940 $cm^{-1}$

$Mo(O)Cl_2(PEt_2Ph)_3$

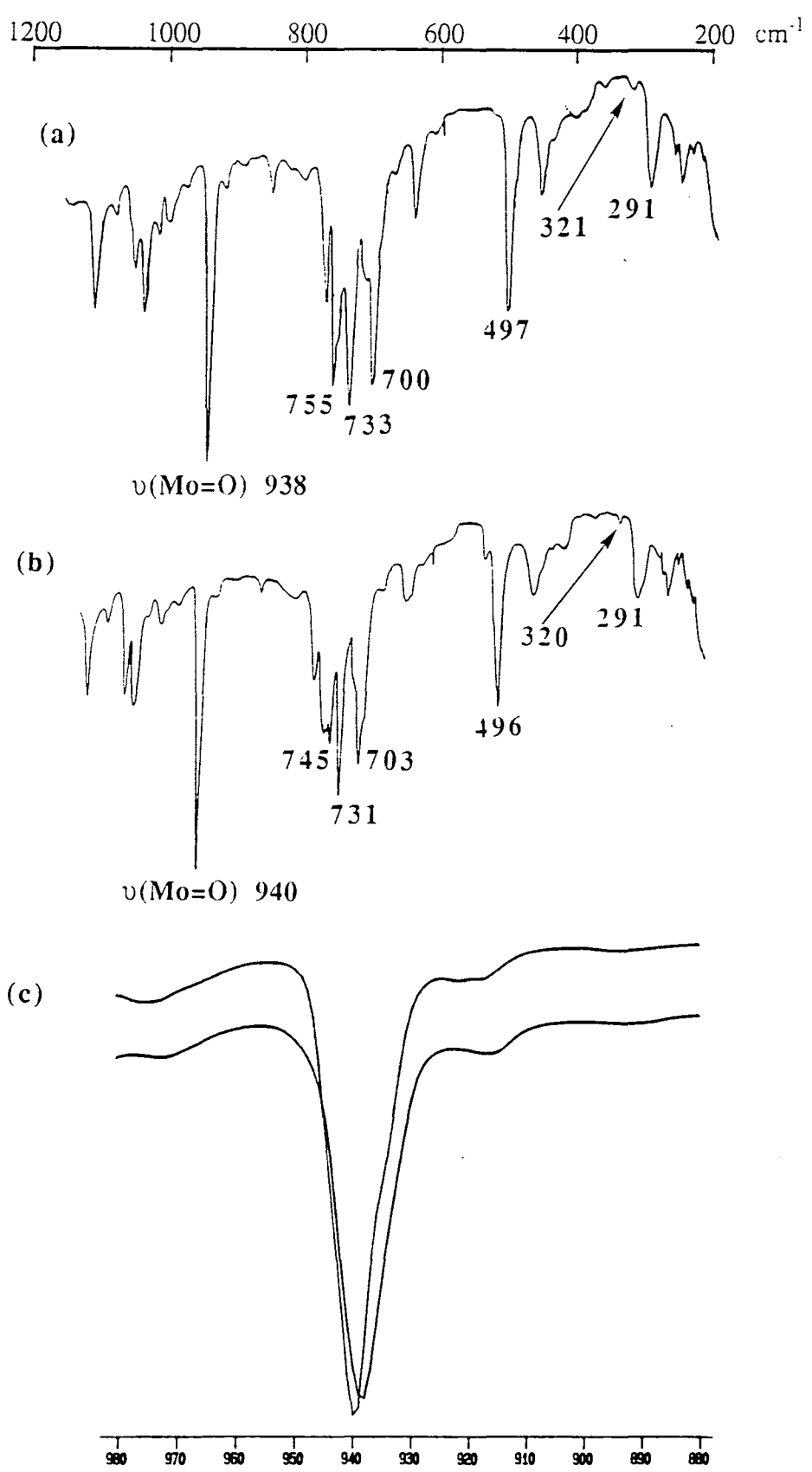


**Figure 3.14:** Infrared spectra (nujol mull) of the green $\nu$(Mo=O) 938 and 940 $cm^{-1}$ forms of *cis-mer*-$Mo(O)Cl_2(PEt_2Ph)_3$ over the range (a,b) 1150 to 200 $cm^{-1}$ and (c) 980 to 880 $cm^{-1}$ highlighting a comparison of the $\nu$(Mo=O) stretching region.

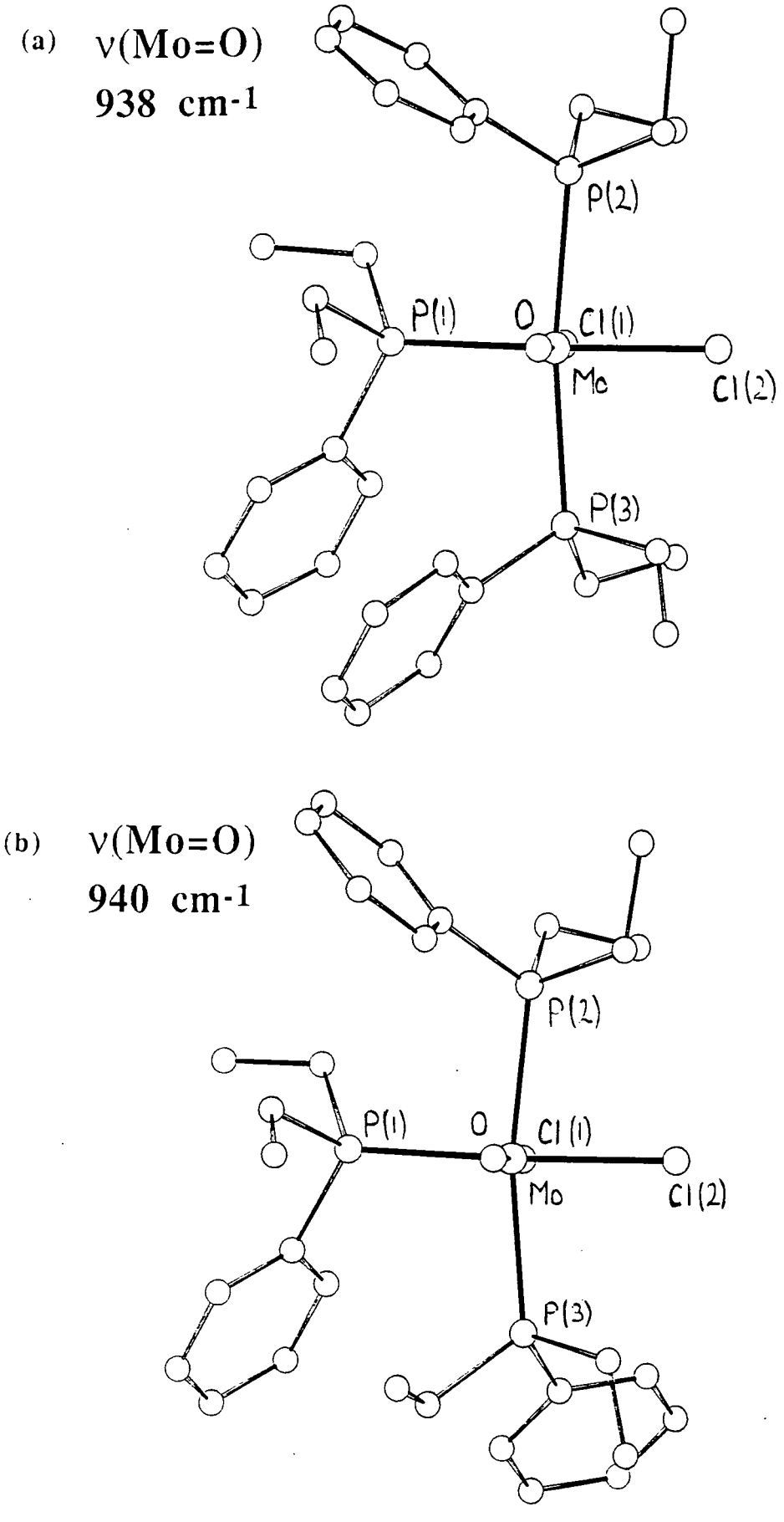


**Figure 3.15:** Molecular structure comparisons of the 938 and 940 $cm^{-1}$ forms of green *cis-mer*-$Mo(O)Cl_2(PEt_2Ph)_3$.

'anti' manner, in the 938 $cm^{-1}$ species these aryl groups are now 'syn' to one another. The two forms represent a rotamer pair.

Particular significant though is the fact that both forms possess abnormally long Mo=O bonds; 1.871(5)Å in the 938 $cm^{-1}$ form and 1.857(6)Å in the 940 $cm^{-1}$ form.[22] This compares with 1.803(11)Å originally reported by Chatt.[5] The abnormal bond lengths have previously been ascribed to the manifestation of trichloride contamination, and thus this raises the question as to whether the trichloride itself exists in two forms where the phosphine substituents adopt different orientations that parallel those observed in the green oxo forms.

However, the evidence for a trichloride impurity resulting in the co-occupancy of the oxo position due to the Mo-$Cl_{axial}$ bond of the trichloride is not as strong in the case of the green forms of $Mo(O)Cl_2(PEt_2Ph)_3$ and remains inconclusive. Both IR and $^1H$ NMR spectroscopy do not confirm whether or not a paramagnetic trichloride impurity is present. In the IR spectrum only a very weak absorption at 320 $cm^{-1}$, typically where a ν(Mo-Cl) stretch for a trichloride is expected, is observed. The 400 MHz $^1H$ NMR spectra in $CDCl_3$ of the two green forms are near identical, consisting of a rather complicated series of multiplets. In the upfield region of the spectrum where the presence of a paramagnetic impurity is typically expected to be observed there is no such evidence for any broad resonances, although in the methyl and methylene region there are a few broad resonances of low variable intensity which suggest the presence of a possible impurity in the samples. However, considering the fact that the level of co-crystallised trichloride required to produce an apparent Mo=O bond length in the range 1.80 to 1.85Å is likely to be only ca. 4% (as estimated from the evidence in the series of green $Mo(O)Cl_2(PMe_2Ph)_3$ species)[17], together with the diastereotopic nature of the methylene and methyl protons, then such resonances due to a paramagnetic impurity are likely to be broadened to such an extent that they may not be distinguishable from the background noise.

This leaves open the possibility that an internal disorder, for example involving the trans-chloro and oxo ligands could account for the elongated Mo=O bonds.

Evidence in support of this postulation may be found in the observed value reported for the Mo-$Cl_{trans\text{-}to\text{-}O}$ bond length which is substantially shorter than expected.[22]

## 3.5 Infrared Spectroscopic Evidence Supporting the Existence of Different Phosphine Orientations as Established by X-Ray Diffraction

With all the evidence now accumulated on the series of complexes $M(O)X_2(PMe_2Ph)_3$ (M= W, X= Cl; M= Mo, X= Cl, Br, I) a comparison can be made of the IR spectra in order to establish whether or not a link exists between the orientations adopted by the phosphine ligands (as established by X-ray structure determination) and the pattern of bands observed in the IR spectra. Those which adopt an 'Enemark-like' configuration showing $C_1$ molecular symmetry are depicted in figure 3.16 and those that are 'Chatt-like' ($C_s$) are shown in figure 3.17.

Inspection of the general features associated with the spectra of the complexes of the series $Mo(O)X_2(PMe_2Ph)_3$ (X= Cl, Br, I) exhibiting ν(Mo=O) stretches in the 940 $cm^{-1}$ region (figure 3.16) show remarkably close similarities, and likewise for the series of complexes $M(O)X_2(PMe_2Ph)_3$ (M= W, X= Cl; M= Mo, X= Cl, Br), where a mid 950s ν(Mo=O) stretch is observed (figure 3.17).

This indicates that a crystal structure determination may no longer be necessary to predict the likely orientation of the phosphine ligands.

The two green forms of $Mo(O)Cl_2(PEt_2Ph)_3$ have been shown by X-ray diffraction to adopt 'syn' and 'anti' orientations of the aryl group on the trans-$PEt_2Ph$ ligands, and this difference is realised both in the slight difference in the ν(Mo=O) stretches (938 and 940 $cm^{-1}$, figures 3.14 and 3.18 (a)) and in the other regions of the IR spectra.

## 3.6 Summary

In this chapter the existence of additional examples of distortional isomerism have been established. For example, the blue $W(O)Cl_2(PMe_2Ph)_3$ complex has also been

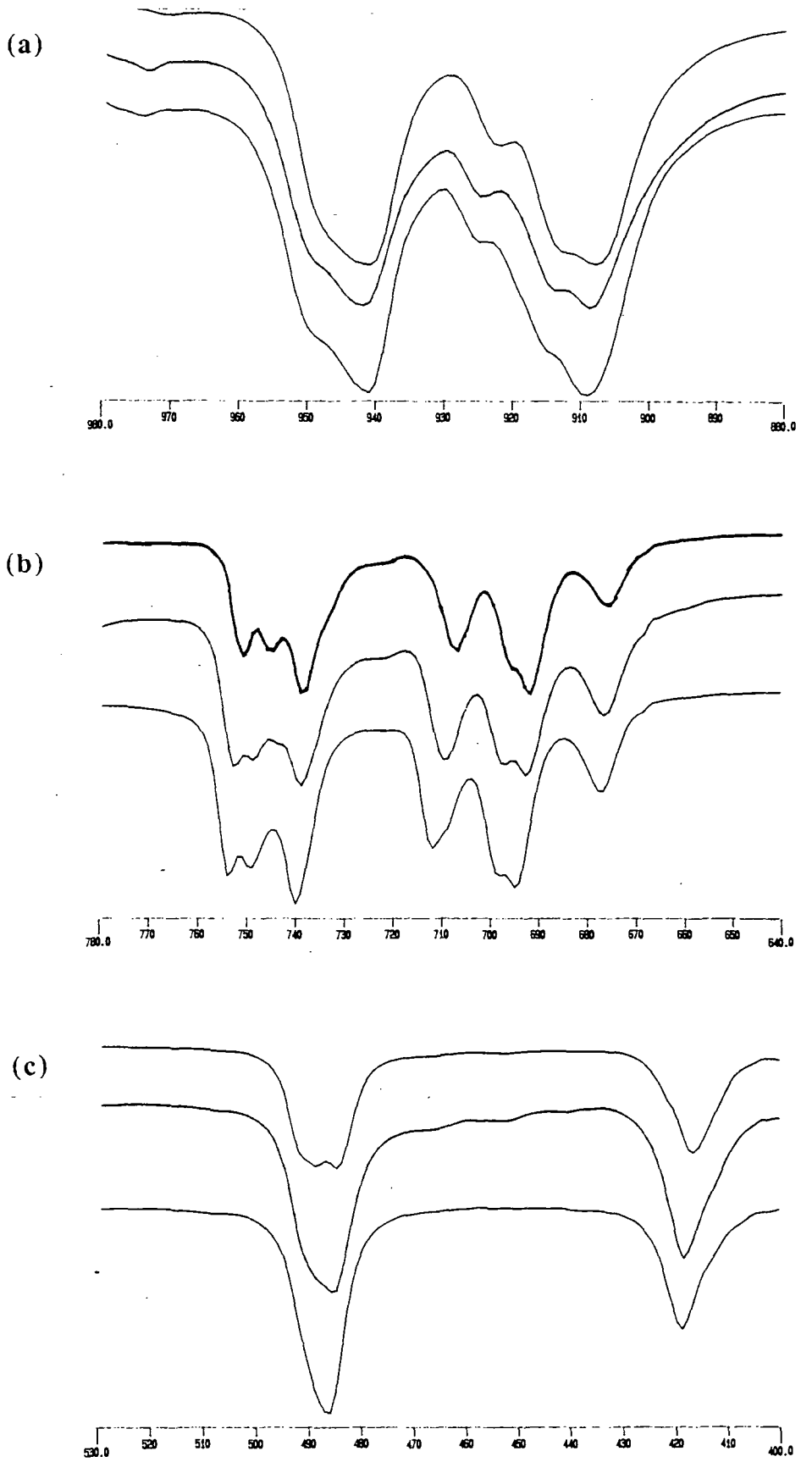


**Figure 3.16:** Solid-state infrared comparisons of 'Enemark-like' $Mo(O)I_2(PMe_2Ph)_3$ (top trace), $Mo(O)Br_2(PMe_2Ph)_3$ (middle), and $Mo(O)Cl_2(PMe_2Ph)_3$ (bottom) over the regions (a) 980-880 $cm^{-1}$, (b) 780-640 $cm^{-1}$, and (c) 530-400 $cm^{-1}$

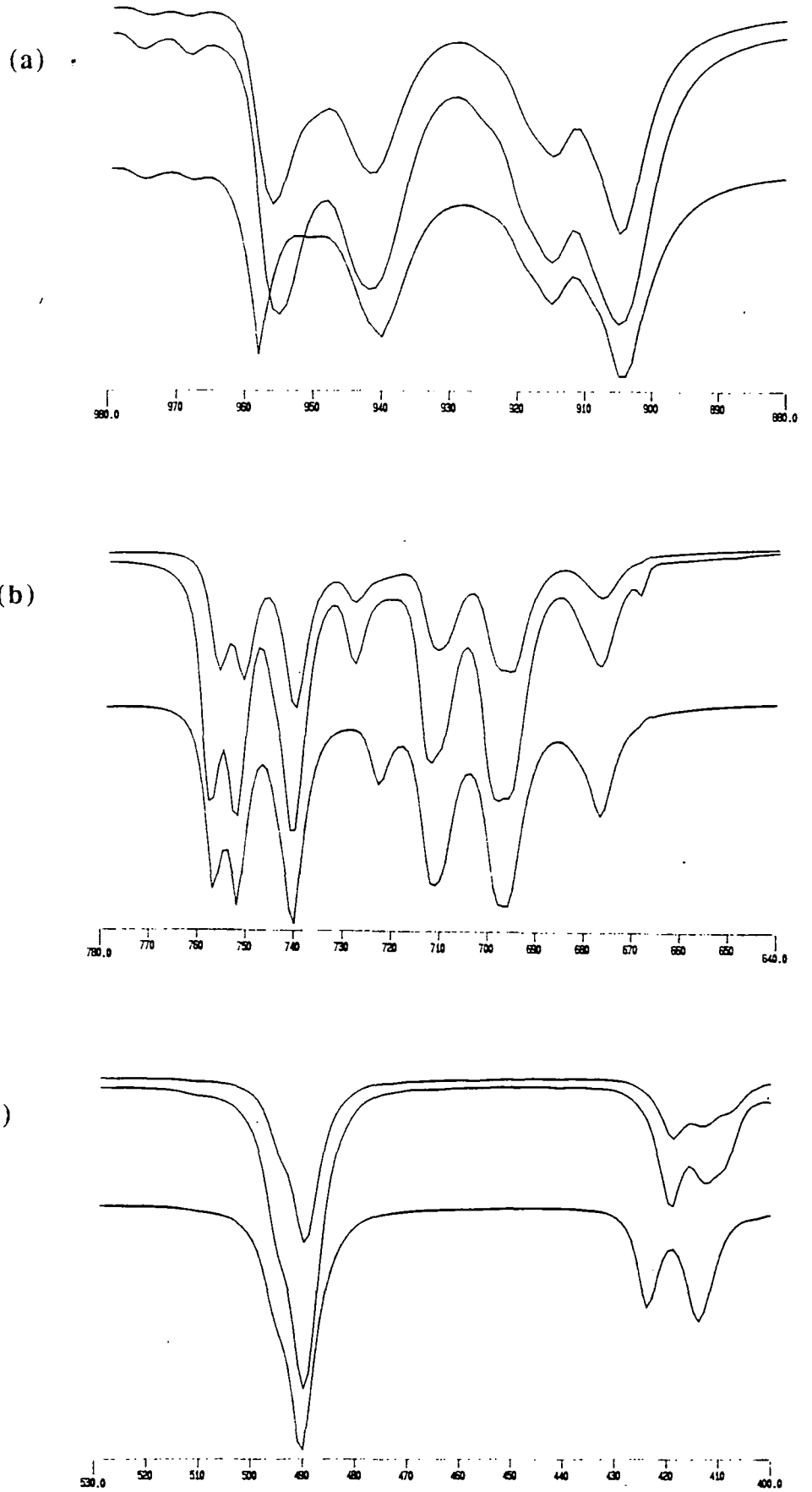


**Figure 3.17:** Solid-state infrared comparisons of 'Chatt-like' $Mo(O)Br_2(PMe_2Ph)_3$ (top trace), $Mo(O)Cl_2(PMe_2Ph)_3$ (middle), and $W(O)Cl_2(PMe_2Ph)_3$ (bottom) over the regions (a) 980-880 $cm^{-1}$, (b) 780-640 $cm^{-1}$, and (c) 530-400 $cm^{-1}$

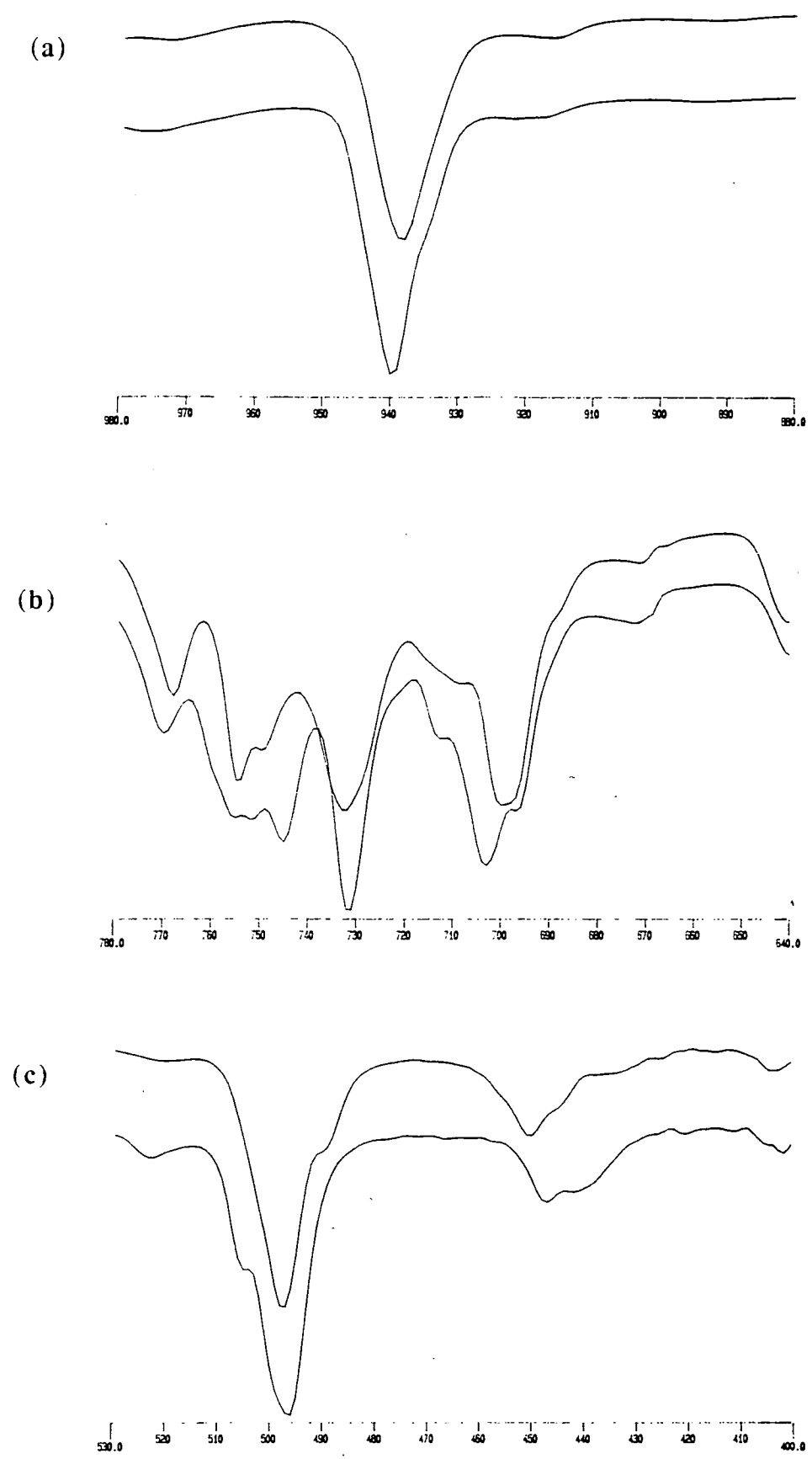


**Figure 3.18:** Solid-state infrared comparisons of the green ν(Mo=O) 938 (top trace), and 940 $cm^{-1}$ (bottom) species $Mo(O)Cl_2(PEt_2Ph)_3$.over the regions (a) 980-880 $cm^{-1}$, (b) 780-640 $cm^{-1}$, and (c) 530-400 $cm^{-1}$

found to exist in two forms which have their parallel counterparts in the molybdenum system.

Furthermore, the existence of two green forms of $Mo(O)Cl_2(PEt_2Ph)_3$, with similar but significantly different ν(W=O) stretches and whose orientations of the organic substituents on the phosphine ligands show close similarities, has led to the speculation for the conceivable existence of more than one form of the potential trichloride contaminant. In addition it has been established that a link exists between the phosphine orientations and the ν(M=O) stretching frequency.

## 3.7 References


1. A.V. Butcher, J. Chatt, *J. Chem. Soc (A)*, **1970**, 2652.
2. Raman spectrum run courtesy of Dr. D.N. Waters.
3. K. Nakamoto, *"Infrared and Raman Spectra of Inorganic and Coordination Compounds"*, Wiley & Sons, New York, 3rd ed., 1978, p270-274 and references therein.
4. P.J. Desrochers, K.W. Nebesny, M.J. LaBarre, S.E. Lincoln, T.M. Loehr, J.H. Enemark, *J.Amer. Chem. Soc.*, 1991, **113**, 9193.
5. (a) Lj. Manojlovic-Muir, *Chem. Commun.* , **1971**, 147; (b) *J. Chem. Soc (A)*, **1971**, 2796.
6. P.R. Brookes, B.L. Shaw, *J. Chem. Soc.*, **1967**, 1079.
7. J.M. Jenkins, B.L. Shaw, *J. Chem. Soc.*, **1966**, 1407.
8. J.M. Jenkins, B.L. Shaw, *Proc. Chem. Soc.*, **1963**, 291.
9. I. Leden, J. Chatt, *J.Chem. Soc.*, **1955**, 2936.
10. A.V. Butcher, J. Chatt, G.J. Leigh, P.L. Richards, *J. Chem. Soc. Dalton Trans.*, **1972**, 1064.
11. E. Carmona, L. Sanchez, M.L. Poveda, R.A. Jones, J.G. Hefner, *Polyhedron*, 1983, **2**, 797.
12. K.W. Chia, D. Lyons, G. Wilkinson, *Polyhedron*, 1983, **2**, 803.
13. F.A. Cotton, S.K. Mandal, *Inorg. Chim. Acta.*, 1992, **194**, 179.
14. K. Yoon, G. Parkin, D.L. Hughes, G.J. Leigh, *J. Chem. Soc. Dalton Trans.*, **1992**, 769.

15. A. Hills, D.L. Hughes, G.J. Leigh, R. Prieto-Alcón, *J. Chem. Soc. Dalton Trans.*, **1991**, 1515.

16. F.A. Cotton, M.P. Diebold, W.J. Roth, *Inorg. Chem.*, 1987, **26**, 2848.

17. K. Yoon, G. Parkin, A.L. Rheingold, *J. Amer. Chem. Soc.*, 1991, **113**, 1437; *J. Amer. Chem. Soc.*, 1992, **114**, 2210; G. Parkin, *Acc. Chem. Res.*, 1992, **25**, 455.

18. W.P. Griffith, *Coord. Chem. Rev.*, 1970, **5**, 459; Z. Dori, *Prog. Inorg. Chem.*, 1981, **28**, 239.

19. F.M. Su, C. Cooper, S.J. Geib, A.L. Rheingold, J.M. Mayer, *J. Amer. Chem. Soc.*,1986, **108**, 3545.

20. J.M. Mayer, *Inorg. Chem.*, 1988, **27**, 3899.

21. J. Chatt, Lj. Manojlovic-Muir, K.W. Muir, *J. Chem. Soc. Chem. Comm.*, **1971**, 655; Lj. Manojlovic-Muir, K.W. Muir, *J. Chem. Soc. Dalton Trans.*, **1972**, 686.

22. Private communication with M. McPartlin.

# CHAPTER FOUR

## Seven Coordinate Oxo-Halides of Niobium

## 4.1 Introduction

In recent years a number of studies have indicated that a new type of isomerism may exist.[1-4] A fundamental idea of isomerism is that there exists a 'real' difference in the three-dimensional arrangement of atoms in a molecule. That is a topological change, not just some internal bond stretch is required. However, there appears to be an increasing body of evidence which supports the existence of molecules in the solid-state and also in solution which interconvert with varying ease, and whose only structural difference is a dramatic difference in the length of one or more bonds. It is unclear whether the existence of the two bond-stretch isomer pairs in the solid-state is simply due to a packing effect or reveals some more fundamental phenomenon.

Very few examples of a fully characterised matched pair of complexes exhibiting bond-stretch isomerism have been published. One such example is from the work of Wieghardt and co-workers[7] of blue and green forms of the hexafluorophosphate salt of the paramagnetic cation $[LW(O)Cl_2]^+$ (L=$NR_3$=1,4,7-trimethyl-1,4,7-triazacyclononane) (figure 1.8). The two isomers are stable both in the solid-state and in solution and differ mainly in the length of the W=O bond. This case thus indicates that distortional isomerism is not solely a solid-state effect arising from crystal packing forces. The elusiveness of suitable crystals of isomer pairs with exactly the same organophosphine ligand meant that the highly significant differences in the Mo=O bond length was for many years classified as 'distortional' isomerism.

## 4.2 Green and Yellow Forms of $Nb(O)Cl_3(PMe_3)_3$

Two structurally isomorphous forms of $Nb(O)Cl_3(PMe_3)_3$ exist.[9,10] The yellow α-$Nb(O)Cl_3(PMe_3)_3$ form, first synthesized by T.P. Kee and R.M. Sorrell[9], is selectively crystallised in toluene from an α,β mix originating from the treatment of $[Nb(O)Cl_3]_n$ with neat $PMe_3$ for ca. 20h. (scheme 4.1). This form is found to possess a Nb-O bond length of 1.781(6)Å[9] (slightly longer than the Nb=O bond distances found in other niobium oxo complexes (table 4.5)). Dissolution of the crude α,β mix arising

from the treatment of $[Nb(O)Cl_3]_n$ or $[Nb(O)Cl_3(CH_3CN)_2]$ with $PMe_3$ in dichloromethane leads to the selective crystallisation of the β-isomer, originally isolated by A. Shaw.[10] Subsequent X-ray determination of its structure revealed an exceptionally long Nb=O bond distance of 2.087(5)Å[9b], the lengthening of the Nb-O bond being accompanied by a small but significant contraction in the Nb-Cl distances by an average of 0.022Å. In β-$Nb(O)Cl_3(PMe_3)_3$ the Nb-O bond length is comparable to the sum of the covalent radii of niobium and oxygen (2.1Å)[11] and on the face of it, initially suggests that the bond order is close to unity. The magnitude of the change in the bond length of the metal-oxo moiety shown (0.3Å) is considerably larger than those shown in $d^1$ and $d^2$ systems. Crystal packing forces were thus thought unlikely to be the cause. It is now known (as discussed in section 4.11) that this lengthening is partially the result of the presence of the isostructurally similar co-crystallised species $NbCl_4(PMe_3)_3$, which results in the shared site occupancy of the oxo position with a chloride from the tetrachloride. Infrared spectroscopic evidence, however, indicate that a difference in Nb=O bond lengths exists, but not to as dramatic an extent as first thought from the X-ray structure determination.

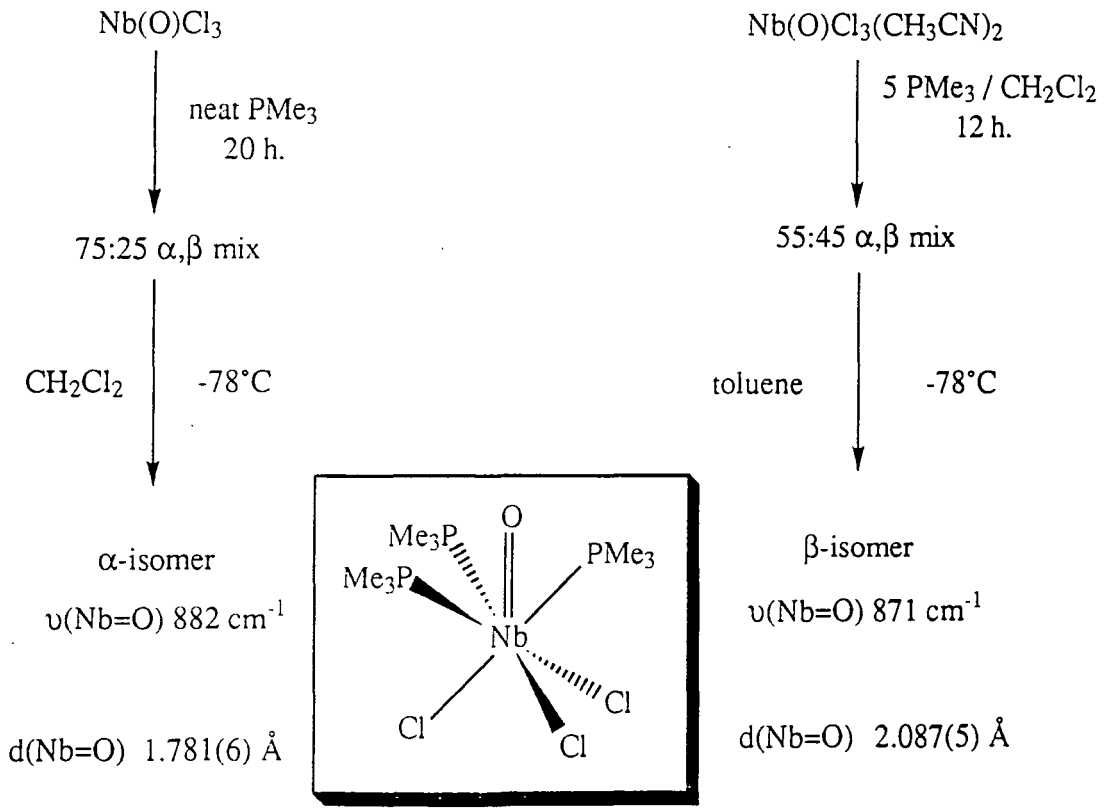


**Scheme 4.1:** Synthetic routes to α- and β- $Nb(O)Cl_3(PMe_3)_3$

In the solid-state the IR nujol mull displays two strong absorptions at 882 and 871 $cm^{-1}$ (figure 4.1), due to the $\alpha$ and $\beta$ isomers respectively. These are consistent with the presence of a terminal oxo ligand. Unique to this system and others in the series $M(E)X_3(PMe_3)_3$ (M=Nb, X=Cl,Br and E=O,S; M=Ta, X=Cl,Br and E=S) is the fact that these two absorptions can be observed not only independently of each other but also co-crystallised in a single sample. This is different from the *cis-mer*-$Mo(O)Cl_2(PMe_2Ph)_3$ system where the absorptions due to $\nu$(Mo=O) can only be observed independently in the pure forms and not as a mixed species (crystallised from solution), since reactivity studies have shown that only one form is preferentially crystallised at any given time in total exclusion of the other. In the case investigated by Parkin[12] of $Mo(O)Cl_2(PMe_3)_3$ only one absorption in the nujol mull IR spectrum is observed at 950 $cm^{-1}$, despite observing by X-ray diffraction two molecules of '*cis-mer*-$Mo(O)Cl_2(PMe_3)_3$' in the same asymmetric unit, one with a normal Mo=O bond length of 1.698Å and the other with an abnormally long Mo=O bond length of 1.866Å. However, on re-examination two new Mo=O bond lengths of 1.772 and 2.154Å were found. These structural discrepancies, on examination of the electron density plots, revealed excess electron density at the oxo position in the abnormally long form. This discrepancy was assigned to compositional disorder arising from the co-crystallisation of *cis-mer*-$Mo(O)Cl_2(PMe_3)_3$ with small quantities of isostructural trichloride complex *mer*-$MoCl_3(PMe_3)_3$.[13] It is this incorporation of chloride into the oxo site that is proposed to lead to the artificial increase of the 'M=O' bond length in both the Mo and Nb systems.

As the basis for the origin of the phenomenon of bond-stretch isomerism was the subject of much controversy, it was decided to undertake a more detailed study into the phenomenon within the controlled system $M(E)X_3(PMe_3)_3$ (M= Nb, Ta; E= O, S; X= Cl, Br).

## 4.3 Synthesis of $Nb(O)X_3(PMe_3)_3$ (X=Cl, Br) Species

### 4.3.1 Synthesis of α- and β- $Nb(O)Cl_3(PMe_3)_3$

*Reaction of $Nb(O)Cl_3$ and $Nb(O)Cl_3(CH_3CN)_2$ with $PMe_3$*

Treatment of either $Nb(O)Cl_3$ or $Nb(O)Cl_3(CH_3CN)_2$ with 5 equivalents of trimethylphosphine, $PMe_3$, in dichloromethane leads to the formation of $Nb(O)Cl_3(PMe_3)_3$, isolated as a pale green amorphous powder in > 95% yield. By infrared spectroscopy, it is revealed to be essentially a mixture of two oxo complexes, the ratio of isomers being dependent upon the starting material used and the reaction time (this assumes that the differing metal-oxo bonds possess similar extinction absorption coefficients and so a direct relation between absorption intensity and isomeric ratio). The Nb=O vibrational stretching bands occur at 882 and 871 $cm^{-1}$. The isomer with the shorter Nb-O bond distance (and hence higher wavenumber) is referred to as the α-isomer while that with the apparently elongated Nb-O bond distance (lower wavenumber) is referred to as the β-isomer.

T.P.Kee[9b] established that an isomeric form could be isolated upon recrystallisation. The yellow α-$Nb(O)Cl_3(PMe_3)_3$ form is selectively crystallised from an α,β mix (76:24), arising from treatment of $[Nb(O)Cl_3]_n$ with 5 equivalents of trimethylphosphine in $CH_2Cl_2$ for 24 h., on cooling to -35°C (42% yield). A better route to selectively form the α-isomer involves treatment of $[Nb(O)Cl_3]_n$ in neat trimethylphosphine for ca. 20 h., which leads to a 73:27 α,β mix from which the α-isomer selectively crystallises in 73% yield. This form was found to possess a Nb-O bond distance of 1.781(6)Å[9a] (slightly longer than the Nb-O distance found in other niobium oxo complexes) with average Nb-Cl bond distances of 2.518(3)Å. Dissolution in toluene of the crude α,β mix, arising from the treatment of $[Nb(O)Cl_3]_n$ or $[Nb(O)Cl_3(CH_3CN)_2]$ with trimethylphosphine in $CH_2Cl_2$, leads to the selective crystallisation of the green β-isomer as plates on cooling to -35°C. X-ray determination of its structure revealed an exceptionally long Nb-O bond distance of 2.087(5)Å[9b], the lengthening of the Nb-O bond being accompanied by a small but significant contraction in the Nb-Cl distances by an average of 0.022Å.

### 4.3.2 Synthesis of β -$Nb(O)Br_3(PMe_3)_3$

***Reaction of $Nb(O)Br_3$ and $Nb(O)Br_3(MeCN)_2$ with $PMe_3$***

Preparation of the crude α,β mix of $Nb(O)Br_3(PMe)_3$ is exactly analogous to that of $Nb(O)Cl_3(PMe)_3$ giving a dark brown amorphous solid in > 95% yield when 5 equivalents of trimethylphosphine are used. However, although β-$Nb(O)Br_3(PMe)_3$ can be selectively crystallised by dissolution of the mixture in toluene and cooling at -35°C, as red cubic crystals (just as for β-$Nb(O)Cl_3(PMe)_3$), the α-form could not be selectively crystallised from $CH_2Cl_2$, $(CHCl_2)_2$ or toluene. Instead an orange crystalline solid is isolated, which by infrared analysis is shown to be a 20:80 isomeric α/β mixture. The Nb=O stretching vibrations occur at 882 and 871 $cm^{-1}$. The stretching frequencies are remarkably similar to those observed for α- and β-$Nb(O)Cl_3(PMe)_3$ suggesting that replacement of the chloride ligands for bromide has little effect on ν(Nb=O) stretch, i.e., the Nb-O stretching vibrations are not significantly perturbed by the metal-halogen vibrations. It also supports the not unreasonable evidence for the existence of the non-isolable α-form of $Nb(O)Br_3(PMe)_3$ as the second oxo species.

## 4.4 Solid-State Infrared Spectroscopy of α- and β-$Nb(O)Cl_3(PMe)_3$

The infrared spectra of α- and β-$Nb(O)Cl_3(PMe_3)_3$ display absorptions typical of coordinated $PMe_3$ at 1277 $cm^{-1}$ ($\sigma(CH_3)$), 951 $cm^{-1}$ ($\rho(CH_3)$) and 737 $cm^{-1}$ ($\upsilon_{as}(PC_3)$).[14] The strong absorptions at 882 and 871 $cm^{-1}$ (figure 4.1) due to the α- and β-isomers respectively are consistent with the presence of a terminal oxo ligand.[15] At one stage a weak absorption at 845 $cm^{-1}$ was thought to be due to a bridging oxo species until comparison with the infrared spectrum of the isostructural $Nb(S)Cl_3(PMe_3)_3$ showed that the band is more likely due to a Nb-$PMe_3$ vibration. The spectra of the oxo and sulphido species are similar with the exception that the niobium-sulphur stretching vibration occurs at 489 $cm^{-1}$ (for the green isomer) leaving only a weak absorption at 845 $cm^{-1}$ in the region 800 to 900 $cm^{-1}$, where Nb=O stretching vibrations are expected for the niobium-oxo species. This strongly indicates that the band is in fact assignable to

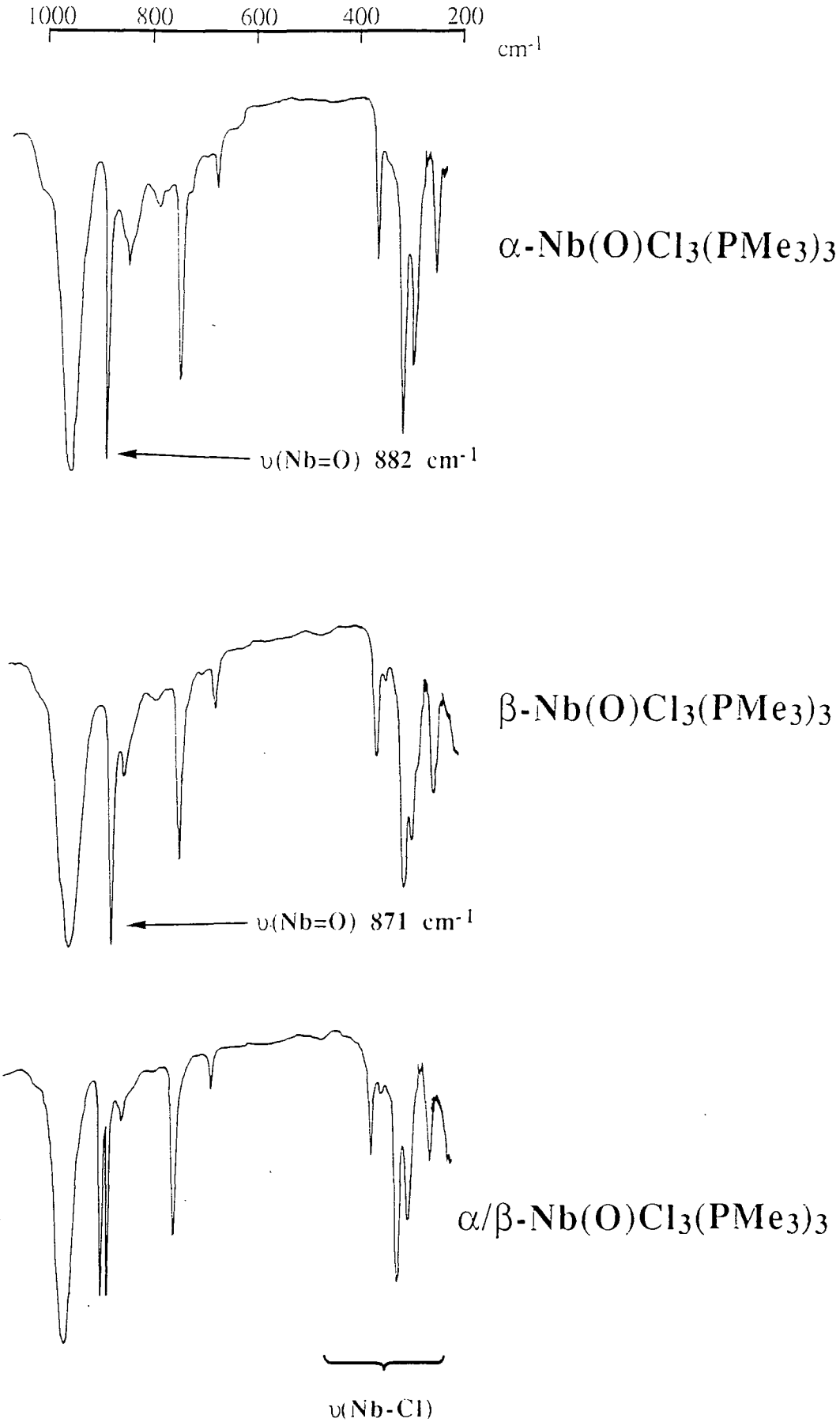


**Figure 4.1:** Solid-state infrared spectra of α-, α/β, and β-$Nb(O)Cl_3(PMe_3)_3$ including the ν(Nb=O) and ν(Nb-Cl) stretching regions.

$PMe_3$. The legitimacy of assigning the bands at 882 and 871 $cm^{-1}$ in the infrared spectra of $Nb(O)Cl_3(PMe_3)_3$ to $\nu$(Nb=O) stretches is discussed in section 4.6 on isotopic labelling.

The very small difference in the $\nu$(Nb=O) stretching frequencies (ca. 11 $cm^{-1}$) for $\alpha$- and $\beta$-$Nb(O)X_3(PMe)_3$ in both the chloride and bromide variants is not initially readily explained considering the magnitude of the change in the Nb=O bond length (0.30Å) originally reported by X-ray structure determination. By using equation 5 (appendix 3) the calculated force constants for the Nb=O bonds of the $\alpha$- and $\beta$-isomers of $Nb(O)Cl_3(PMe)_3$ are 705.3 and 686.2 $Nm^{-1}$ respectively. These are not significantly different considering the change in bond length associated with these isomers, and correspond to only an associated change of ca. 0.023Å and not 0.30Å. Group theory ought to lead to a better understanding of the origin of these bands by considering the mixing of all vibrations within the molecule. However, a simple qualitative comparison of the IR spectra of $\alpha$- and $\beta$-$Nb(O)X_3(PMe)_3$ (X=Cl, Br), which possess virtually identical metal-oxo stretching frequencies in each of the corresponding $\nu$(Nb=O) forms, suggests that this vibration is not perturbed to any significant extent by the changes in the halide ligand.

A plausible explanation first put forward to explain the large (0.30Å) change in the Nb=O bond length involved postulating an enhanced ionic contribution in the elongated Nb-O bond of the $\beta$-isomer resulting in a form similar to canonical (III) (scheme 4.2).

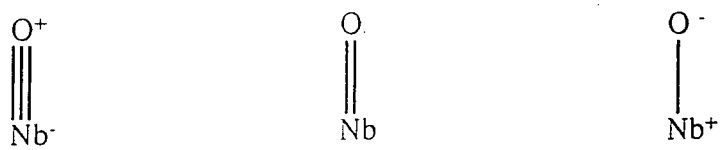


I II III

**Scheme 4.2:** Proposed formalisation of Nb-O bonds in the isomers

The possibility of an increased contribution due to the ionic form III with its related enhanced bond length compared to an equivalent covalent bond of unity bond order would have reasonably accounted for the fact that the Nb-O stretching frequency

does not correlate with the covalent bond order thus accounting for a higher stretching frequency than expected, should the ionic contribution be significant.

It is now realised that the magnitude of the lengthening in the Nb=O bond in the green β-isomer is in fact due to the presence of the impurity $NbCl_4(PMe_3)_3$, which by the virtue of its isostructural nature with $Nb(O)Cl_3(PMe_3)_3$ leads to a crystallographic disorder in the oxo position due to superimposed chloride. The presence of this impurity has now been established by $^1H$ NMR, elemental analysis, X-ray crystallography, as well as by infrared spectroscopy.

In Parkin's investigation[12,16] of the *cis-mer*-$Mo(O)Cl_2(PMe_2Ph)_3$ system he was able to isolate forms that varied in the colour from blue (ν(Mo=O) 941 $cm^{-1}$), through green-blue, to emerald green (ν(Mo=O) 943 $cm^{-1}$). Parkin inferred from his observations that with this colour and bond length variation there should be an accompanying variation in the bond-stretch frequencies, ν(Mo=O). However, only one ν(Mo=O) stretch at 941 $cm^{-1}$ was observed. Similarly in the cases of α- and β-$Nb(O)Cl_3(PMe_3)_3$ only two absorption frequencies corresponding to the metal-oxo bond stretches are observed and not a continuous series, but unlike the *cis-mer*-$Mo(O)Cl_2(PMe_2Ph)_3$ system, here there is no dramatic variation in the colour of the crystals, and two ν(Nb=O) stretches are observed. Parkin, however, in contrast to the studies reported herein, was unable to reproduce the synthesis of Chatt's blue form of *cis-mer*-$Mo(O)Cl_2(PMe_2Ph)_3$ which shows a ν(Mo=O) stretch at 955 $cm^{-1}$. Two forms are observed when grown from toluene, a yellow normal Nb=O bond length form and a light green form with an abnormally long Nb=O bond. The nujol mull IR spectra of the β form gives independently a strong absorption at 871 $cm^{-1}$ corresponding to a ν(Nb=O) stretch. Thus, this is a distinct species which can be observed independently of the 882 $cm^{-1}$ yellow form. There is, however, some evidence for the presence of $NbCl_4(PMe_3)_3$ in the IR spectrum of the green 871 $cm^{-1}$ isomer in the form of a weak absorption at 336 $cm^{-1}$. The $NbCl_4(PMe_3)_3$ impurity is observed only in the β form at a constant contamination level of 4.5% , as shown by $^1H$ NMR. It is the colour of the dark green $NbCl_4(PMe_3)_3$ contaminant that gives rise to the the green colouration of the β-form. In fact, use of dichloroethane as the solvent to selectively crystallise the β-form has been

able to produce yellow crystals exhibiting a ν(Nb=O) absorption at 871 $cm^{-1}$ characteristic of the β-form. $^1H$ NMR analysis still, however, indicated a very low level of tetrachloride contaminant being present. This seemingly indicates that the β-form could possibly be isolated as crystals with a true yellow colour, without the presence of co-crystallised tetrachloride and that crystallisation of the β-form is susceptible to co-crystallisation with tetrachloride $NbCl_4(PMe_3)_3$.

In order to ascertain whether $NbCl_4(PMe_3)_3$ was perturbing the 882 $cm^{-1}$ ν(Nb=O) stretching vibration, known molar ratio mixtures of α-$Nb(O)Cl_3(PMe_3)_3$ and $NbCl_4(PMe_3)_3$ were mixed in solution in $CH_2Cl_2$ and the nujol mull IR spectra recorded of the solid remaining after removing all volatiles. A series of spectra (figure 4.2) were produced showing that in the presence of $NbCl_4(PMe_3)_3$, the α-$Nb(O)Cl_3(PMe_3)_3$ was converted to the β-form at a rate that was greater than the control reaction where α-$Nb(O)Cl_3(PMe_3)_3$ was stirred by itself in $CH_2Cl_2$. The presence of $NbCl_4(PMe_3)_3$ could be inferred from an absorption at 336 $cm^{-1}$ and a general broadening of the Nb-Cl stretches. No evidence was seen for the perturbation of the ν(Nb=O) stretching frequency leading to a general broadening of the region as would be expected if the 'Nb=O' bond was to vary continuously in length. However, it does establish that the presence of co-crystallised $NbCl_4(PMe_3)_3$ leads to the ν(Nb=O) 871 $cm^{-1}$ form being selectively crystallised.

The Nb-Cl bond stretching vibration region also provides evidence of the uniqueness of the two forms (figure 4.3) and the presence of $NbCl_4(PMe_3)_3$ impurity. By applying group theory it can be shown that since $Nb(O)Cl_3(PMe_3)_3$ and $NbCl_4(PMe_3)_3$ belong to the $C_{3v}$ point group (figure 4.4 and 4.5), having a pseudo $C_3$ rotation axis along the Nb-O and Nb-Cl (axial) bonds respectively, the ν(Nb-Cl) stretching vibrations in $Nb(O)Cl_3(PMe_3)_3$ ($\chi_{stretch}$(3 0 1)) are found to transform as $A_1$+ E. Therefore, two infrared active ν(Nb-Cl) stretches are expected in the spectrum, since two of the three are degenerate. In the case of $NbCl_4(PMe_3)_3$, the ν(Nb-Cl) stretching vibrations ($\chi_{stretch}$(4 1 2)) are found to transform as $2A_1$+ E and so three infrared active ν(Nb-Cl) stretches are expected. However, in each isomer four absorptions are seen in this region, three of which at 353, 301 and 237 $cm^{-1}$ are common to both. Additionally

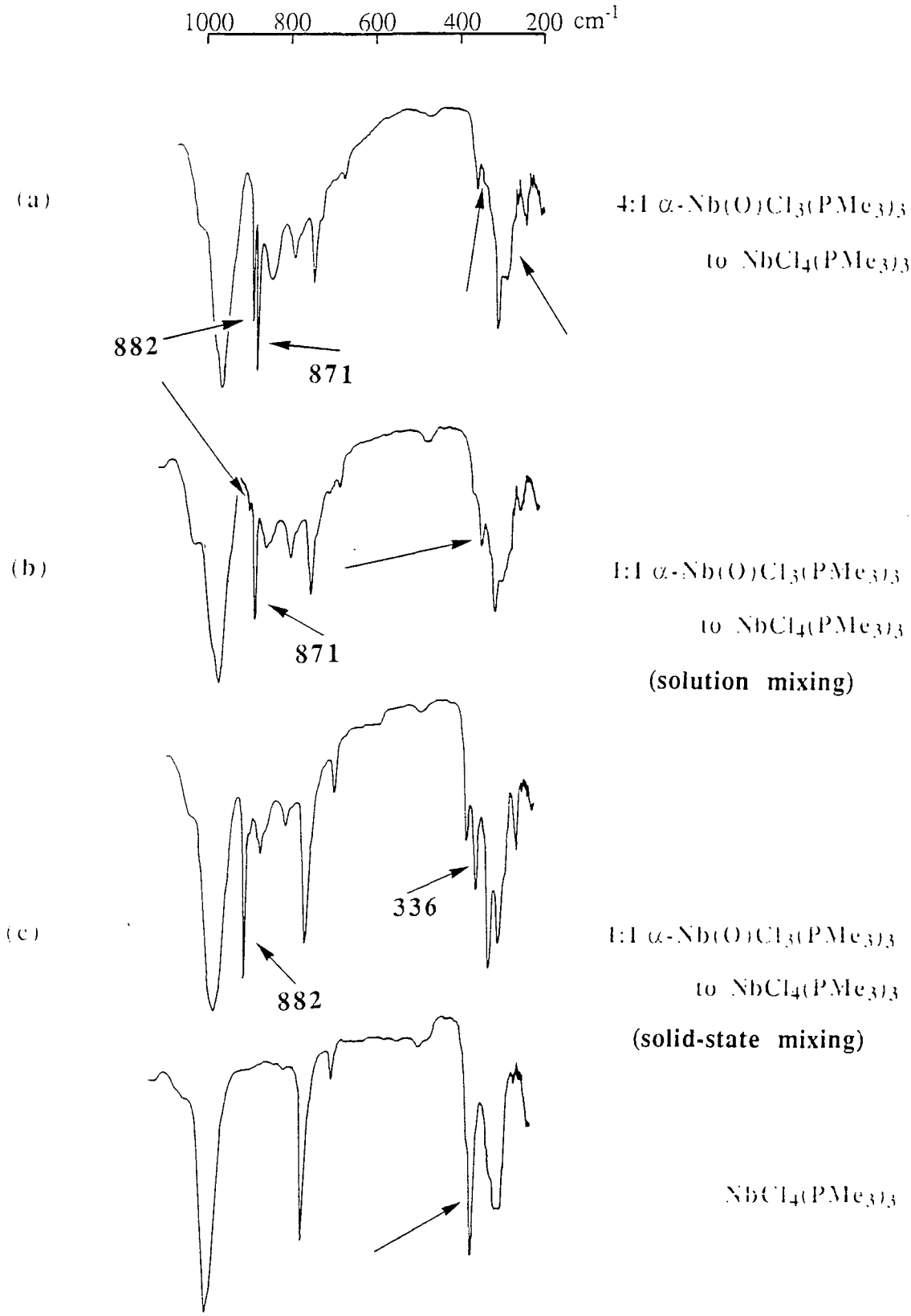


**Figure 4.2:** Infrared spectra showing that (a,b) the mixing of $NbCl_4(PMe_3)_3$ in solution with $\alpha$-$Nb(O)Cl_3(PMe_3)_3$ causes enhanced conversion to $\beta$-$Nb(O)Cl_3(PMe_3)_3$, whereas (c) no effect is observed on solid-state mixing of $\alpha$-$Nb(O)Cl_3(PMe_3)_3$ and $NbCl_4(PMe_3)_3$.

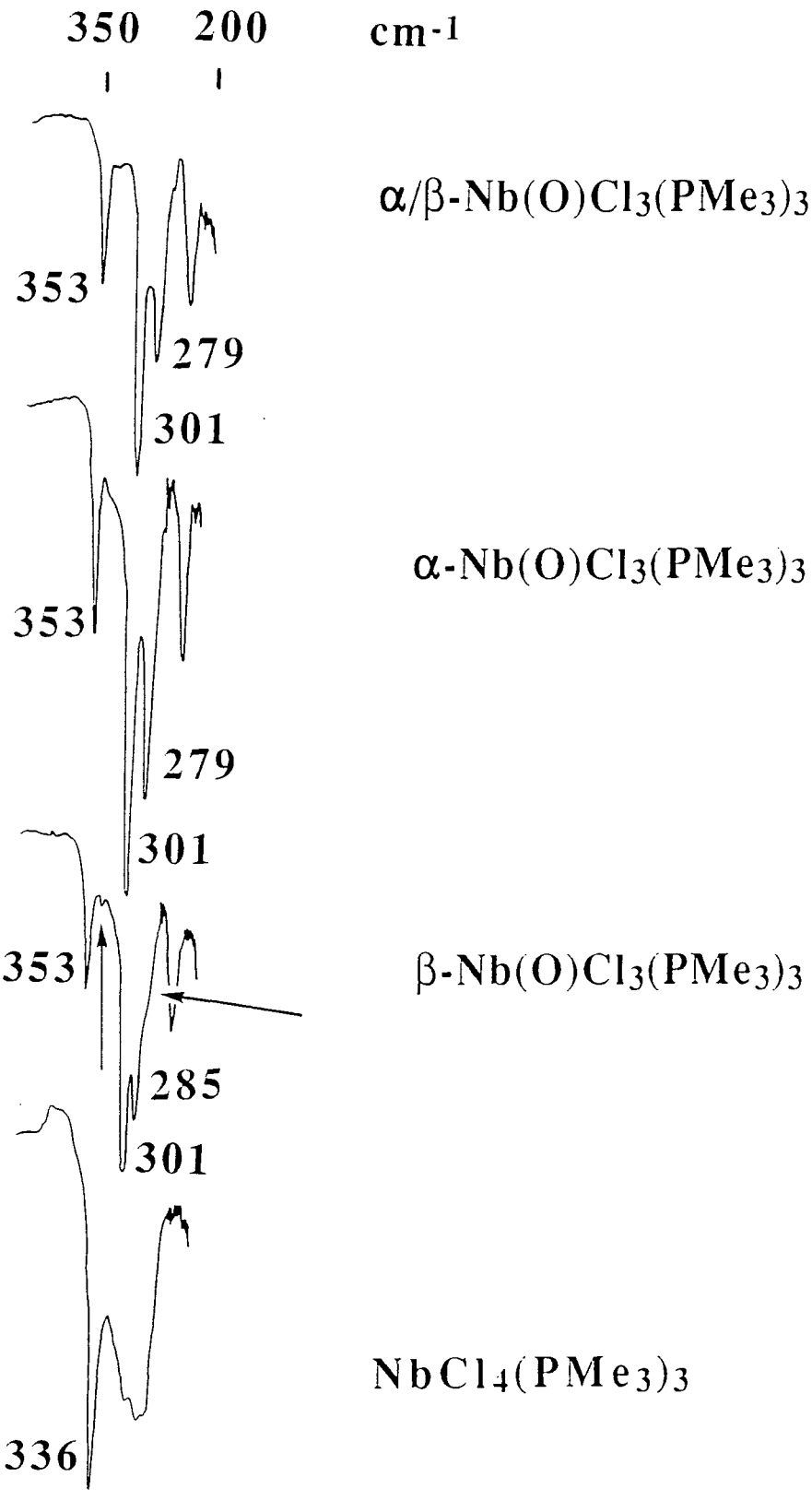


**Figure 4.3:** Solid-state infrared spectra of α- and β-$Nb(O)Cl_3(PMe_3)_3$ and $NbCl_4(PMe_3)_3$ in the ν(Nb-Cl) stretch region.

in the α-form there is a unique peak at 279 $cm^{-1}$ and in the β-form one at 285 $cm^{-1}$, along with a weak absorption at 336 $cm^{-1}$ due to co-crystallised $NbCl_4(PMe_3)_3$ (figure 4.3). In establishing which of these stretches are due to Nb-Cl stretching vibrations one must remember that group theory dictates that two ν(Nb-Cl) stretches are expected in the α and β forms of $Nb(O)Cl_3(PMe_3)_3$, and so the bands at 301 (common to both forms) and at 279 and 285 $cm^{-1}$ respectively are assigned to the ν(Nb-Cl) stretches. This assignment is also reflective of the requirement that in $NbCl_4(PMe_3)_3$ three absorptions are dictated for the ν(Nb-Cl) stretches, two of which appear at 275 and 265 $cm^{-1}$ as a broad band, and a sharp peak at 336 $cm^{-1}$, which because of its unique clarity is tentatively assigned to the totally symmetric stretch of all four Nb-Cl bonds in phase. This all gives credence to the belief that it is the presence of co-crystallised $NbCl_4(PMe_3)_3$ which causes an approximately 0.023Å change (implied by the 11 $cm^{-1}$ difference in the ν(Nb=O) stretches) in the length of the niobium-oxo bond.

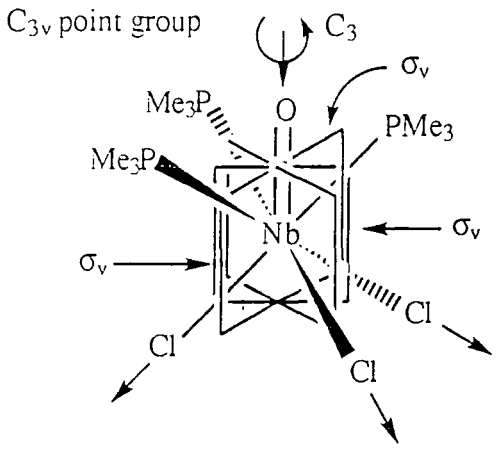


**Figure 4.4:** $C_{3v}$ point group of $Nb(O)Cl_3(PMe_3)_3$

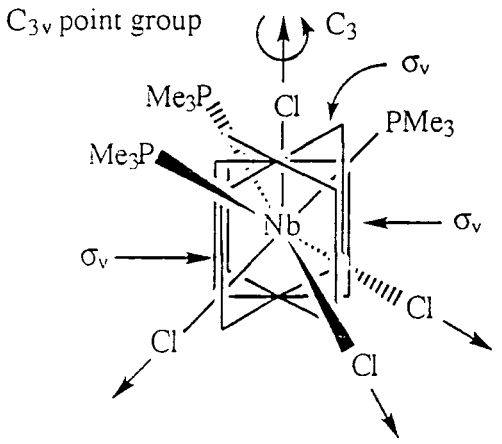


**Figure 4.5:** $C_{3v}$ point group of $NbCl_4(PMe_3)_3$

## 4.5 Solution Infrared and UV-Visible Spectroscopic Studies

In preparing the isomers according to equations 4.1 and 4.2 it was noted that the longer the α/β isomer mix was left standing in solution ($CH_2Cl_2$) the greater was the proportion of the β-form in the IR spectrum of the amorphous crude product of the reaction prior to dissolution for selective recrystallisation. In addition β-$Nb(O)Cl_3(PMe_3)_3$ was found to be unchanged on standing in solution. It was thus envisaged that because conversion between the isomers occurs in solution involving solely the transformation of the α-form to the apparently thermodynamically more stable β-form, that this conversion could be monitored by solution IR or UV-visible techniques.

$$Nb(O)Cl_3 \xrightarrow[PMe_3]{\text{neat}} \alpha/\beta\text{-}Nb(O)Cl_3(PMe_3)_3 \qquad \textbf{(4.1)}$$

$$Nb(O)Cl_3 \xrightarrow[CH_2Cl_2]{PMe_3} \alpha/\beta\text{-}Nb(O)Cl_3(PMe_3)_3 \qquad \textbf{(4.2)}$$

$^1H$ NMR studies had already shown that conversion could not be monitored via this technique, only one signal being observed (before decomposition), presumably due to the equivalent nature of the phosphine ligands produced by free-rotation about the Nb-P bonds creating an averaged environment. However, in solution IR spectroscopy studies it was the Nb=O stretching vibration that was of direct interest, and not the solution averaged phosphine environments.

As dichloromethane exhibits a strong absorption at 890 $cm^{-1}$ very close to the region of interest, dibromomethane which has a similarly strong absorption but shifted to 815 $cm^{-1}$ was deemed to be the better choice of solvent for the solution IR studies.

However, dissolution of α-$Nb(O)Cl_3(PMe_3)_3$ in $CH_2Br_2$ was observed to give the same spectrum as for β-$Nb(O)Cl_3(PMe_3)_3$ dissolved in solution, namely a ν(Nb=O) stretch at 871 $cm^{-1}$ indicative of β-$Nb(O)Cl_3(PMe_3)_3$ being the sole species

present in solution (figure 4.6). The low frequency region of the spectra (figure 4.7) confirmed this was the case and that conversion to the β-form had occurred since a weak absorption at 336 $cm^{-1}$ indicated the presence of $NbCl_4(PMe_3)_3$ which is invariably associated with β-$Nb(O)Cl_3(PMe_3)_3$. This is consistent with the findings of $^1H$ NMR analysis which shows a build up of the levels of $NbCl_4(PMe_3)_3$ on leaving the α-form in solution for 3 days (figure 4.10). A parallel control reaction showed that β-$Nb(O)Cl_3(PMe_3)_3$ was also the only species found in the solid-state IR spectrum.

On the premise that the α-form could not be seen in solution due to the influence of acid-catalysis, acid-free $CH_2Br_2$ was produced by 'scrubbing'. This involved the literature purification procedure for chlorocarbons of treating solvents with a 5% solution of sodium carbonate, followed by washing with de-ionised water, and finally drying over $CaCl_2$ before distilling from calcium hydride.

However, even using acid-free solvents the α-isomer was not observed in solution, and so solution IR spectroscopy was not a viable technique to monitor the progress of the reaction. This observation is in agreement with solution IR spectroscopic studies on the *cis-mer*-$Mo(O)Cl_2(PMe_2Ph)_3$ system (section 2.4) where two blue forms are observable in the solid-state (ν(Mo=O) 941 and 954 $cm^{-1}$), but only one ν(Mo=O) stretch at 946 $cm^{-1}$ is observed in solution. The two systems do differ, however, in that in the niobium system the 'abnormally' long form is observed, whereas in the molybdenum system a signal intermediate between those found for the two isomers is observed. Chatt[5] remarks that on warming in organic solvent the green isomer (1.80Å) is converted irreversibly to the blue (1.68Å) form. However, this is a consequence of recrystallisation from a solution where the level of the $MoCl_3(PMe_2Ph)_3$ impurity in solution is reduced, and hence selective recrystallisation (aided by this reduction in the level of the trichloride) of the *cis-mer*-$Mo(O)Cl_2(PMe_2Ph)_3$ form (ν(Mo=O) 954 $cm^{-1}$), which by X-ray analysis[6] has phosphine orientations that do not mimic those observed in *mer*-$MoCl_3(PMe_2Ph)_3$. Nevertheless, it must remembered that the two blue forms can be obtained free of impurity, and it is possibly the level of trichloride impurity in the crystallising solution that determines which orientation the alkyl and aryl fragments on the phosphine ligands adopt, as is reflected in the levels of ca. 20% and 0.3% of trichloride

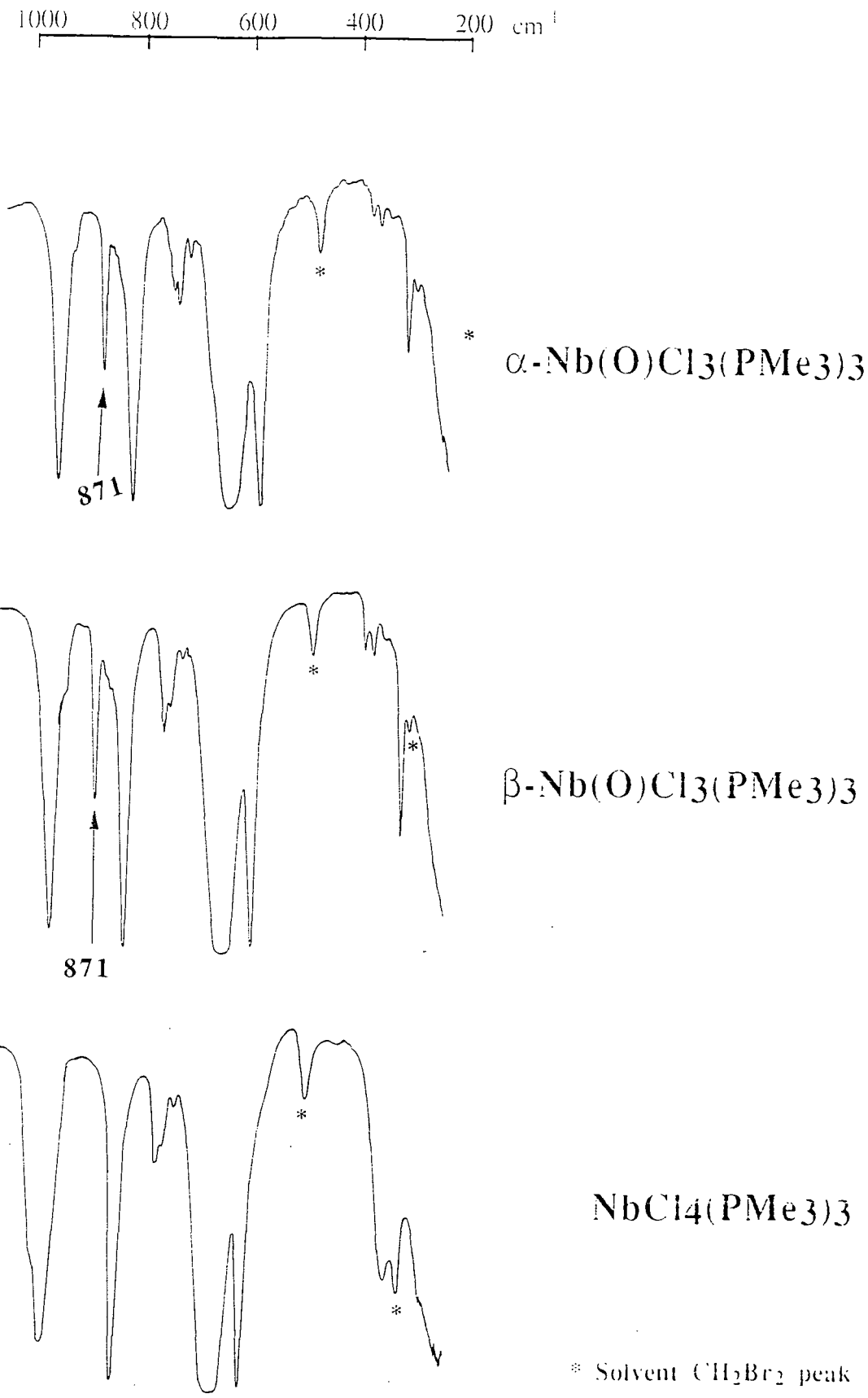


**Figure 4.6:** Solution infrared spectra showing the result of dissolving α- and β-$Nb(O)Cl_3(PMe_3)_3$, and $NbCl_4(PMe_3)_3$ in $CH_2Br_2$ over the range 1050 to 200 $cm^{-1}$.

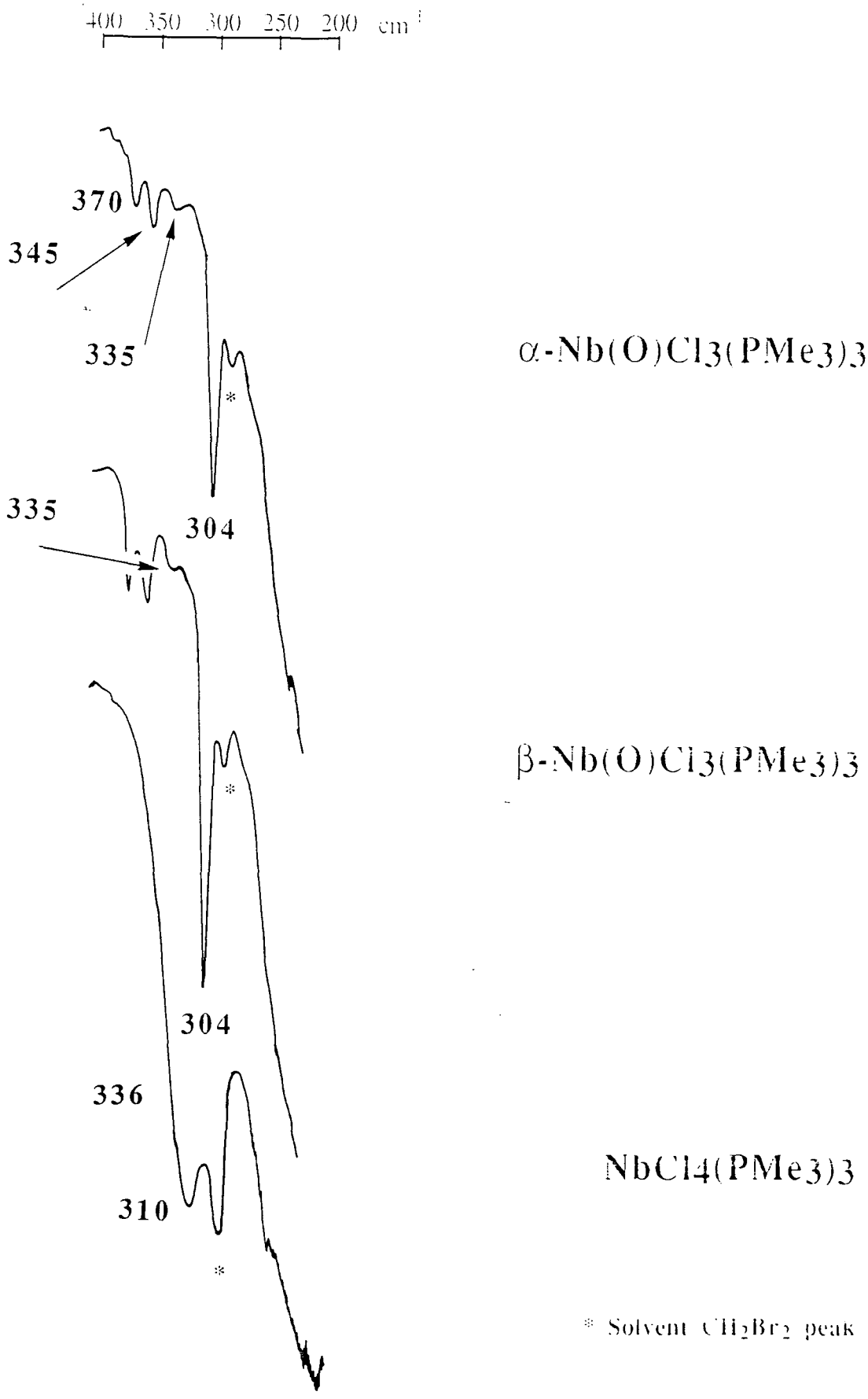


**Figure 4.7:** Solution infrared spectra of α- and β-$Nb(O)Cl_3(PMe_3)_3$ in $CH_2Br_2$ in the ν(Nb-Cl) stretch region.

found in the Enemark and Chatt green forms respectively by both elemental analysis and $^1H$ NMR.

UV-visible spectroscopy proved unsuccessful for resolving α- and β-$Nb(O)Cl_3(PMe_3)_3$ due to the low extinction coefficients and similar colours (hence identical absorption wavelengths) of the two isomers.

## 4.6 Isotopic Labelling Studies ($^{17}O$ and $^{18}O$)

### 4.6.1 Synthesis of the $Nb(^*O)Cl_3$ and $Nb(^*O)Cl_3(MeCN)_2$ Precursors to $Nb(^*O)Cl_3(PMe_3)_3$

By treating the metal-oxo stretching frequencies as arising from a pseudo-diatomic molecule it is thus possible to calculate predicted metal-oxo stretching frequencies on isotopic substitution and compare them with the experimentally determined values.

Experimentally the oxygen isotopes were introduced into the species $M(O)Cl_3$ by using isotopically substituted hexamethyldisiloxane, $(Me_3Si)_2{}^*O$. This is prepared by adding isotopically enriched water, $H_2{}^*O$ (de-oxygenated), to a chilled (-78°C, acetone/$CO_2$) mixture of two equivalents of both trimethylsilyl chloride ($Me_3SiCl$) and lutidene (2,6-dimethylpyridine), in diethyl ether (dried over Na) and vigorously stirring whilst refluxing for 3 h.. The ethereal solution was dried over phosphorus pentoxide and the $(Me_3Si)_2{}^*O$ distilled off collecting in the range 102-106°C, depending on the isotope.

$$2\ Me_3SiCl + H_2{}^*O + 2\ (CH_3)_2C_5H_3N: \xrightarrow[3\ h.]{reflux} (Me_3Si)_2{}^*O + 2\ [(CH_3)_2C_5H_3NH]^+.Cl^-$$

Table 4.1 shows that both $Nb(^{17}O)Cl_3$ and $Nb(^{18}O)Cl_3$ give stretching frequencies for the metal-oxo bond within 1% of that expected. The calculated stretching

frequencies for the isotopically substituted species are based on that observed for the naturally occurring O-16 labelled form and are calculated from equation 4 in appendix 3.

| Isotope | $\nu_{expt}$ ($cm^{-1}$) | $\nu_{calc}$ ($cm^{-1}$) | $k_{xo}$ ($Nm^{-1}$) |
|---|---|---|---|
| $^{16}O$ | 790±2 | ----- | 544.6±2.8 |
| $^{17}O$ | 776±2 | 768.2±1.9 | 556.7±2.9 |
| $^{18}O$ | 746±2 | 748.3±1.9 | 541.3±2.9 |

**Table 4.1:** Table showing the calculated and experimentally determined values for the ν(Nb=O) stretches in the isotopically labelled oxyhalides $Nb(O^*)Cl_3$

O-18 labelling studies were also of use in assigning the ν(Nb=O) stretch in the six-coordinate $Nb(O)Cl_3(MeCN)_2$ complex. In the IR spectrum of the normal O-16 labelled form three strong peaks are observed in the Nb=O fingerprint region at 956, 943 and 930 $cm^{-1}$. The IR spectrum of $Nb(^{18}O)Cl_3(MeCN)_2$, produced by the reaction between $NbCl_5$ and one equivalent of $(Me_3Si)_2{}^{18}O$, exhibited an additional strong absorption at 908 $cm^{-1}$ strongly indicating that the stretch at 956 $cm^{-1}$ was due to $\nu(Nb=^{16}O)$. There was no evidence of any absorptions at 892.1 or 879.8 $cm^{-1}$ corresponding to O-18 isotopic shifts for the other two strong bands in the IR spectrum of the O-16 labelled form (table 4.2).

| Isotope | $\nu_{expt}$ ($cm^{-1}$) | $\nu_{calc}$ ($cm^{-1}$) |
|---|---|---|
| $^{16}O$ | 956±2 | ----- |
| $^{18}O$ | 908±2 | 904.3±1.9 |

**Table 4.2:** Table showing the calculated and experimentally determined values for the ν(Nb=O) stretches in the isotopically labelled $Nb(O^*)Cl_3(MeCN)_2$

### 4.6.2 Synthesis of $Nb(^{18}O)Cl_3(PMe_3)_3$

Treatment of $Nb(^{18}O)Cl_3$ with 5 equivalents of $PMe_3$ in $CH_2Cl_2$ for 8 h. leads to the formation of crude $Nb(^{18}O)Cl_3(PMe_3)_3$ in > 95% yield. Comparison of its IR spectrum with that of $Nb(^{16}O)Cl_3(PMe_3)_3$ reveals them to be identical in every respect with the exception of three additional peaks in the ν(Nb=O) stretching region. These

occur at 856 (m), 835 (vs) and 822 (m) $cm^{-1}$, indicating the probable formation of α,β isotopically substituted isomer pairs of $^{16}O$, $^{17}O$ and $^{18}O$ (figures 4.8 and 4.9). However, the peak possibly due to α-$Nb(^{17}O)Cl_3(PMe_3)_3$ was surprisingly strong considering $^{17}O$'s enrichment of only ca. 3%.

In order to assign each band and confirm the existence of α,β-$Nb(^*O)Cl_3(PMe_3)_3$ the α-forms were selectively recrystallised from $CH_2Cl_2$ at -78°C and similarly the β-forms from toluene at -78°C. The β-forms can also be selectively recrystallised by dissolution of the crude product from the reaction between $Nb(^*O)Cl_3(MeCN)_2$ and $PMe_3$ in $CH_2Cl_2$, in toluene at -78°C.

The IR spectrum of α-$Nb(^*O)Cl_3(PMe_3)_3$ gives ν(Nb=*O) bands at 882, 856 and 835 $cm^{-1}$ (figure 4.9, middle). That of β-$Nb(^*O)Cl_3(PMe_3)_3$ gives peaks at 871 and 824 $cm^{-1}$ (figure 4.9, bottom). At first glance this would seem to point to the existence of 3 α- and 2 β-forms.

Using equation 4 (appendix 3) the expected stretching frequencies of the isotopically substituted metal-oxo can be calculated using $M_X$= M ($NbCl_3(PMe_3)_3$)=427.4900. Table 4.3 gives the values of the frequencies found and calculated for ν(Nb=*O) stretching vibrations.

Each band is in excellent agreement with that expected so proving the original assignment of the bands at 882 and 871 $cm^{-1}$ as ν(Nb=O) stretching vibrations of α- and β-$Nb(^{16}O)Cl_3(PMe_3)_3$ respectively to be correct.

A band at 848 $cm^{-1}$ in the IR spectrum of β-$Nb(^*O)Cl_3(PMe_3)_3$ could not for certain be assigned to a ν(Nb=$^{17}$O) band for β-$Nb(^{17}O)Cl_3(PMe_3)_3$ since there exists at this region a band due to Nb-$PMe_3$.

| Isotope | α-$Nb(O)Cl_3(PMe_3)_3$ | | β-$Nb(O)Cl_3(PMe_3)_3$ | |
|---|---|---|---|---|
| O* | ν(expt) $cm^{-1}$ | ν(calc) $cm^{-1}$ | ν(expt) $cm^{-1}$ | ν(calc) $cm^{-1}$ |
| 16 | 882±2 | ---- | 871±2 | ---- |
| 17 | 856±2 | 855.7±1.9 | ---- | 844.0±1.9 |
| 18 | 835±2 | 832.5±1.9 | 824±2 | 823.0±1.9 |

**Table 4.3:** The observed and calculated values for the Nb=O stretching frequencies in the isotopically labelled $Nb(O)Cl_3(PMe_3)_3$ species

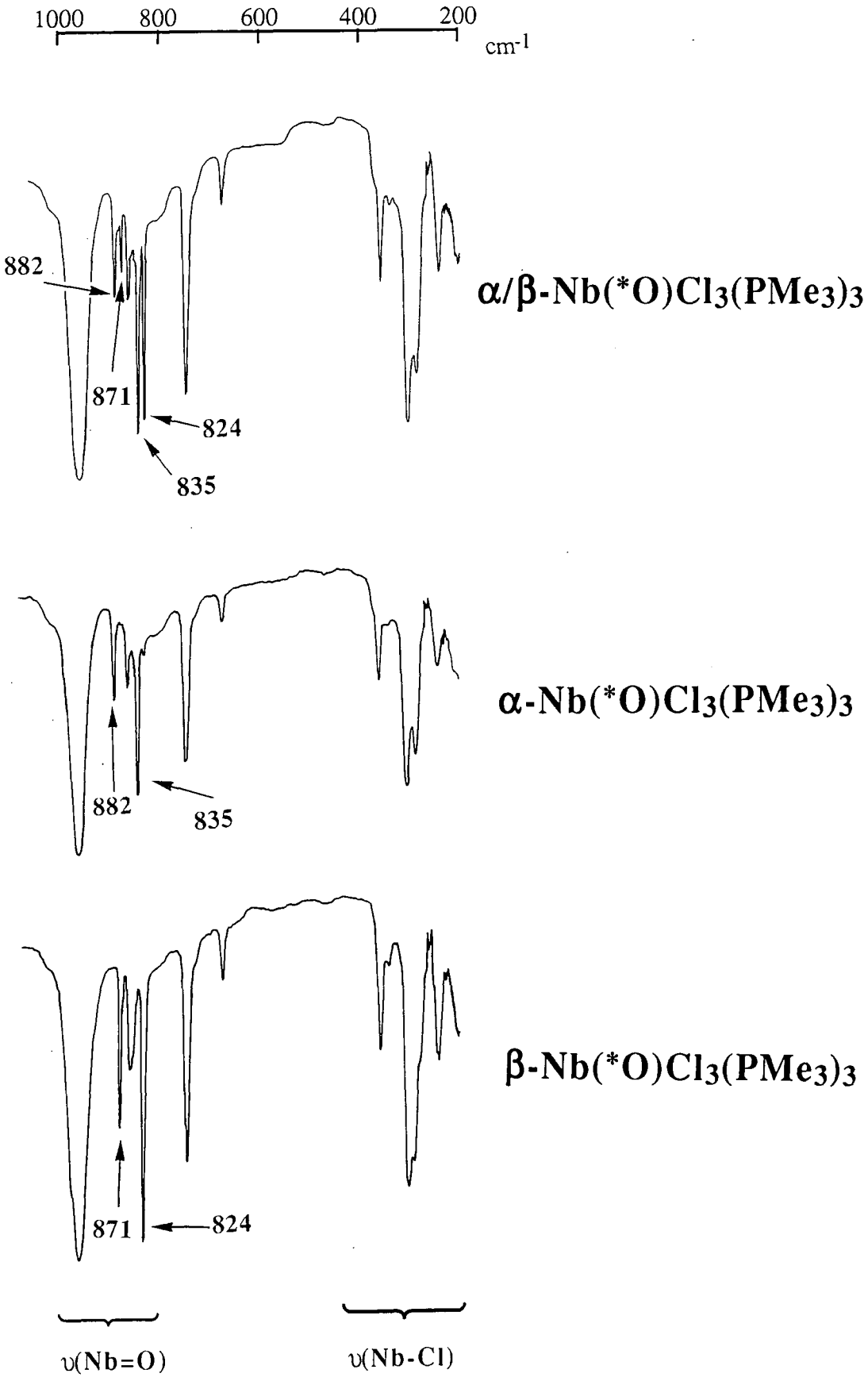


**Figure 4.8:** Infrared spectra of the isotopically labelled species α, α/β and β-$Nb(^*O)Cl_3(PMe_3)_3$ ($^*$=16, 17, 18) in the ν(Nb=O) region.

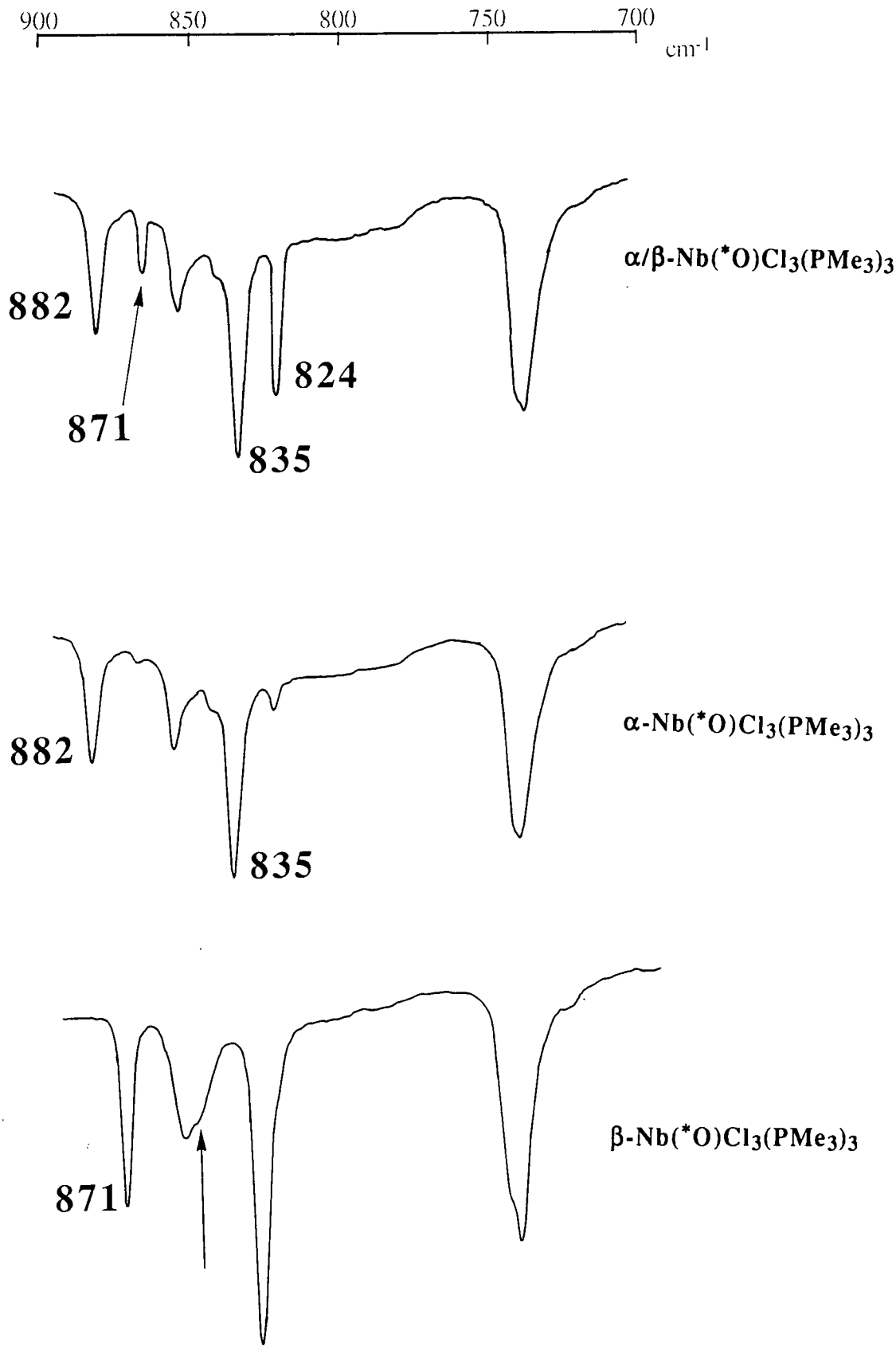


**Figure 4.9:** Solid-state infrared spectra over the ν(Nb=O) stretching region (900 to 700 $cm^{-1}$) for the yellow α and green β forms of $Nb(^*O)Cl_3(PMe_3)_3$ where an oxygen-18 label has been introduced (asterisk represents isotopic label).

## 4.7 NMR Studies of Yellow α- and Green β-$Nb(O)Cl_3(PMe_3)_3$

The results of $^1H$ NMR analysis of the yellow and green forms of $Nb(O)Cl_3(PMe_3)_3$ are similar to the findings of solution infrared spectroscopic studies. Whether the solvent used is $CD_2Cl_2$ or $CDCl_3$, no unique signal is observed independently for each species. Instead both yellow α- and green β-$Nb(O)Cl_3(PMe_3)_3$ forms show a doublet at δ 1.44 ppm in $CD_2Cl_2$ with a $^2J(PH)$ coupling constant of 7.20 Hz ((figures 4.10 and 4.11), the coincidence of the peaks suggesting an averaged environment of the phosphine ligands in solution due to free rotation about the Nb-P bonds. Whereas in the case of the six co-ordinate *cis-mer*-$Mo(O)Cl_2(PMe_2Ph)_3$ system a doublet and two 1:2:1 virtual triplets are observed for the methyl protons indicative of the cis (~90°) and trans (~180°) phosphine environments, in the seven co-ordinate $Nb(O)Cl_3(PMe_3)_3$ system a single doublet is observed, indicative of equivalent phosphine environments in solution and an approximately 'cis' phosphine stereochemistry. Indeed, X-ray determination shows the average P-Nb-P bond angle to be 114.7°±1.7° and 114.5°±2.8° in the yellow and green forms respectively.

Evidence for the co-crystallisation of $NbCl_4(PMe_3)_3$ with the β form is provided by examination of the $^1H$ NMR spectra. $NbCl_4(PMe_3)_3$ is paramagnetic and thus normally escapes detection in the normal range +12 to -1 ppm usually scanned. It is however observed as a broad resonance at δ -3.05ppm ($\Delta_{1/2}$=72Hz) in $CD_2Cl_2$ (figure 4.11, top). An examination of the 400 MHz $^1H$ NMR spectra ($CD_2Cl_2$) for the α and β forms reveals that initially the paramagnetic contaminant is observed only in the β form (figure 4.11), the level being constant at ca. 1.5% over a 6h. period of time. Both isomers show a single doublet at δ 1.44 ppm ($^2J(PH)$=7.20Hz). There is no evidence for any interconversion taking place. After 5 days the solutions become progressively more green with no observation of isomer conversion. Instead decomposition occurs (with solid dropping out of solution) to an unknown species exhibiting in each case a broad resonance (α-isomer: δ 1.25ppm, $\Delta_{1/2}$=12Hz; β-isomer δ 1.22ppm, $\Delta_{1/2}$=16Hz), there being no evidence of free $PMe_3$ at 1.02 ppm in the $^1H$ NMR or in the $^{31}P$ NMR spectrum at ca. δ -62 ppm. Despite the absence of free $PMe_3$ this broadened resonance in the $^1H$

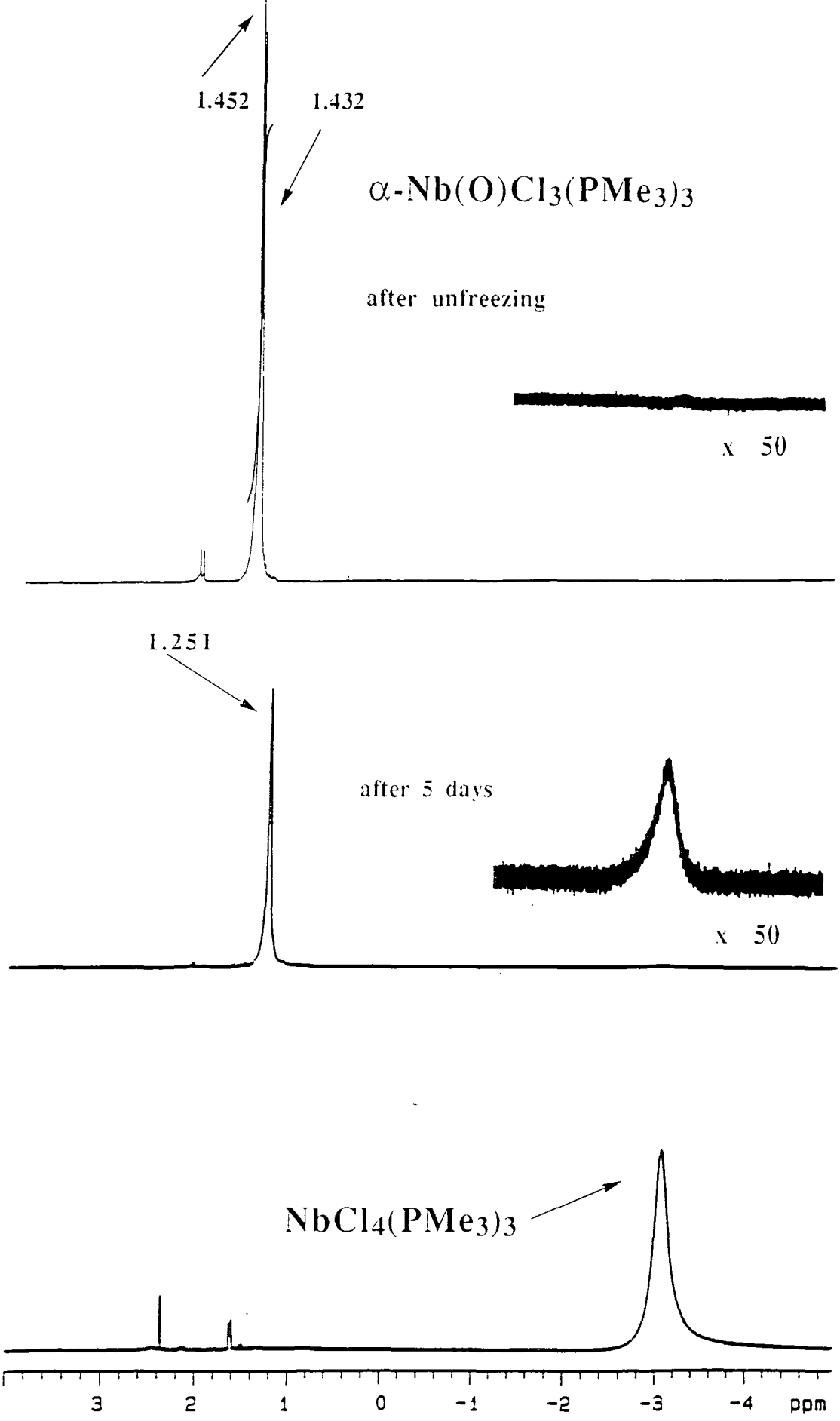


**Figure 4.10:** 400 MHz $^1$H NMR spectrum of α-Nb(O)$Cl_3$($PMe_3$)$_3$ in $CD_2Cl_2$ over the range +4 to -5 ppm.

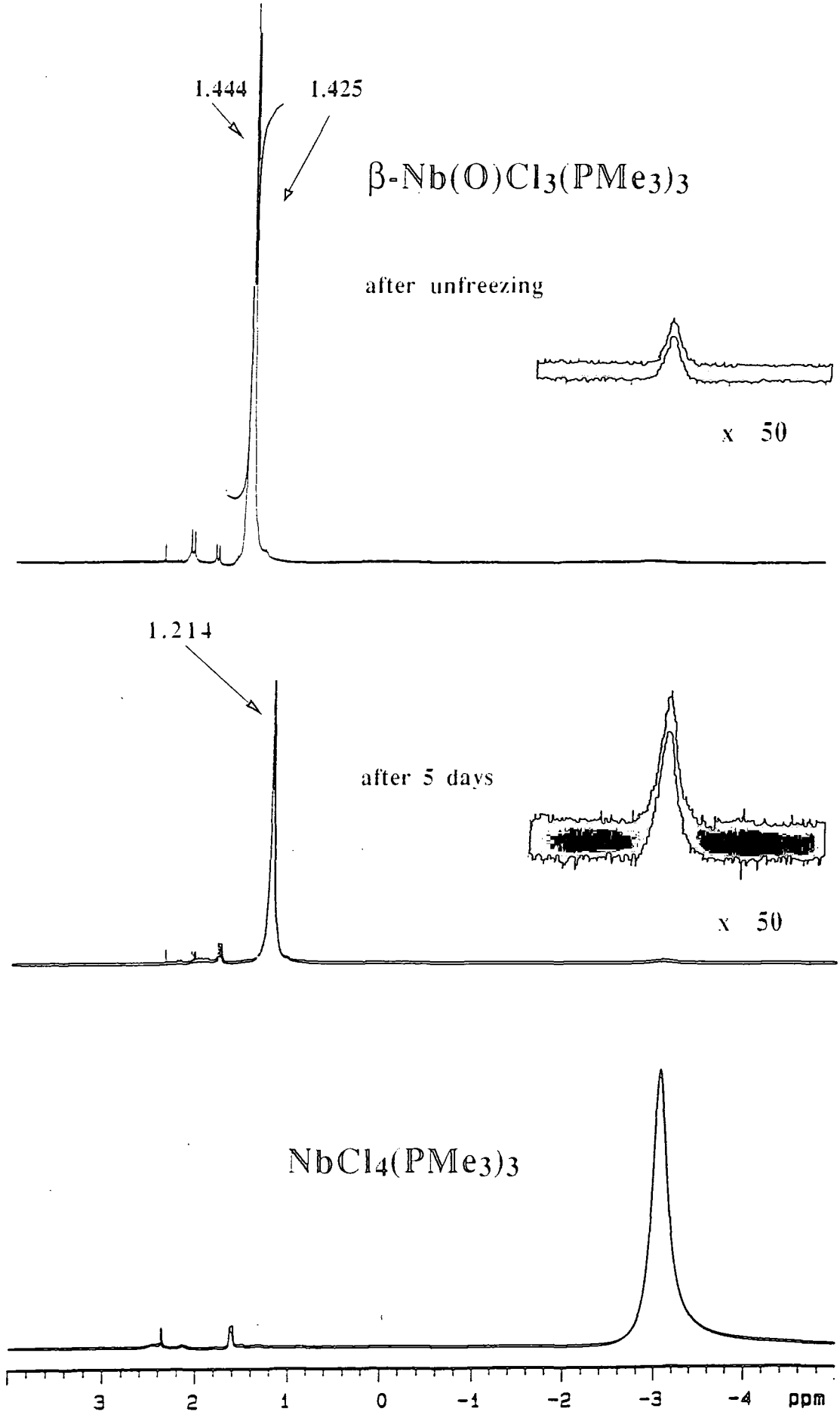


**Figure 4.11:** 400 MHz $^1$H NMR spectrum of β-Nb(O)$Cl_3$($PMe_3$)$_3$ in $CD_2Cl_2$ over the range +4 to -5 ppm.

NMR at δ 1.25 ppm is proposed to be due to the species $[Nb(O)Cl_3(PMe_3)_2]_2$, being consistent with the finding of T. Kee[9a] that in $CDCl_3$ the $^1H$ NMR of the related species $Nb(O)Cl_3(PPh_2Me)_2$ similarly consists of a broadened resonance for the methyl protons, suggesting the occurrence of ligand exchange on the NMR timescale. The broadening is also consistent with the effect of contact shifting due to the build up of the paramagnetic species $NbCl_4(PMe_3)_3$, but does not account for the shift with time. The species $[Nb(O)Cl_3(PMe_3)_2]_2$ was, however, found by myself and T. Kee to be insoluble in aromatic, aliphatic and chlorinated hydrocarbons upon isolation. Furthermore, solution infrared studies revealed that the yellow α- and green β-$Nb(O)Cl_3(PMe_3)_3$ when left standing in solution were thermally converted to $[Nb(O)Cl_3(PMe_3)_2]_2$, as indicated by the observation of absorptions at 920 $cm^{-1}$ (typical of a terminally bonded Nb=O moiety) and 322 $cm^{-1}$, in the solid-state and solution IR spectra, assignable to the known species $[Nb(O)Cl_3(PMe_3)_2]_2$.[9b] In both cases the paramagnetic contamination had risen to a steady level of 3.83% (green β form) and 4.33% (yellow α form) (figures 4.11 and 4.10) and so although $NbCl_4(PMe_3)_3$ is present in the β-isomer its level is constant. Whether its presence gives rise to the β-isomer or not is unclear from the $^1H$ NMR evidence. Since solid is seen to be deposited from solution, which is consistent with the increased signal of the solvent relative to the sample, the levels of paramagnetic contaminant have been determined relative to the total number of protons in the solution. Infrared data does, however, show that the presence of $NbCl_4(PMe_3)_3$ increases the rate at which the yellow (882 $cm^{-1}$) isomer converts to the green (871 $cm^{-1}$) isomer relative to allowing the yellow form to stand in solution. In the case of the α-isomer the $NbCl_4(PMe_3)_3$ impurity is only evident after decomposition has occurred. The origin of the tetrachloride impurity is not known but seems likely to be due to either disproportionation or reduction by $PMe_3$.

G. Parkin[12,16] in his re-investigation of the structures of *cis-mer*-$Mo(O)Cl_2(PMe_2Ph)_3$ also encountered the presence of a paramagnetic contaminant, $MoCl_3(PMe_2Ph)_3$. His studies, combining X-ray diffraction results with $^1H$ NMR spectra of solutions used to grow the crystals, indicate that the apparent 'Mo=O' bond length varies as a function of the composition.

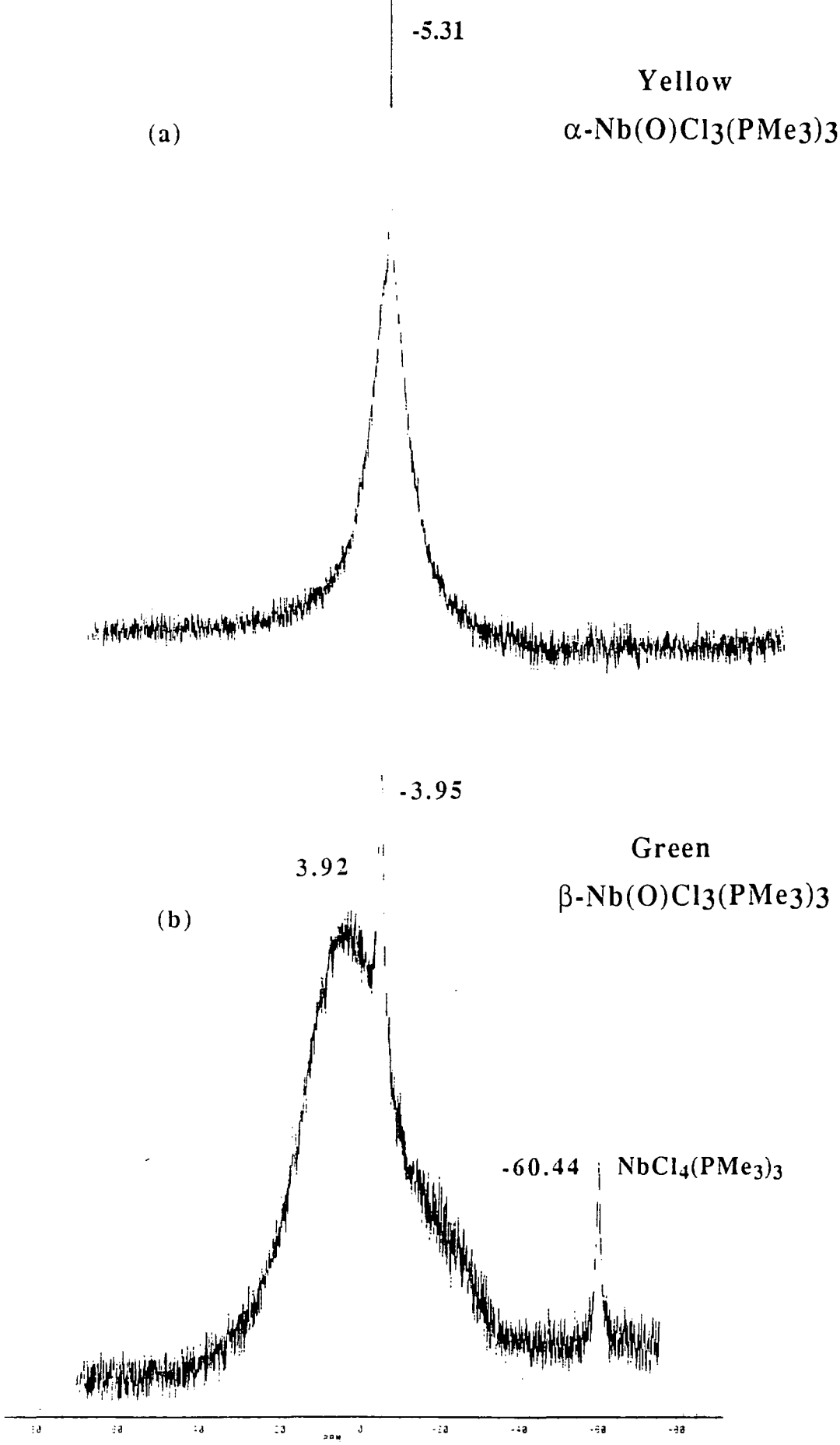


**Figure 4.12:** 101.26 MHz $^{31}P\{^{1}H\}$ NMR spectra of (a) yellow α-$Nb(O)Cl_3(PMe_3)_3$ and (b) green β-$Nb(O)Cl_3(PMe_3)_3$.

The $^{31}P\{^{1}H\}$ NMR spectra of the yellow α- and green β-$Nb(O)Cl_3(PMe_3)_3$ both show two resonances, one of which is broad and the other relatively sharp, consistent with the solution IR and $^{1}H$ NMR data that ligand exchange is occurring in solution. However, the peaks are also intrinsically broad due to $^{93}Nb$ quadrapolar coupling, the extra degree of broadening suggesting that an additional factor is causing further broadening. Both forms show a sharp peak at ca. δ -5.31 ($\Delta^1/_2$= 250 Hz) and δ -3.95 ($\Delta^1/_2$= 415 Hz) ppm in the yellow and green forms respectively, which are constant in position with time. In the case of yellow α-$Nb(O)Cl_3(PMe_3)_3$ the broad resonance is centred at δ -5.31 ppm ($\Delta^1/_2$= 1000 Hz). Similarly, in the case of green β-$Nb(O)Cl_3(PMe_3)_3$ the broad resonance remains static, but at 3.92 ppm ($\Delta^1/_2$= 2500 Hz, figure 4.12). The chemical shifts are consistent with $PMe_3$ being co-ordinated to a metal centre, the sharper resonance being tentatively assigned to the initial $Nb(O)Cl_3(PMe_3)_3$ species, where the $PMe_3$ ligands are 'locked' in fixed co-ordination sites, whereas the broad resonances suggest ligand exchange is occurring, and are thus assigned to the developing species $[Nb(O)Cl_3(PMe_3)_2]_2$, on the basis of the solution IR data and the fact that in the case of the green β-$Nb(O)Cl_3(PMe_3)_3$ form ligand exchange appears to be more rapid on the evidence of the $^{1}H$ NMR data, which shows signs of broadening at an earlier stage. $NbCl_4(PMe_3)_3$ is known to give a broad peak at δ -60.44 ppm ($\Delta^1/_2$ = 250Hz) in its 101.26 MHz $^{31}P\{^{1}H\}$ NMR spectrum in $CDCl_3$, and is observed only in the green β-$Nb(O)Cl_3(PMe_3)_3$ form.

## 4.8 Solid-State Reactivity

A sample of $Nb(O)Cl_3(PMe_3)_3$ with a 75:25 α,β mix stored under nitrogen for one week at room temperature, showed by IR spectroscopy to be a mixture with an isomeric ratio now of 57:43 indicating that solid-state α→β conversion is occurring. Pure α-$Nb(O)Cl_3(PMe_3)_3$ shows a similar α→β conversion. In the absence of light α→β conversion still occurs giving a 67:33 α,β mix indicating that the process proceeds thermally (just as for $Ta(S)Cl_3(PMe_3)_3$ as reported by A.Shaw[30]) as well as photochemically. β→α conversion of pure β-$Nb(O)Cl_3(PMe_3)_3$ crystals is however not

observed suggesting that the interconversion is irreversible and in favour of the thermodynamically more stable β-form.

## 4.9 Determination of the Level of $NbCl_4(PMe_3)_3$ by Elemental Analysis

Along with $^1H$ NMR analysis and infrared spectroscopy, elemental analysis suggests the presence of a contaminant. It has been established by both of the former techniques that this impurity is $NbCl_4(PMe_3)_3$. As with the other techniques elemental analysis can be used to determine the level of impurity present in each of the two forms of $Nb(O)Cl_3(PMe_3)_3$. Using the equation 4.3, where x represents the mole fraction of $NbCl_4(PMe_3)_3$ (determined using the same reasoning as for equation 2.2, section 2.7), the results of repeated elemental analysis can be tabulated (table 4.4) in order to give an indication of the degree of contamination. The mole fraction of $NbCl_4(PMe_3)_3$ in the green form of $Nb(O)Cl_3(PMe_3)_3$ is estimated to be 0.105±0.038, whereas in the yellow form the amount is negligible, -0.035±0.051. These findings are reflected by those

$$x = \frac{\%Cl.RMM[Nb(O)Cl_3(PMe_3)_3] - 300.RMM[Cl]}{100.RMM[Cl] - \%Cl.RMM[(Cl) - (O)]}$$

$$= \frac{443.5044\ \%Cl - 10635.9}{3545.3 - 19.454\ \%Cl} \qquad \textbf{(4.3)}$$

| | %C | %H | %Cl | Average %Cl | $\%NbCl_4(PMe_3)_3$ |
|---|---|---|---|---|---|
| Calculated | 24.37 | 6.14 | 23.98 | ---- | ---- |
| Yellow $Nb(O)Cl_3(PMe_3)_3$ | 24.91 | 6.33 | 24.09 | 23.74 | -3.54 |
| | 24.04 | 6.36 | 23.38 | | |
| | 24.21 | 6.27 | | | |
| | 24.36 | 6.08 | | | |
| Green $Nb(O)Cl_3(PMe_3)_3$ | 23.77 | 6.10 | 25.01 | 24.70 | 10.45 |
| | 24.04 | 6.36 | 24.73 | | |
| | | | 24.37 | | |

**Table 4.4:** Elemental analysis for the yellow and green forms of $Nb(O)Cl_3(PMe_3)_3$

established by $^1H$ NMR, which indicate 0.000±0.001 and 0.013±0.001 mole fractions of $NbCl_4(PMe_3)_3$ in the yellow and green forms respectively.

## 4.10 The Molecular Structures of Yellow and Green $Nb(O)Cl_3(PMe_3)_3$

The isolation of two isomeric compounds with the formula $Nb(O)Cl_3(PMe_3)_3$ was described in section 4.3. Both forms, yellow $Nb(O)Cl_3(PMe_3)_3$[9a] and green $Nb(O)Cl_3(PMe_3)_3$[9b,10] have been subjected to X-ray diffraction analysis by Prof. M. McPartlin and co-workers at the University of North London and the results of these studies are described below.

### 4.10.1 Yellow $Nb(O)Cl_3(PMe_3)_3$ ($\nu$(Nb=O) 882 $cm^{-1}$)

The crystal data are collected in appendix 1A and the molecular structure is illustrated in figures 4.13 and 4.14(a). Selected bond angles and distances are given in appendix 4A.

The complex is monomeric for which the coordination geometry is best described as distorted, monocapped octahedral with facial arrangements of chloro and trimethylphosphine ligands giving the molecule virtual $C_{3v}$ symmetry (figure 4.13). The oxo group is in a site capping the face defined by the phosphine ligands and lies 1.16Å above the P(1), P(2), P(3) plane, with the niobium atom 0.62Å below this plane. This coordination is similar to that observed in $NbCl_4(PMe_3)_3$[17], yet very different to the seven coordinate complex $Nb(O)(S_2CNEt_2)_3$[8], in which the niobium atom is at the centre of a distorted pentagonal bipyramid.

The Nb=O bond length of 1.781(6)Å is significantly longer than the Nb=O distances usually observed in four to seven coordinate oxo-niobium complexes (average ca. 1.7Å, table 4.5). This presumably arises due to the presence of three, highly basic electron releasing $PMe_3$ ligands within the crowded coordination sphere of yellow $Nb(O)Cl_3(PMe_3)_3$.

(a)

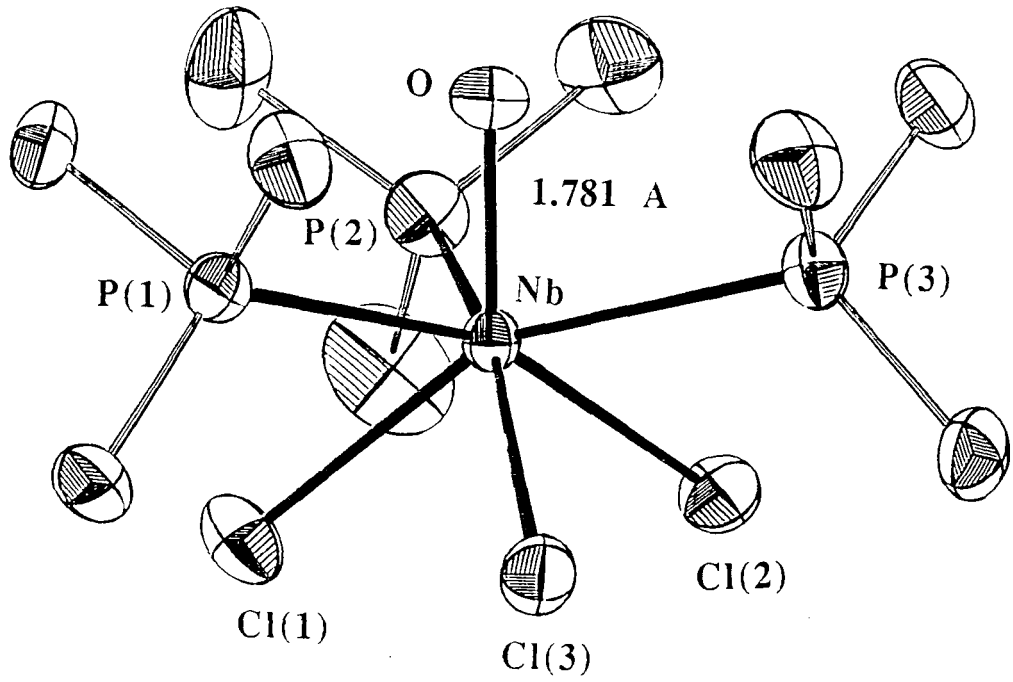


(b)

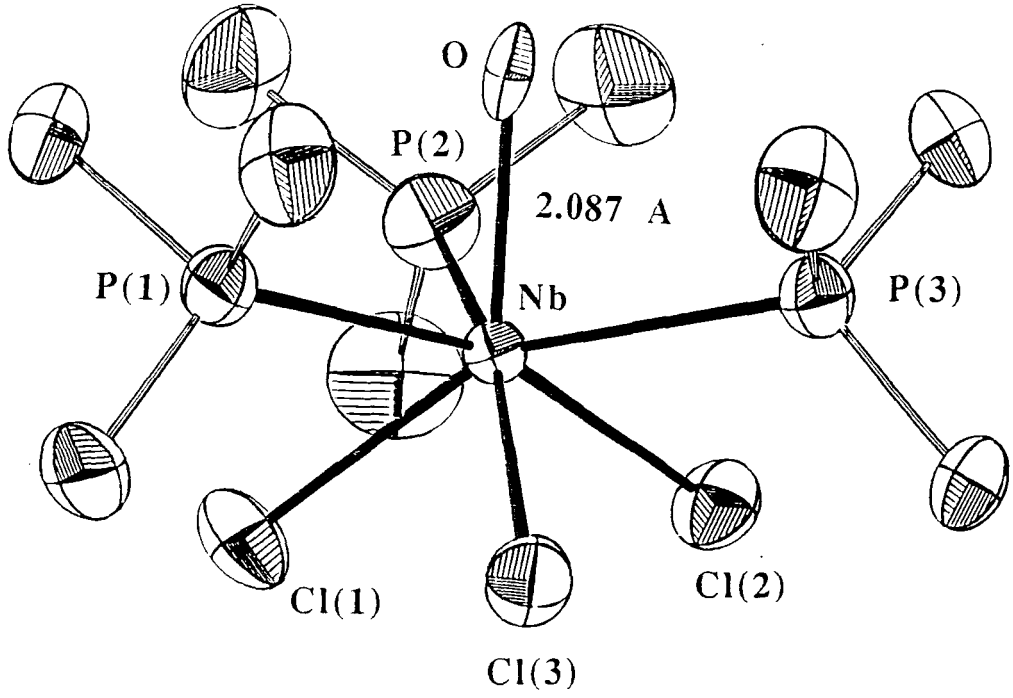


**Figure 4.14:** Comparison of the structures of (a) yellow α- (ν(Nb=O) 882 $cm^{-1}$), and (b) green β- (ν(Nb=O) 871 $cm^{-1}$) forms of $Nb(O)Cl_3(PMe_3)_3$ showing the elongated thermal ellipsoid of the oxygen atom in the green form.

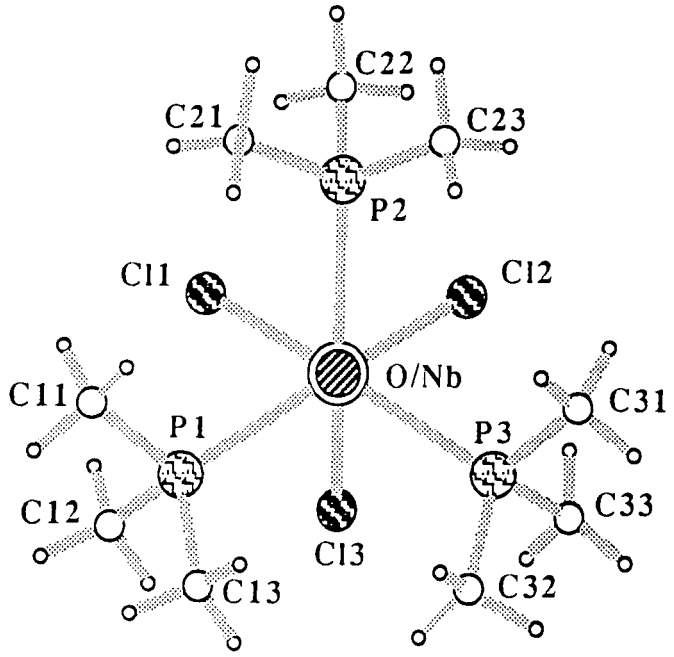


**Figure 4.13:** View down the oxygen-niobium bond of yellow $Nb(O)Cl_3(PMe_3)_3$

The compounds yellow $Nb(O)Cl_3(PMe_3)_3$ and $NbCl_4(PMe_3)_3$[17] are isomorphous (space group $P2_{1/c}$). The average Nb-Cl distances in yellow $Nb(O)Cl_3(PMe_3)_3$ (2.518(8)Å) are slightly longer than the average facial Nb-Cl distances in $NbCl_4(PMe_3)_3$ (2.453(13)Å) the opposite of the trend predicted on the basis of oxidation state. Since both compounds possess average P-Nb-$Cl_{trans}$ angles of ca. 159°, a similar average trans influence is anticipated due to the oxo ligand. Therefore, the average lengthening observed in yellow $Nb(O)Cl_3(PMe_3)_3$ may be attributed to the presence of the oxo ligand.

Interestingly, the Nb-Cl (2) bond is the longest (2.533(3)Å) whilst also having the most acute O-Nb-Cl angle of 121.2°, an observation at variance with an oxo ligand trans influence. However, since the trans P-Nb-Cl angle for Cl(2) is the largest (161.9°), this atom may experience a slightly larger $PMe_3$ trans influence.

The Nb-P bonds have an average length of 2.640(4)Å in yellow $Nb(O)Cl_3(PMe_3)_3$ and 2.651(6)Å in $NbCl_4(PMe_3)_3$, the former having the slightly shorter distances as expected for niobium (V) over niobium (IV).

The acute O-Nb-P angles (average 76.5(2)°) led to a staggered arrangement of $PMe_3$ substituents with respect to the capping oxygen atom (as viewed along the P-Nb

vector) in order to minimise interligand repulsions. A similar arrangement is found in $NbCl_4(PMe_3)_3$. Consequently, close O···H contacts result, in the range 2.79 - 2.97Å.

| No. | Complex | de⁻ | CN | Nb=O (Å) | υ ($cm^{-1}$) | Ref. |
|---|---|---|---|---|---|---|
| 1. | $[Nb(O)Cl_4]^-[NbCl_4(diars)_2]^+$ | 0 | 5[a] | 1.70(2) | | 18 |
| 2. | $[Nb(O)(NCS)_5](AsPh_4)_2$ | 0 | 6 | 1.70(4) | | 19 |
| 3. | $[Nb(O)F_5]^{2-}[N_2H_6]^{2+}$ | 0 | 6 | 1.75(2) | | 20 |
| 4. | $[Nb(O)Cl_5](AsPh_4)_2$ | 0 | 6 | 1.967(6) | | 21 |
| 5. | $[Nb(O)Cl_4(MeCN)]PPh_3Me$ | 0 | 6 | 1.688(2) | | 22 |
| 6. | $[Nb(O)Cl_4(H_2O)]PPh_4$ | 0 | 6 | 1.74(1) | | 23 |
| 7. | $[Nb(O)Cl_4(THF)]^-[CpNbCl(MeCN)_4]^+$ (trans) | 0 | 6 | 1.665(11) | | 24 |
| 8. | $[Nb(O)Cl_4(OPCl_2O)](PPh_4)_2$ | 0 | 6 | 1.77(1) | | 23 |
| 9. | $Nb(O)Cl_3[CF_3C(O)CHC(O)(c\text{-}C_4H_3S)]$ | 0 | 6 | 1.704(3) | | 25 |
| 10. | $Nb(O)Cl_3$ | 0 | 6 | | 790 | |
| 11. | $Nb(O)Br_3$ | 0 | 6 | | 758 | |
| 12. | $Nb(O)Cl_3(MeCN)_2$ (mer) | 0 | 6 | 1.68(2) | 956 | 29 |
| 13. | $Nb(O)Br_3(MeCN)_2$ (mer) | 0 | 6 | | 952 | |
| 14. | $Nb(O)Cl_3(hmpa)_2$ (mer) | 0 | 6 | 1.692(5) | | 26 |
| 15. | $Nb(O)Cl_3(THF)_2$ | 0 | 6 | | 960 | |
| 16. | $Nb(O)Cl_2(OEt)bipy$ | 0 | 6 | 1.710(35) | | 19 |
| 17. | $[Nb(O)(C_2O_4)_3](NH_4)_3$ | 0 | 7 | 1.710(10) | | 27 |
| 18. | α-$Nb(O)Cl_3(PMe_3)_3$ | 0 | 7 | 1.781(6) | 882 | 9 |
| 19. | β-$Nb(O)Cl_3(PMe_3)_3$ | 0 | 7 | 2.087(1)<br>1.929(6) | 871 | 9b<br>10 |
| 20. | $Nb(O)(S_2CNEt_2)_3$ | 0 | 7 | 1.74(1) | | 8 |

**Table 4.5:** Table of Nb=O bond lengths found in selected Nb(V) oxo complexes

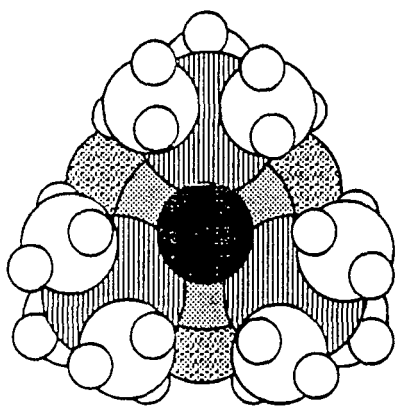

**Figure 4.15:** Space filling diagram of yellow $Nb(O)Cl_3(PMe_3)_3$ viewed down the oxygen-niobium bond

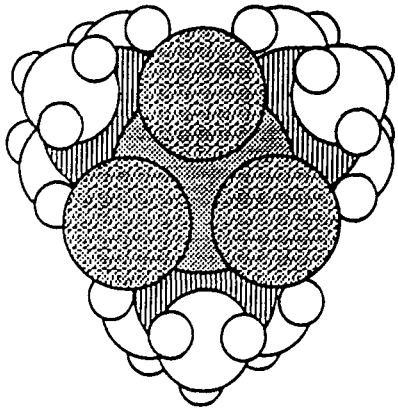

**Figure 4.16:** Space filling diagram of yellow $Nb(O)Cl_3(PMe_3)_3$ viewed through the facial chlorine plane

Figure 4.15 represents a space filling diagram of yellow $Nb(O)Cl_3(PMe_3)_3$ viewed down the O=Nb vector illustrating the extremely close contacts between the oxygen atom and six phosphine methyl hydrogens (H-H). Figure 4.16 is a similar diagram viewed through the facial chlorine plane.

### 4.10.2 Green $Nb(O)Cl_3(PMe_3)_3$ ($\nu$(Nb=O) 871 $cm^{-1}$)

The crystal data are collected in appendix 1B and the molecular structure is illustrated in figure 4.14(b). Selected bond angles and distances are given in appendix 4B.

The green compound $Nb(O)Cl_3(PMe_3)_3$ is isomorphous to yellow $Nb(O)Cl_3(PMe_3)_3$ (space group $P2_1/c$) and the average interatomic distances and angles are essentially identical, although the 871 $cm^{-1}$ isomer shows larger individual deviations.

The Nb-Cl distances are slightly shorter and the Nb-P distances marginally longer for the $\nu$(Nb=O) 871 $cm^{-1}$ isomer.

### 4.10.3 Solid-State Structure of $NbCl_4(PMe_3)_3$

$NbCl_4(PMe_3)_3$ was originally prepared and characterised crystallographically by Cotton and co-workers.[17] $NbCl_4(PMe_3)_3$ forms monoclinic crystals (space group $P2_1/c$) and is structurally isomorphous with that of the yellow and green forms of

| | | | |
|---|---|---|---|
| Nb - Cl(1) | 2.449(3) | P(2) - Nb - P(1) | 116.3(1) |
| Nb - Cl(2) | 2.476(3) | P(3) - Nb - P(1) | 106.5(1) |
| Nb - Cl(3) | 2.433(4) | P(3) - Nb - P(2) | 117.5(1) |
| | | | |
| Nb - P(1) | 2.647(3) | Cl(4) - Nb - Cl(1) | 122.5(2) |
| Nb - P(2) | 2.643(4) | Cl(4) - Nb - Cl(2) | 120.0(1) |
| Nb - P(3) | 2.664(4) | Cl(4) - Nb - Cl(3) | 134.8(1) |
| | | | |
| | | Cl(4) - Nb - P(1) | 75.8(1) |
| Nb - Cl(4) | 2.409(4) | Cl(4) - Nb - P(2) | 74.0(1) |
| | | Cl(4) - Nb - P(3) | 75.0(1) |
| | | | |
| Cl(2) - Nb - Cl(1) | 95.5(1) | P(1) - Nb - Cl(1) | 77.2(1) |
| Cl(3) - Nb - Cl(1) | 85.3(1) | P(1) - Nb - Cl(2) | 163.7(1) |
| Cl(3) - Nb - Cl(2) | 87.6(1) | P(1) - Nb - Cl(3) | 77.3(1) |
| | | P(2) - Nb - Cl(1) | 74.3(1) |
| | | P(2) - Nb - Cl(2) | 74.7(1) |
| | | P(2) - Nb - Cl(3) | 151.2(1) |
| | | P(3) - Nb - Cl(1) | 162.1(1) |
| | | P(3) - Nb - Cl(2) | 76.1(1) |
| | | P(3) - Nb - Cl(3) | 78.6(1) |

**Table 4.6:** Selected bond distances (Å) and angles (°) for green $NbCl_4(PMe_3)_3$[17]

$Nb(O)Cl_3(PMe_3)_3$, having what can be best described as a distorted monocapped octahedral geometry (an *axial* chlorine occupying the site of the oxygen atom in $Nb(O)Cl_3(PMe_3)_3$). Its molecular structure is illustrated in an ORTEP drawing in figure 4.17. Selected bond distances and angles are given in table 4.6.

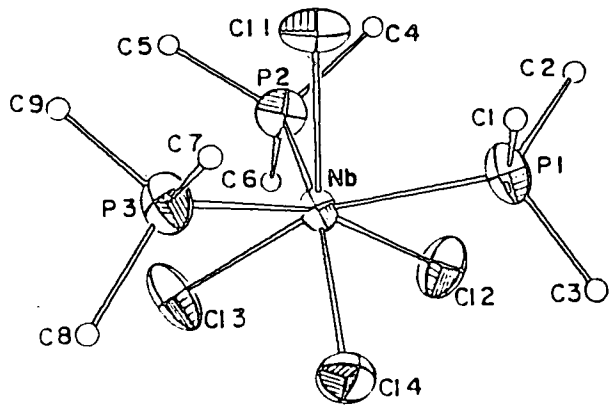


**Figure 4.17:** The structure $NbCl_4(PMe_3)_3$ shown in an ORTEP drawing

### 4.10.4 A Comparison of the Molecular Structures of the Yellow and Green Forms of $Nb(O)Cl_3(PMe_3)_3$ and Green $NbCl_4(PMe_3)_3$

Comparative values of selected parameters for yellow and green $Nb(O)Cl_3(PMe_3)_3$ and green $NbCl_4(PMe_3)_3$ are displayed in table 4.7.

Without doubt, the most marked difference between the $Nb(O)Cl_3(PMe_3)_3$ isomers is the length of the niobium-oxygen bond. In green $Nb(O)Cl_3(PMe_3)_3$ this bond has been apparently lengthened by ca. 0.306Å over that in yellow $Nb(O)Cl_3(PMe_3)_3$ and is ca. 0.400Å longer than is usually found in niobium oxo compounds. Indeed this distance of 2.087(5)Å seen in the green form is approaching the sum of the covalent radii of niobium and oxygen (2.1Å)[11] and was originally regarded as representing a Nb-O bond order considerably less than 2 and in fact close to unity. Consistently the Nb=O bond length is between representative values of niobium-oxygen single bonds in $\mu_2$-bridging oxo compounds (ca. 1.91Å)[28] and niobium-oxygen dative covalent bonds, as for example in $[Cp'NbCl_3(H_2O)]_2$ ($\mu$-O) where [Nb-O($H_2O$)] is 2.19Å (Cp' = $C_5H_4Me$).[28] However, it has now been established that this lengthening is the manifestation of the substantially longer axial Nb-Cl bond (2.355(8)Å) of co-crystallised $NbCl_4(PMe_3)_3$.

Although the green form of $Nb(O)Cl_3(PMe_3)_3$ was originally considered to possibly be a geometric isomer of the yellow form on the basis of the second independently observable $\nu$(Nb=O) stretch at 871 $cm^{-1}$, X-ray structure analysis showed its structure to be virtually identical in all respects to that of the yellow form, except for the bond lengths to the metal. This is also backed-up by IR spectroscopic evidence that in the low frequency region (350 to 200 $cm^{-1}$) the two forms exhibit near identical $\nu$(Nb-Cl) stretches (figure 4.3). Although there are slight variations in the O-Nb-Cl angles, the mean values are not significantly different between the two isomers. In the initial refinement on the green form an extremely long Nb=O bond of 2.087(5)Å was observed and the oxygen atom anisotropic thermal ellipsoid showed a marked elongation in the Nb=O bond vector direction. Furthermore, residual electron density in this direction beyond the oxygen atom indicated the possibility of the presence of a second virtually

isostructural molecule, with an axial chlorine in the capping site of the oxygen atom. Refinement using an 80% occupancy of the axial positions by an oxygen atom and 20% by a chlorine atom, gave a Nb=O bond length of 1.929(6)Å and a Nb-$Cl_{axial}$(4) bond length of 2.355(8)Å (a value close to that reported by Cotton[22] for the Nb-$Cl_{axial}$ bond of 2.409(6)Å in the green tetrachloride $NbCl_4(PMe_3)_3$).

In the green isomer of $Nb(O)Cl_3(PMe_3)_3$ the Nb=O bond length of 1.929(6)Å is 0.148Å (ca. 25 standard deviations) longer than that observed earlier[9a] in the yellow form. This lengthening is accompanied by a relatively small but significant contraction in the Nb-Cl distances (mean 0.023Å, ca. 10 standard deviations). The difference is, however, still substantially larger than that expected from a consideration of the 11 $cm^{-1}$ difference in the ν(Nb=O) stretches, which implies a 0.023Å change in the Nb-O bond length.

| Parameter | Yellow $Nb(O)Cl_3(PMe_3)_3$ | Green $Nb(O)Cl_3(PMe_3)_3$ | $NbCl_4(PMe_3)_3$ |
|---|---|---|---|
| (Nb=O/Nb-$Cl_{axial}$) | 1.781(6) | 2.087(5) | 2.409(4) |
| $(Nb-Cl)_{av}$ | 2.518(8) | 2.496(7) | 2.543(13) |
| $(Nb-P)_{av}$ | 2.640(2) | 2.642(3) | 2.651(6) |
| O-Nb-$Cl_{av}$ | 125.0(2) | 125.2(3) | 125.7(8) |
| O-Nb-$P_{av}$ | 76.5(2) | 76.3(7) | 74.9(4) |
| P-Nb-$P_{av}$ | 114.7(1) | 114.5(2) | 113.4(4) |
| Cl-Nb-$Cl_{av}$ | 90.4(1) | 90.2(1) | 89.4(8) |
| P-Nb-$Cl_{trans,\ av}$ | 158.5(2) | 158.5(1) | 159.0(1) |

**Table 4.7:** Comparative values of some parameters for yellow and green $Nb(O)Cl_3(PMe_3)_3$

## 4.11 Structural Disorder

Original indications from spectroscopic, $^1H$ NMR and X-ray structural studies of the two forms of $Nb(O)Cl_3(PMe_3)_3$ appeared to suggest that this system provided evidence for the phenomenon of bond-stretch isomerism. Unlike previously reported examples which involved an octahedral geometry at a $d^1$ or $d^2$ metal centre, here the

molecules exhibited seven co-ordinate geometry and a $d^0$ configuration. The first structurally characterised yellow α-$Nb(O)Cl_3(PMe_3)_3$ form (ν(Nb=O) 882 $cm^{-1}$) was found to have a mono-capped distorted octahedral structure (figure 4.14 (a)), with each of the three chloro and phosphine ligands occupying facial octahedron sites with the oxo ligand capping the '$P_3$' face. The Nb=O bond length of 1.781(6)Å was typical of a Nb=O double bond.

The subsequent use of an alternative starting material, the monomeric base-stabilised $Nb(O)Cl_3(MeCN)_2$, instead of the 'polymeric' base-free $Nb(O)Cl_3$, led to the isolation of a green form with the same elemental analysis, and an infrared spectrum which closely resembled that of the yellow form apart from the ν(Nb=O) stretch being at 871 $cm^{-1}$ (figure 4.1). It was originally postulated, as in the case of Chatt's $Mo(O)Cl_2(PMe_2Ph)_3$ system, that the two forms were geometric isomers. However, X-ray structure determination revealed that the crystals were isomorphous, with very similar overall geometries, even down to the orientations of the methyl fragments of the phosphine ligands. The green form, however, showed an extremely long Nb=O bond length of 2.087(5)Å . Infrared and $^1H$ NMR analysis did not reveal the presence of a hydroxy group in order to explain this abnormality. This was backed-up by vibrating-sample magnetometry, which indicated a fundamentally diamagnetic compound, whereas a hydroxy complex would have a $d^1$ configuration and so be paramagnetic. As shown in section 4.6.2, the assignment of the two IR bands at 882 and 871 $cm^{-1}$ due to Nb=O stretches was confirmed by O-18 labelling (figures 4.8 and 4.9).

The evidence for bond-stretch isomerism at this stage was quite compelling. However, a marked elongation in the anisotropic ellipsoid of the axial oxo, along with the psuedo $C_3$ axis (figure 4.14 (b)), and together with a residual electron density corresponding to ca. 1.5 electrons in the axial position 0.51Å beyond the oxygen atom in the Nb-O lengthened green form, suggested all was not quite as it seemed. The residual peak of electron density indicated the presence of a second co-crystallised isostructural species with a longer axial bond; X-ray analysis only being able to show an average structure. Systematic testing showed the occupancy of the oxygen atom site was reduced to 80%, and 20% was assigned to the site of the smaller peak. The parameter of the

atoms refined satisfactorily, giving a Nb=O bond distance of 1.929(6)Å and an axial Nb-Cl bond length of 2.355(8)Å.[2] There still remained the inescapable fact that IR spectroscopic studies revealed two independent bands assignable to ν(Nb=O) stretches. Without recourse to the phenomenon of bond-stretch isomerism, a solid-state model in which 80% of the normal Nb=O bond length yellow form (d(Nb=O) 1.781Å, ν(Nb=O) 882 $cm^{-1}$) had co-crystallised with 20% of a geometric isomer was considered. This model would require a chloro ligand in the capping axial site and the oxo ligand replacing it to be in an octahedral site (figure 4.18 (a)) and thus be assigned to the ν(Nb=O) 871 $cm^{-1}$ band. Detection of the oxygen atom of 20% occupancy would by X-ray determination be very difficult, and completely impossible if rotational disorder of the 20% geometric isomer was also invoked, such that each of the three equivalent octahedral sites (fully occupied in 80% of the molecules by three chloro ligands of the yellow isomer), was randomly occupied by the oxo ligand of the geometric isomer in the remaining 20%.

The disorder model despite giving a satisfactory explanation of the X-ray results showing the apparent lengthening of the Nb=O bond as an artifact of the disorder, was still not able to explain the occurrence of a single ν(Nb=O) stretch at 871 $cm^{-1}$ in all samples of the green form. Secondly, no evidence was seen of the band at 882 $cm^{-1}$ due to the yellow isomer, presumed in this model to be the source of the 80% axial oxo ligand.

The concept of a geometric isomer as the reason for the disorder was therefore dropped in favour of a model where the crystallographic disorder was due to the co-crystallisation of 20% of the tetrachloride $NbCl_4(PMe_3)_3$ (figure 4.18 (b)). This species was thought to arise due to some source of decomposition. $^1H$ NMR studies have been able (section 4.7) to detect the presence of such a paramagnetic contaminant, in an upfield region of the spectrum (δ -3.01ppm) not normally scanned. As can be seen from figure 4.19, replacement of some of the oxo molecules by tetrachloride has little affect on the overall crystal packing since the three phosphine groups overshadow any axial ligand.

On the basis of X-ray analysis it is thus concluded that only one oxo species is present in the yellow and green forms of '$Nb(O)Cl_3(PMe_3)_3$', and that in the green form

(a)

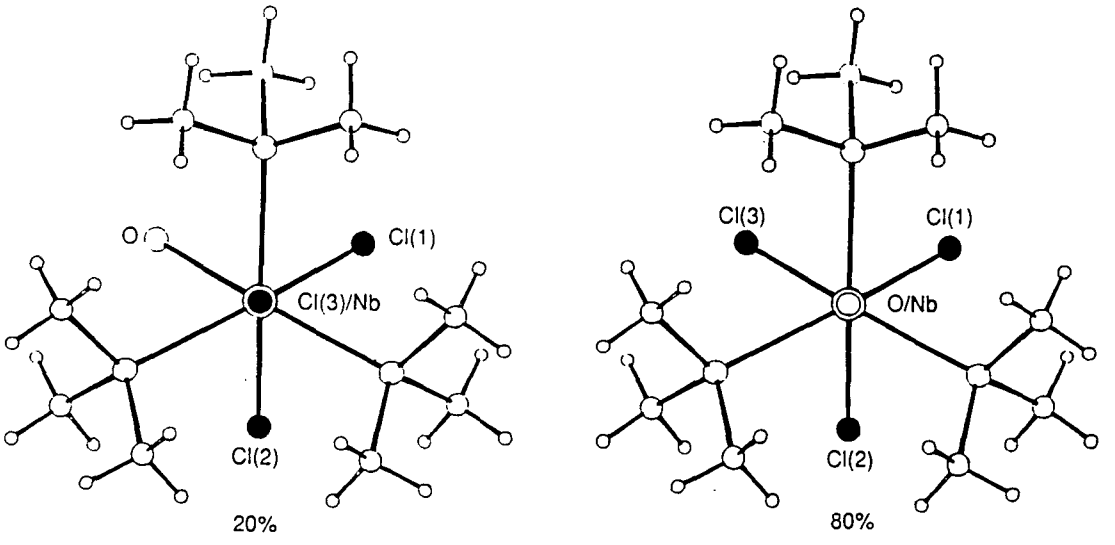


(b)

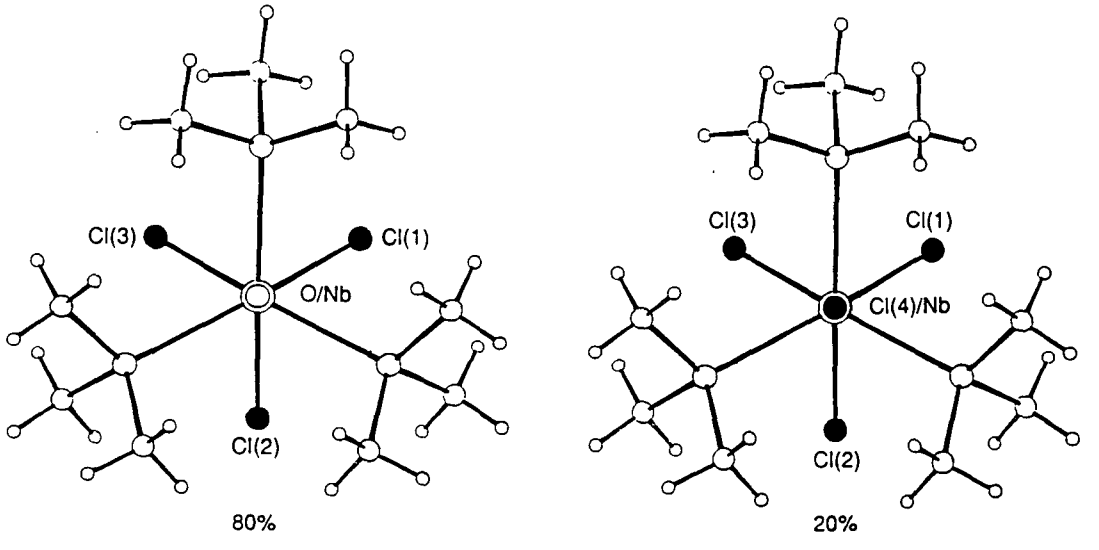


**Figure 4.18:** Disorder models to rationalise the observed crystallographic results on the green form of $Nb(O)Cl_3(PMe_3)_3$: (a) 80% of an axial oxo species with 20% of a geometrical isomer (oxygen atom occupying an octahedral site), and (b) 80% of an axial oxo species contaminated with 20% of $NbCl_4(PMe_3)_3$.

(a)

$Nb(O)Cl_3(PMe_3)_3$

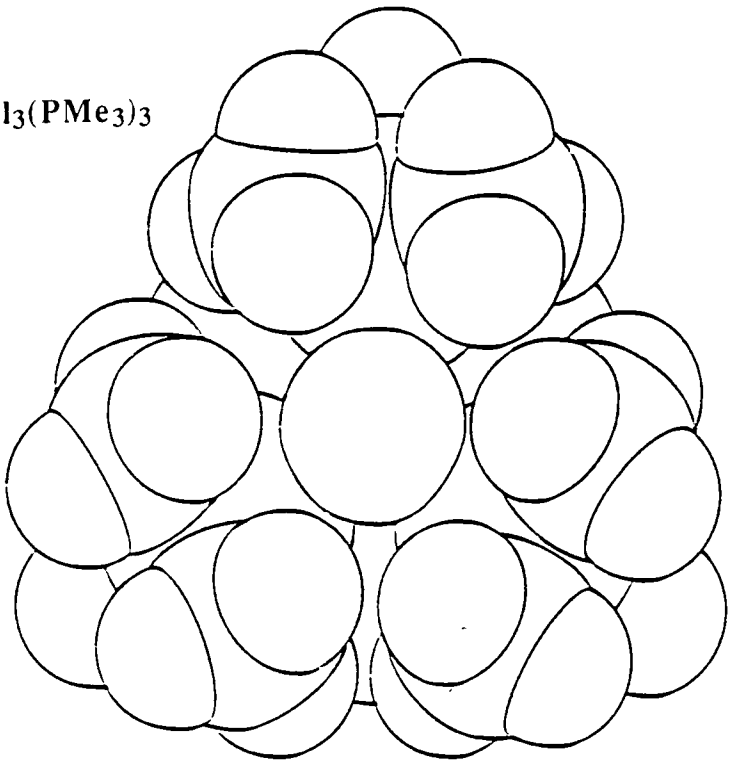

(b)

$NbCl_4(PMe_3)_3$

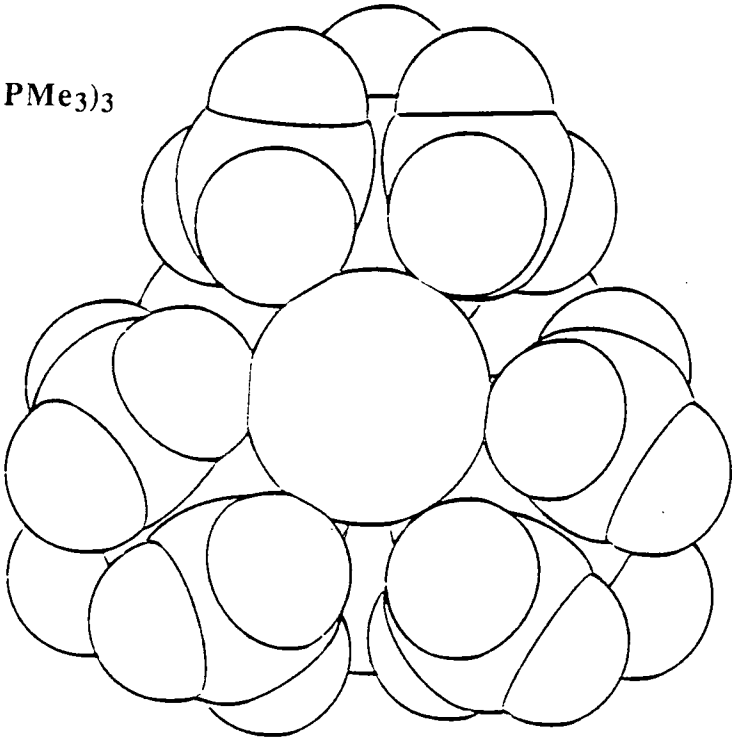

**Figure 4.19:** Comparison of space filling representations of α-$Nb(O)Cl_3(PMe_3)_3$ and $NbCl_4(PMe_3)_3$.

the oxygen atom in the axial site is partially occupied by chloride from the tetrachloride. Nevertheless, infrared data clearly indicates that the two oxo species are distinguishable, so re-enforcing the postulation that in principle bond-stretch isomerism can exist, since the difference in the ν(Nb=O) stretches must implicitly be linked to a real difference in the Nb=O bond lengths in the two forms (if not to the extent first indicated by X-ray determination).

## 4.12 β-$Nb(O)Br_3(PMe_3)_3$

Treatment of $Nb(O)Br_3$ in neat $PMe_3$ for 18 h. followed by dissolution of the crude orange-brown product in dichloroethane and cooling at -35°C for 1 week produces red cubic crystals, first isolated by A. Shaw.[30] IR spectroscopy shows a ν(Nb=O) absorption at 871 $cm^{-1}$ (figure 4.20), identical to that shown by β-$Nb(O)Cl_3(PMe_3)_3$. However, the Nb-X stretching vibrations are different. β-$Nb(O)Cl_3(PMe_3)_3$ shows peaks in this region at 351, 290 and 274 $cm^{-1}$ (figure 4.3). The pattern is also immediately recognisable as being different. The presence of any paramagnetic $NbBr_4(PMe_3)_3$ by infrared spectroscopy can not be commented upon since the species has yet to be synthesized. Although the ν(Nb=O) stretching vibration frequencies for the niobium oxo-halides are coincident the absorption in the metal-halide region of the IR spectrum conclusively point to the two species being different and not simply the result of chloride-bromide exchange to produce the oxochloro analogue.

The 400 MHz $^1H$ NMR spectrum ($CD_2Cl_2$) consists of a doublet at δ 1.57 ppm ($^2J(PH)$=9.60 Hz, figure 4.21). This contrasts with β-$Nb(O)Cl_3(PMe_3)_3$ which exhibits a doublet at δ 1.43 ppm ($^2J(PH)$=7.20 Hz). The different chemical shifts for the bromo and chloro derivatives indicate that the two species are unique, whereas from IR data it is not initially obvious since both species exhibit a ν(Nb=O) stretch at 871 $cm^{-1}$ (the possibility of chloride-bromide metathesis occurring during synthesis in a chlorinated solvent not being unreasonable). Even the presence of a different paramagnetic species $NbBr_4(PMe_3)_3$ at δ -3.45 ppm ($\Delta_{1/2}$=295 Hz) can not be proposed as perturbing the

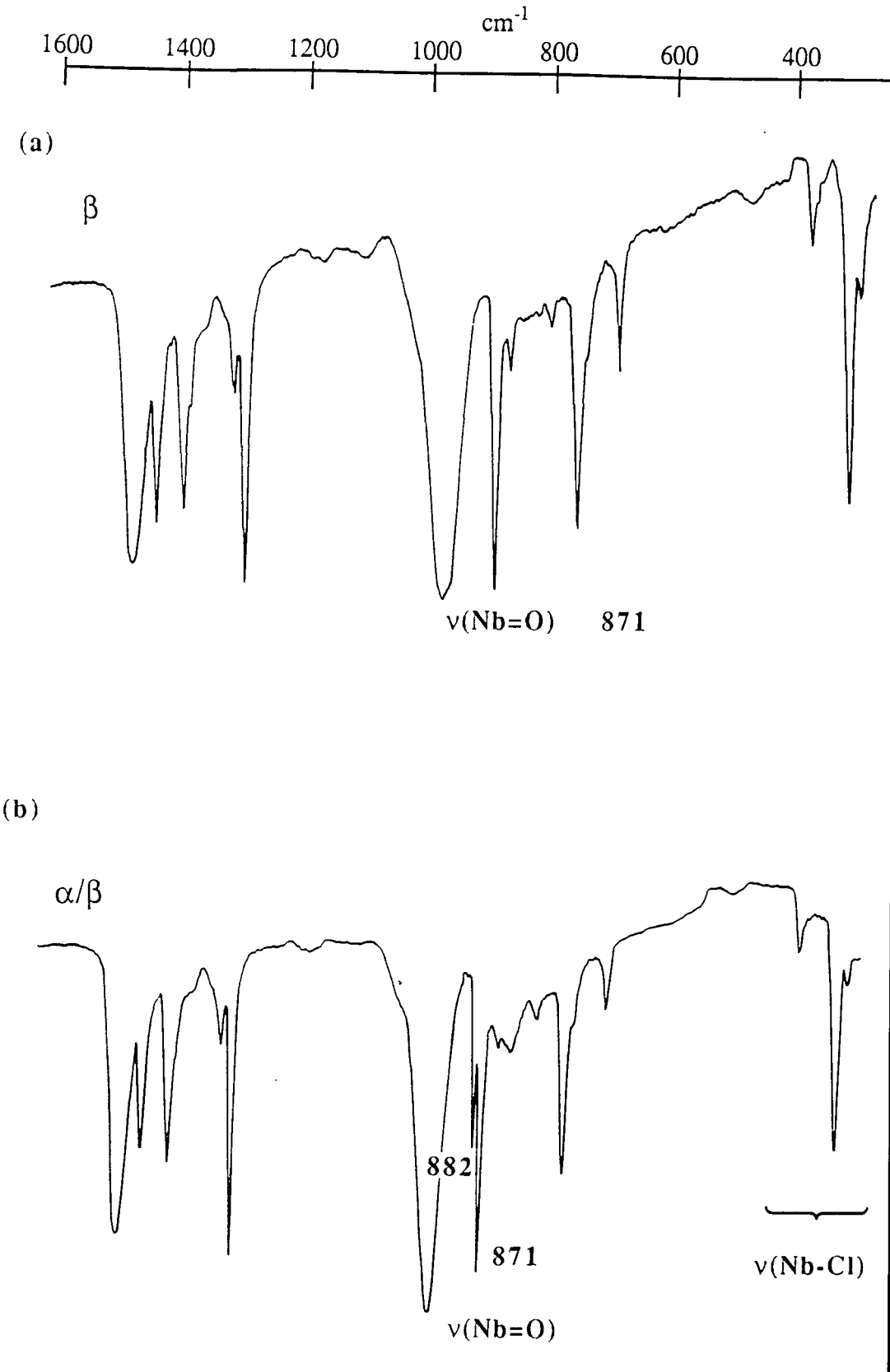


**Figure 4.20:** Solid-state infrared spectrum of β-$Nb(O)Br_3(PMe_3)_3$.

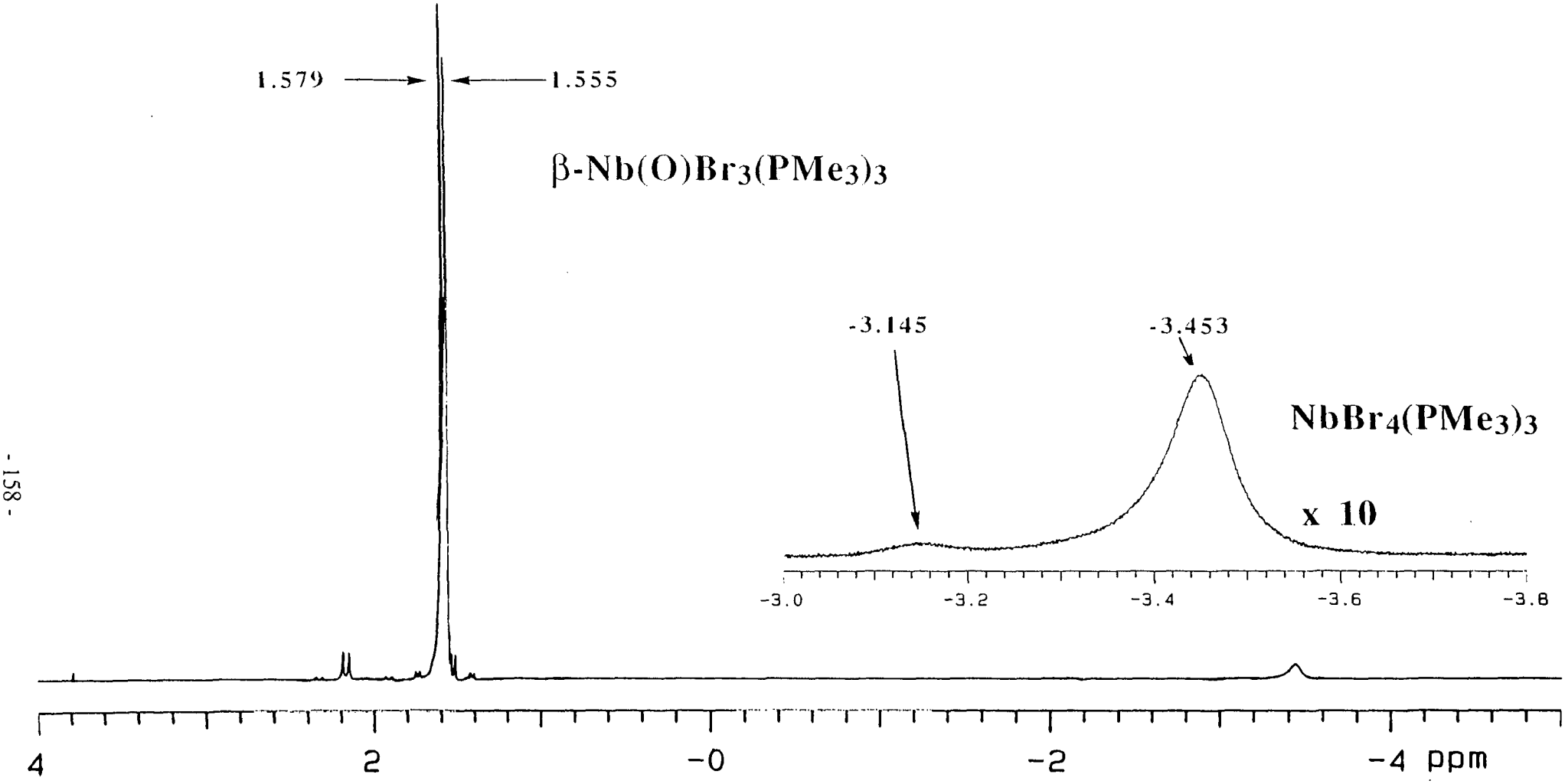


**Figure 4.21:** 400 MHz $^1$H NMR spectrum of β-Nb(O)Br$_3$(PMe$_3$)$_3$ in $CD_2Cl_2$ over the range +4 to -5 ppm.

signal since the chemical shift of the broad resonance is further up-field. The level of contamination is similarly low at 4.6% (figure 4.21).

## 4.13 Summary

This chapter has established that despite the abnormal Nb=O bond length in the green form being the manifestation of co-crystallisation of the oxo complex with the isostructural species $NbCl_4(PMe_3)_3$, that two forms are still evident from the infrared and isotopic labelling studies, and so the the existence of two forms cannot be dismissed on the basis of a trichloride contaminant. Indeed, the observation of two unique, independently observable ν(Nb=O) stretches must be associated with a difference in the Nb=O bond length since the phosphine orientations are identical.

## 4.14 References


1. J.M. Mayer, *Angew Chem.*, 1992, **104**, 293; *Angew. Chem. Int. Ed. Engl.*, 1992, **31**, 286; G. Parkin, *Acc. Chem. Res.*, 1992, **25**, 455.
2. V.C. Gibson, M. McPartlin, *J. Chem. Soc. Dalton. Trans.*, **1992**, 947.
3. R. Baum, *Chem. Eng. News*, 1991, **69**, (9) 20; I. Amato, *Science*, **1991**, 254, 1452.
4. L. Milgrom, *New Sci.*, **1991**, 131 (1788) 22.
5. A.V. Butcher, J. Chatt, *J. Chem. Soc. A*, **1970**, 2652.
6. Lj. Manojlovic-Muir, *J. Chem. Soc. A*, **1971**, 2796.
7. K. Wieghardt, G. Backes-Dahmann, B. Nuker, J. Weiss, *Angew. Chem. Int. Ed. Engl.*, 1985, **24**, 777.
8. M.G.B. Drew, D.A. Rice and D.M. Williams, *J. Chem. Soc. Dalton Trans.*, **1985**, 1821.
9. (a) V.C. Gibson, T.P. Kee, R.M. Sorrell, A.P. Bashall, M. McPartlin, *Polyhedron*, 1988, **7**, 2221; (b) T.P. Kee, *Ph.D. Thesis*, Durham University, 1989.
10. A.P. Bashall, V.C. Gibson, T.P. Kee, M. McPartlin, O.B. Robinson, A. Shaw, *Angew. Chem. Int. Ed. Engl.*, 1991, **30**, 980.

11. W.W. Porterfield, '*Inorganic Chemistry- A Unified Approach*', Addison-Wesley, New York, 1984.

12. K. Yoon, G. Parkin, A.L. Rheingold, *J. Amer. Chem. Soc.*, 1991, **113**, 1437.

13. J.L. Alwood, W.E. Hunter, E. Carmona-Guzman, G. Wilkinson, *J. Chem. Soc. Dalton Trans.*, **1980**, 467.

14. J. Nieman, J.H. Teuben, J.C. Huffmann, K.G. Caulton, *J. Organometal. Chem.*, 1983, **255**, 193.

15. V. Katovic, C. Djordevic, *Inorg. Chem.*, 1970, **9**, 1720; C.G. Barraclough, J. Lewis, R.S. Nyholm, *J. Chem. Soc.*, **1959**, 3552; W.P. Griffith, *Coord. Chem. Rev.*, 1970, **5**, 459.

16. K. Yoon, G. Parkin, A.L. Rheingold, *J. Amer. Chem. Soc.*, 1992, **114**, 2210.

17. F.A. Cotton, M.P. Diebold and W.J. Roth, *Polyhedron,* 1985, **4**, 110.

18. J.C. Dewan, D.L. Kepert, C.L. Raston, A.H. White, *J. Chem. Soc. Dalton Trans.*, **1975**, 2031.

19. C.K. Prout, B. Kamenar, *J. Chem. Soc. (A)*, **1970**, 2379.

20. Yu E. Gorbunov, V.I. Pakhomov, V.G. Kuznetsov, E.S. Kovaleva, *Zh. Strukh. Khim.*, 1972, **13**, 165.

21. U. Müller, I. Lorenz, *Z. Anorg. Allg. Chem.*, 1980, **463**, 110.

22. W. Hiller, J. Strähle, H. Prinz, K. Dehnicke, *Z. Naturforsch.*, 1984, **39B**, 107.

23. P. Klingelhofer, U. Müller, *Z. Anorg. Allg. Chem.*, 1984, **516**, 85.

24. H.C. Aspinall, M.M. Roberts, S.J. Lippard, *J. Inorg. Chem.*, 1984, **23**, 1782.

25. J. -C. Daran, Y. Jeannin, J.E. Guerchais, R. Kergoat, *Inorg. Chim. Acta.*, 1979, **33**, 81.

26. L.G. Hubert-Pfalzgraf, A.A. Pinkerton, *Inorg. Chem.*, 1977, **16**, 1895.

27. G. Mathern, R. Weiss, *Acta. Cryst.*, 1971, **B27**, 1610.

28. C.K. Prout, J.-C. Daran, *Acta. Cryst.*, 1979, **B35**, 2882.

29. C. Chavant, J.-C. Daran, Y. Jeannin, G. Constant, R. Morancho, *Acta. Cryst.*, 1975, **B31**, 1823.

30. A. Shaw, *Ph.D. Thesis*, Durham University, 1989.

# CHAPTER FIVE

## Seven Coordinate Sulphido-Halides of Niobium and Tantalum

## 5.1 Introduction

The observation of the phenomenon of bond-stretch isomerism in the $Nb(O)X_3(PMe_3)_3$ (X= Cl, Br) systems[1] led to the obvious proposal as to whether such a situation might exist in the analogous niobium and tantalum sulphido systems. The ready accessibility of the niobium and tantalum sulphido-halide starting materials meant that the occurrence of bond-stretch isomers in other analogous seven coordinate systems could be investigated.

Two forms of $Nb(S)Cl_3(PMe_3)_3$ exhibiting two independently observable Nb=S stretching frequencies were first synthesized by A. Shaw.[2,20] X-ray structure determinations revealed two different bond lengths, but surprisingly the distances did not correlate with the order of the observed stretching frequencies. A high frequency form of $Ta(S)Cl_3(PMe_3)_3$ was also synthesized and structurally characterised by A. Shaw.[2] In view of the irregularities it was decided to re-investigate the sulphido systems.

## 5.2 Green and Orange Forms of $Nb(S)Cl_3(PMe_3)_3$

### 5.2.1 Reaction of $Nb(S)Cl_3$ and $Nb(S)Cl_3(MeCN)_2$ with $PMe_3$

Treatment of $Nb(S)Cl_3$ with $3^1/_2$ equivalents of $PMe_3$ in dichloromethane[2] leads to the isolation of a yellow crystalline material. Infrared spectroscopy revealed that it was in fact a mixture of two species, showing peaks at 489 and 455 $cm^{-1}$ (in an 80:20 ratio) which is consistent, if a little low, for terminal Nb=S stretching vibrations. Dissolution of this crude mixture in toluene gave selective crystallisation at -35°C of green cubic crystals, the nujol mull IR spectrum now showing only an absorption at 489 $cm^{-1}$.

The reaction between $Nb(S)Cl_3(MeCN)_2$ and $3^1/_2$ equivalents of $PMe_3$ in dichloromethane[2] leads to a 55:45 crude mixture (the higher ν(Nb=S) being quoted first). Dissolution of this mixture in toluene led to selective crystallisation at -35°C of cubic yellow-orange crystals, which by IR spectroscopy showed exclusively an absorption at 455 $cm^{-1}$.

### 5.2.2 Solid-State Infrared Spectroscopy

From reactions with niobium sulphido-halide starting materials crystals of two forms of $Nb(S)Cl_3(PMe_3)_3$ can be obtained which are readily distinguished not only by their colour (yellow-orange and green), but also by a marked difference in their IR spectra; ν(Nb=S) stretches are observed at 455 $cm^{-1}$ for the orange-yellow form and 489 $cm^{-1}$ for the green form (figure 5.1).

A significant feature of their IR spectra are the low values observed for the ν(Nb=S) stretching vibrations. Previously characterised compounds containing sulphur terminally bound to niobium are observed to give stretching vibrations typically greater than 500 $cm^{-1}$ (table 5.1). The decreased frequency of these absorptions may be a reflection of the high coordination number of the complexes and the highly basic nature of the $PMe_3$ ligand (the phosphine 'off-loading' excess electron density, through interaction with the metal, onto the sulphur moiety, and thus reducing the 'bond order' and hence the ν(Nb=S) stretching frequency).

In fact it was shown by A. Shaw[2] that curiously the Nb=S stretching frequency does not appear to correlate with the Nb=S bond distances reported for these isomers. This is surprising since a correlation is observed for other terminally bonded niobium sulphides (figure 5.2). Subsequent crystal structure re-determinations furnished two shorter Nb=S bond lengths for the high frequency form, now known to be the consequence of a reduced level of tetrachloride, $NbCl_4(PMe_3)_3$, impurity.

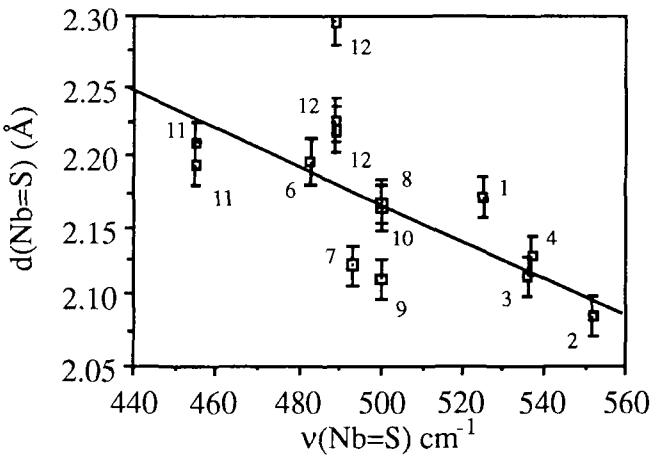


**Figure 5.2:** Plot of d(Nb=S) (Å) versus ν(Nb=S) ($cm^{-1}$)

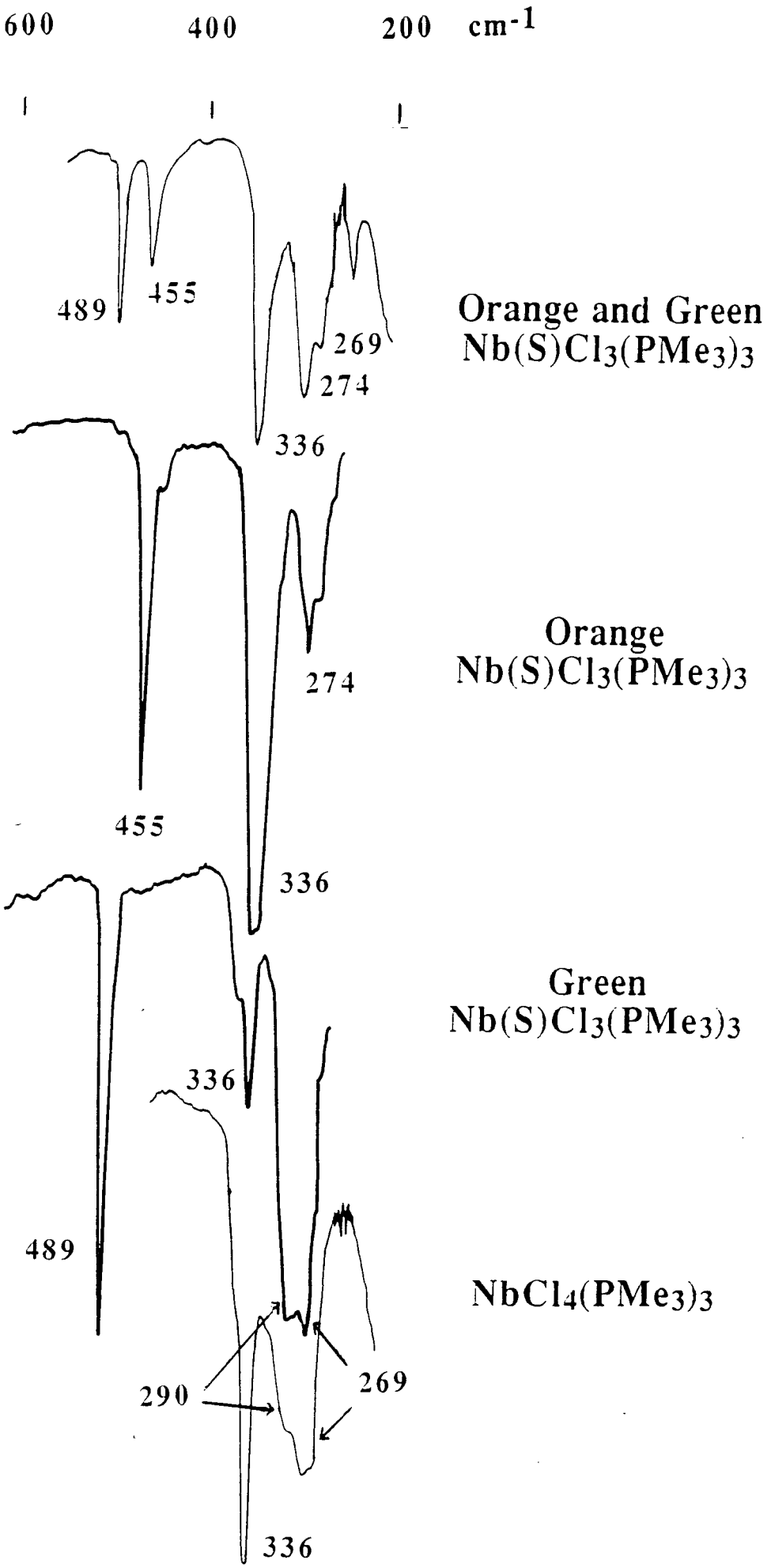


**Figure 5.1:** Low frequency solid-state infrared spectra of the green and orange forms of $Nb(S)Cl_3(PMe_3)_3$.

| No. | Complex | de⁻ | CN | Nb=S (Å) | ν ($cm^{-1}$) | Ref. |
|---|---|---|---|---|---|---|
| 1. | $Nb(S)(SPh_4)^-$ | 0 | 5 | 2.171(2) | 525 | 3 |
| 2. | $Nb(S)Cl_4^-$ | 0 | 5 | 2.085(5) | 552 | 4 |
| 3. | $Nb(S)Cl_3(SPPh_3)$ | 0 | 5 | 2.114(4) | 536 | 5 |
| 4. | $[Nb(S)Cl_3(SPPh_3)]_2$ | 0 | 6 | 2.129 | 537 | 6 |
| 5. | $Nb(S)Br_3(THT)_2$ | 0 | 6 | 2.09(8) | | 7 |
| 6. | $Nb_6S_{17}^{4-}$ | 0 | 6 | 2.196(4) | 483 | 8 |
| 7. | $Nb(S)(S_2CNEt_2)_3$ | 0 | 7 | 2.122(1) | 493 | 9 |
| 8. | $Nb(S)(S_2CNEt_2)_3$ | 0 | 7 | 2.168(1) | 500 | 9 |
| 9. | $Nb(S)(S_2CNEt_2)_3$ | 0 | 7 | 2.112(3) | 500 | 10 |
| 10. | $Nb(S)(S_2CNEt_2)_3$ | 0 | 7 | 2.164(3) | 500 | 10 |
| 11. | α-$Nb(S)Cl_3(PMe_3)_3$ | 0 | 7 | 2.194(2)<br>2.210(3) | 455 | 2<br>This work |
| 12. | β-$Nb(S)Cl_3(PMe_3)_3$ | 0 | 7 | 2.296(1)<br>2.225(3)<br>2.219(3) | 489 | 2<br>This work<br>This work |
| 13. | $Nb(S)Cl_3$ | 0 | 6 | | 542 | 11 |
| 14. | $Nb(S)Br_3$ | 0 | 6 | | 552 | 12 |
| 15. | $Nb(S)Cl_3(MeCN)_2$ | 0 | 6 | | 523 | |
| 16. | $Nb(S)Br_3(MeCN)_2$ | 0 | 6 | | 528 | |
| 17. | $Nb(S)Cl_3(THF)_2$ | 0 | 6 | | 529 | |

**Table 5.1:** Nb=S bond lengths and wavelengths of absorptions for selected niobium sulphides

As to the presence of $NbCl_4(PMe_3)_3$, which is found in the low frequency 871 $cm^{-1}$ form of $Nb(O)Cl_3(PMe_3)_3$, figure 5.1 shows a comparison between the solid-state IR spectra of the orange-yellow and green forms of $Nb(S)Cl_3(PMe_3)_3$ together with $NbCl_4(PMe_3)_3$ in the low frequency region and includes both the Nb-Cl and Nb=S stretching vibrations. It shows that common to each species is a strong ν(Nb-Cl) absorption at 336 $cm^{-1}$, conspicuous by its virtual absence in the niobium-oxo system and presence in the IR spectrum of $NbCl_4(PMe_3)_3$, to be initially attributable to $NbCl_4(PMe_3)_3$. However, the $^1H$ NMR of the orange-yellow form (figure 5.9) shows that the paramagnetic $NbCl_4(PMe_3)_3$ is absent, and so the peak must be coincidentally common to both the orange-yellow form of $Nb(S)Cl_3(PMe_3)_3$ and $NbCl_4(PMe_3)_3$.

Evidence of the absence of $NbCl_4(PMe_3)_3$ impurity in the orange-yellow form is also supplied in the IR spectrum by the absence of a general broad absorption between 290 and 260 $cm^{-1}$ which typifies $NbCl_4(PMe_3)_3$. The green form in addition to the peak at 336 $cm^{-1}$ shows two strong absorptions at 290 $cm^{-1}$ and 269 $cm^{-1}$, which together with the general broadness of this region points to the presence of co-crystallised $NbCl_4(PMe_3)_3$. Furthermore, the fact that the broad absorption is stronger than the peak at 336 $cm^{-1}$ indicates a high level of impurity. This is backed up by $^1H$ NMR evidence which indicates levels of ca. 20%.

The stability and interconversion of isomers is of importance in furthering the understanding of the phenomenon of bond-stretch isomerism. Solid-state studies reveal that as in the $Nb(O)Cl_3(PMe_3)_3$ system the conversion is invariably from one form to the other and is irreversible. Stored under an atmosphere of nitrogen the green form ($\nu$(Nb=S) 489 $cm^{-1}$) converts to a 30:70 mixture over a period of four weeks, the lower $\nu$(Nb=S) stretching species now being predominant (figure 5.3).

The orange-yellow form is found to be unchanged over a period of one week (figure 5.4). In neither the green nor orange-yellow form is any evidence of decomposition to give $S{=}PMe_3$ observed, as is also the case in solution, so strengthening the evidence for isomer conversion in the solid-state. However, unlike the $Nb(O)Cl_3(PMe_3)_3$ system, which although similarly shows a conversion to the lower $\nu$(Nb=E) stretching frequency species (E= O, S), the sulphido system involves conversion in the solid-state to a form that is free of impurity in its pure state, although from the study the presence of $NbCl_4(PMe_3)_3$ is still evident from the broadness of the peak at 284 $cm^{-1}$. The fact that conversion is occurring is also evident from the absorptions at 336 and 284 $cm^{-1}$ (orange-yellow) increasing in intensity, while those at 290 and 269 $cm^{-1}$ (green) now appear as shoulders on the 284 $cm^{-1}$ absorption.

### 5.2.3 Solution Infrared Spectroscopic Studies

Unlike the $Nb(O)Cl_3(PMe_3)_3$ system where only the green $\beta$-isomer with $\nu$(Nb=O) absorption at 871 $cm^{-1}$ is observed in solution, in the $Nb(S)Cl_3(PMe_3)_3$ case

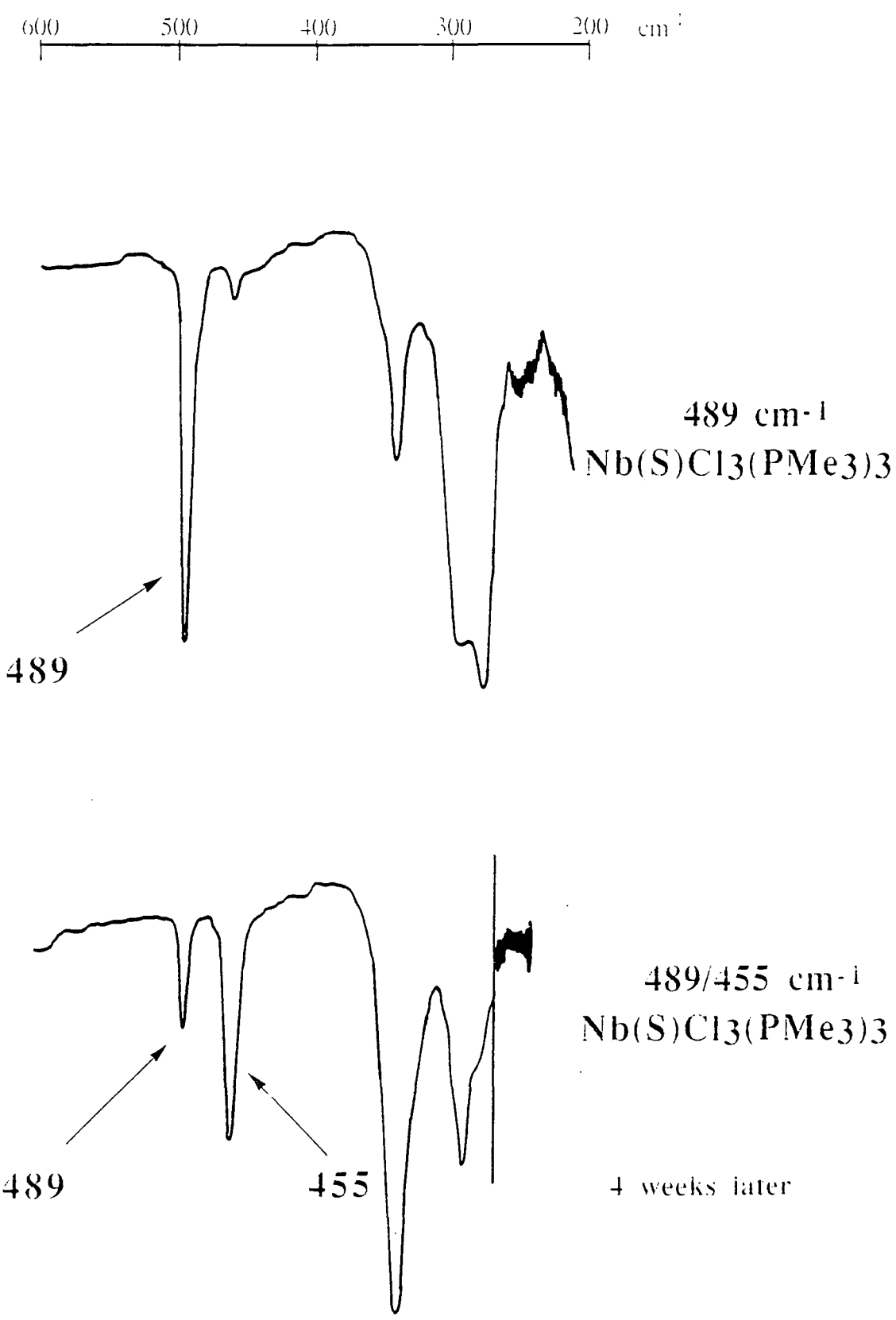


**Figure 5.3:** Low frequency solid-state infrared spectra showing the solid-state conversion of the green form to the orange form of $Nb(S)Cl_3(PMe_3)_3$.

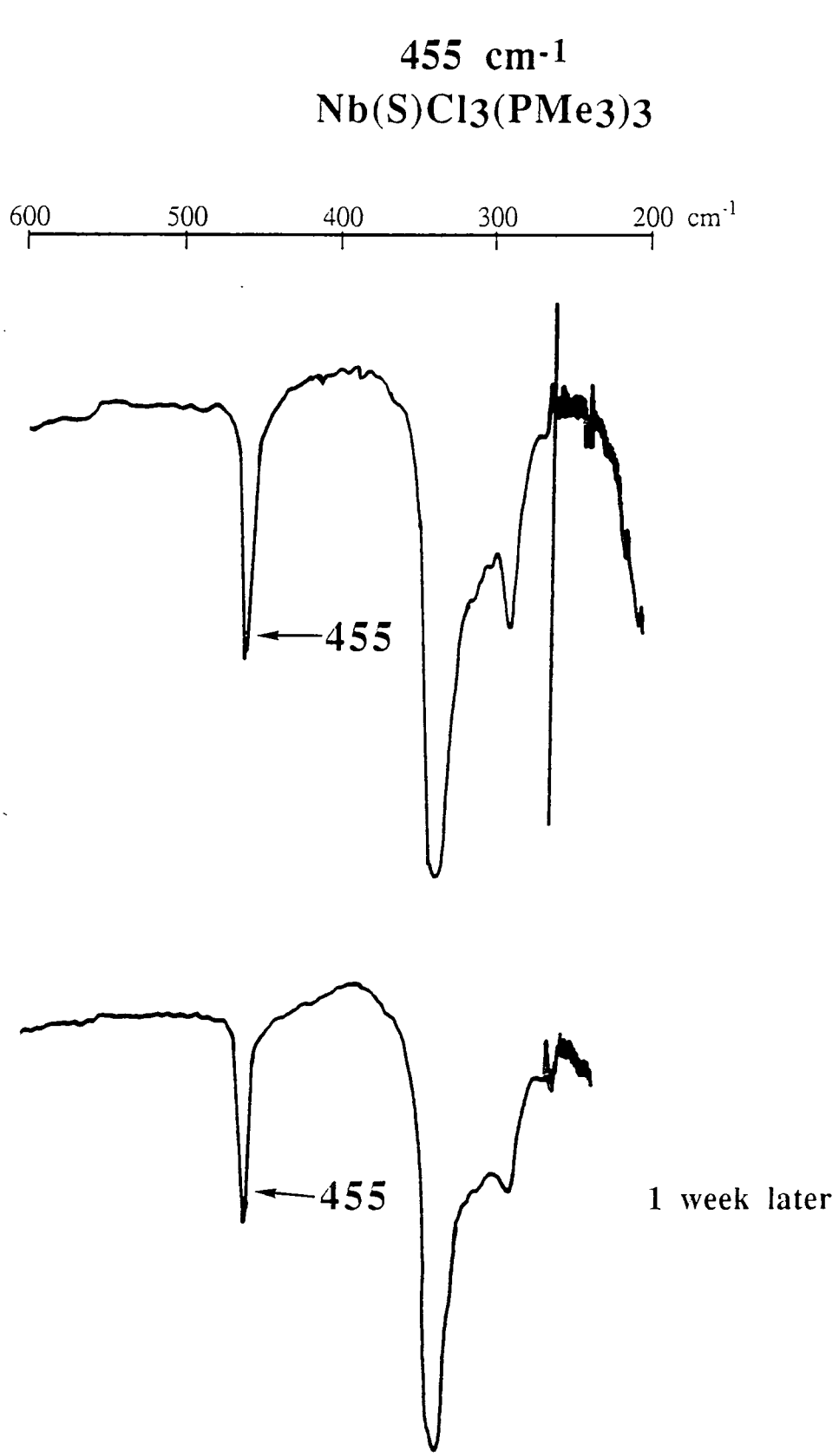


**Figure 5.4:** Low frequency solid-state infrared spectra showing the solid-state stability of the orange form of $Nb(S)Cl_3(PMe_3)_3$.

both forms are visible in solution. A sample of the green form that shows a single absorption at 489 $cm^{-1}$ in the solid state IR spectrum, shows absorptions at 484 and 453 $cm^{-1}$ in an 85:15 ratio immediately after dissolution in $CH_2Cl_2$, with a shoulder at 271 $cm^{-1}$ on the solvent peak verifying that the green form is unambiguously visible in solution (figure 5.5, top). After stirring for 5 minutes in $CH_2Cl_2$ the solution IR spectrum now shows a 40:60 (484:453) mix, conversion being 100% complete to the orange-yellow 453 $cm^{-1}$ form after 10 minutes. The nujol mull IR spectrum after 5 minutes confirms that conversion has occurred (figure 5.5, bottom).

A sample of the pure orange-yellow form (ν(Nb=S) 455 $cm^{-1}$) dissolved in $CH_2Cl_2$ shows only a peak at 453 $cm^{-1}$ for the ν(Nb=S) stretch (figure 5.5, middle), confirming the irreversible nature of the isomer conversion. No absorption is distinguishable in the Nb-Cl stretching region since the ν(Nb-Cl) stretches for the orange-yellow form are masked by the solvent peak.

The presence of $NbCl_4(PMe_3)_3$ impurity in the green form is established by the weak shoulder absorption at 337 $cm^{-1}$. In the case of the orange-yellow form, however, an absorption of approximately equal intensity is observed at 336 $cm^{-1}$ in the Nb-Cl stretching vibration region indicating that this signal can indeed be attributed to a ν(Nb-Cl) stretch due to the orange-yellow form, as well as for $NbCl_4(PMe_3)_3$ in the green form, since its $^1H$ NMR spectrum establishes that the orange-yellow form is free of paramagnetic contaminant (figure 5.9).

### 5.2.4 Raman Spectroscopy

The existence of two terminally bonded sulphur $Nb(S)Cl_3(PMe_3)_3$ species is unclear from Raman spectroscopic evidence. The ν(Nb=S) stretch in such molecules showing virtual $C_{3v}$ symmetry should be Raman (as well as infrared) active according to group theory. The Raman spectrum for the green ν(Nb=S) 489 $cm^{-1}$ form shows a single absorption at 487 $cm^{-1}$ (figure 5.6, bottom), whilst that of a sample showing a 60:40 mix by IR spectroscopy of the 489 and 455 $cm^{-1}$ forms, possesses only one absorption at 487 $cm^{-1}$ (figure 5.6, top). As to whether the orange-yellow ν(Nb=S) 455

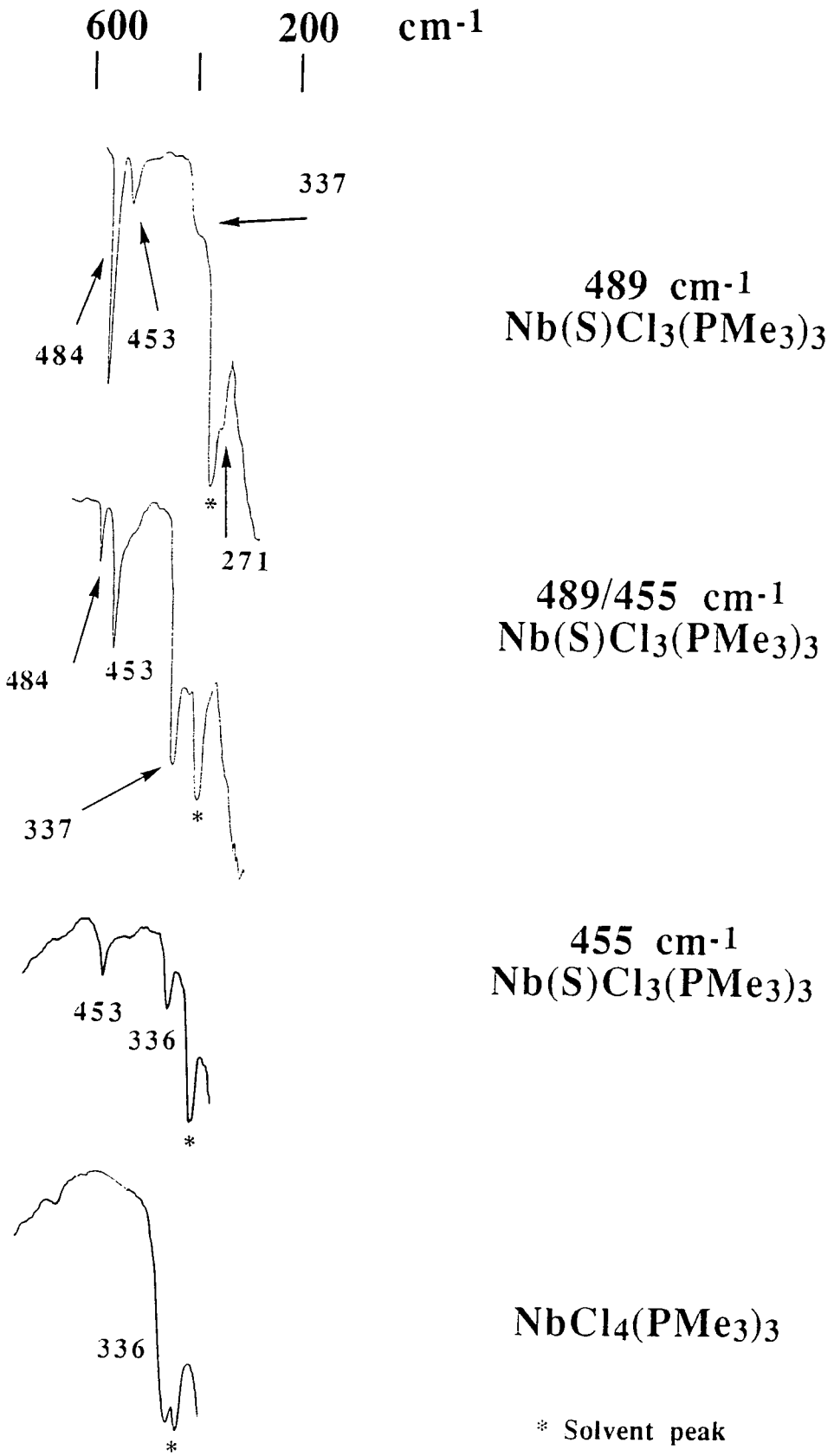


**Figure 5.5:** Low frequency solution ($CH_2Cl_2$) infrared spectra of the green and orange forms of $Nb(S)Cl_3(PMe_3)_3$.

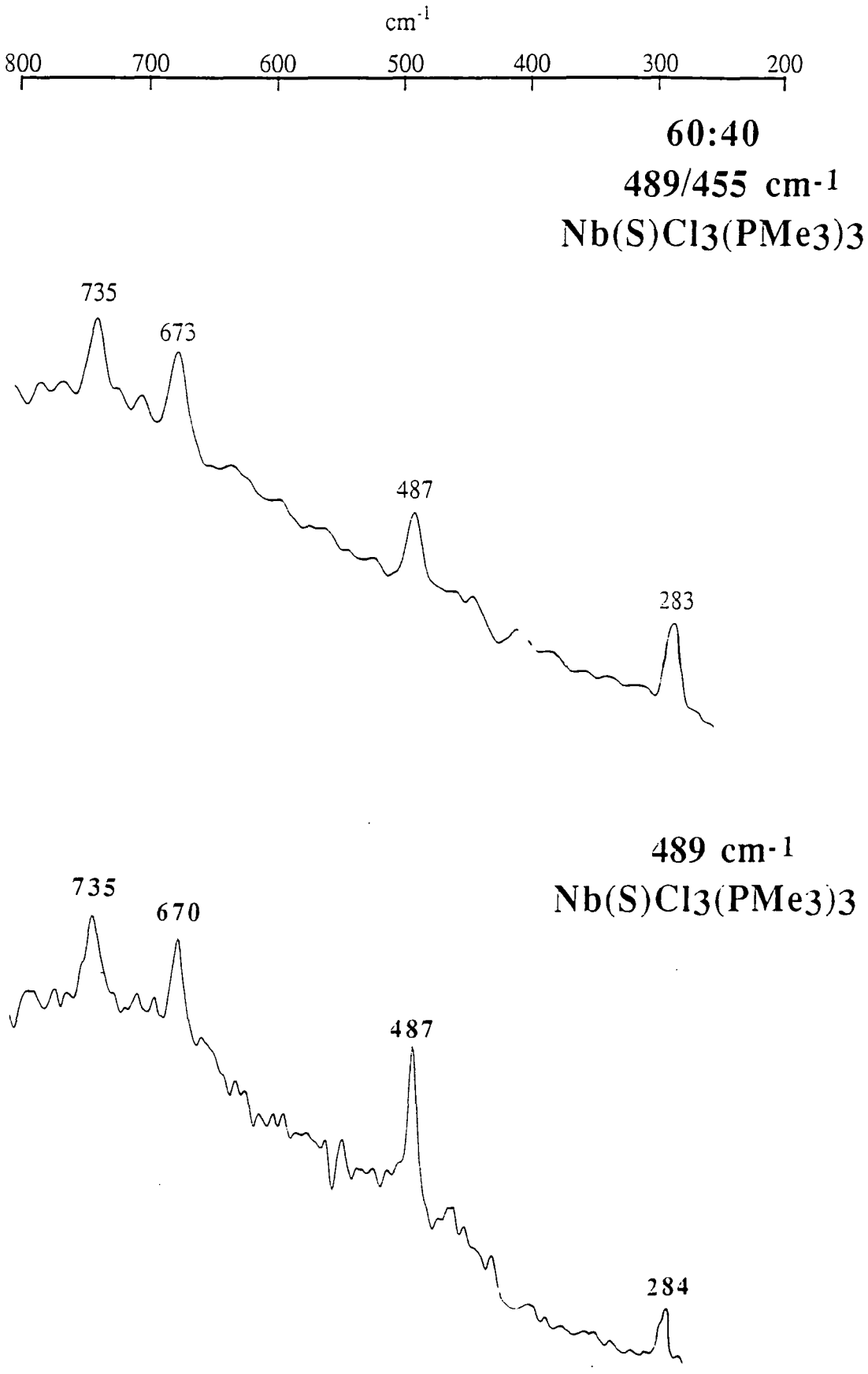


**Figure 5.6:** Raman spectra (solid-state) of pure 489 $cm^{-1}$ ν(Nb=S) and a 60:40 mix of 489/455 $cm^{-1}$ ν(Nb=S) of $Nb(S)Cl_3(PMe_3)_3$ over the range 800 to 250 $cm^{-1}$.

$cm^{-1}$ form of $Nb(S)Cl_3(PMe_3)_3$ possesses a terminal sulphur atom, this is not confirmed by the Raman data. Elemental analysis (section 5.2.7), however, confirms a stoichiometry consistent with $Nb(S)Cl_3(PMe_3)_3$, and the presence of a strong $^1H$ NMR signal is further indication of a diamagnetic, presumably niobium (V) species.

In the ν(Nb-Cl) stretching vibration region, where two Raman active bands are expected for $Nb(S)Cl_3(PMe_3)_3$ and three for $NbCl_4(PMe_3)_3$, only one absorption at 284 $cm^{-1}$ is observed in the spectra of both samples. So despite the high level of $NbCl_4(PMe_3)_3$ impurity in the green form, as indicated by both elemental and $^1H$ NMR analyses, its presence is not able to be observed in the Raman spectrum, unlike that of *mer*-$MoCl_3(PMe_2Ph)_3$ in the green '*cis-mer*-$Mo(O)Cl_2(PMe_2Ph)_3$' species (section 2.3.2). The absorption at 336 $cm^{-1}$ of $NbCl_4(PMe_3)_3$ is not active in the Raman spectrum.

### 5.2.5 UV-Visible Spectroscopy

The UV-visible spectrum for the green form, with ν(Nb=S) at 489 $cm^{-1}$, shows an absorbance at 270 nm ($\varepsilon = 4.5 \times 10^3$ $mol^{-1}$ $cm^2$) which remains unchanged over a period of 8 hours (figure 5.7, top). The orange-yellow species, with ν(Nb=S) at 455 $cm^{-1}$, gives two absorbances, one at 270 nm ($\varepsilon = 5.0 \times 10^3$ $mol^{-1}$ $cm^2$) and another at 324 nm ($\varepsilon = 2.1 \times 10^3$ $mol^{-1}$ $cm^2$). Over a period of 3 hours the absorbance at 270 nm decreases in intensity, while that at 324 nm grows in intensity (figure 5.7, bottom). First impressions might suggest that an isomer conversion is proceeding, consistent with what is observed in the solid-state, since two absorptions would suggest two differently coloured species, as is observed for the crystals. However, bearing in mind the evidence from the $Nb(O)Cl_3(PMe_3)_3$ system, that the green colouration of the ν(Nb=O) 871 $cm^{-1}$ form is due to the green colouration of the $NbCl_4(PMe_3)_3$ impurity (yellow crystals of the 871 $cm^{-1}$ form having been isolated), it seems more than likely that a similar situation exists for the green ν(Nb=S) 489 $cm^{-1}$ $Nb(S)Cl_3(PMe_3)_3$ species. Significantly different wavelengths of absorbance would thus not be expected for the Nb=S chromophore, since the 'true' colour of the ν(Nb=S) 489 $cm^{-1}$ form is likely to be close to that of the orange-

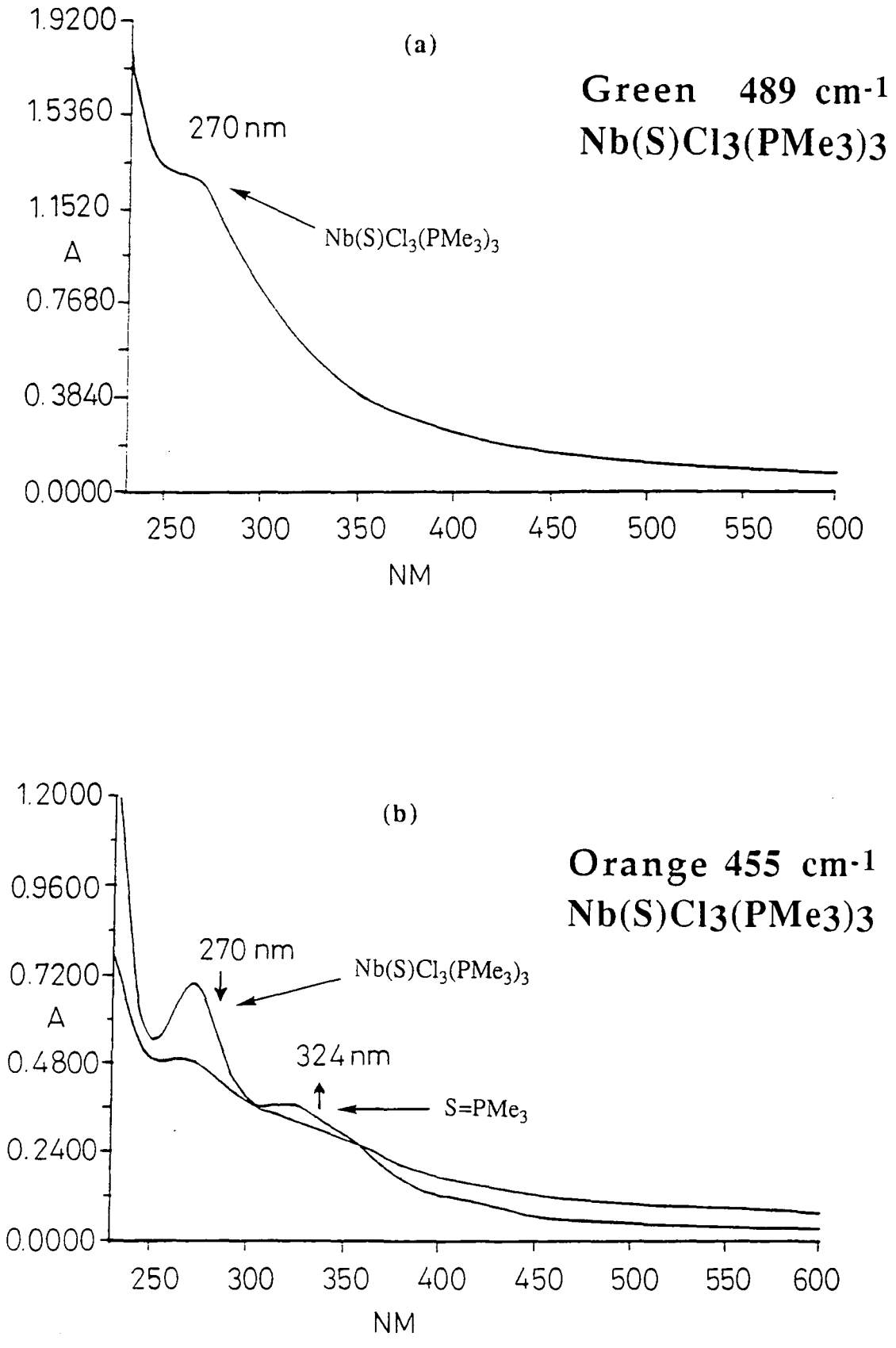


**Figure 5.7:** UV-visible spectra in dichloromethane of the green (ν(Nb=S) 489 $cm^{-1}$) and orange (ν(Nb=S) 455 $cm^{-1}$) forms of $Nb(S)Cl_3(PMe_3)_3$.

yellow ν(Nb=S) 455 $cm^{-1}$ form. UV-visible spectroscopic studies, in fact, mimic those seen in solution by $^1H$ NMR. The green form is observed to be considerably more stable in solution than is the orange-yellow form, the green form showing no visible change after 6 hours, while the orange-yellow form is seen to decompose (reduction in the 270 nm $Nb(S)Cl_3(PMe_3)_3$ absorbance) over a period of 3 hours to $S=PMe_3$ (324 nm). This is consistent with the observations by $^1H$ NMR and solution IR where absorptions due to $S=PMe_3$, 1.75 ppm ($^2J(PH)$ = 13.2 Hz) and 570 $cm^{-1}$ respectively, are observed to grow in. The change in the UV-visible spectrum of the orange-yellow form is thus due to decomposition resulting in the liberation of $S=PMe_3$. This is not to say that isomer conversion in solution can be ruled out by this technique.

### 5.2.6 NMR Studies

The 400 MHz $^1H$ NMR spectrum in $CD_2Cl_2$ of green (ν(Nb=S) 489 $cm^{-1}$) $Nb(S)Cl_3(PMe_3)_3$ initially consists of a broadened singlet resonance at δ 1.61 ppm ($\Delta^1/_2$ = 16 Hz) and a broad resonance at δ -3.01 ppm ($\Delta^1/_2$ = 98 Hz) due to the paramagnetic impurity $NbCl_4(PMe_3)_3$, the level of contamination being ca. 20% (figure 5.8). Left at room temperature the broadened singlet diminishes in intensity, while a doublet at δ 1.75 ppm ($^2J(PH)$ = 13.6 Hz) due to the formation of $S=PMe_3$ grows in. Over a period of 5 days the broadened singlet due to $Nb(S)Cl_3(PMe_3)_3$ continues to diminish, while the $S=PMe_3$ doublet and $NbCl_4(PMe_3)_3$ broad resonance upfield increase in intensity. The $S=PMe_3$ signal now comprises 19% and the $NbCl_4(PMe_3)_3$ 38% (being constant for 3 days) of the integrated $^1H$ resonances. Although the initial level of paramagnetic contaminant can vary between samples, being as low as 5%, it consistently rises to a level in the mid-30% region. The addition of excess $PMe_3$ in the NMR tube is found to reduce the rate of decomposition, in accordance with a ligand exchange mechanism being involved.

The 400 MHz $^1H$ NMR spectrum in $CD_2Cl_2$ of orange-yellow (ν(Nb=S) 455 $cm^{-1}$) $Nb(S)Cl_3(PMe_3)_3$ shows signals due to the $Nb(S)Cl_3(PMe_3)_3$ species at δ 1.60 ppm ($\Delta^1/_2$ = 14.5 Hz) and $S=PMe_3$ at δ 1.75 ppm ($^2J(PH)$ = 12.8 Hz) immediately after

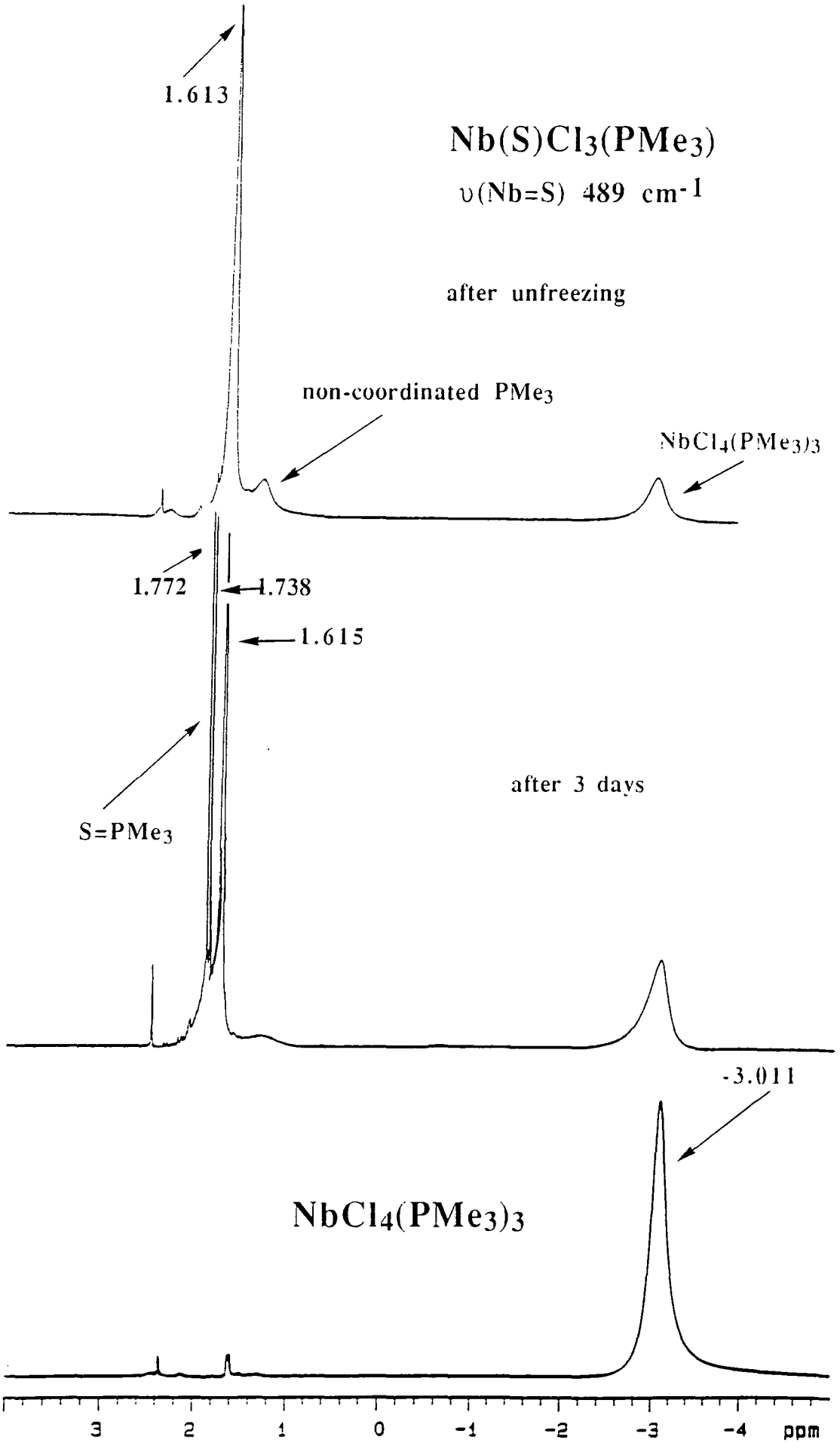


**Figure 5.8:** 400 MHz $^{1}H$ NMR spectra of green $Nb(S)Cl_3(PMe_3)_3$ ($\nu$(Nb=S) 489 $cm^{-1}$) in $CD_2Cl_2$ over the range +4 to -5 ppm.

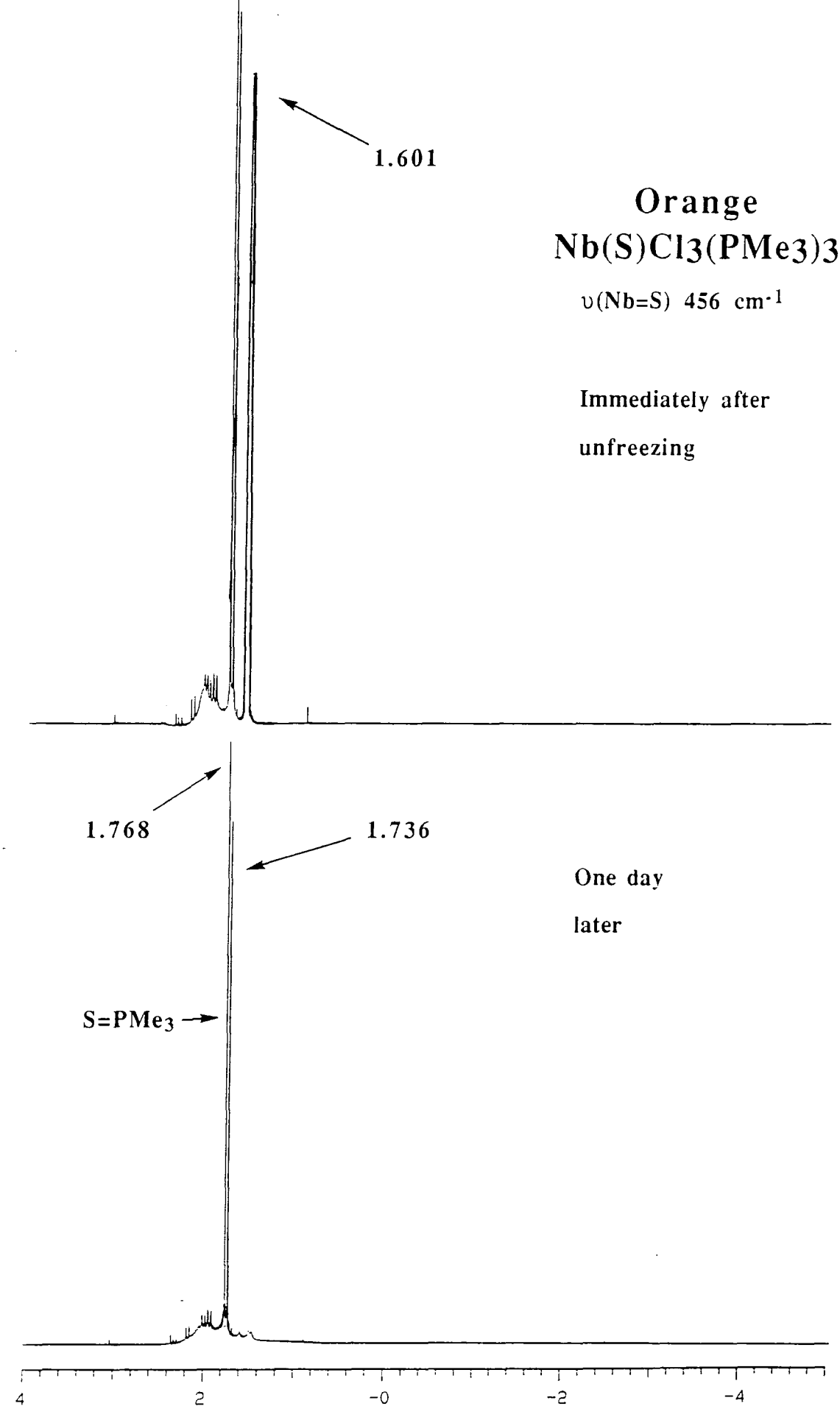


**Figure 5.9:** 400 MHz $^{1}H$ NMR spectra of orange $Nb(S)Cl_3(PMe_3)_3$ ($\nu$(Nb=S) 455 $cm^{-1}$) in $CD_2Cl_2$ over the range +4 to -5 ppm.

unfreezing the sample, but unlike the green form there is no evidence of any paramagnetic $NbCl_4(PMe_3)_3$ impurity (figure 5.9). After only one day the only signal observed is due to $S{=}PMe_3$. Decomposition of the orange-yellow form thus appears to occur via a pathway not involving the formation of $NbCl_4(PMe_3)_3$. In fact the lack of $NbCl_4(PMe_3)_3$ in both the crystal lattice of the orange-yellow form of $Nb(S)Cl_3(PMe_3)_3$ and its decomposition route in solution as seen by $^1H$ NMR is consistent with NMR scale preparative reactions from $Nb(S)Cl_3(MeCN)_2$. This suggests that formation of the orange-yellow species does not result in the formation of or decomposition to $NbCl_4(PMe_3)_3$. The use of $Nb(S)Cl_3$ as the starting sulphido-halide is found to lead to $NbCl_4(PMe_3)_3$ contaminant, both on a preparative and NMR scale. As to whether $NbCl_4(PMe_3)_3$ is produced thus seems to depend upon the nature of the thiohalide starting material; the fact that $Nb(S)Cl_3(MeCN)_2$ is monomeric and $Nb(S)Cl_3$ is 'polymeric' possibly having something to do with it. This raises the question as to whether there is the possibility for the formation of a polymeric '$NbCl_4$' impurity, which upon subsequent reaction with trimethylphosphine produces the $NbCl_4(PMe_3)_3$ contaminant.

101.26 MHz $^{31}P\{^1H\}$ NMR spectra were found to be variable, possibly due to low solubility. The $^{31}P\{^1H\}$ spectrum of the green form of $Nb(S)Cl_3(PMe_3)_3$ did not reveal any signal at room temperature. However, that of the orange-yellow form consisted of two broad resonances at $\delta$ 5.19 ppm ($\Delta^1/_2$ = 146 Hz) and $\delta$ -23.75 ppm ($\Delta^1/_2$ = 83 Hz), and a sharp peak at $\delta$ 26.59 ppm (assigned to free $S{=}PMe_3$ due to decomposition). The broadness of two of the peaks is attributed to ligand exchange occurring in solution, the peak at $\delta$ 5.19 ppm being assigned to $Nb(S)Cl_3(PMe_3)_3$ on the basis that integration of the signal shows this band to represent the predominant species, in-line with what is observed in the $^1H$ NMR spectrum of orange-yellow $Nb(S)Cl_3(PMe_3)_3$. The peak at $\delta$ -23.75 ppm is tentatively attributed to a species sometimes observed in the $^1H$ NMR spectrum as a virtual triplet.

### 5.2.7 Elemental Analysis

Using equation 5.1, where x once again represents the mole fraction of $NbCl_4(PMe_3)_3$ present in the green and orange-yellow forms of $Nb(S)Cl_3(PMe_3)_3$, determined from the chlorine content of each sample, table 5.2 can be drawn up.

$$x = \frac{\%Cl.RMM[Nb(S)Cl_3(PMe_3)_3] - 300.RMM[Cl]}{100.RMM[Cl] - \%Cl.RMM[(Cl) - (O)]}$$

$$= \frac{459.5694\ \%Cl - 10635.9}{3545.3 - 3.389\ \%Cl} \qquad \textbf{(5.1)}$$

Analyses reveal that the mole fraction of $NbCl_4(PMe_3)_3$ in the green ($\nu$(Nb=S) 489 $cm^{-1}$) form is estimated to be 0.264±0.071, and in the orange-yellow ($\nu$(Nb=S) 455 $cm^{-1}$) form to be 0.108±0.032. These findings are not entirely reflected by those determined from $^1H$ NMR data, which indicates the mole fraction of impurity in the green and orange-yellow forms to be 0.047 to 0.173±0.005 and 0.000±0.005 respectively. The reason for this is unclear, and infrared and Raman spectroscopy are unable to shed further light on the disagreement of information.

| | %C | %H | %Cl | Average %Cl | %$NbCl_4(PMe_3)_3$ |
|---|---|---|---|---|---|
| Calculated | 23.52 | 5.92 | 23.14 | ---- | ---- |
| Orange-yellow $Nb(S)Cl_3(PMe_3)_3$ | 23.05 | 5.92 | 23.69 | 23.95 | 10.75 |
| | 22.94 | 5.96 | 24.01 | | |
| | | | 24.16 | | |
| Green $Nb(S)Cl_3(PMe_3)_3$ | 23.52 | 6.00 | 24.60 | 25.13 | 26.36 |
| | 23.39 | 5.99 | 24.72 | | |
| | 23.10 | 5.95 | 24.72 | | |
| | 23.30 | 5.90 | 24.73 | | |
| | | | 24.76 | | |
| | | | 25.33 | | |
| | | | 25.52 | | |
| | | | 25.79 | | |
| | | | 25.97 | | |

**Table 5.2:** Elemental analysis data for the orange-yellow and green forms of $Nb(S)Cl_3(PMe_3)_3$

## 5.3 Yellow and Orange Forms of $Ta(S)Cl_3(PMe_3)_3$

### 5.3.1 Reaction of $Ta(S)Cl_3$ and $Ta(S)Cl_3(MeCN)_2$ with $PMe_3$

Treatment of $Ta(S)Cl_3$ with $3^1/_2$ equivalents of trimethylphosphine in dichloromethane for 6 hours leads to the isolation of a yellow crystalline material from a green solution at -78°C. The IR spectrum shows the crystalline material to be a 10:90 mixture[2] of two species which exhibit Ta=S stretching vibrations at 470 and 430 $cm^{-1}$ respectively (figure 5.10, top). Dissolution of the crude mixture in toluene resulted in selective crystallisation at -35°C of orange cubic crystals, showing solely a ν(Ta=S) stretch at 470 $cm^{-1}$ (the minor component in the mixture). If, however, the solution is left stirring for 2 days the crude mixture now shows a 90:10 ratio of the ν(Ta=S) stretching bands, the higher frequency species now being predominant. Dissolution of this mixture in toluene leads to the selective crystallisation at -35°C of orange crystals which once again exhibited solely a ν(Ta=S) stretch at 470 $cm^{-1}$ (figure 5.10, bottom). Preparative studies thus reveal that the longer the reaction is allowed to be stirred at room temperature, the higher was the proportion of the 470 $cm^{-1}$ species in the mixture, thus suggesting that conversion was occurring in solution. This obviously accounts for the reason as to why the 430 $cm^{-1}$ form could not be isolated in its entirely pure form, due to its conversion in solution during the period it takes to obtain crystals. The $CI^+$ mass spectrum shows an envelope at m/z 546 which is attributed to the parent ion, with daughter species at m/z 470 ($[M\text{-}PMe_3]^+$), 435 ($[M\text{-}PMe_3, Cl]^+$), and 400 ($[M\text{-}PMe_3, 2Cl]^+$).

The reaction of $Ta(S)Cl_3(MeCN)_2$ with $3^1/_2$ equivalents of $PMe_3$ in dichloromethane leads to the isolation of a 90:10 (470/430 $cm^{-1}$) crude mixture, which on recrystallisation from toluene at -35°C affords once again cubic orange crystals, whose IR spectrum shows exclusively a ν(Ta=S) stretch at 470 $cm^{-1}$.

### 5.3.2 Solid-State Infrared Spectroscopy

Both the yellow mixture and pure orange form show absorptions in the nujol mull IR spectrum that are typical of coordinated $PMe_3$ at 1298 (σ(Me)), 950 (ρ(Me)), and

730 $cm^{-1}$ ($\nu_{as}$(Me)). The most overwhelmingly significant feature of their IR spectra is the observation of two stretches at 470 and 430 $cm^{-1}$ attributed to ν(Ta=S) stretching vibrations, only the 470 $cm^{-1}$ form being completely observable as an independent species (figure 5.10). Previously reported compounds containing a single terminal tantalum-sulphur moiety invariably exhibit ν(Ta=S) bands at above 500 $cm^{-1}$ (table 5.3). As for the niobium analogues, the low values of these species is thought to reflect the high coordination number (c.f. $Ta(S)(S_2CNEt_2)_3$[13]) and the presence of three highly basic $PMe_3$ ligands.

A comparison of the infrared spectra of the 470 and 470/430 $cm^{-1}$ forms of $Ta(S)Cl_3(PMe_3)_3$ with those of the closely related compounds $Nb(S)Cl_3(PMe_3)_3$ and

| Complex | de⁻ | CN | Ta=S (Å) | ν ($cm^{-1}$) | Ref. |
|---|---|---|---|---|---|
| $Ta(S)(S_2CNEt_2)_3$ | 0 | 7 | 2.181(1) | 483 | 13 |
| $Ta(S)Cl_3$(bpte) | 0 | 6 | 2.204(5) | 516/510 | 14 |
| α-$Ta(S)Cl_3(PMe_3)_3$ | 0 | 7 | | 430 | 20 |
| β-$Ta(S)Cl_3(PMe_3)_3$ | 0 | 7 | 2.219(2)<br>2.198(3) | 470 | 20 |
| $Ta(S)Br_3$ | 0 | 6 | | 448 | 15 |
| $Ta(S)Cl_3$ | 0 | 6 | | 460 | |
| $Ta(S)Cl_3(MeCN)_2$ | 0 | 6 | | 513 | This work |
| $Ta(S)Br_3(MeCN)_2$ | 0 | 6 | | 508 | 14 |
| $Ta(S)Cl_3(tht)_2$ | 0 | 6 | | 505 | 14 |
| $Ta(S)Br_3(tht)_2$ | 0 | 6 | | 504 | 14 |
| $Ta(S)Cl_3(dms)_2$ | 0 | 6 | | 510 | 14 |
| $Ta(S)Br_3(dms)_2$ | 0 | 6 | | 506 | 14 |
| $Ta(S)Br_3$(bpte) | 0 | 6 | | 512/508 | 14 |

**Table 5.3:** ν(Ta=S) and Ta=S bond lengths of selected terminal tantalum-sulphur compounds

$Nb(O)Cl_3(PMe_3)_3$ means that any vibration modes due to the co-ordinated $PMe_3$ ligand can be eliminated. This enables the bands at 470 and 430 $cm^{-1}$ to be attributed to ν(Ta-S) stretching vibrations. In the parent chalcogenide $Ta(S)Cl_3$ the ν(Ta=S) stretch occurs at 460 $cm^{-1}$ and is attributed to bridging sulphur atoms. On adduct formation it is not surprising to observe an increase in the Ta-S stretching frequency to 470 $cm^{-1}$ in the pure

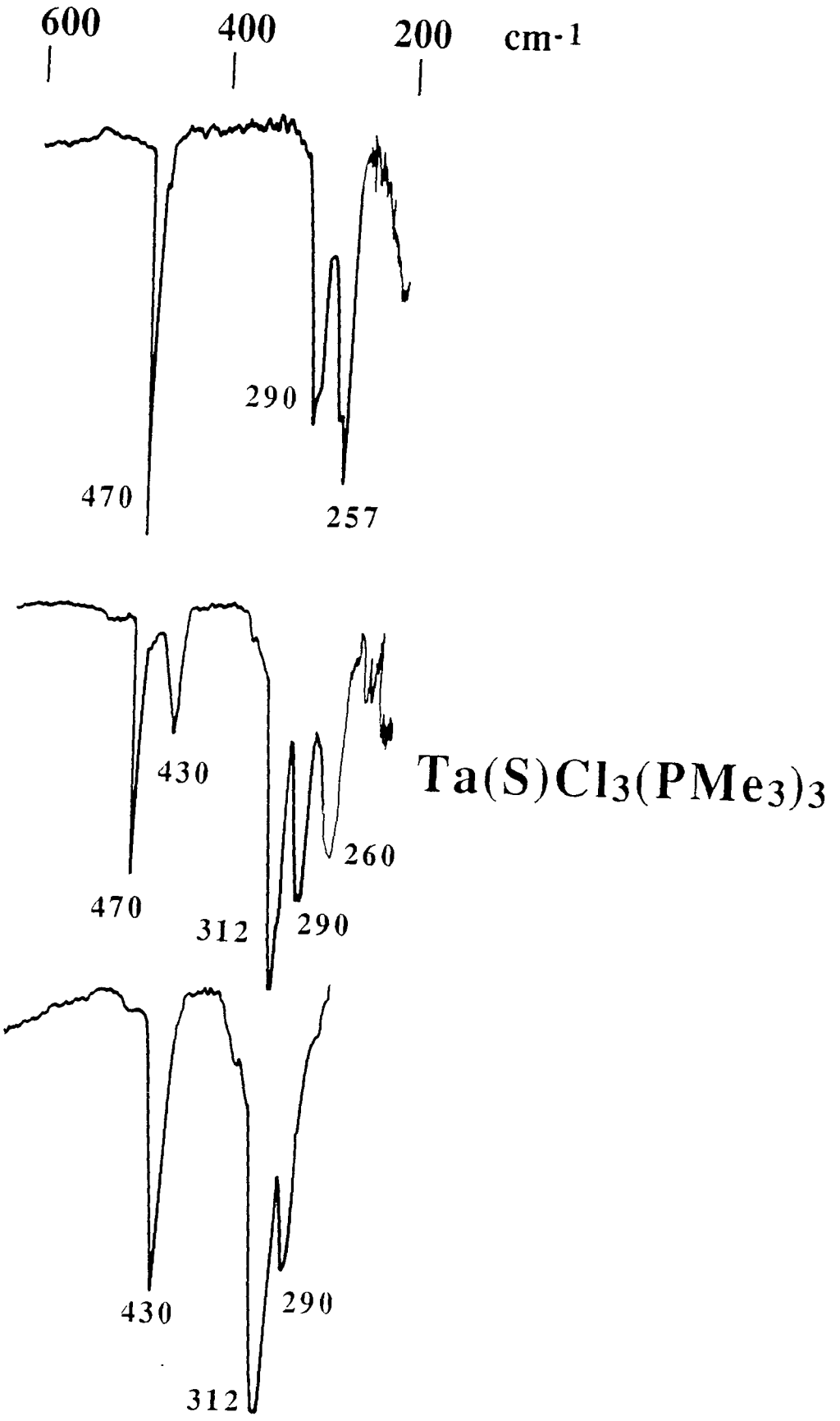


**Figure 5.10:** Low frequency solid-state infrared spectra of the ν(Ta=S) 470 $cm^{-1}$ and 470/430 $cm^{-1}$ forms of $Ta(S)Cl_3(PMe_3)_3$.

orange form, indicative of the fact that these bridges are being broken to give a terminal sulphur moiety. However, it is harder to rationalise the existence of the 430 $cm^{-1}$ absorption being due to the presence of terminal sulphur atoms. Furthermore, it is worth remarking on the observation that considering the ν(M=S) stretching frequencies in the species $M(S)Cl_3$ and $M(S)Cl_3(MeCN)_2$ (M = Ta, Nb), the observed trend is for the frequency of the absorption to decrease (table 5.3) on going from the base-stabilised form (with well defined 6 co-ordination geometry) to the base-free form in the tantalum system. This is indicative of the terminal nature of the sulphur atom in $Ta(S)Cl_3(MeCN)_2$ compared to its bridging nature in $Ta(S)Cl_3$. The possibility for bridging sulphur atoms is seen in the EI mass spectrum at m/z 534 corresponding to the decomposition fragment $Ta_2(S)Cl_4$. However, an opposite trend is observed in the niobium system, which suggests that there is a difference in the nature of the bonding involved for sulphur in these species. Additionally, EI mass spectroscopy shows a daughter fragment at m/z 426 corresponding to $Nb_2(S)_2Cl_5$ as plausible evidence for bridging occurring through chlorine atoms, and hence a terminal nature for the sulphur moiety would be implied.

In the ν(Ta-Cl) stretching region two absorptions are predicted by group theory for $Ta(S)Cl_3(PMe_3)_3$ with $C_{3v}$ symmetry. In the pure orange ν(Ta=S) 470 $cm^{-1}$ form two peaks at 290 and 257 $cm^{-1}$ are observed (figure 5.10, bottom). In the spectrum of a 10:90 mixture of the 470/430 $cm^{-1}$ forms, two peaks are also observed, but now at 312 and 290 $cm^{-1}$ (figure 5.10, top). A 60:40 mixture displays all three bands (figure 5.10, middle). The Ta-Cl stretching region thus seems to suggest that the geometry of the chloride ligands is different in the two species giving rise to the absorptions at 470 and 430 $cm^{-1}$. Furthermore, the low chlorine content for the mixed form (section 5.3.6) would also seem to indicate a difference in the stoichiometry for the two species. In section 5.3.7 it is suggested that the species giving rise to the 430 $cm^{-1}$ absorption is $[Ta(S)Cl_2(PMe_3)_2]_2$.

At this stage it is interesting to make a comparison (table 5.4) of the ν(M-Cl) stretching frequencies reported for the analogous series of compounds $M(E)Cl_3(PMe_3)_3$ (M=Nb, E=O, S; M=Ta, E=S). From this table it can be seen that the stretches in the two forms of $Nb(O)Cl_3(PMe_3)_3$ and the high frequency forms of $Nb(S)Cl_3(PMe_3)_3$ and

$Ta(S)Cl_3(PMe_3)_3$ show similar values, which is indicative of the well defined stoichiometry found in these species corresponding to $M(E)Cl_3(PMe_3)_3$ (the level of $NbCl_4(PMe_3)_3$ contaminant in the 871 $cm^{-1}$ form of $Nb(O)Cl_3(PMe_3)_3$ being low enough (4.5% maximum in solution) to consider it as virtually a pure sample, unlike the 455 $cm^{-1}$ $Nb(S)Cl_3(PMe_3)_3$ species which shows a level of contamination in the order or 20%).

However, in the lower ν(M=S) stretching forms of $M(E)Cl_3(PMe_3)_3$ (M=Nb, Ta) two similar absorptions are observed but at higher frequencies. In the case of ν(Nb=S) 455 $cm^{-1}$ $Nb(S)Cl_3(PMe_3)_3$, despite the coincidence that an absorption occurs at 336 $cm^{-1}$, the same position at which $NbCl_4(PMe_3)_3$ possesses an absorption, the peak is assigned to its ν(Nb-Cl) stretch since the $^1H$ NMR revealed no paramagnetic contaminant. Similarly, in ν(Ta=S) 430 $cm^{-1}$ $Ta(S)Cl_3(PMe_3)_3$ no paramagnetic species

| Species ν(M=E) $cm^{-1}$ | ν(M-Cl) $cm^{-1}$ | |
|---|---|---|
| 882 $Nb(O)Cl_3(PMe_3)_3$ | 300 | 285 |
| 871 $Nb(O)Cl_3(PMe_3)_3$ | 298 | 275 |
| 489 $Nb(S)Cl_3(PMe_3)_3$ | 290 | 269 |
| 455 $Nb(S)Cl_3(PMe_3)_3$ | 336 | 274 |
| 489 $Ta(S)Cl_3(PMe_3)_3$ | 290 | 257 |
| 430 $Ta(S)Cl_3(PMe_3)_3$ | 312 | 290 |

**Table 5.4:** A comparison of the ν(M-Cl) stretching frequencies in the series of compounds $M(E)Cl_3(PMe_3)_3$ (M=Nb, E=O, S; M=Ta, E=S)

is observed in the $^1H$ NMR spectrum and so the 312 $cm^{-1}$ absorption has been attributed to a ν(Ta-Cl) stretch due to this species.

A sample of 40:60 ratio 470/430 $cm^{-1}$ $Ta(S)Cl_3(PMe_3)_3$ stored under nitrogen in the absence of light converts to a 65:35 mix after a period of one month at room temperature. A similar observation is made in the presence of light, although at an increased rate. This suggests a solid-state conversion from the lower frequency form to the 470 $cm^{-1}$ species is occurring which is enhanced photochemically.

A sample of the 470 $cm^{-1}$ form remains unchanged both in absorption frequency and colour, whether or not it is photochemically exposed, indicating that the process is irreversible, affording the thermodynamically favoured form.

### 5.3.3 Solution Infrared Spectroscopy

A sample of orange 470 $cm^{-1}$ $Ta(S)Cl_3(PMe_3)_3$ in $CH_2Cl_2$ shows a stable ν(Ta=S) absorption at 463 $cm^{-1}$ (figure 5.11, top). A 70:30 ratio 470/430 $cm^{-1}$ yellow mixture similarly shows two invariant absorptions at 463 and 430 $cm^{-1}$ (figure 5.11, bottom), whose ratio mimics that observed in the solid-state IR spectrum.

In the ν(Ta-Cl) stretching region the pure orange form shows a single absorption at 257 $cm^{-1}$, the 290 $cm^{-1}$ peak being masked by a solvent absorption. In the yellow mixture two peaks at 257 and 313 $cm^{-1}$ are observed. Solution infrared spectroscopy thus reinforces what is observed in the solid-state and infers that the two ν(Ta=S) stretches are not an artifact of a solid-state effect.

### 5.3.4 Electronic UV-Visible Spectroscopy

The electronic UV-visible spectrum in $CH_2Cl_2$ of the orange $Ta(S)Cl_3(PMe_3)_3$ (ν(Ta=S) at 470 $cm^{-1}$) exhibits a single absorbance at 318 nm (ε = 315 $mol^{-1}$ $cm^2$) which remains unchanged after 20 hours (figure 5.12, top). An 80:20 mixture of the 470/430 $cm^{-1}$ forms gives two absorbances, one at 286 nm (ε = 385 $mol^{-1}$ $cm^2$) and another at 308 (ε = 367 $mol^{-1}$ $cm^2$) with a shoulder on the high frequency side of the band (figure 5.12, bottom). After a period of 20 hours a single absorbance at 320 nm (ε = 134 $mol^{-1}$ $cm^2$) is observed corresponding to the ν(Ta=S) 470 $cm^{-1}$ form, and indicating a conversion to this species in solution. This is in agreement with the slower solid-state conversion and the fact that longer reaction time preparations produce a higher proportion of the 470 $cm^{-1}$ form in the crude mixture. Although $S=PMe_3$ is known to absorb at 324 nm, the thio-tantalum system is appreciably more stable than the thio-niobium system (as seen by $^1H$ NMR) and so the change is not thought to be the result of the liberation of $S=PMe_3$. In fact $^1H$ NMR studies show that $S=PMe_3$ is only a very minor component of the decomposition mixture, $PMe_3$ being the dominant product.

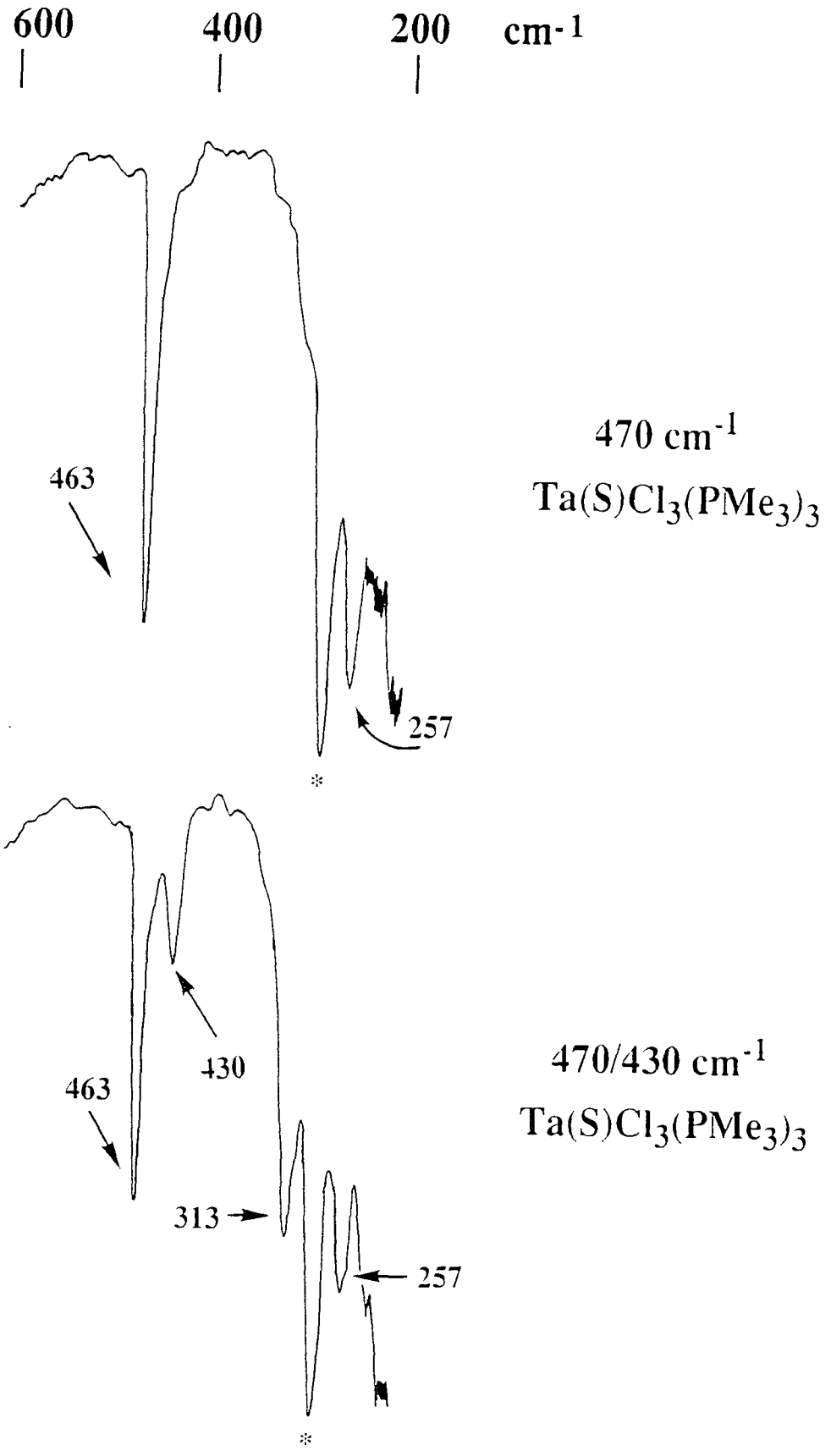


* Solvent peak

**Figure 5.11:** Low frequency solution ($CH_2Cl_2$) infrared spectra of the ν(Ta=S) 470 $cm^{-1}$ and 470/430 $cm^{-1}$ forms of $Ta(S)Cl_3(PMe_3)_3$.

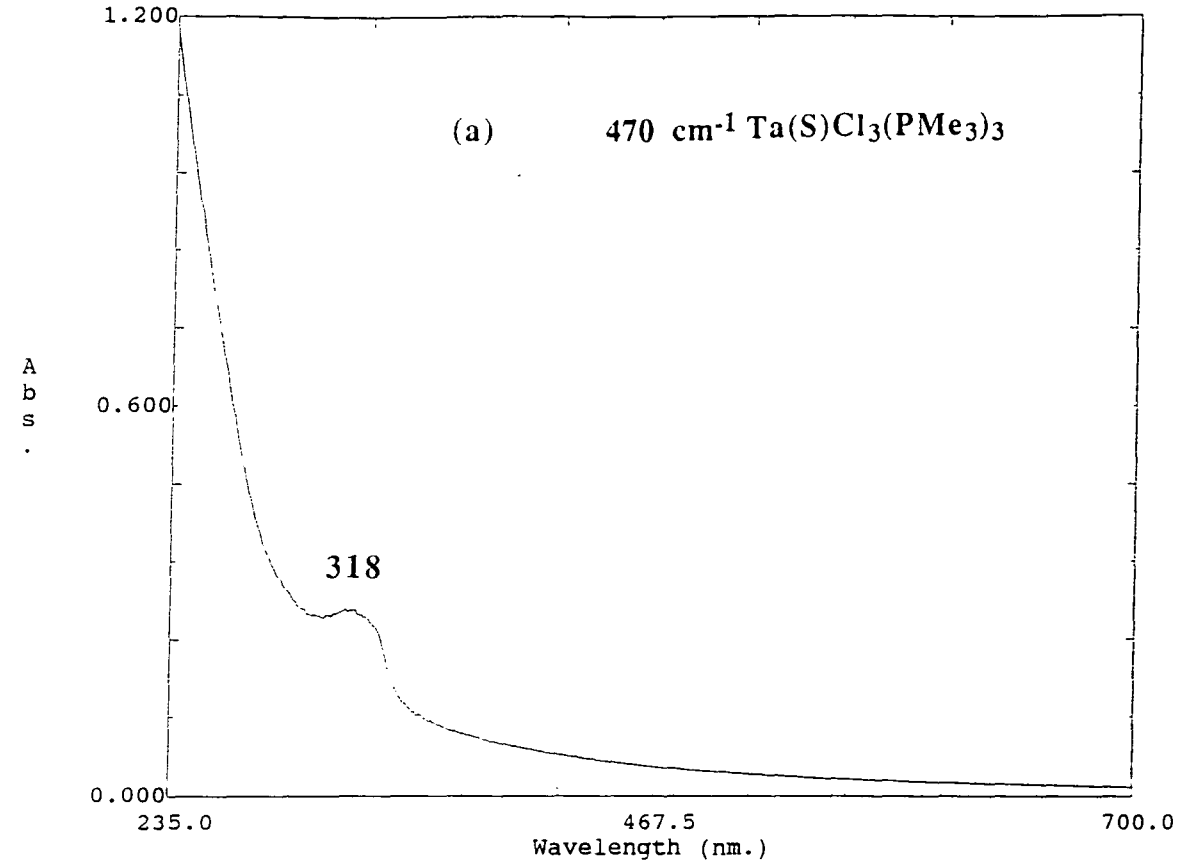


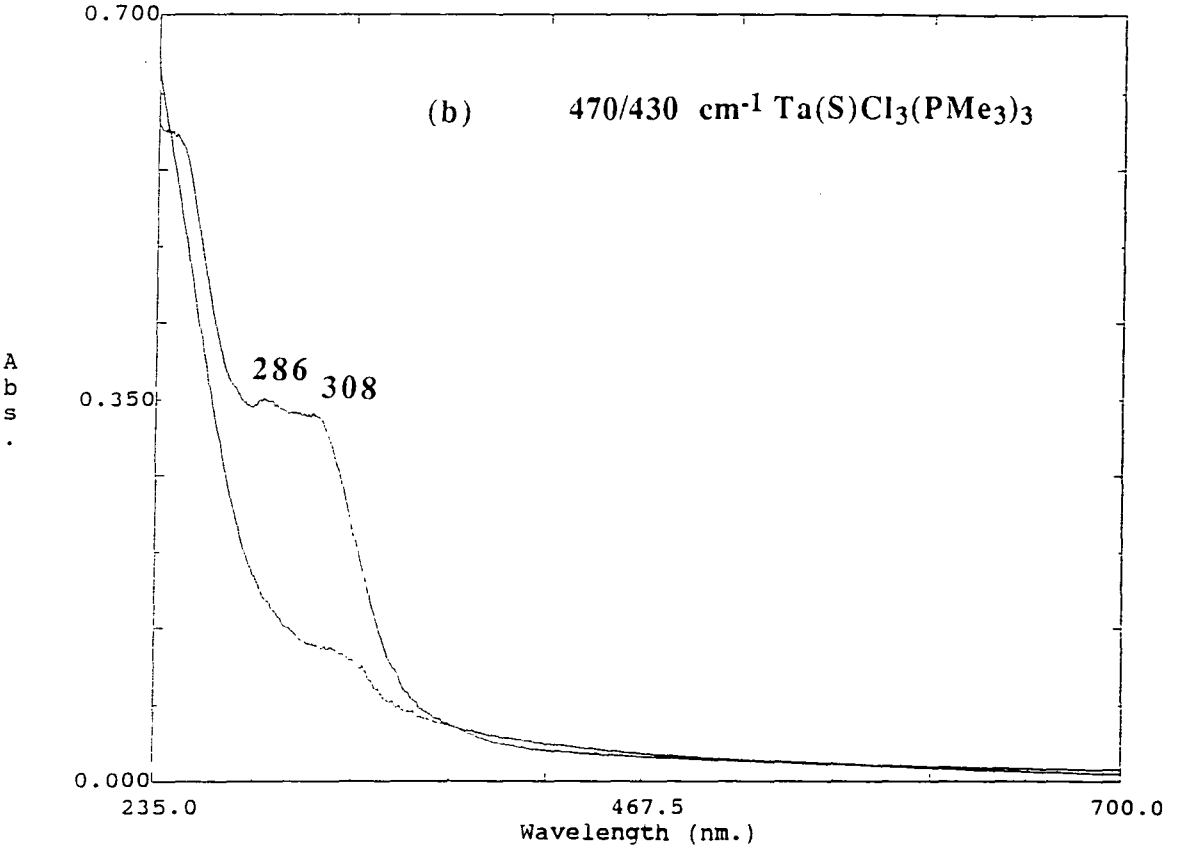


**Figure 5.12:** UV-visible spectra in dichloromethane of the ν(Ta=S) 470 $cm^{-1}$ and 470/430 $cm^{-1}$ forms of $Ta(S)Cl_3(PMe_3)_3$.

### 5.3.5 Raman Spectroscopy

It has been seen in both solid-state and solution infrared spectroscopic studies that two absorptions attributed to ν(Ta=S) stretches can be observed. However, Raman spectroscopy points to only one of the absorptions, that at 470 $cm^{-1}$ in the IR spectrum, being active in the Raman mode at 466 $cm^{-1}$ (figure 5.13), in both the pure 470 $cm^{-1}$ and 470/430 $cm^{-1}$ forms. It is the 470 $cm^{-1}$ species which has both a confirmed stoichiometry as $Ta(S)Cl_3(PMe_3)_3$ and a terminal sulphur moiety (d(Ta=S) 2.219(2)Å), as has been been established by X-ray structure analysis. Elemental analysis of the mixed species (section 5.3.6) shows a lower than expected chlorine content, and together with $^1H$ and $^{31}P$ NMR, mass spectroscopic data and infrared data, it is proposed in section 5.3.7 that the 430 $cm^{-1}$ absorption is due to an unknown species that possesses a bridging sulphur linkage.

In the ν(Ta-Cl) stretching region the pure 470 $cm^{-1}$ $Ta(S)Cl_3(PMe_3)_3$ with its psuedo $C_{3v}$ symmetry is expected to exhibit two Raman active Ta-Cl stretching vibrations, for which there is evidence of in the absorptions at 285 and 251 $cm^{-1}$. However, an 80:20 (470/430 $cm^{-1}$) mixture shows evidence of only one absorption at 289 $cm^{-1}$. The 312 $cm^{-1}$ band, so evident in the IR spectrum and characteristic of the 430 $cm^{-1}$ species, is only very weakly absorbing in the Raman spectrum.

### 5.3.6 Elemental Analysis

Elemental analysis of the $Ta(S)Cl_3(PMe_3)_3$ species which shows a sole absorption at 470 $cm^{-1}$ for the ν(Ta=S) stretch agrees with the stoichiometry (table 5.5). However, the 470/430 $cm^{-1}$ mixture shows a chlorine content that is lower than expected for the stoichiometry $Ta(S)Cl_3(PMe_3)_3$. It has been established by $^1H$ NMR that the mixture does not contain any paramagnetic $TaCl_4(PMe_3)_3$ contaminant (25.74% chlorine). Moreover, if such a species were present it would cause an increase in the observed chlorine content, which conflicts with the reduced chlorine content that is observed. It has been suggested on the basis of infrared and $^1H$ and $^{31}P$ NMR evidence

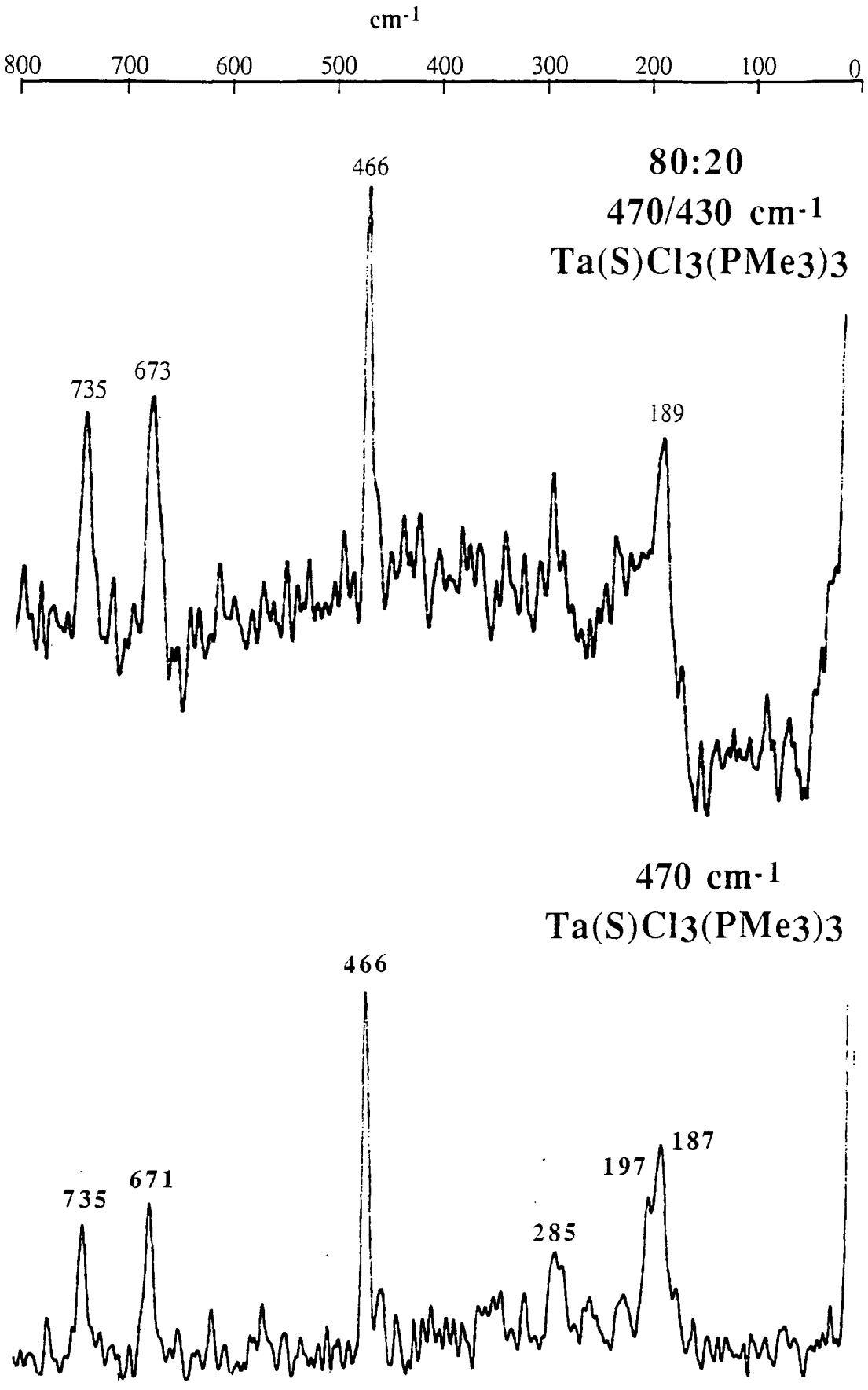


**Figure 5.13:** Raman spectra (solid-state) of pure 470 $cm^{-1}$ $\nu$(Ta=S) and a 80:20 mix of 470/430 $cm^{-1}$ $\nu$(Ta=S) of $Ta(S)Cl_3(PMe_3)_3$ over the range 800 to 0 $cm^{-1}$.

that the 430 $cm^{-1}$ stretch could be due to the dimeric species $[Ta(S)Cl_2(PMe_3)_2]_2$ (16.26% Cl). It can be established that, using the chlorine content values, the mole fraction of such a species in the mixture can be represented by the expression:-

$$x = \frac{\%Cl.RMM[Ta(S)Cl_3(PMe_3)_3] - 300.RMM[Cl]}{100.RMM[Cl] - \%Cl.RMM[Ta(S)Cl(PMe_3)]}$$

$$= \frac{547.613\ \%Cl - 10635.9}{3545.3 - 325.547\ \%Cl}$$

Using this the level of the impurity is calculated at 0.178±0.020 and 0.236±0.023 in the mixed species which compares favourably with the observed 80:20 and 75:25 ratios of the intensities of the ν(Ta=S) stretches in the mixed species.

| | %C | %H | %Cl | Average %Cl | %$[Ta(S)Cl_2(PMe_3)_2]_2$ |
|---|---|---|---|---|---|
| Calculated | 19.74 | 4.97 | 19.42 | ---- | ---- |
| 470 $cm^{-1}$ $Ta(S)Cl_3(PMe_3)_3$ | 19.64 | 4.55 | | 19.38 | 0.96 |
| | 19.48 | 4.48 | | | |
| | 19.39 | 4.90 | 19.30 | | |
| | 19.39 | 4.98 | 19.45 | | |
| 470/430 $cm^{-1}$ $Ta(S)Cl_3(PMe_3)_3$ | 18.48 | 4.64 | 18.61 | 18.50 | 20.71 |
| | 18.16 | 4.65 | 18.38 | | |

**Table 5.5:** Elemental analysis data for the orange and yellow forms of $Ta(S)Cl_3(PMe_3)_3$

### 5.3.7 $^1H$ and $^{31}P$ NMR Studies

The room temperature 400 MHz $^1H$ NMR spectrum in $CD_2Cl_2$ of the orange (ν(Ta=S) 470 $cm^{-1}$) form of $Ta(S)Cl_3(PMe_3)_3$ shows a broadened singlet at δ 1.68 ppm ($\Delta^1/_2$ = 13.0 Hz) and a virtually coupled triplet at δ 2.01 ppm ($^2J(PH)$ = 3.6 Hz) which contributes to 3.0% of the total $^1H$ integral summation (figure 5.14, top). A doublet at δ 1.75 ppm ($^2J(PH)$ = 13.2 Hz) can be assigned to free $S=PMe_3$ (ca. 3.0%). There is no evidence of any paramagnetic $TaCl_4(PMe_3)_3$ at δ -3.21 ppm in the spectrum. The broadness of the singlet suggests that in solution the phosphine ligands have equivalent environments, or the possibility of rapid ligand exchange (not unreasonable considering

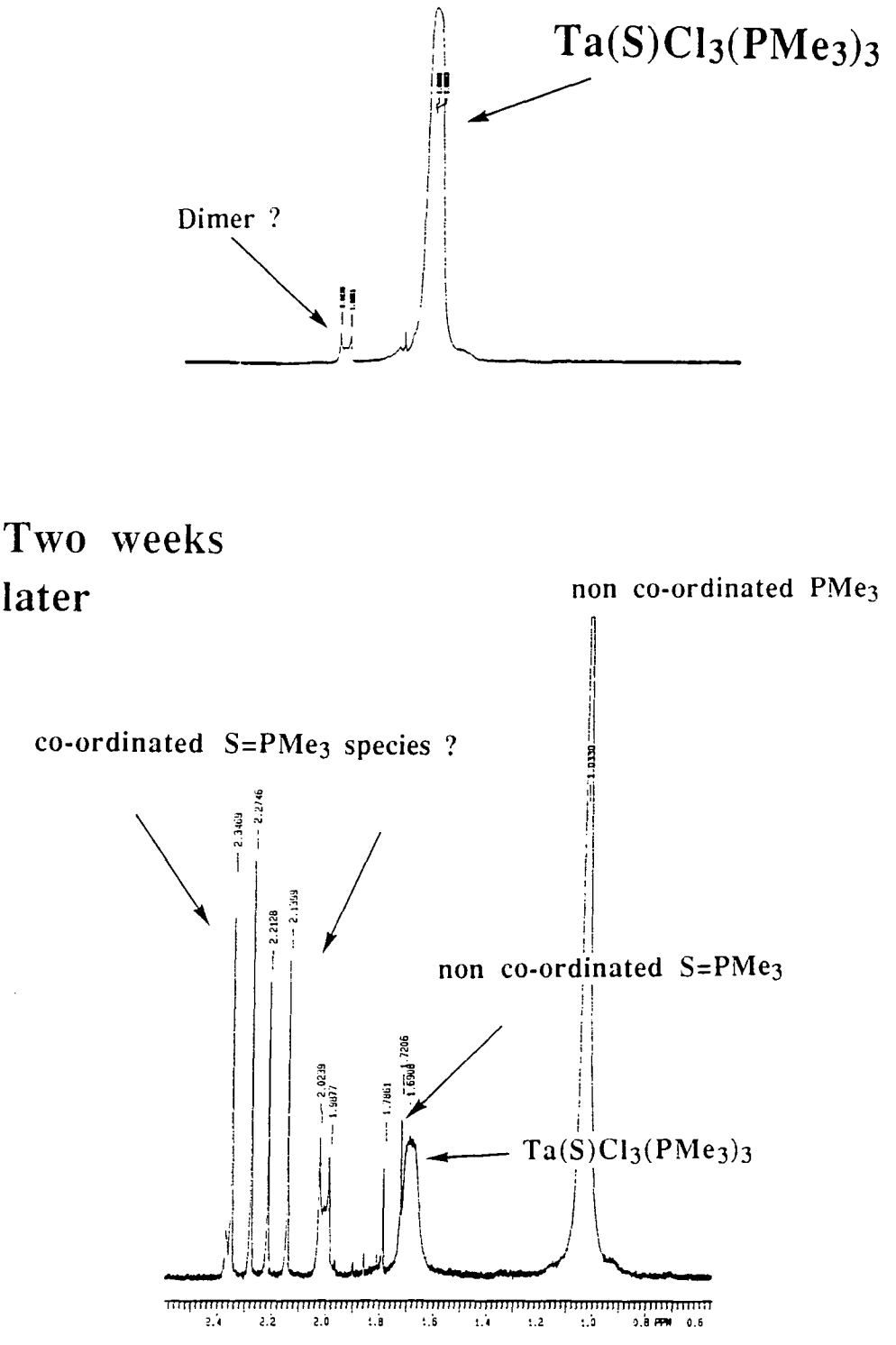


**Figure 5.14:** 400 MHz $^1$H NMR spectra of orange $Ta(S)Cl_3(PMe_3)_3$ ($\nu$(Ta=S) 470 $cm^{-1}$) in $CD_2Cl_2$ over the range +0.8 to +2.5 ppm.

the possible origin of the virtual triplet due to $[Ta(S)Cl_2(PMe_3)_2]_2$ which is discussed later).

The room temperature 161.9 MHz $^{31}P$ NMR spectrum ($CD_2Cl_2$) reveals two unique phosphine environments as sharp singlets at δ 34.14 and -32.46 ppm, in a ratio which suggests that the downfield signal is due to the orange (ν(Ta=S) 470 $cm^{-1}$) $Ta(S)Cl_3(PMe_3)_3$ species and that the upfield signal is due to the species which exhibits a virtually coupled triplet in the $^1H$ NMR spectrum.

Stability studies on a 200 MHz spectrometer revealed that the signals were stable for up to one week in solution, after which the originally golden-yellow solution became yellow-green in colour, the $^1H$ NMR spectrum showing evidence of significant amounts of free $PMe_3$ as a broadened singlet at δ 1.04 ppm ($\Delta^1/_2$ = 9.9 Hz) and small amounts of free $S{=}PMe_3$ (figure 5.14, bottom). The virtual triplet had increased with respect to the singlet at δ 1.68 ppm, although their overall contribution to the signal had decreased to 22%. After two weeks, further decomposition had occurred liberating $PMe_3$ and depositing a yellow solid out of solution, which was shown by IR to be $Ta(S)Cl_3$. There was no evidence of any paramagnetic $TaCl_4(PMe_3)_3$ in the upfield region.

The 200 MHz $^1H$ NMR spectrum ($CD_2Cl_2$) of an 80:20 mixture of the ν(Ta=S) 470/430 $cm^{-1}$ yellow crystalline material gave a yellow-orange solution and similarly exhibited a virtually coupled triplet at δ 2.01 ppm ($^2J(PH)$ = 3.69 Hz) (63% of the $^1H$ signal) and a broadened singlet at δ 1.68 ppm ($\Delta^1/_2$ = 12.5 Hz) (37%) (figure 5.15, top). These two signals were invariant over a period of one week at room temperature, and after two weeks the virtual triplet had increased in intensity while that of the broadened singlet had decreased. The spectrum now showed evidence of free $PMe_3$ as a broadened singlet at δ 1.03 ppm ($\Delta^1/_2$ = 5.2 Hz), and free $S{=}PMe_3$ as a doublet at δ 1.75 ppm ($^2J(PH)$ = 13.1 Hz). There was no evidence of any paramagnetic $TaCl_4(PMe_3)_3$ in the spectrum at δ -3.21 ppm (figure 5.15, bottom).

The 101.26 MHz $^{31}P$ NMR spectrum of the 470/430 $cm^{-1}$ mixture showed two singlets at δ 27.76 and -36.71 ppm, the integral ratio suggesting that the downfield signal is due to the ν(Ta=S) 470 $cm^{-1}$ species and the upfield signal is due to the species

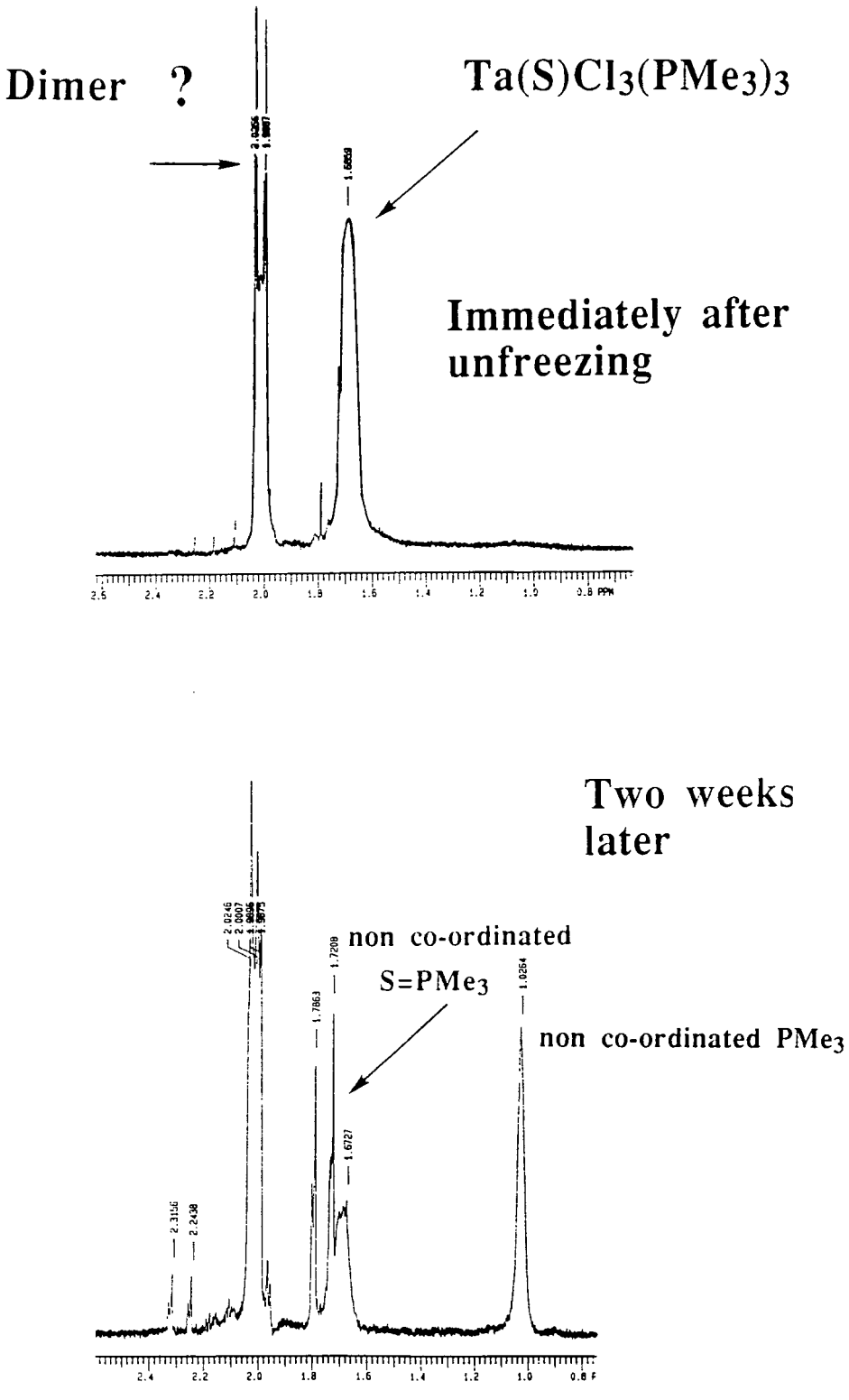


**Figure 5.15:** 400 MHz $^1$H NMR spectra of yellow $Ta(S)Cl_3(PMe_3)_3$ ($\nu$(Ta=S) 440/430 $cm^{-1}$) in $CD_2Cl_2$ over the range +0.8 to +2.5 ppm.

which exhibits a virtual triplet in the $^1H$ NMR spectrum, and hence to the species that absorbs at 430 $cm^{-1}$ in the IR spectrum.

$^1H$ and $^{31}P$ NMR studies thus infer that the ν(Ta=S) 470 and 430 $cm^{-1}$ species are independently observable, showing signals that imply equivalent phosphine environments within the geometry of each molecule. Additionally, the 6-coordinate complex $TaCl_6(PMe_3)_4$[16] is known to have two phosphine environments; one that is axial and the other equatorial. This is reflected in the $^{31}P\{^1H\}$ NMR ($C_6D_6$) which shows signals due to these configurational differences at δ -31.1 (equatorial) and -52.3 ppm (axial). This suggests that the configuration of the phosphine groups in this unknown species which exhibits a virtual triplet in the $^1H$ NMR are in an equatorial environment. Furthermore, the near doublet nature of the virtually coupled triplet signal suggests that the P-Ta-P angle is significantly closer to a *cis*-90° configuration than to a *trans*-180° configuration. In fact, an angle of about 90° to 100° does not seem unreasonable. From consideration of the infrared spectroscopic data which shows a third additional ν(Ta-Cl) stretch at 312 $cm^{-1}$, and elemental analysis data which reveals a reduced chlorine content in the mixed 470/430 $cm^{-1}$ species, it is suggested that the ν(Ta=S) stretch at 430 $cm^{-1}$ is possibly due to the species $[Ta(S)Cl_2(PMe_3)_2]_2$. There is additional evidence for this species in the $CI^+$ mass spectrum which gives a molecular ion at m/z 437. The dimer can have two possible geometries for a non-bridging sulphur model, a trans-sulphur configuration (figure 5.17) or a cis-sulphur configuration (figure 5.16).

$C_{2v}$ point group

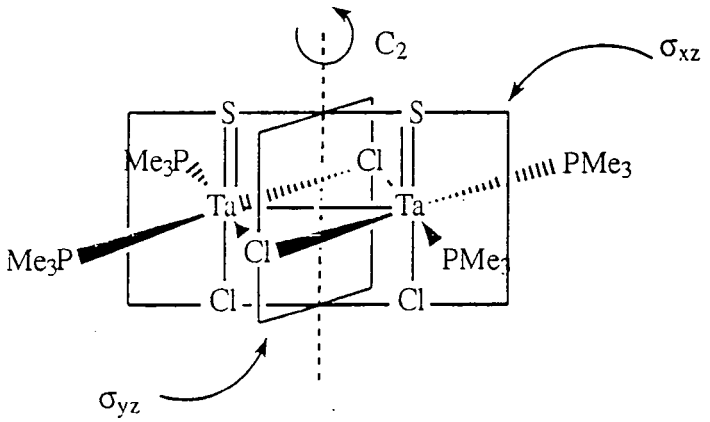


**Figure 5.16:** $C_{2v}$ point group for μ-Cl dimer $[Ta(S)Cl_2(PMe_3)_2]_2$

These have $C_{2h}$ and $C_{2v}$ molecular symmetries respectively. Considering the six Ta-Cl stretching vibrations, then group theory leads to the conclusion that $2A_g+A_u+B_g+2B_u$ and $2A_1+A_2+2B_1+B_2$ ($\Gamma_{Ta\text{-}Cl}$) respectively span the vibrations for the two cases. However, not all of these vibrations are infrared active, and for the $C_{2h}$ case this reduces to $A_u+2B_u$ (i.e., three vibrations) and for the $C_{2v}$ scenario to $2A_1+2B_1+B_2$ (i.e., five vibrations). Now the infrared spectrum for the mixed tantalum species shows three Ta-Cl stretching vibrations (312, 290 and 257 $cm^{-1}$), while the infrared spectra of a 90:10 and 10:90[2] each show only two absorptions, at 290 and 257 $cm^{-1}$, and at 312 and 290 $cm^{-1}$ respectively (figure 5.10). This indicates that the 312 $cm^{-1}$ is unique to the 430 $cm^{-1}$ species, just as the 257 $cm^{-1}$ absorption is to the 470 $cm^{-1}$ stretching species. Thus, neither of the bridging chlorine models fits the IR data. Considering that the ν(Ta=S)

$C_{2h}$ point group

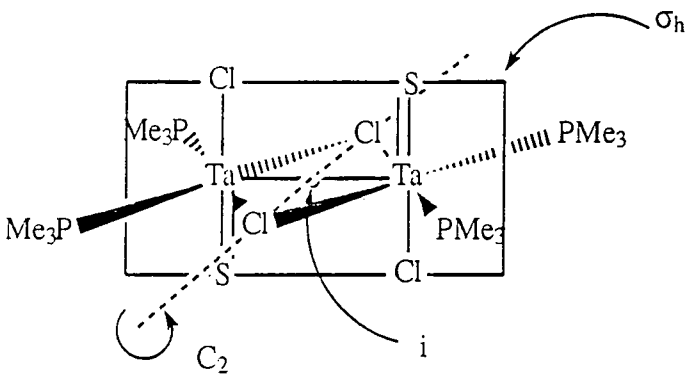


**Figure 5.17:** $C_{2h}$ point group for μ-Cl dimer $[Ta(S)Cl_2(PMe_3)_2]_2$

stretch of the base-free $Ta(S)Cl_3$ which occurs at 460 $cm^{-1}$ implies a bridging sulphur atom being present, it seems not unreasonable to propose that a similar situation exists in this dimer. With bridging sulphur atoms this molecule (figure 5.18) now has $D_{2h}$ symmetry and the four Ta-Cl bonds have stretching vibrations that transform as $A_g+B_{1u}+B_{2g}+B_{3u}$. However, only $B_{1u}+B_{3u}$ are infrared active and thus account for the two ν(Ta-Cl) stretches observed for the unknown species giving rise to the 430 $cm^{-1}$ ν(Ta=S) stretch. This postulation would also account for the low value observed for the ν(Ta=S) stretch being due to a bridging sulphur atom and not to a terminally bound

sulphur atom. This is substantiated by the Raman evidence which shows that only one ν(Ta=S) stretch is Raman active (466 $cm^{-1}$), corresponding to the 470 $cm^{-1}$ ν(Ta=S)

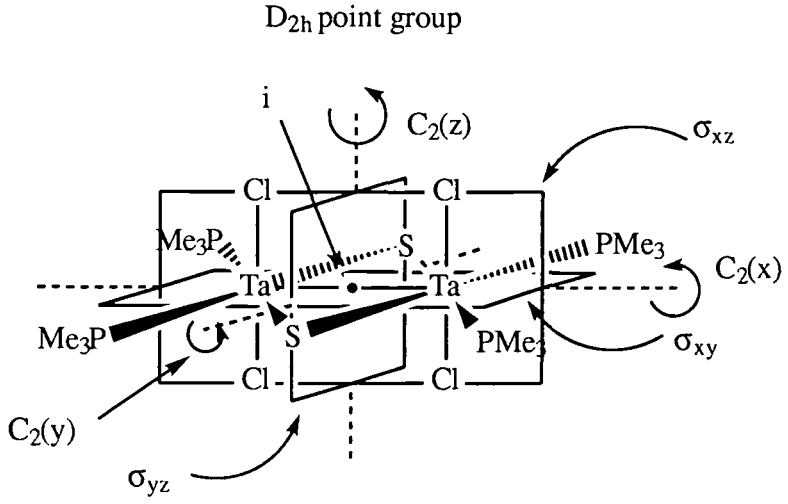


**Figure 5.18:** $D_{2h}$ point group for μ-S dimer $[Ta(S)Cl_2(PMe_3)_2]_2$

stretch observed in the infrared spectrum for a terminally bound sulphur atom (as established by X-ray structure determination (section 5.4.3)). Vibrations of a bridging sulphur atom are not Raman active.

However, it must be noted that in such a dimeric species the niobium centre formally has a +4 oxidation state ($d^1$), and so coupling of the unpaired electrons to form a Ta–Ta bond (which formally doesn't contribute to the metal's oxidation state) must be invoked in order for the species to be diamagnetic.

Another possibility, also considered in the case of green $Nb(S)Cl_3(PMe_3)_3$, which would account for the reduced chlorine content in the mixed tantalum species, is to envisage the replacement of one of the chlorine ligands in the seven-coordinate complex by a thiolate or hydroxide. However, using the elemental analysis data leads to the conclusion that these values would represent contamination levels due to such species of 13.00% (SH) and 13.40% (OH), which are significantly lower than the ca. 20% proposed for the dimer, and the level calculated from the IR data (20-25%). Furthermore, $^1H$ NMR data does not appear to indicate the presence of SH or OH groups, which despite the intrinsically broad nature expected of their resonances would be expected to be observed considering the intensity of the two signals in the $^1H$ NMR

spectrum for the mixed species. Thus the μ-S dimer is proposed to be the best candidate for the species giving rise to the ν(Ta=S) stretch at 430 $cm^{-1}$.

## 5.4 The Molecular Structures of Orange-Yellow and Green $Nb(S)Cl_3(PMe_3)_3$ and Orange $Ta(S)Cl_3(PMe_3)_3$

The isolation of two isomeric compounds with the formula $Nb(S)Cl_3(PMe_3)_3$ was described in section 5.2.1. Both forms, orange-yellow and green $Nb(S)Cl_3(PMe_3)_3$[19,20] have been subjected to X-ray diffraction analysis by Prof. M. McPartlin and co-workers at the University of North London and the results of these studies are described below.

### 5.4.1 Orange-Yellow $Nb(S)Cl_3(PMe_3)_3$ (ν(Nb=S) 455 $cm^{-1}$)

The crystal data are collected in appendix 1D and the molecular structure is illustrated in figures 5.19, 5.20 and 5.23(a). Selected bond angles and distances are given in appendix 4C.

The complex is monomeric for which the coordination geometry is best described as distorted, monocapped octahedral (figure 5.19) with facial arrangements of chloro and trimethylphosphine ligands giving the molecule virtual $C_{3v}$ symmetry (figure 5.20). The sulphido group is in a site capping the face defined by the phosphine ligands and lies above the P(1), P(2), P(3) plane, with the niobium atoms below this plane. This coordination is similar to that observed in $NbCl_4(PMe_3)_3$[17], yet very different to the seven coordinate complex $Nb(S)(S_2CNEt_2)_3$[10], in which the niobium atom is at the centre of a distorted pentagonal bipyramid.

The Nb=S bond length of 2.194(1)Å is at the far end of the range of distances usually observed in four to seven coordinate sulphido-niobium complexes (2.085(5) - 2.196(4)Å) (table 5.1). This presumably arises due to the presence of three, highly electron releasing $PMe_3$ ligands within the crowded coordination sphere of orange-yellow $Nb(S)Cl_3(PMe_3)_3$.

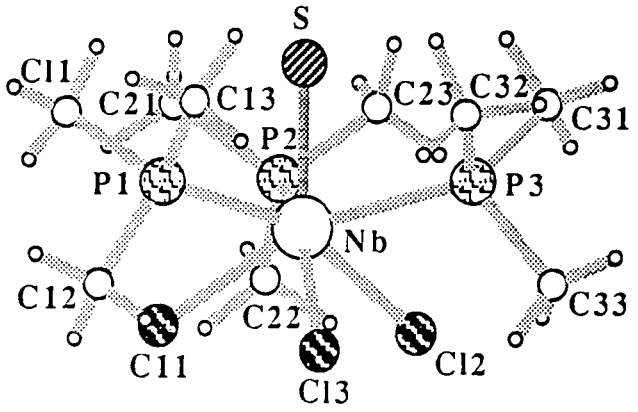


**Figure 5.19:** Molecular structure of orange-yellow $Nb(S)Cl_3(PMe_3)_3$

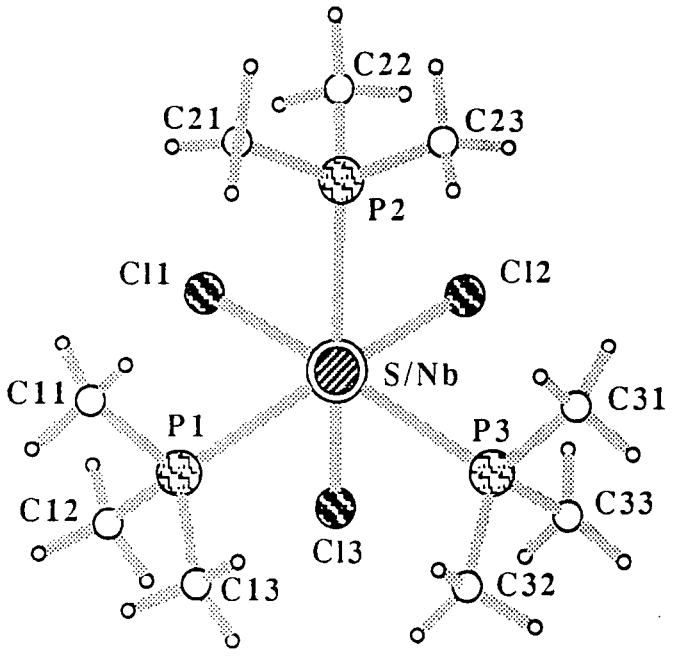


**Figure 5.20:** View down the sulphur-niobium bond of orange-yellow $Nb(S)Cl_3(PMe_3)_3$

The compounds orange-yellow $Nb(S)Cl_3(PMe_3)_3$ and $NbCl_4(PMe_3)_3$[17] are isomorphous (space group $P2_{1/c}$). The average Nb-Cl distances in orange-yellow $Nb(S)Cl_3(PMe_3)_3$ (2.499(2)Å) are slightly longer than the average facial Nb-Cl distances in $NbCl_4(PMe_3)_3$ (2.453(13)Å) the opposite of the trend predicted on the basis of oxidation state. Since both compounds possess average P-Nb-$Cl_{trans}$ angles of ca. 157°, a similar average trans influence is anticipated due to the sulphido ligand. Therefore, the average lengthening observed in orange-yellow $Nb(S)Cl_3(PMe_3)_3$ may be attributed to the presence of the sulphido ligand.

Interestingly, the Nb-Cl (2) bond is the longest (2.501(1)Å) whilst also having the most acute S-Nb-Cl angle of 121.8°, an observation at variance with a

(a)

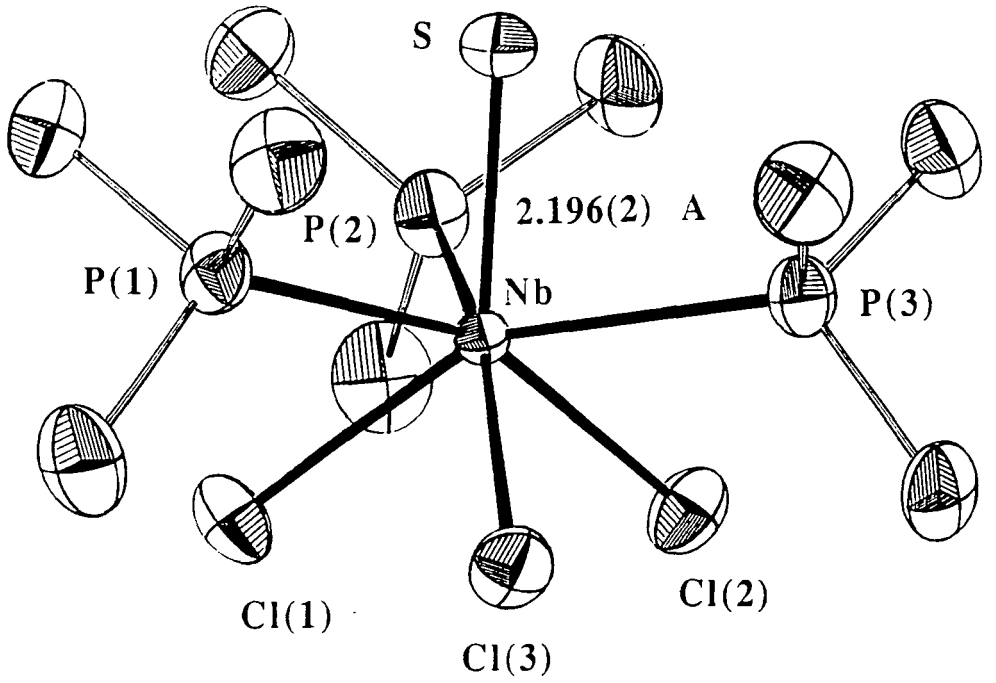


(b)

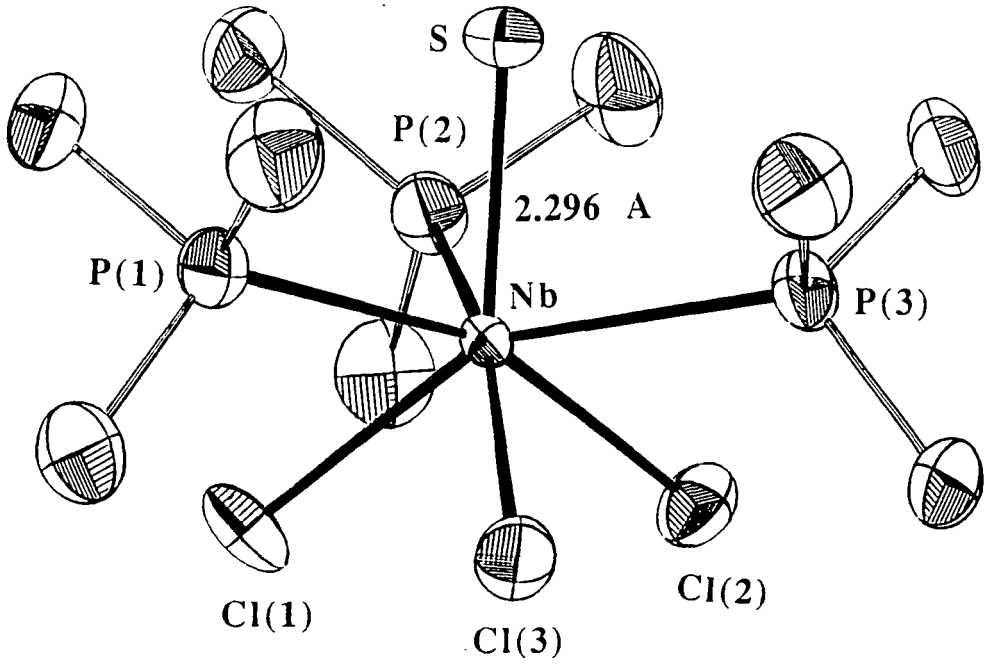


**Figure 5.23:** Comparison of the structures of (a) the yellow-orange (ν(Nb=S) 455 $cm^{-1}$) and (b) the green (ν(Nb=S) 489 $cm^{-1}$) forms of $Nb(S)Cl_3(PMe_3)_3$, showing the absence of a distortion of the thermal ellipsoid of the sulphur atom in the green form.

sulphido ligand trans influence. However, since the trans P-Nb-Cl angle for Cl(2) is the largest (158.9°), this atom may experience a slightly larger $PMe_3$ trans influence.

The Nb-P bonds have an average length of 2.639(1)Å in orange-yellow $Nb(S)Cl_3(PMe_3)_3$ and 2.651(6)Å in $NbCl_4(PMe_3)_3$, the former having the slightly shorter distances as expected for niobium (V) over niobium (IV).

The acute S-Nb-P angles (average 77.6(1)°) led to a staggered arrangement of $PMe_3$ substituents with respect to the capping sulphur atom (as viewed along the P-Nb vector) in order to minimise inter-ligand repulsions. A similar arrangement is found in $NbCl_4(PMe_3)_3$. Consequently, close S···H contacts result, in the range 2.83 - 3.03Å.

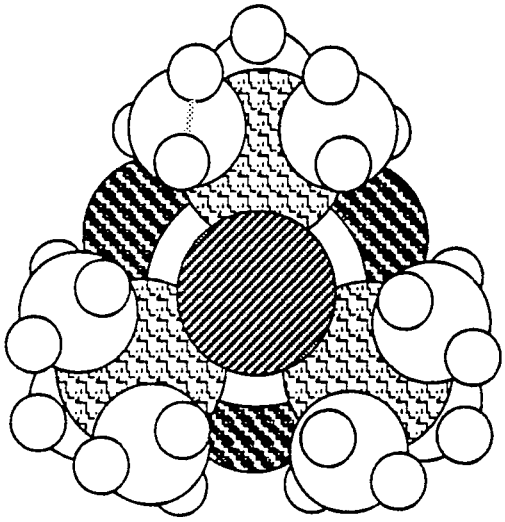

**Figure 5.21:** Space filling diagram of orange-yellow $Nb(S)Cl_3(PMe_3)_3$ viewed down the sulphur-niobium bond

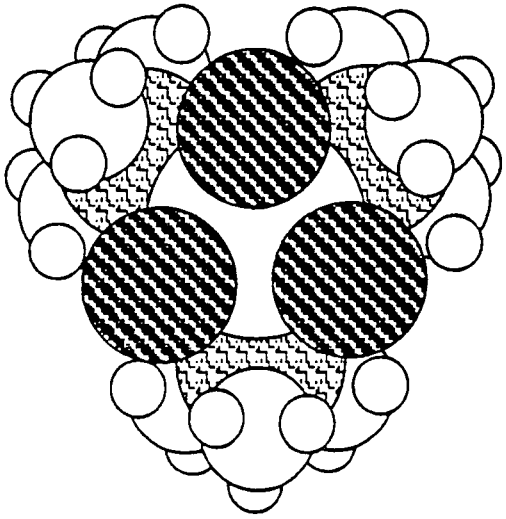

**Figure 5.22:** Space filling diagram of orange-yellow $Nb(S)Cl_3(PMe_3)_3$ viewed through the facial chlorine plane

Indeed these distances are comparable to the sum of the van der Waals radii of niobium and sulphur (3.0Å).[18] Figure 5.21 represents a space filling diagram of orange-yellow $Nb(S)Cl_3(PMe_3)_3$ viewed down the S=Nb vector illustrating the extremely close contacts between the sulphur atom and six phosphine methyl hydrogens (H-H). Figure 5.22 is a similar diagram viewed through the facial chlorine plane.

### 5.4.2 Green $Nb(S)Cl_3(PMe_3)_3$ ($\nu$(Nb=S) 489 $cm^{-1}$)

The crystal data are collected in appendix 1E and the molecular structure is illustrated in figures 5.23(b), and is compared with that of the yellow-orange form. Selected bond angles and distances are given in appendix 4D and comparative values of selected parameters for orange-yellow and green $Nb(S)Cl_3(PMe_3)_3$, and for a tantalum analogue (orange $Ta(S)Cl_3(PMe_3)_3$) described later are displayed in table 5.6.

| Parameter | Orange-yellow $Nb(S)Cl_3(PMe_3)_3$ | Green $Nb(S)Cl_3(PMe_3)_3$ | Orange $Ta(S)Cl_3(PMe_3)_3$ |
|---|---|---|---|
| (M=S) | 2.194(2) | 2.296(1) | 2.219(2) |
| $(M\text{-}Cl)_{av}$ | 2.499(2) | 2.486(1) | 2.486(2) |
| $(M\text{-}P)_{av}$ | 2.639(2) | 2.649(1) | 2.635(2) |
| $S\text{-}M\text{-}Cl_{av}$ | 126.0(1) | 125.8(1) | 126.4(1) |
| $S\text{-}M\text{-}P_{av}$ | 77.6(1) | 76.3(1) | 77.5(1) |
| $P\text{-}M\text{-}P_{av}$ | 115.5(1) | 114.6(1) | 115.4(1) |
| $Cl\text{-}M\text{-}Cl_{av}$ | 89.1(1) | 89.3(1) | 88.3(1) |
| $P\text{-}M\text{-}Cl_{trans,\ av}$ | 156.5(1) | 157.7(1) | 156.1(1) |

**Table 5.6:** Comparative values of some parameters for orange-yellow and green $Nb(S)Cl_3(PMe_3)_3$ and orange $Ta(S)Cl_3(PMe_3)_3$

The green compound $Nb(S)Cl_3(PMe_3)_3$ is isomorphous to orange-yellow $Nb(S)Cl_3(PMe_3)_3$ (space group $P2_1/c$) and the average interatomic distances and angles are essentially identical, although the 489 $cm^{-1}$ isomer shows larger individual deviations.

The Nb-Cl distances are slightly shorter and the Nb-P distances marginally for the $\nu$(Nb=S) 489 $cm^{-1}$ isomer.

Without doubt, the most marked difference between the isomers is the length of the niobium-sulphur bond. In green $Nb(S)Cl_3(PMe_3)_3$ this bond has been lengthened by ca. 0.10Å over that in orange-yellow $Nb(S)Cl_3(PMe_3)_3$ and is ca. 0.15Å longer than is usually found in niobium sulphido compounds. Indeed this distance is approaching the sum of the covalent radii of niobium and sulphur (2.39Å)[18] and could therefore be regarded as representing a bond order considerably less than 2. There is also a slight contraction in the Nb-Cl bond lengths (mean 0.013Å) in going from the green form to the orange-yellow form.

### 5.4.3 Orange $Ta(S)Cl_3(PMe_3)_3$ ($\nu$(Ta=S) 470 $cm^{-1}$)

Orange $Ta(S)Cl_3(PMe_3)_3$ ($\nu$(Ta=S) 470 $cm^{-1}$) has been subjected to X-ray diffraction analysis by Prof. M. McPartlin and co-workers at the University of North London. The crystal data are collected in appendix 1F and the molecular structure is illustrated in figures 5.24 (a). Selected bond angles and distances on a refined structure are given in table 5.7 and the original crystal structure determination[2] is presented in appendix 4E.

The compound is isomorphous to orange-yellow and green $Nb(S)Cl_3(PMe_3)_3$ (space group $P_{21/c}$). Values of selected parameters for orange $Ta(S)Cl_3(PMe_3)_3$ are displayed along side orange-yellow and green $Nb(S)Cl_3(PMe_3)_3$ in table 5.6 and essentially, the average bond lengths and angles are identical.

The most significant feature is the length of the tantalum-sulphur bond. In orange $Ta(S)Cl_3(PMe_3)_3$ this is 0.015Å longer than the longest (Ta=S) bond previously reported for six coordinate $Ta(S)Cl_3(bpte)$[14] and 0.038Å longer than the seven coordinate complex $Ta(S)Cl_3(S_2CNEt_2)_3$.[13] A re-examination of the molecular structure has since given a value of 2.198(3)Å for the Ta=S bond length, 0.020(9)Å shorter than that previously reported.[2] This form has been established by $^1H$ NMR to be paramagnetic contaminant free, and so the source of this discrepancy in the two values is unknown.

| | | | |
|---|---|---|---|
| Ta - Cl(1) | 2.479(2) | P(2) - Ta - P(1) | 113.0(1) |
| Ta - Cl(2) | 2.501(2) | P(3) - Ta - P(1) | 116.3(1) |
| Ta - Cl(3) | 2.480(2) | P(3) - Ta - P(2) | 117.0(1) |
| | | | |
| Ta - P(1) | 2.631(2) | S - Ta - Cl(1) | 129.7(1) |
| Ta - P(2) | 2.639(2) | S - Ta - Cl(2) | 123.3(1) |
| Ta - P(3) | 2.637(2) | S - Ta - Cl(3) | 126.2(1) |
| | | | |
| Ta - S | 2.219(2) | S - Ta - P(1) | 77.8(1) |
| | | S - Ta - P(2) | 77.3(1) |
| P(1) - C(11) | 1.824(9) | S - Ta - P(3) | 77.2(1) |
| P(1) - C(12) | 1.822(9) | | |
| P(1) - C(13) | 1.826(10) | C(11) - P(1) - Ta | 113.0(3) |
| P(2) - C(21) | 1.830(9) | C(12) - P(1) - Ta | 118.9(3) |
| P(2) - C(22) | 1.832(10) | C(13) - P(1) - Ta | 113.5(3) |
| P(2) - C(23) | 1.820(9) | C(21) - P(2) - Ta | 114.6(3) |
| P(3) - C(31) | 1.822(9) | C(22) - P(2) - Ta | 117.8(3) |
| P(3) - C(32) | 1.816(10) | C(23) - P(2) - Ta | 112.3(3) |
| P(3) - C(33) | 1.819(8) | C(31) - P(3) - Ta | 113.6(3) |
| | | C(32) - P(3) - Ta | 113.2(3) |
| Cl(2) - Ta - Cl(1) | 88.0(1) | C(33) - P(3) - Ta | 118.3(3) |
| Cl(3) - Ta - Cl(1) | 86.4(1) | | |
| Cl(3) - Ta - Cl(2) | 90.7(1) | C(12) - P(1) - C(11) | 103.0(5) |
| | | C(13) - P(1) - C(11) | 104.6(5) |
| P(1) - Ta - Cl(1) | 75.2(1) | C(13) - P(1) - C(12) | 102.2(4) |
| P(1) - Ta - Cl(2) | 158.8(1) | C(22) - P(2) - C(21) | 102.7(5) |
| P(1) - Ta - Cl(3) | 75.5(1) | C(23) - P(2) - C(21) | 103.4(5) |
| P(2) - Ta - Cl(1) | 75.4(1) | C(23) - P(2) - C(22) | 104.5(4) |
| P(2) - Ta - Cl(2) | 74.1(1) | C(32) - P(3) - C(31) | 103.1(4) |
| P(2) - Ta - Cl(3) | 156.5(1) | C(33) - P(3) - C(31) | 103.2(4) |
| P(3) - Ta - Cl(1) | 153.0(1) | C(33) - P(3) - C(32) | 103.7(4) |
| P(3) - Ta - Cl(2) | 74.0(1) | | |
| P(3) - Ta - Cl(3) | 74.2(1) | | |

**Table 5.7:** Selected bond lengths (Å) and angles (°) for orange $Ta(S)Cl_3(PMe_3)_3$

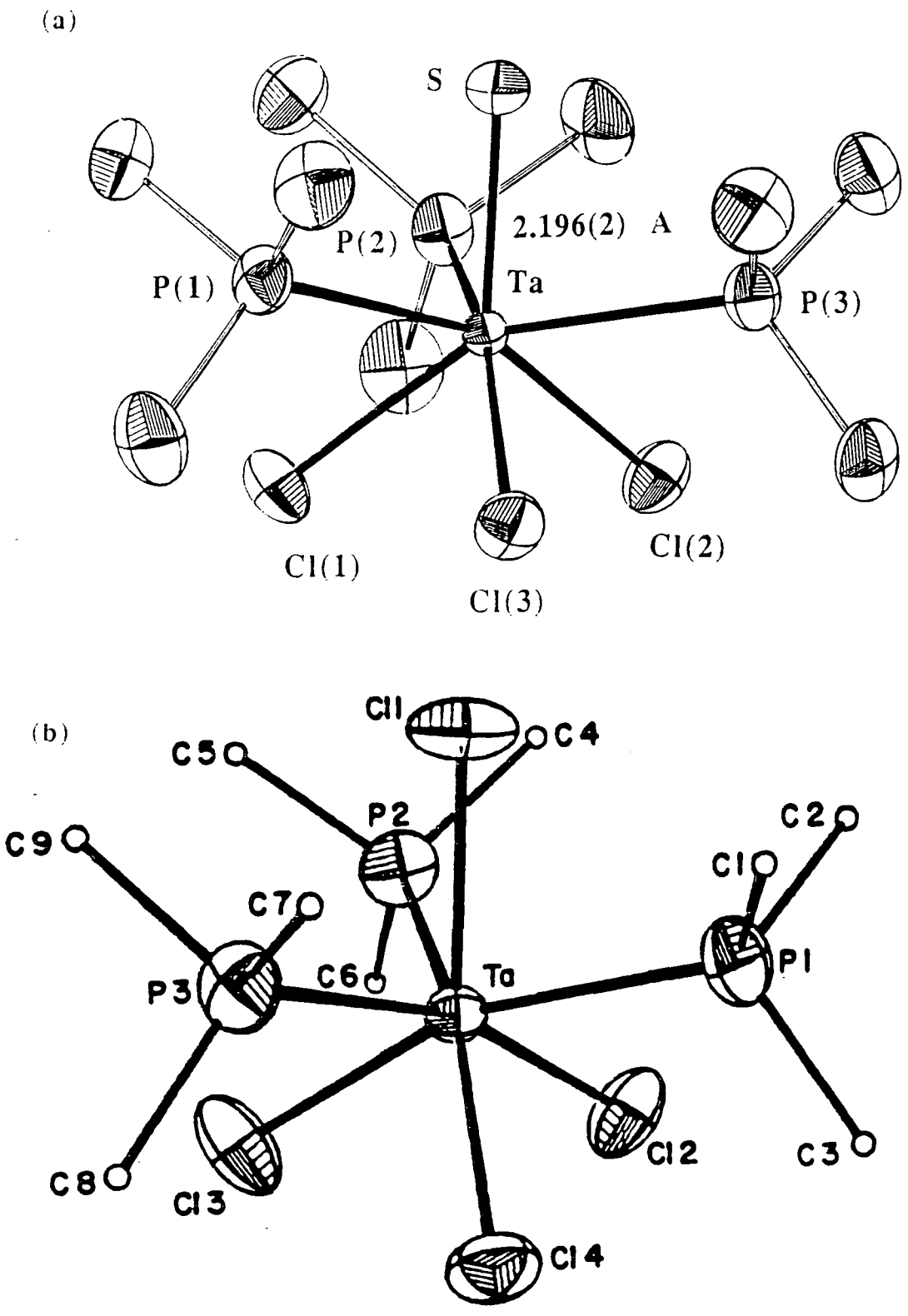


**Figure 5.24:** ORTEP comparison of the structures of 470 $cm^{-1}$ $Ta(S)Cl_3(PMe_3)_3$ and $TaCl_4(PMe_3)_3$.

### 5.4.4 Crystallographic Disorder

X-ray structure determination of the orange-yellow and green forms of $Nb(S)Cl_3(PMe_3)_3$ reveals the two structures to be almost indistinguishable (figure 5.23). These crystals are isomorphous not only with each other but also with the two forms of $Nb(O)Cl_3(PMe_3)_3$ and the tetrachloride impurity $NbCl_4(PMe_3)_3$. The main differences as we have seen in the previous sections have been centred on the bond lengths, and of course the ν(Nb=E) stretching frequencies. In addition to the small differences in Nb-Cl and Nb-P distances, there is a marked variation in the length of the Nb=S bond in the two forms, being 2.194(2)Å in the orange-yellow form and 2.296(1)Å in the green form. This variation is the opposite to that expected on the basis of the ν(Nb=S) stretch observed in their respective IR spectra; the green form being expected to have had the longer Nb=S bond length. This discrepancy between the bond length in relation to the IR spectra led to the postulation again of a possible disorder model. The similarity between the $Nb(S)Cl_3(PMe_3)_3$ and $Nb(O)Cl_3(PMe_3)_3$ systems first envoked thoughts of the presence of an impurity, $NbCl_4(PMe_3)_3$, being considered. However, the similar number of electrons in sulphur and chlorine atoms means that signs of disorder in the structures would be almost impossible to detect. However, despite the thermal ellipsoids for the two sulphur atoms being normal (figure 5.23), and there being no sign of any excess electron density at the sulphur position in the structure of the green form, the possibility of co-crystallised $NbCl_4(PMe_3)_3$ (or some other S/Cl disorder) in this long-bonded form can not be ruled out. The possibility of a geometric isomer disordered with the tetrachloride, or alternatively that a pure green geometric isomer was three-fold disordered (figure 5.25), were considered. Both these models fit the IR spectroscopic data, supplying explanations for the different ν(Nb=S) stretches of the orange-yellow (455 $cm^{-1}$) and green forms (489 $cm^{-1}$). However, they still left unexplained the fact that the axial bond length of the green form was too short (even allowing for the differences in oxidation state between the sulphido and tetrachloride) to be a single Nb-Cl length; 2.296(1)Å compared to 2.409Å in the tetrachloride. A simple disorder of the orange-yellow form with the tetrachloride (as depicted for the oxo system in figure 4.18),

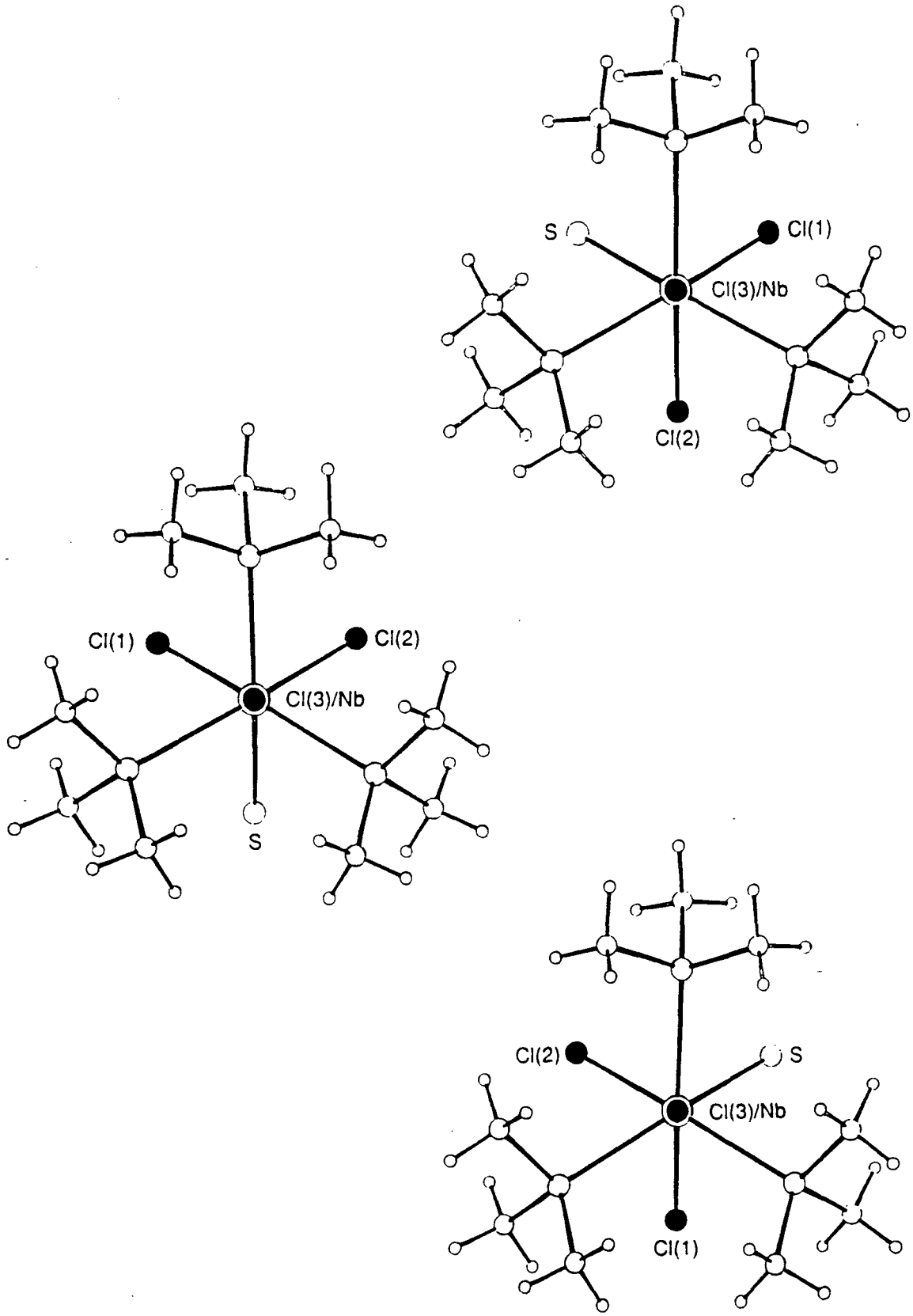


**Figure 5.25:** A three-fold disorder model for a pure geometrical isomer of $Nb(S)Cl_3(PMe_3)_3$ which would fit the spectroscopic data, but requires a longer bond length for the axial ligand than observed.

although feasible on crystallographic grounds, does not readily explain the observed differences in the ν(Nb=S) stretches between the green and orange-yellow forms. The fact that the IR spectra were recorded in nujol means that some solid-state effect, produced by the presence of tetrachloride in the crystals, seemed to be the only explanation of the differences in the IR spectra for this model. In this event the solution IR spectra of the two forms would be expected to show the same ν(Nb=S) stretch. However, as we seen in section 5.2.3 the spectra of the orange-yellow and green forms in $CH_2Cl_2$ show two characteristic ν(Nb=S) stretches corresponding to those observed in the solid-state nujol mull spectra. This clearly means that the differences in the ν(Nb=S) stretches between the orange-yellow and green forms of $Nb(S)Cl_3(PMe_3)_3$ is not a solid-state artifact and so the possibility of these two forms being genuine examples of bond-stretch isomers, regardless of whether the green form is contaminated by tetrachloride, must be reconsidered.

In view of the co-crystallised $NbCl_4(PMe_3)_3$ present in the green $Nb(O)Cl_3(PMe_3)_3$ samples, the thioniobium system (where any disorder could not be directly detected from one structure determination) was re-investigated in the hope that if there were an undetected mixture of two components present in the green isomer, the proportion might change between successive preparations. Two additional batches of suitable crystals were subsequently examined and significantly, although the bulk sample exhibited only a single absorption at ν(Nb=S) 489 $cm^{-1}$ characteristic of the green isomer, the X-ray structure determinations revealed two new, very much shorter Nb=S bond lengths of 2.225(3)Å and 2.219(3)Å[19] compared to that of 2.296(1)Å[20] in the original evaluation. This implies that the green form of $Nb(S)Cl_3(PMe_3)_3$, like its oxo analogue, contained a proportion of co-crystallised $NbCl_4(PMe_3)_3$ thus giving the appearance of an apparent Nb=S bond length which can vary depending on the fraction of tetrachloride present. This observation does, however eliminate the possibility of a disordered pure geometric isomer with chloride in the axial site accounting for the differences in the ν(Nb=S) stretches, as the major component in these crystals must have an axial sulphur in order to explain both the short and variable nature of the axial bond lengths observed. As only one ν(Nb=S) at 489 $cm^{-1}$ is present in all these cases it must be attributed to this

axial Nb=S, and not to an undetected Nb=S in an octahedral site. Thus, the demonstration of disorder in the green form of $Nb(S)Cl_3(PMe_3)_3$ makes it difficult to rule out bond-stretch isomerism in these compounds.

Using the crystallographic data for the two forms of $Nb(S)Cl_3(PMe_3)_3$ it was attempted to explain the results by invoking co-crystallisation of the orange-yellow form with different proportions of tetrachloride. This means that the IR spectroscopic evidence of two ν(Nb=S) stretches was ignored, as Parkin[21] had done in his re-evaluation of the *cis-mer*-$Mo(O)Cl_2(PMe_2Ph)_3$ system. In these studies the difference of 0.0456Å between the mean octahedral Nb-Cl length in the tetrachloride (2.4527Å) from that of the orange-yellow form were used to estimate the fractional composition of the mixture by the method outlined in section 2.9, although in this case the difference in M-Cl lengths are very small so that the estimates are of limited accuracy. In this way, the fraction of chloride in these samples was estimated to range from 0.09 to 0.26 using the original crystal data for the green form, and when a plot of the observed axial 'Nb-S/Nb-Cl' length against composition was drawn up, a fairly gentle curve was once again obtained. The plot was thus able to confirm how contamination contributes to an apparent lengthening in the axial 'Nb-S/Nb-Cl'. It cannot be a true representation of the situation as we have deliberately neglected the infrared evidence since in these three green samples, all exhibiting a ν(Nb=S) stretch at 489 $cm^{-1}$, it is not the orange-yellow form (ν(Nb=S) 455 $cm^{-1}$) that is co-crystallised with the tetrachloride contaminant, but the form with a ν(Nb=S) stretch at 489 $cm^{-1}$, for which no 'pure' Nb=S bond length is available (as the green form is unable to be isolated in its pure form).

Isolation of the ν(Ta=S) 430 $cm^{-1}$ form of '$Ta(S)Cl_3(PMe_3)_3$' has not been forthcoming and consequently it has not been possible to establish the length of the Ta-S linkage. Thus it is difficult to put any significance on the two values of 2.198(3) and 2.219(2)Å reported for the pure ν(Ta=S) 470 $cm^{-1}$ form. Although the presence of $NbCl_4(PMe_3)_3$ was noted in the green $Nb(S)Cl_3(PMe_3)_3$ species, there is no evidence of such an analogous paramagnetic $TaCl_4(PMe_3)_3$[22] contaminant in this species (as indicated by $^1H$ NMR) to account for the variation in the reported Ta=S bond lengths.

In view of this it is difficult to postulate the discrepancy arising due to co-occupancy of the sulphido site by chloride from a co-crystallised isostructural tetrachloride impurity. Moreover, the thermal ellipsoid for the sulphur atom is normal and shows no evidence of any elongation in the direction of the Ta-S bond vector that might indicate the presence of another species. A comparison of the ORTEP drawings of 470 $cm^{-1}$ $Ta(S)Cl_3(PMe_3)_3$ and $TaCl_4(PMe_3)_3$ are presented in figure 5.24.

The similarity (within $3\sigma$) in the geometrical parameters of the analogous niobium and tantalum tetrachlorides is noted in table 5.8.

| | $NbCl_4(PMe_3)_3$ | $TaCl_4(PMe_3)_3$ |
|---|---|---|
| $M\text{-}Cl_{ax}$ | 2.409(4) | 2.417(3) |
| $(M\text{-}Cl)_{av}$ | 2.543(13) | 2.447(8) |
| $(M\text{-}P)_{av}$ | 2.651(6) | 2.640(5) |
| $(Cl_{ax}\text{-}M\text{-}Cl)_{av}$ | 125.7(8) | 126.3(3) |
| $(Cl_{ax}\text{-}M\text{-}P)_{av}$ | 74.9(4) | 74.8(3) |
| $(P\text{-}M\text{-}P)_{av}$ | 113.4(4) | 113.3(3) |
| $(Cl\text{-}M\text{-}Cl)_{av}$ | 89.4(8) | 88.8(3) |
| $(P\text{-}M\text{-}Cl_{trans})_{av}$ | 159.0(1) | 158.6(3) |

**Table 5.8:** Comparison of selected bond lengths (Å) and angles (°) for $MCl_4(PMe_3)_3$ where M= Nb, Ta.

## 5.5 Summary

In this chapter two forms of $Nb(S)Cl_3(PMe_3)_3$ have been studied in detail, each exhibiting unique $\nu(Nb{=}S)$ stretches which have been established by X-ray diffraction studies to be due to terminal sulphur moieties. The anomaly between the reported bond lengths and the observed $\nu(Nb{=}S)$ stretching frequencies (the trend being the reverse to that observed in the oxoniobium system) can be attributed to contamination by the isostructural species $NbCl_4(PMe_3)_3$ in the high frequency form as compared with the low frequency form in the oxo case. The presence of a tetrachloride contaminant in the long bonded form of $Nb(S)Cl_3(PMe_3)_3$ does not, however, rule out the possibility of bond-stretch isomerism and in fact makes the case for its existence quite compelling. In

fact it is not unrealistic to expect that under the right conditions a pure form of the ν(Nb=S) 489 $cm^{-1}$ species could be isolated and shown to possess a Nb=S bond length shorter than that reported for the pure lower stretching ν(Nb=S) 455 $cm^{-1}$ form.

## 5.6 References


1. T.P. Kee, *Ph.D.Thesis*, Durham University, 1989; V.C. Gibson, T.P. Kee, R.M. Sorrell, A.P. Bashall, M. McPartlin, *Polyhedron*, **7**, 2221.
2. A. Shaw, *Ph.D.Thesis*, Durham University, 1989.
3. G. Christou, J.C. Huffman, J.L. Seela, *Polyhedron*, 1989, **8**, 1797.
4. P. Klingelhofer, U. Müller, *Z. Anorg. Allg. Chem.*, 1984, **510**, 109.
5. M.G.B. Drew, R.J. Hobson, *Inorg. Chim. Acta.*, 1983, **72**, 233.
6. K. Gebreyes, J. Zubieta, T.A. George, L.M. Koczon, *Inorg. Chem.*, 1986, **25**, 405.
7. M.G.B. Drew, D.A. Rice, D.M. Williams, *J. Chem. Soc. Dalton Trans.*, **1983**, 2251.
8. J.M. Berg, R.H. Holm, *Inorg. Chem.*, 1985, **24**, 1706.
9. Y. Do, R.H. Holm, *Inorg. Chim. Acta.*, 1985, **104**, 33.
10. M.G.B. Drew, D.A. Rice, D.M. Williams, *J. Chem. Soc. Dalton Trans.*, **1985**, 1821.
11. M.G.B. Drew, I.B. Tomkins, *J. Chem. Soc. A*, **1970**, 22.
12. G. Ferguson, M. Mercer, D.W.A. Sharp, *J. Chem. Soc. A*, **1969**, 2415
13. T.M. Brown, R.B. von Dreele, E.J. Peterson, *Inorg. Chem.*, 1978, **14**, 1410.
14. M.G.B. Drew, D.A. Rice, D.M. Williams, *J. Chem. Soc. Dalton Trans.*, **1984**, 845.
15. M.G.B. Drew, I.B. Tomkins, *Acta. Crystallogr.Sect. B*, 1970, **26**, 1161.
16. A.P. Sattelberger, R.B. Wilson, J.C. Huffman, *Inorg. Chem.*, 1982, **21**, 2392.
17. F.A. Cotton, M.P. Diebold, W.J. Roth, *Polyhedron*, 1985, **4**, 1103.
18. W.W. Porterfield, "*Inorganic Chemistry-A Unified Approach*", Addison-Wesley, New York (1984).

19. V.C. Gibson, M. McPartlin, *J. Chem. Soc. Dalton Trans.*, **1992**, 947.

20. A.P. Bashall, V.C. Gibson. T.P. Kee, M. McPartlin, O.B. Robinson, A. Shaw, *Angew. Chem. Int. Ed. Engl.*, 1991, **30**, 980.

21. K. Yoon, G. Parkin, A. Rheingold, *J. Amer. Chem. Soc.*, 1991, **113**, 1437; *J. Amer. Chem. Soc.*, 1992, **114**, 2210.

22. F.A. Cotton, S.A. Duraj, W.J. Roth, *Inorg. Chem.*, 1984, **23**, 4046.

# CHAPTER SIX

## A Summary and Conclusion on Distortional and Bond-Stretch Isomerism

## 6.1 A Discussion on the Evidence For and Against Distortional and Bond-Stretch Isomerism

The results of work carried out on the oxomolybdenum[1-5] and thio- and oxo-niobium systems[5-9] has clearly established that the apparent differences in bond distances observed by X-ray structure determination of 'bond-stretch isomer' pairs, differing in colour, are artifacts of unresolved disorder of the components of co-crystallisation with the amorphous chloride species; the colour of the impurity giving rise to the differences in colour.

All transition metal systems claimed to exhibit distortional or bond-stretch isomerism, with the exception of the aquooxocyanomolybdate examples of Weighardt[10], possess three important common characteristics. All have terminal metal-oxo or -sulphido units; all have terminal halogen ligands; and all have bulky organic amine or phosphine ligands. In light of the current evidence for co-crystallisation, it seems likely that all these examples are actually mixtures in which the terminal oxo or sulphido atom is replaced by a halogen atom in a fraction of the molecules. For example, consider the yellow and green forms of $Nb(O)Cl_3(PMe_3)_3$ where the oxygen atom caps the face of three $PMe_3$ ligands. Here, the unusually long Nb=O bond length of 2.087(5)Å reported in the structure data for the original green form[11] is an artifact of compositional disorder in a co-crystallised mixture of $Nb(O)Cl_3(PMe_3)_3$ and $NbCl_4(PMe_3)_3$. X-ray model calculation studies by Desrochers and Enemark[12] on the blue and green $[LW(O)Cl_2]PF_6$ similarly suggest that compositional disorder accounts for the unusual W=O and W-Cl bond lengths in this pair.

Our work, along with that of the two groups of Parkin[1,2] and Enemark[3], have established that the blue and green forms of '*cis-mer*-$Mo(O)Cl_2(PMe_2Ph)_3$' exhibiting a ν(Mo=O) stretch at 941 $cm^{-1}$ are not bond-stretch isomers, but rather that the green form is a mixture of blue *cis-mer*-$Mo(O)Cl_2(PMe_2Ph)_3$ (ν(Mo=O) 941 $cm^{-1}$) and the yellow *mer*-$MoCl_3(PMe_2Ph)_3$. The chlorine analyses are somewhat high, but not alarmingly so. The small differences in the $^1H$ NMR spectra of the original blue (ν(Mo=O) 955 $cm^{-1}$) and green (ν(Mo=O) 943 $cm^{-1}$) reported by Chatt would have been

undetectable on the original 60 MHz NMR spectrometer. The assignment of the IR bands in the region 900 to 1000 $cm^{-1}$ is ambiguous and Raman spectroscopy is required to distinguish ligand bands from the Mo=O band. The XPS data of Enemark[3] requires careful line shape analysis in order to reveal that the Enemark green is a mixture. Of the original data[13], only the low frequency infrared data and the UV-visible electronic spectra suggest that the green is a mixture.[17] The accumulated evidence supports the persuasive argument that *ipso facto* the phenomenon of bond-stretch isomerism is an artifact of contamination. However, it is not that simple and a number of questions remain unanswered.

The $Nb(S)Cl_3(PMe_3)_3$ system so far represents the best case that illustrates the possible reality of the phenomenon of bond-stretch isomerism. Although it is now clear from our experimental data that the green form of $Nb(S)Cl_3(PMe_3)_3$ ($\nu$(Nb=S) 489 $cm^{-1}$) is not a pure species, its properties cannot be explained simply due to its being a mixture of the orange form ($\nu$(Nb=S) 455 $cm^{-1}$) and the green tetrachloride $NbCl_4(PMe_3)_3$, as was sufficient for the '$Mo(O)Cl_2(PMe_2Ph)_3$' case. This parallel argument breaks down because it does not offer an explanation for the difference in the observed stretching frequencies between the orange and green forms. As the two characteristic $\nu$(Nb=S) stretches are clearly identified in solution ($CH_2Cl_2$) and in nujol mull, the stretches cannot be a solid-state artifact (i.e., crystal packing effect). Therefore, it must be concluded that the green form contains a different thioniobium species from that present in the orange form, and yet the X-ray structure determination of the two forms reveals no structural distinction between the two, apart from slight bond length differences (the thermal ellipsoids being normal). In particular, the nature of the established disorder confirms that the thio ligand in this mystery species must be in the axial (face capping) site as it is in the orange form, so that the difference in the $\nu$(Nb=S) stretching frequencies cannot be explained by it being a geometric isomer with the thio ligand in an octahedral site. Thus there appears to be only one other possibility, apart from the conclusion that bond-stretch isomerism is a true effect, that is that the unknown thioniobium species could have some undetected difference in the non-sulphur ligand set. This cannot be dismissed on crystallographic grounds because, for example, replacement

of one of the chloride ligands by a thiolate ligand (SH), a possible product of decomposition to the tetrachloride, would be undetectable if accompanied by a three-fold disorder involving interchange of the sulphur and chlorine sites (figure 6.1). Another possibility is for one of the chlorides to become replaced by a hydroxide arising from partial hydrolysis, due to the extreme moisture sensitive nature of the species. However, neither of these explains the observation that for the green $Nb(S)Cl_3(PMe_3)_3$ form the chlorine content by elemental analysis is consistently high. The presence of up to ca. 20% tetrachloride would not explain this if one of the three chloride ligands had been replaced by OH or SH, and furthermore the IR spectra show no evidence of either of these functionalities being present.

The presence of chloride contaminant in the 'long-bonded' green form of $Nb(S)Cl_3(PMe_3)_3$ clearly does not provide sufficient evidence to rule out bond-stretch isomerism, and unexpectedly it in fact makes the case for this type of isomerism quite hard to disprove. Originally the bond lengthening in the green form was an embarrassment to the case, because on the basis of the infrared spectra the orange form ($\nu$(Nb=S) 455 $cm^{-1}$) was expected to have a longer Nb=S bond than that of the green form ($\nu$(Nb=S) 489 $cm^{-1}$). It is now clear that the actual Nb=S bond length in the green form of $Nb(S)Cl_3(PMe_3)_3$ is as yet not established and may well in fact be shorter than that in the orange form. It is interesting to offer the supposition that the true colour of the $\nu$(Nb=S) 489 $cm^{-1}$ species may well also prove to be orange-yellow, as the observed green colouration for this form may be entirely due to the green tetrachloride with which it co-crystallises, just as the two green '$Mo(O)Cl_2(PMe_2Ph)_3$' species were due to the mixing of two different blue *cis-mer*-$Mo(O)Cl_2(PMe_2Ph)_3$ forms with yellow *mer*-$MoCl_3(PMe_2Ph)_3$.

The research into the phenomenon of distortional or bond-stretch isomerism has highlighted the subtle effects that undetected crystallographic disorder can play in the determination of the molecular structure based on single X-ray diffraction. The incorrect determination of bond lengths serves to emphasize that the observation of low R values, low e.s.d.'s, and well-behaved thermal parameters are not always sufficient indications of a *true* structure. Central to the subject has been disorder due to the presence of

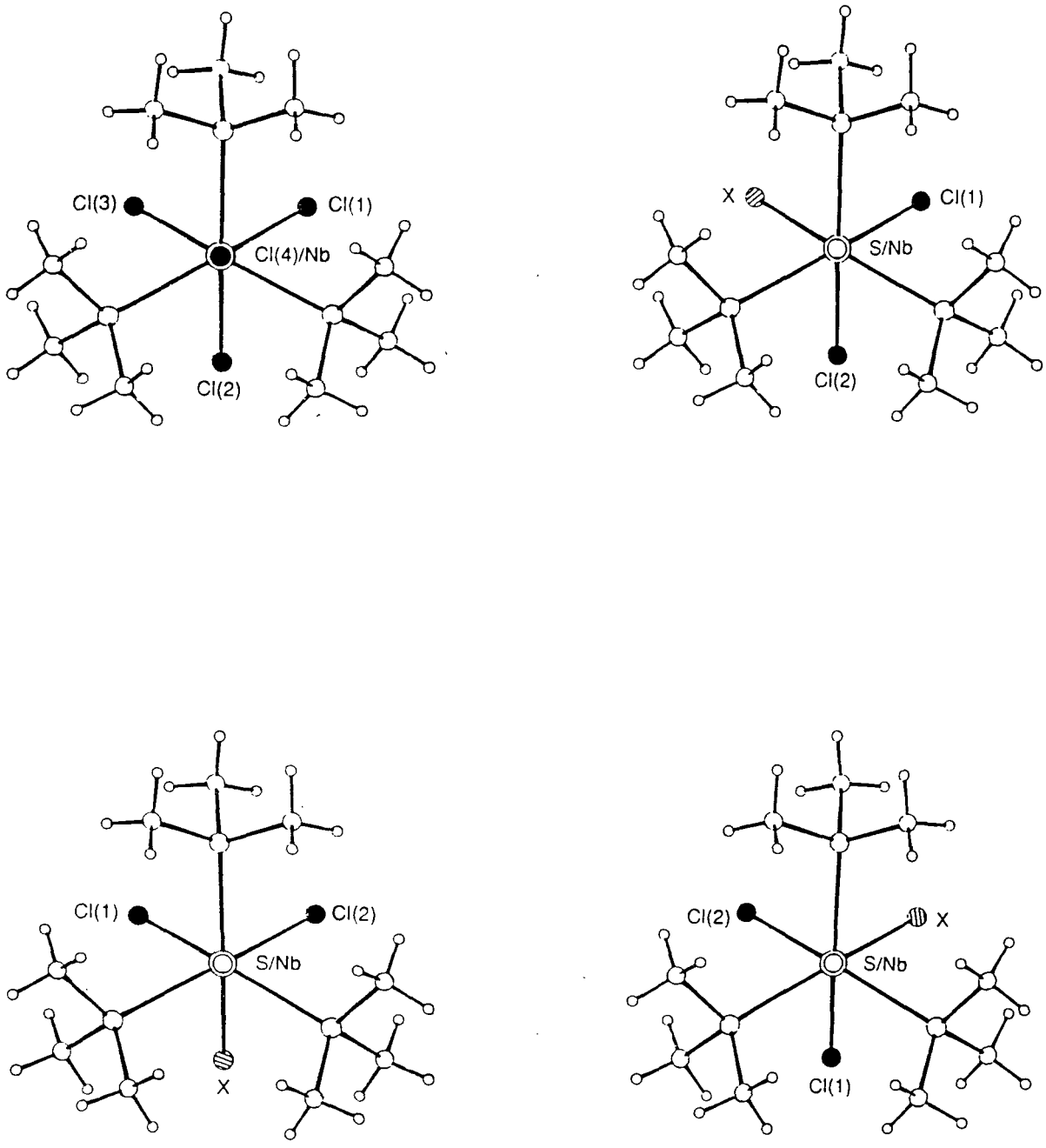


**Figure 6.1:** The type of disorder model that might be the explanation of the difference in ν(Nb=S) in the green isomer. One of the chloro ligands has been replaced by another ligand X (such as OH or SH); this molecule might be three-fold disordered in addition to being contaminated with some $NbCl_4(PMe_3)_3$.

impurities in single crystals. It is very likely that a contributing factor to the discussions has been the neglect of compositional disorder in X-ray determined structures, due the common belief that single crystals are inherently pure, even though it is recognised that such a method of doping paramagnetic complexes into crystals of isostructural diamagnetic complexes is used extensively in single crystal EPR studies.[14] It is the general belief that single crystals are pure, compounded by the subtlety of the disorder problem, that results in mis-interpretations. Crystallisation is usually considered a purifying process, and yet crystallisation, for example of the green '*cis-mer*-$Mo(O)Cl_2(PMe_2Ph)_3$' species returns green, apparently homogeneous crystals. A free energy change ($\Delta G_{cryst}$) associated with the crystallisation process can be envisaged:[15]

$$\Delta G_{cryst} = \Delta H_{cryst} - T\Delta S_{cryst}$$

The enthalpy ($\Delta H_{cryst}$) contains contributions from intermolecular interactions as well as intramolecular conformational energies. Now in the case of blue *cis-mer*-$Mo(O)Cl_2(PMe_2Ph)_3$ ($\nu$(Mo=O) 941 $cm^{-1}$) and yellow *mer*-$MoCl_3(PMe_2Ph)_3$, which are known to readily co-crystallise each molecule contains three bulky meridional dimethylphenylphosphine ligands, and have molecular volumes of 699.4 and 703.8 $Å^3$/molecule respectively that differ by less than 1%.[16] Most of their molecular volume is due to the bulky phosphines and so there may be little difference in their polarities. Thus the $\Delta H_{cryst}$ contributions of these individual molecules can be considered to be similar and that it is thus the increased entropy ($\Delta S_{cryst}$) afforded by the process of co-crystallisation that provides the thermodynamic driving force[15] for the formation of compositionally disordered crystals. A similar argument could be applied to the $M(E)X_3(PMe_3)_3$ systems (M= Nb, Ta; E= O, S; X= Cl, Br).

The interpretation of X-ray diffraction data in order to verify the experimental observations of distortional isomerism in *cis-mer*-$Mo(O)Cl_2(PMe_2Ph)_3$ represents an extreme example of the subtlety of the disorder problem. Moreover, it is the influential power of X-ray structure determination providing a true, exact , unequivocal representation of a molecule's structure that often leads to the inherent belief that 'nothing

beats a crystal structure'.[20] While this may be true for the majority of structures, it is important to recognise that the technique has its limitations and so its results must not be over-interpreted.[21] For example, even the interpretation of the e.s.d.'s that are commonly associated with crystal structure determinations requires care, since systematic error is generally not considered, and therefore the values represent only the lower degree of the error.

Currently the only irrefutable evidence for bond-stretch isomerism is spectroscopic. Although X-ray studies are essential evidence in order to demonstrate the existence of species with virtually indistinguishable structures, the evidence of bond lengthening from these data is either suspect or wrong in all the published cases. However, there is strong spectroscopic evidence in at least two cases, the oxo- and sulphido- niobium systems, that nevertheless two 'isomers' do exist and probably do differ in their Nb=E bond lengths because the two ν(Nb=E) stretches are different in each case. As it has clearly been demonstrated that evidence of co-crystallisation of a contaminant does not rule out bond-stretch isomerism in the niobium system it may be argued that the case against it in the oxomolybdenum system, which appears to be widely accepted without question , is not so. For in fact, in this research it has been established that two blue forms of *cis-mer*-$Mo(O)Cl_2(PMe_2Ph)_3$ (ν(Mo=O) stretches at 941 and 955 $cm^{-1}$) do exist, the first as synthesized by Enemark and co-workers[3], both by direct synthesis and by purification of the green form (ν(Mo=O) 941 $cm^{-1}$), and that which was originally reported by Chatt and Butcher[13] in 1971 (ν(Mo=O) 955 $cm^{-1}$) but considered by many to be the result of a misassignment of the ν(Mo=O) stretch for this blue isomer. Enemark was, however, unaware of the significance of his discovery. However, one must remember that whereas the niobium system represents a possible candidate for bond-stretch isomerism (since coordination geometries and conformations of the organic ligands of the phosphines are virtually identical), the oxomolybdenum system represents distortional isomerism, where the slight but significant variations in the metal-ligand bond distances are the manifestation of the different conformations adopted by the organic fragments of the phosphines in the two blue forms. Further support for this may be gleaned from a comparison of the structures observed by X-ray analysis of the Chatt blue

isomer by Manojlovic-Muir[22] with that of the blue form studied by Parkin and co-workers[2] ( tables 2.5 and 2.7) which shows very different Mo-Cl bond lengths trans to the Mo=O (2.551(3) and 2.528(1)Å respectively). In the two unique forms of blue *cis-mer*-$Mo(O)Cl_2(PMe_2Ph)_3$ isolated by our group it is observed that a significant increase in the Mo=O bond length (1.663(2) to 1.682(3)Å) is accompanied by a decrease in the length of the Mo-Cl bond trans to the oxo moiety (2.538(1) to 2.523(1)Å).

Furthermore, the more widespread prevalence of distortional isomerism is supported by the observation of two unique forms of blue *cis-mer*-$W(O)Cl_2(PMe_2Ph)_3$ complex that parallel those originally reported in molybdenum complex, and the observation of two closely similar forms of green $Mo(O)Cl_2(PEt_2Ph)_3$. The latter of these examples additionally raises the question of the possible existence of more than one form of trichloride contaminant in any given series of distortional isomers, the presence of which in solution is thought to influence the orientation adopted by the phosphine ligands in the form that crystallises from solution. There is also evidence to suggest that a link exists between the general features of the IR spectrum (e.g. $\nu$(M=O) stretching frequency) and the phosphine orientations, as determined by X-ray crystallography.

Thus, overall it may be concluded that distortional isomerism is a real phenomenon whilst rationalisation of bond-stretch isomerism as a mere solid-state artifact does not fit all the observations so far reported. However, the evidence is that if the phenomenon is a fact, chemists will be faced with the problem of spotting examples where the structures are almost identical and have the same colour.

## 6.2 References


1. K. Yoon, G. Parkin, A.L. Rheingold, *J.Amer. Chem. Soc.*, 1991, **113**, 1437.
2. K. Yoon, G. Parkin, A.L. Rheingold, *J.Amer. Chem. Soc.*, 1992, **114**, 2210.
3. P.J. Desrochers, K.W. Nebesny, M.J. LaBarre, S.E. Lincoln, T.M. Loehr, J.H. Enemark, *J.Amer. Chem. Soc.*, 1991, **113**, 9193.
4. G. Parkin, *Acc. Chem. Res.*, 1992, **25**, 455.

5. V.C. Gibson, M. McPartlin, *J. Chem. Soc. Dalton. Trans.*, **1992**, 947.

6. A.P. Bashall, M. McPartlin, poster presented at 15th IUC International Conference of Crystallography, Bordeaux 19th-28th July 1990.

7. V.C. Gibson, T.P. Kee, R.M. Sorrell, A.P. Bashall, M. McPartlin, *Polyhedron*, 1988, **7**, 2221.

8. A.P. Bashall, V.C. Gibson, T.P. Kee, M. McPartlin, O.B. Robinson, A. Shaw, *Angew. Chem. Int. Ed. Engl.*, 1991, **30**, 980.

9. A.P. Bashall, S.W. Annie Bligh, A.J. Edwards, V.C. Gibson, M. McPartlin, O.B. Robinson, *Angew. Chem. Int. Ed. Engl.*, 1992, **31**, 1607.

10. K. Wieghardt, G. Backes-Dahmann, B. Nuber, J. Weiss, *Angew. Chem. Int. Ed. Engl.*, 1985, **24**, 777.

11. T.P. Kee, *Ph.D. Thesis*, Durham University, 1989.

12. Unpublished results.

13. A.V. Butcher, J. Chatt, *J. Chem. Soc (A)*, **1970**, 2652.

14. J.L. Petersen, L.F. Dahl, *J. Amer. Chem. Soc.*, **1975**, 97, 6416; J.L. Petersen, L.F. Dahl, *J. Amer. Chem. Soc.*, **1975**, 97, 6422.

15. D.F. Shriver, P.W. Atkins, C.H. Langford, *'Inorganic Chemistry'*, W.H. Freeman and Co., New York, 1990, p.573.

16. Calculated using unit cell parameters from ref. 1.

17. The original report[13] of Enemark green (ν(Mo=O) 943 $cm^{-1}$) notes that this material is difficult to separate from a yellow species formulated as $MoCl_3(PMe_2Ph)_3$. However, pure yellow *mer*-$MoCl_3(PMe_2Ph)_3$ was not prepared until 1976[18], five years after the original proposal of distortional isomerism.[19]

18. M.W. Anker, J. Chatt, G.J. Leigh, G.A. Wedd, *J. Chem. Soc. Dalton Trans.*, **1975**, 2639.

19. J. Chatt, Lj. Manojlovic-Muir, W.K.Muir, *J. Chem. Soc. Chem. Commun.*, **1971**, 655.

20. E.A.V. Ebsworth, D.W. Rankin, S. Cradock, *'Structural Methods in Inorganic Chemistry'*, 2nd Ed., CRC Press, Boca Raton, 1991.

21. P.G. Jones, *Chem. Soc. Rev.*, 1984, **13**, 157.

22. Lj. Manojlovic-Muir, *J. Chem. Soc. A*, **1971**, 2796.

# CHAPTER SEVEN

## Experimental Details

## 7.1 General

### 7.1.1 Experimental Techniques

All manipulations of air and/or moisture sensitive materials were performed on a conventional vacuum/inert atmosphere (nitrogen or argon) line using standard Schlenk and cannula techniques, or in an inert atmosphere (nitrogen or argon) filled glove box.

Elemental analysis was performed by the microanalytical services of this department.

Infrared spectra were recorded on Perkin-Elmer 577, 457 and 1020X grating spectrophotometers using CsI windows. Absorptions abbreviated as: vs (very strong), s (strong), m (medium), w (weak), br (broad), sp (sharp) and sh (shoulder).

Mass spectra were recorded on a VG 7070E Mass Spectrometer.

NMR spectra were recorded on the following instruments at the frequencies listed: Varian VXR400, $^{1}H$ (399.95 MHz), $^{13}C$ (100.58 MHz), $^{31}P$ (161.90 MHz); Bruker AC250, $^{1}H$ (250.13 MHz), $^{31}P$ (101.26 MHz); Varian Gemini 200, $^{1}H$ (199.98 MHz), $^{13}C$ (50.29 MHz). The following abbreviations have been used for band multiplicities and shapes: s (singlet), d(doublet), t (triplet), m (multiplet), br (broad). Chemical shifts are quoted as $\delta$ in ppm downfield from the following references : $^{1}H$ ($C_6D_6$, 7.15ppm; $CD_2Cl_2$, 5.35ppm; $CDCl_3$, 7.263ppm); $^{13}C$ ($C_6D_6$, 128.0ppm; $CDCl_3$, 78.0 ppm); $^{31}P$ ($CD_2Cl_2$, 0.00 ppm; $CDCl_3$, 0.00 ppm).

### 7.1.2 Solvents and Reagents

The following solvents were dried by prolonged reflux over a suitable drying agent (in parenthesis), being freshly distilled and de-oxygenated before use: toluene (sodium metal), petroleum ether 40-60°C (lithium aluminium hydride), octane (lithium aluminium hydride), tetrahydrofuran (sodium benzophenone ketyl), acetonitrile (calcium hydride), dichloromethane (calcium hydride), 1,2-dichloroethane (calcium hydride), n-pentane (lithium aluminium hydride), dimethoxy ethylene glycol (potassium metal) and

diethyl ether (lithium aluminium hydride), ethanol (magnesium turnings, iodine), methanol (magnesium turnings, iodine).

The following NMR solvents were dried by vacuum distillation from a suitable drying agent (in parenthesis) and stored over activated 4A molecular sieves: benzene-$d_6$ (phosphorus (V) oxide), chloroform-$d_1$ (phosphorus (V) oxide) and dichloromethane-$d_2$ (phosphorus (V) oxide).

### 7.1.3 Preparation of Trimethylphosphine

A 5L round-bottomed flask, fitted with a pressure equalising dropping funnel, efficient mechanical stirrer and a dry-ice condenser, was charged with magnesium turnings (180g, 7.5mol) and di-n-butyl ether, $(CH_3(CH_2)_3)_2O$, (2.5L, molecular sieve dried and de-oxygenated) and the apparatus then purged with nitrogen. Methyl iodide (1000g, 7.05mol) in an equal volume of di-n-butyl ether was added dropwise to the vigorously stirred suspension of magnesium over a period of 2 h., at such a rate as to maintain a reaction temperature of ca. 30°C. Upon completion of the addition the mixture was stirred for a further 2 h. whilst being allowed to cool to room temperature. To the methyl magnesium iodide, formed *in situ* a degased solution of triphenylphosphite, $P(OPh)_3$, (660g, 2.13mol) in an equal volume of di-n-butyl ether was added dropwise with vigorous stirring over a period of 3 h., making sure the reaction does not become too viscous due to the precipitation of magnesium salts. The mixture was stirred for a further 2 h. allowing the mixture to cool to room temperature. The dropping funnel was then replaced with a distillation system with a 500ml round-bottomed flask cooled in dry-ice/acetone for collection. The reaction mixture was heated to ca. 140°C using an oil bath and the fraction boiling between 35-80°C was collected (ca. 350ml). This fraction was further distilled with the fraction coming over at 40°C proving to be pure $PMe_3$ (102g, 63.1%).

Infrared data (Nujol, CsI, $cm^{-1}$): 2974 (vs), 2962 (vs), 2953 (s,sh), 2915 (s,sh), 2904 (vs), 2838 (m), 2821 (m), 1444 (vs), 1432 (s), 1422 (m,sh), 1314 (m), 1300 (m), 1286 (m), 947 (vs), 938 (vs), 716 (s) and 705 (s).

## 7.2 Experimental Details to Chapter Two Synthesis of Oxymolybdenum and Tungsten Phosphines Complexes

### 7.2.1 Synthesis of Chatt Blue *cis-mer*-$Mo(O)Cl_2(PMe_2Ph)_3$

#### 7.2.1.1 *Reaction of $MoCl_4(THF)_2$ with $PMe_2Ph$ and $H_2O$*

A suspension of $MoCl_4(THF)_2$ (0.500g, 1.34 mmol) in THF (30 ml) was treated with $PMe_2Ph$ (0.90g, 6.52 mmol) upon which the dark orange mixture produced a green solution. $H_2O$ (24µl, 1.33 mmol) was added and the mixture stirred overnight at room temperature. The mixture was filtered, and the volatiles removed under reduced pressure. The oily residue was washed with n-pentane, giving a green solid. This was extracted into hot methanol and filtered. Cooling to room temperature led to the deposition of blue crystals of *cis-mer*-$Mo(O)Cl_2(PMe_2Ph)_3$ (1.697g, 89.8%).

#### 7.2.1.2 *Reaction of $Mo(O)_2Cl_2$ with $PMe_2Ph$ and EtMgCl*

$Mo(O)_2Cl_2$ (0.500g, 2.51 mmol) was added slowly to a stirred solution of DME (15ml) to give a colourless solution. The solution was then frozen and ethyl magnesium chloride (1.26ml, 2.51mmol) syringed in, along with $PMe_2Ph$ (1.39g, 10.06mmol) in DME (5ml) being added via cannula. The mixture was allowed to warm to room temperature to give a purple solution, and stirred for 2 hours leading to the precipitation of magnesium chloride and a green solution. The solution was filtered and the $MgCl_2$ washed with DME (2x10ml). The solution was then pumped down to give a green oil, which was washed with n-pentane (10ml) to give a green solid. The solid was redissolved in hot methanol, filtered and allowed to cool to room temperature, giving rise to the deposition of blue crystals (1.14g, 75.9%).

### 7.2.1.3 *Reaction of $MoCl_4(MeCN)_2$ with $PMe_2Ph$ and $H_2O$*

A suspension of $MoCl_4(MeCN)_2$ (0.500g, 1.56 mmol) in THF (30 ml) was treated with $PMe_2Ph$ (1.080g, 7.80 mmol) producing a green solution. $H_2O$ (24µl, 1.56 mmol) was added and the mixture stirred overnight at room temperature. The mixture was filtered, and the volatiles removed under reduced pressure to give a green oil. The oily residue was washed with n-pentane, giving a green solid. This was extracted into hot methanol and filtered. Cooling to room temperature led to the deposition of blue crystals of *cis-mer*-$Mo(O)Cl_2(PMe_2Ph)_3$ (0.834g, 89.3%).

### 7.2.1.4 *Reaction of $MoCl_5$ with $PMe_2Ph$ and $H_2O$*

Dry ethanol (3 ml) was added dropwise to molybdenum pentachloride (0.500g, 1.83 mmol), giving rise to a green oil. The reaction is vigorous, with copious amounts of hydrogen chloride being evolved. 33µl (1.83 mmol) of $H_2O$ (de-oxygenated) was added, giving rise to a brown oil. The oil was dissolved in ethanol (20ml) and $PMe_2Ph$ (2.100g, 15.20mmol) in ethanol (10ml) added dropwise to the stirred solution at room temperature. The mixture was then heated at 80°C for 15 mins., producing a royal blue solution which was then filtered and cooled to room temperature, giving rise to blue crystals (0.987g, 90.3%).

### 7.2.1.5 *UV-visible Photolysis of Enemark Blue cis-mer-$Mo(O)Cl_2(PMe_2Ph)_3$*

1.00g of Enemark Blue *cis-mer*-$Mo(O)Cl_2(PMe_2Ph)_3$ was dissolved in 30ml of ethanol, filtered and irradiated with a mercury lamp UV-visible source for 30 minutes, producing a royal blue solution. On cooling to -20°C blue cubic crystals of *cis-mer*-$Mo(O)Cl_2(PMe_2Ph)_3$ were formed (0.878g, 87.8%).

*Characterising data for Chatt Blue cis-mer-$Mo(O)Cl_2(PMe_2Ph)_3$*

Elemental Analysis for $C_{24}H_{33}P_3Cl_2OMo$: refer to section 2.7.

Infrared data (Nujol, CsI, $cm^{-1}$): 1571 (w), 1434 (m), 1413 (w), 1314 (w), 1294 (w), 1286 (m), 1282 (m), 1269 (w), 1106 (m), 1001 (w), 955 (vs,sp), 942 (vs,sp), 915 (vs), 905 (vs), 860 (w), 834 (m), 828 (w), 757 (s), 752 (s), 740 (s), 728 (m), 712 (s), 698 (s), 695 (s,sh), 677 (w), 490 (s,sp), 422 (w,sh), 419 (w), 405 (w), 345 (w), 335 (vw,sh), 315 (vw,sh), 297 (s), 285 (m,sh), 252 (s), 225 (w).

Infrared data (CsI disc, $cm^{-1}$): 1001 (w), 955 (vs,sp), 942 (vs,sp), 915 (vs), 905 (vs), 834 (m), 828 (w), 757 (s), 752 (s), 740 (s), 728 (w), 712 (m), 698 (s,sh), 696 (s), 677 (m), 490 (m,sp), 420 (m), 413 (m,sh), 345 (w), 315 (w), 288 (m), 278 (m,sh), 252 (m), 223 (w), 214 (vw).

Raman data ($cm^{-1}$): 1588 (s), 1575 (vw), 1414 (m), 1164 (w), 1104 (m), 1029 (m), 1002 (vs), 954 (m), 904 (w), 858 (w), 750 (m), 735 (vw), 719 (w), 698 (s), 623 (w), 490 (vw), 345 (m), 310 (w), 263 (w), 251 (w), 207 (m), 187 (vw).

Solution Infrared data ($CH_2Br_2$, CsI, $cm^{-1}$): 1492 (w), 1440 (m), 1420 (m), 1299 (w), 1285 (w), 1002 (vw), 946 (s), 920 (m,sh), 907 (s), 744 (s), 708 (m), 694 (s), 492 (m), 425 (w,sh), 420 (w), 290 (w).

UV-visible data ($CH_2Cl_2$, nm ($mol^{-1}$ $cm^2$)): 587 (924), 393 (1911).

$^1$H NMR data (400 MHz, d-chloroform, 298K, ppm): 1.217 (d, $^2J(PH)$=8.8Hz, cis-P**Me**$_2$Ph), 1.725 (t, $^2J(PH)$=4.2Hz, trans-P**Me**(Me)Ph), 1.927 (t, $^2J(PH)$=4.2Hz, trans-P(Me)**Me**Ph), 7.07 (m), 7.13 (m), 7.35 (m), 7.56 (m).

(200 MHz, d-chloroform, 298K, ppm): 1.215 (d, $^2J(PH)$=8.6Hz), 1.721 (t, $^2J(PH)$=4.1Hz), 1.925 (t, $^2J(PH)$=4.1Hz), 7.08 (m), 7.21 (m), 7.35 (m), 7.53 (m).

(400 MHz, $d_2$-dichloromethane, 298K, ppm): 1.250 (d, $^2J(PH)$=8.8Hz), 1.662 (t, $^2J(PH)$=4.0Hz), 1.870 (t, $^2J(PH)$=4.0Hz), 7.13 (m), 7.26 (m), 7.40 (m), 7.56 (m).

(200 MHz, $d_2$-dichloromethane, 298K, ppm): 1.277 (d, $^2J(PH)$=8.6Hz), 1.688 (t, $^2J(PH)$=4.1Hz), 1.886 (t, $^2J(PH)$=4.0Hz), 7.14 (m), 7.25 (m), 7.40 (m), 7.57 (m).

### 7.2.2 Synthesis of Chatt Blue $Mo(^{18}O)Cl_2(PMe_2Ph)_3$

*Reaction of $MoCl_4(THF)_2$ with $PMe_2Ph$ and $H_2{}^{18}O$*

A suspension of $MoCl_4(THF)_2$ (0.500g, 1.34 mmol) in THF (30 ml) was treated with $PMe_2Ph$ (0.900g, 6.52 mmol) upon which the dark orange mixture produced a green solution. $H_2{}^{18}O$ (27µl, 1.35 mmol) was added and the mixture stirred overnight at room temperature. The mixture was filtered, and the volatiles removed under reduced pressure. The oily residue was washed with n-pentane, giving a green solid. This was extracted into hot methanol and filtered. Cooling at room temperature led to the deposition of blue crystals of *cis-mer*-$Mo(^{18}O)Cl_2(PMe_2Ph)_3$ (0.657g, 82.3%).

*Characterising data for Chatt Blue cis-mer-$Mo(^{18}O)Cl_2(PMe_2Ph)_3$*

Elemental Analysis for $C_{24}H_{33}P_3Cl_2{}^{18}OMo$ F(R): %C, 48.46 (48.10), %H, 5.59 (5.55), %Cl, 11.78 (11.83)

Infrared data (Nujol, CsI, $cm^{-1}$): 1571 (w), 1433 (m), 1424 (m), 1413 (w), 1294 (w), 1287 (m), 1282 (m), 1269 (w), 1107 (m), 1001 (w), 954 (m), 941 (s), 920 (s), 916 (s), 905 (vs), 902 (s,sh), 860 (w), 834 (m), 828(w), 758 (s), 752 (s), 740 (s), 728 (m), 712 (m), 698 (s), 693 (s), 677 (w), 490 (s,sp), 422 (m,sh), 421 (m), 419 (w), 403 (w), 347 (w), 343 (w,sh), 315 (vw), 298 (s), 251 (s).

Raman data ($cm^{-1}$): 1588 (s), 1575 (vw), 1413 (m), 1165 (w), 1107 (m), 1022 (m), 1001 (vs), 953 (vw), 905 (s), 740 (m), 676 (s), 612 (w), 334 (m), 300 (w), 255 (w), 240 (w), 213 (vw), 198 (vw).

Solution Infrared data ($CH_2Br_2$, CsI, $cm^{-1}$): 1490 (w), 1438 (m), 1418 (m), 1298 (w), 1284 (w), 1002 (vw), 946 (s), 920 (s,sh), 907 (vs), 900 (s,sh), 870 (vw), 838 (m), 744 (s), 710 (m), 694 (s), 492 (m), 422 (w), 290 (w).

UV-visible data ($CH_2Cl_2$, nm ($mol^{-1}$ $cm^2$)): 608 (613), 394 (1417).

$^1$H NMR data (200 MHz, d-chloroform, 298K, ppm): 1.218 (d, $^2J(PH)$=8.6Hz, cis-P**Me**$_2$Ph)), 1.725 (t, $^2J(PH)$=4.1Hz, trans-P**Me**(Me)Ph), 1.928 (t, $^2J(PH)$=4.1Hz, trans-P(Me)**Me**Ph), 7.08 (m), 7.37 (m), 7.55 (m).

### 7.2.3 Synthesis of Chatt Green *cis-mer*-$Mo(O)Cl_2(PMe_2Ph)_3$

Samples of Chatt green *cis-mer*-$Mo(O)Cl_2(PMe_2Ph)_3$ were obtained from preparations of Chatt blue *cis-mer*-$Mo(O)Cl_2(PMe_2Ph)_3$ where a small level of yellow $MoCl_3(PMe_2Ph)_3$ contamination, of unknown origin, led to co-crystallisation of the two species.

*Characterising data for Chatt Green cis-mer-$Mo(O)Cl_2(PMe_2Ph)_3$*

Elemental Analysis for $C_{24}H_{33}P_3Cl_2OMo$: refer to section 2.7.

Infrared data (Nujol, CsI, $cm^{-1}$): 1571 (w), 1433 (m), 1424 (m), 1413 (w), 1314 (w), 1294 (w), 1287 (m), 1282 (m), 1270 (w), 1182 (w), 1107 (m), 1001 (w), 955 (vs), 942 (vs), 915 (vs), 904 (vs), 868 (w), 860 (w), 834 (m), 827 (m), 757 (vs), 752 (vs), 740 (s), 728 (m), 712 (s), 698 (s), 694 (s), 677 (m), 490 (s,sp), 421 (m,sh), 419 (m), 413 (w,sh), 344 (m), 315 (w), 296 (s), 285 (m,sh), 252 (s), 225 (w).

Infrared data (CsI disc, $cm^{-1}$): 1001 (w), 955 (vs), 942 (vs), 915 (vs), 905 (vs), 834 (m), 828 (w), 757 (vs), 752 (vs), 740 (s), 728 (w), 712 (m), 698 (s,sh), 696 (s), 676 (m), 490 (s,sp), 420 (m), 413 (m,sh), 345 (w), 315 (w,sh), 288 (m), 278 (m,sh), 252 (m), 223 (w), 214 (vw).

Raman data ($cm^{-1}$): 1588 (s), 1575 (vw), 1414 (m), 1157 (m), 1107 (m), 1029 (s), 1002 (vs), 954 (s), 904 (s),858 (w), 750 (m),735 (vw), 719 (w), 698 (s), 623 (w),490 (vw), 345 (m), 310 (w), 263 (w), 251 (w), 225 (vw), 207 (w).

Solution Infrared data ($CH_2Br_2$, CsI, $cm^{-1}$): 1492 (w), 1440 (m), 1420 (m), 1299 (w), 1285 (w), 1002 (vw), 946 (s), 920 (m,sh), 907 (s), 744 (s), 708 (m), 694 (s), 492 (m), 422 (w), 290 (w).

UV-visible data ($CH_2Cl_2$, nm ($mol^{-1}$ $cm^2$)): 603 (510), 397 (1585).

$^1H$ NMR data (400 MHz, d-chloroform, 298K, ppm): 1.216 (d, $^2J(PH)$=8.6Hz, cis-P**Me**$_2$Ph)), 1.724 (t, $^2J(PH)$=4.1Hz, trans-P**Me**(Me)Ph), 1.927 (t, $^2J(PH)$=4.1Hz, trans-P(Me)**Me**Ph), 7.08 (m), 7.37 (m), 7.55 (m), -22.7 (vw,br), -40.7 (vw,br).

### 7.2.4 Synthesis of Enemark Blue *cis-mer*-$Mo(O)Cl_2(PMe_2Ph)_3$

Dry ethanol (3 ml) was added dropwise to molybdenum pentachloride (0.500g, 1.83mmol), giving rise to a green oil. The reaction is vigorous, with copious amounts of hydrogen chloride being evolved. The oil was dissolved in ethanol (20ml) and $PMe_2Ph$ (2.100g, 15.20mmol) in ethanol (10ml) added dropwise to the stirred solution at room temperature. The mixture was then heated at 80°C for 15 mins., giving rise to a pale blue solution which was then filtered and cooled to room temperature, giving rise to needle-like blue crystals (1.03g, 94.3%).

*Characterising data for Enemark Blue cis-mer-$Mo(O)Cl_2(PMe_2Ph)_3$*

Elemental Analysis for $C_{24}H_{33}P_3Cl_2OMo$: refer to section 2.7.

Infrared data (Nujol, CsI, $cm^{-1}$): 1571 (w), 1439 (m), 1420 (w), 1315 (w), 1290 (w), 1278 (w), 1106 (m), 1001 (w), 949 (vs,sh), 941 (vs), 909 (vs), 868 (w), 856 (w), 839 (m), 800(m,br), 754 (s), 749 (s), 740 (s), 722 (m), 712 (m), 698 (s), 695 (s), 677 (w), 617 (w), 486 (s,sp), 419 (w), 403 (vw), 355 (w), 308 (m), 285 (s), 274 (m,sh), 256 (m,sh), 251 (s).

Infrared data (CsI disc, $cm^{-1}$): 1001 (w), 949 (vs,sh), 941 (vs), 925 (m,sh), 909 (vs), 839 (m), 754 (s), 749 (s), 740 (s), 712 (m), 698 (s), 695 (s), 677 (m), 486 (m,sp), 419 (m), 355 (w), 340 (vw), 313 (w,sh), 288 (m), 251 (m), 230 (w), 210 (w).

Raman data ($cm^{-1}$): 1588 (s), 1575 (vw), 1420 (m), 1106 (m), 1031 (m), 1002 (vs), 941 (m), 858 (w), 754 (w), 711 (w), 677 (s), 619 (w), 353 (m),338 (w), 307 (w),282 (w), 266 (w), 244 (w), 203 (w).

Solution Infrared data ($CH_2Br_2$, CsI, $cm^{-1}$): 1492 (w), 1440 (s), 1420 (m), 1299 (w), 1285 (w), 1002 (vw), 946 (vs), 920 (s,sh), 907 (vs), 868 (w), 838 (m), 744 (s), 710 (m), 694 (s), 492 (m), 422 (m), 300 (m,sh), 290 (m).

UV-visible data ($CH_2Cl_2$, nm ($mol^{-1}$ $cm^2$)): 604 (621), 395 (1688).

$^1H$ NMR data (400 MHz, d-chloroform, 298K, ppm): 1.215 (d, $^2J(PH)$=8.4Hz, cis-P**Me**$_2$Ph)), 1.724 (t, $^2J(PH)$=4.2Hz, trans-P**Me**(Me)Ph), 1.926 (t, $^2J(PH)$=4.2Hz, trans-P(Me)**Me**Ph), 7.07 (m), 7.13 (m), 7.35 (m), 7.53 (m).

(200 MHz, d-chloroform, 298K, ppm): 1.238 (d, $^2J(PH)$=8.7Hz), 1.724 (t, $^2J(PH)$=4.1Hz), 1.927 (t, $^2J(PH)$=4.0Hz), 7.06 (m), 7.21 (m), 7.36 (m), 7.54 (m).

(400 MHz, $d_2$-dichloromethane, 298K, ppm): 1.276 (d, $^2J(PH)$=8.8Hz), 1.688 (t, $^2J(PH)$=4.2Hz), 1.886 (t, $^2J(PH)$=4.0Hz), 7.15 (m), 7.27 (m), 7.40 (m), 7.57 (m).

(200 MHz, $d_2$-dichloromethane, 298K, ppm): 1.298 (d, $^2J(PH)$=8.6Hz), 1.689 (t, $^2J(PH)$=4.1Hz), 1.887 (t, $^2J(PH)$=4.0Hz), 7.15 (m), 7.27 (m), 7.43 (m), 7.57 (m).

### 7.2.5 Synthesis of Enemark Green *cis-mer*-$Mo(O)Cl_2(PMe_2Ph)_3$

Dimethylphenylphosphine (2.80g, 20.27 mmol) was added dropwise to a suspension of $MoCl_4(MeCN)_2$ (1.00g, 3.13 mmol) in ethanol (20ml), and the solution heated for 15 mins. The resulting green solution was cooled to room temperature, affording green crystals (1.651g, 88.4%). These were recrystallised from methanol.

*Characterising data for Enemark Green cis-mer-$Mo(O)Cl_2(PMe_2Ph)_3$*

Elemental Analysis for $C_{24}H_{33}P_3Cl_2OMo$: refer to section 2.7.

Infrared data (Nujol, CsI, $cm^{-1}$): 1571 (w), 1437 (m), 1420 (w), 1317 (w), 1294 (w), 1288 (w), 1281 (m), 1281 (w), 1162 (w), 1103 (m), 1001 (w), 962 (m), 952 (s), 942 (vs), 928 (s), 917 (vs), 909 (vs), 881 (w), 871 (w), 852 (w), 843 (w), 803 (w,br), 754 (m,sh), 748 (s), 741 (s), 731 (m), 715 (m), 708 (m), 698 (s,sh), 695 (s), 679 (w), 618 (w), 491 (m), 483 (m), 421 (m), 419 (m,sh), 405 (w), 321 (m), 310 (m,sh), 304 (m), 297 (m), 286 (m), 254 (m).

Infrared data (CsI disc, $cm^{-1}$): 1001 (w), 962 (m), 952 (s), 941 (vs), 928 (s), 917 (vs), 909 (vs), 754 (s,sh), 748 (s), 740 (s), 731 (m), 715 (m), 708 (m), 677 (m), 491 (m), 483 (m), 420 (m), 413 (m,sh), 322 (m), 306 (m), 287 (m), 274 (m,sh), 254 (m).

Infrared data (KBr disc, $cm^{-1}$): 3141 (w), 3078 (w), 3047 (m), 2981 (w), 2962 (w), 2916 (m), 2910 (m), 2850 (w), 2360 (w), 2342 (w), 1970 (w), 1899 (w), 1817 (w), 1772 (w), 1734 (w), 1718 (w), 1700 (w), 1696 (w), 1684 (w), 1675 (w), 1653 (w), 1647 (w), 1635 (w), 1617 (w), 1586 (w), 1571 (w), 1559 (w), 1540 (w), 1507 (w), 1488 (m), 1483 (m), 1436 (s), 1419 (m), 1399 (w), 1317 (w), 1294 (m), 1288 (w),

1281 (m), 1276 (m), 1262 (w), 1193 (w), 1161 (w), 1103 (m), 1076 (w), 1027 (w), 1001 (w), 961 (m), 952 (s), 942 (vs), 927 (s), 917 (vs), 908 (vs), 881 (m), 871 (w), 852 (w), 842 (w), 803 (w), 748 (vs), 740 (vs), 730 (s), 715 (m), 708 (s), 694 (vs), 678 (m), 618 (m), 491 (s), 482 (m), 420 (m), 403 (sh), 321 (m), 310 (sh), 304 (m), 297 (m), 286 (m), 274 (sh), 254 (m).

Raman data ($cm^{-1}$): 1588 (s), 1575 (vw), 1420 (w), 1106 (m), 1031 (m), 1002 (vs), 942 (m), 754 (w), 711 (w), 677 (s), 619 (w).

Solution Infrared data ($CH_2Br_2$, CsI, $cm^{-1}$): 1492 (w), 1440 (s), 1420 (m), 1299 (w), 1285 (w), 1002 (vw), 946 (vs), 920 (s,sh), 907 (vs), 871 (vw), 838 (m), 744 (vs), 710 (m), 694 (s), 492 (m), 421 (w), 325 (w), 290 (m).

UV-visible data ($CH_2Cl_2$, nm ($mol^{-1}$ $cm^2$)): 409 (1752).

$^1$H NMR data (400 MHz, d-chloroform, 298K, ppm): 1.249 (d, $^2$J(PH)=8.8Hz, cis-P**Me**$_2$Ph)), 1.756 (t, $^2$J(PH)=4.0Hz, trans-P**Me**(Me)Ph), 1.958 (t, $^2$J(PH)=4.0Hz, trans-P(Me)**Me**Ph), 7.11 (m), 7.26 (m), 7.75 (m), 7.57 (m), 7.971 (br), 9.173 (br), 11.283 (br), -22.5 (br), -40.62 (br).

(200 MHz, d-chloroform, 298K, ppm): 1.240 (d, $^2$J(PH)=8.6Hz), 1.756 (t, $^2$J(PH)=4.1Hz), 1.958 (t, $^2$J(PH)=4.1Hz), 7.11 (m), 7.40 (m), 7.58 (m), 7.97 (br), 9.16 (br), 9.47 (br), 11.27 (br).

### 7.2.6 Synthesis of Blue *cis-mer*-Mo(O)Br$_2$(PMe$_2$Ph)$_3$ (ν(Mo=O) 956 $cm^{-1}$)

A mixture of Enemark green or blue Mo(O)Cl$_2$(PMe$_2$Ph)$_3$ (1.0g, mmol) and lithium bromide (2.0g, mmol) were stirred in boiling ethanol (25ml) for 30 minutes. The solution was filtered, and on cooling gave rise to blue crystals of Mo(O)Br$_2$(PMe$_2$Ph)$_3$ (0.77g, %).

Elemental Analysis for $C_{24}H_{33}P_3Br_2OMo$ F(R): %C, 42.10 (42.01); %H, 5.42 (4.85); %Br, 24.83 (23.29)

Infrared data (Nujol, CsI, $cm^{-1}$): 1571 (vw), 1434 (ms), 1413 (m), 1314 (w), 1298 (m), 1288 (m), 1285 (m), 1274 (m), 1108 (m), 1001 (w), 956 (vs), 942 (vs), 915 (vs), 905 (vs), 868 (w), 850 (w), 834 (m), 827(w,sh), 757 (vs), 752 (vs), 740 (vs), 728 (m), 712 (s), 698 (s), 696 (s,sh), 677 (m), 490 (s), 425 (w,sh), 417 (m), 405 (w,sh), 345 (w), 337 (vw,sh), 310 (w), 298 (m), 288 (w,sh), 263 (w,sh), 252 (m), 233 (vw).

$^1$H NMR data (400MHz, d-chloroform, 298K, ppm): 1.197 (d, $^2$J(PH)= 8.8Hz), 1.218 (d, $^2$J(PH)= 7.2Hz), 1.267 (d, $^2$J(PH)= 8.4Hz), 1.285 (d, $^2$J(PH)= 8.8Hz), 1.724 (t, $^2$J(PH)= 3.8Hz), 1.763 (t, $^2$J(PH)= 4.0Hz), 1.812 (t, $^2$J(PH)= 4.0Hz), 1.853 (t, $^2$J(PH)= 4.1Hz), 1.926 (t, $^2$J(PH)= 4.0Hz), 1.948 (t, $^2$J(PH)= 3.9Hz), 2.014 (t, $^2$J(PH)= 4.0Hz), 2.041 (t, $^2$J(PH)= 4.1Hz), 7.10 - 7.70 (m).

### 7.2.7 Blue *cis-mer*-$Mo(O)Br_2(PMe_2Ph)_3$ ($\nu$(Mo=O) 942 $cm^{-1}$)

This sample was kindly supplied by Subashini Balakvmar of the University of North London.

Infrared data (Nujol, CsI, $cm^{-1}$): 1571 (w), 1438 (ms), 1419 (m), 1290 (m), 1277 (m), 1262 (m), 1105 (m), 999 (w), 942 (vs), 925 (m,sh), 913 (m,sh), 909 (vs), 869 (w), 856 (w), 839 (m), 753 (vs), 749 (s), 739 (vs), 710 (s), 697 (s), 693 (s,sh), 677 (m), 486 (s), 419 (m), 354 (w), 335 (vw), 305 (w,br), 282 (w,sh), 246 (m).

$^1$H NMR data (400MHz, d-chloroform, 298K, ppm): 1.197 (d, $^2$J(PH)= 8.8Hz), 1.218 (d, $^2$J(PH)= 7.2Hz), 1.267 (d, $^2$J(PH)= 8.4Hz), 1.285 (d, $^2$J(PH)= 8.8Hz), 1.724 (t, $^2$J(PH)= 4.0Hz), 1.763 (t, $^2$J(PH)= 4.0Hz), 1.812 (t, $^2$J(PH)= 4.0Hz), 1.853 (t, $^2$J(PH)= 4.1Hz), 1.926 (t, $^2$J(PH)= 3.9Hz), 1.948 (t, $^2$J(PH)= 4.1Hz), 2.014 (t, $^2$J(PH)= 4.0Hz), 2.041 (t, $^2$J(PH)= 3.9Hz), 7.10 - 7.70 (m).

### 7.2.8 Synthesis of Blue *cis-mer*-$Mo(O)I_2(PMe_2Ph)_3$

A mixture of Enemark blue *cis-mer*-$Mo(O)Cl_2(PMe_2Ph)_3$ (1.0g, mmol) and sodium iodide (2.5g, mmol) were stirred in boiling ethanol (25ml) for 30 minutes. The solution was filtered, and on cooling gave rise to green crystals of $Mo(O)I_2(PMe_2Ph)_3$ (1.14g, %).

Elemental Analysis for $C_{24}H_{33}P_3I_2OMo$ F(R): %C, 38.69 (36.95); %H, 4.41 (4.26).

Infrared data (Nujol, CsI, $cm^{-1}$): 1436 (m), 1291 (m), 1277 (m), 1103 (m), 1000 (w), 949 (m,sh), 941 (vs), 922 (m,sh), 912 (s,sh), 908 (vs), 840 (m), 751 (m), 745 (m), 739 (s), 707 (s), 695 (s,sh), 692 (s), 676 (m), 489 (s), 485 (s,sh), 417 (m), 331 (vw), 259 (w,sh), 246 (m).

$^1$H NMR data (200MHz, d-chloroform, 298K, ppm): 1.179 (d, $^2$J(PH)= 7.6Hz), 1.335 (d, $^2$J(PH)= 8.6Hz), 1.950 (t, $^2$J(PH)= 4.1Hz), 2.058 (t, $^2$J(PH)= 4.0Hz), 2.142 (t, $^2$J(PH)= 3.9Hz), 2.240 (t, $^2$J(PH)= 4.0Hz), 7.10 (m), 7.35(m), 7.55 (m), 7.70 (m).

### 7.2.9 Synthesis of $MoCl_3(MeCN)_2$

Molybdenum pentachloride (10g, 36.5 mmol) was added slowly over 30 mins. through a connecting tube to a stirred solution of acetonitrile (50ml). Addition of acetonitrile to molybdenum pentachloride can produce sufficient local heating to cause the acetonitrile to froth. The reaction proceeds smoothly, an instantaneous reaction occurring with mild heat evolution and the formation of an orange-brown solid. The resulting suspension is stirred for 2 hours and is then allowed to stand at room temperature overnight. The solid was filtered, washed with acetonitrile (10ml), and dried *in vacuo* . The product is obtained as a fine orange-brown powder (9.96g, 85%).

Elemental analysis for $C_4H_6N_2Cl_3Mo$ F(R): %C, 15.02 (15.26); %H, 1.89 (1.89); %N, 8.59 (8.76).

Infrared data (Nujol mull, CsI, cm$^{-1}$): 2312 (s), 2284 (s), 1360 (m), 1264 (w), 430 (m), 419 (m), 346 (s,br), 318 (m), 310 (m,sh).

### 7.2.10 Synthesis of $MoCl_3(THF)_2$

Tetrahydrofuran (40ml) was vacuum transferred onto frozen solid $MoCl_3(MeCN)_2$ (10g, 26.0 mmol) and the mixture warmed to room temperature and stirred for 2 hours to give a yellow suspension of tetrachlorobis(tetrahydrofuran)molybdenum(IV). The complex is filtered, washed with freshly vacuum transferred THF (10ml), and dried *in vacuo*. The product is obtained as a microcrystalline orange-yellow powder (8.10g, 68%).

Infrared data (Nujol mull, CsI, cm$^{-1}$): 1346 (m), 1039 (s), 1012 (vs), 923 (sh), 909 (m), 853 (vs), 850 (sh), 332 (vs), 320 (vs), 309 (sh), 289 (w), 282 (m).

### 7.2.11 Synthesis of *mer*-$MoCl_3(PMe_2Ph)_3$

$PMe_2Ph$ (0.774g, 5.60 mmol) was added to a stirred suspension of $MoCl_4(PMe_2Ph)_3$ (0.500g, 1.20 mmol) and zinc granules (0.300g, 4.60 mmol). The mixture was stirred overnight at room temperature, giving rise to a yellow-brown solution. The mixture was filtered and the volatiles removed under reduced pressure, giving a brown solid which when washed with n-pentane gave *mer*-$MoCl_3(PMe_2Ph)_3$ as a yellow solid. Crystals of *mer*-$MoCl_3(PMe_2Ph)_3$ were obtained from a concentrated THF solution at room temperature.

Elemental analysis for $C_{24}H_{33}P_3Cl_3Mo$ F(R): %C, 46.01 (46.74); %H, 5.49 (5.39); %Cl, 17.72 (17.25).

Infrared data (Nujol mull, CsI, $cm^{-1}$): 1572 (w), 1489 (m), 1483 (m), 1437 (s), 1429 (m), 1418 (m), 1411 (m), 1400 (w), 1377 (m), 1319 (w), 1296 (m), 1289 (m), 1282 (m), 1262 (w), 1193 (w), 1162 (w), 1103 (m,br), 1076 (w), 1028 (w), 1001 (w), 962 (m), 952 (s), 948 (m,sh), 929 (m,sh), 919 (s), 911 (vs), 881 (w), 853 (w), 838 (w), 801 (w,br), 754 (s), 749 (s), 740 (vs), 730 (m), 714 (w), 708 (m), 698 (m), 694 (s), 678 (w), 669 (w), 618 (w), 495 (m,sh), 490 (m), 482 (w), 423 (w), 415 (w), 322 (vs), 306 (s), 298 (m,sh), 284 (w), 275 (vw).

Infrared data (CsI disc, $cm^{-1}$): 1001 (w), 962 (m), 952 (s), 948 (m,sh), 929 (m,sh), 919 (s,sh), 911 (vs), 754 (s), 749 (s), 740 (vs), 731 (m), 714 (m), 708 (m), 698 (s), 694 (s), 678 (m), 493 (m,sh), 487 (m), 482 (m), 420 (w), 412 (m), 323 (m), 307 (s), 300 (m,sh), 282 (w), 250 (w), 235 (vw).

Raman data ($cm^{-1}$): 1588 (s), 1575 (w), 1419 (w), 1162 (m), 1103 (m), 1031 (m), 1001 (vs), 706 (w), 677 (s), 619 (m), 411 (w), 314 (sh), 295 (m), 280 (m), 203 (m).

UV-visible data ($CH_2Cl_2$, nm ($mol^{-1}$ $cm^2$)): 415 (3138), 355 (3719).

$^1$H NMR data (400 MHz, d-chloroform, 298K, ppm): 12.0 (v.br), 11.296 (s), 9.472 (s), 9.190 (s), 7.991 (s), -22.47 (br), -40.59 (br).

(200 MHz, d-chloroform, 298K, ppm): 12.0 (v.br), 11.304 (s), 9.478 (s), 9.195 (s), 7.993 (s).

## 7.3 Experimental Details for Chapter Three
## The Synthesis of Additional Compounds Relating to Distortional Isomerism

### 7.3.1 Synthesis of $Mo(O)(NCS)_2(PMe_2Ph)_3$

A mixture of Enemark blue *cis-mer*-$Mo(O)Cl_2(PMe_2Ph)_3$ (1.0g, mmol) and potassium thiocyanate (2.5g, mmol) were stirred in boiling ethanol (25ml) for 30 minutes. The solution was filtered, and on cooling gave rise to blue crystals of $Mo(O)(NCS)_2(PMe_2Ph)_3$ (0.93g, %).

Elemental analysis for $C_{26}H_{33}P_3N_2S_2OMo$ F(R): %C, 48.13 (48.60); %H, 5.09 (5.18); %N, 4.21 (4.36).

Infrared data (Nujol mull, CsI, $cm^{-1}$): 2070 (vs), 2040 (vs), 1593 (w), 1439 (s), 1430 (m), 1415 (m), 1299 (m), 1287 (m), 1108 (m,br), 1002 (w), 950 (vs), 941 (vs,sh), 920 (vs,sh), 908 (vs), 860 (m), 844 (s), 838 (s), 800 (w,br), 747 (s), 740 (vs), 708 (s), 693 (vs), 675 (m), 490 (vs,sp), 425 (s), 310 (vw), 300 (w,sh), 288 (m), 255 (m).

Raman data ($cm^{-1}$): 1001 (s), 952 (vs), 845 (m), 840 (m), 679 (m), 325 (w), 296 (w), 283 (w), 249 (w).

$^1$H NMR data (200 MHz, d-chloroform, 298K, ppm): 1.219 (d, $^2J(PH)$=8.2Hz, cis-P**Me**$_2$Ph)), 1.646 (t, $^2J(PH)$=3.9Hz, trans-P**Me**(Me)Ph), 1.855 (t, $^2J(PH)$=4.0Hz, trans-P(Me)**Me**Ph).

### 7.3.2 Blue $W(O)Cl_2(PMe_2Ph)_3$

#### 7.3.2.1 *Reaction of $W(O)_2Cl_2$ with $PMe_2Ph$ and EtMgCl*

$W(O)_2Cl_2$ (0.500g, 1.74 mmol) was added slowly to a stirred solution of DME (30ml) to give a colourless solution. The solution was then frozen and ethyl magnesium chloride (0.87ml, 1.74mmol) syringed in, along with $PMe_2Ph$ (0.970g, 6.96mmol) in DME (10ml) being added via cannula. The mixture was allowed to warm to room temperature and stirred for 3 hours leading to the precipitation of magnesium chloride and a brown solution. The solution was filtered and the $MgCl_2$ washed with

DME (2x10ml). The solution was then pumped down leaving a brown oil, which was washed with n-pentane (10ml) to give brown solid. The solid was re-extracted into hot ethanol, filtered and allowed to cool to room temperature, giving rise to the deposition of purple-blue crystals (0.867g, 72.6%).

### 7.3.2.2 *Reaction of $WCl_6$ with $PMe_2Ph$*

Dry ethanol (2 ml) was added dropwise to tungsten hexachloride (0.500g, 1.26mmol), giving rise to a yellow oil. The reaction is vigorous, with copious amounts of hydrogen chloride being evolved. The oil was dissolved in ethanol (10ml) and $PMe_2Ph$ (1.390g, 10.06mmol) in ethanol (10ml) added dropwise to the stirred solution at room temperature, forming a white precipitate and a pale red solution. The mixture was then heated at 70°C for 1 hour, resulting in a purple solution. Filtration and cooling to room temperature gave rise to deep blue-purple crystals (0.438g, 50.7%).

Elemental Analysis for $C_{24}H_{33}P_3Cl_2OW$ F(R): %C, 41.82 (42.07); %H, 4.96 (4.85), %Cl, 10.53 (10.35).

Infrared data (Nujol, CsI, $cm^{-1}$): 1571 (w), 1489 (s), 1436 (vs), 1426 (m), 1421 (m), 1414 (m), 1407 (m), 1329 (m), 1314 (m), 1298 (m), 1295 (m), 1286 (vs), 1282 (s), 1279 (m,sh), 1269 (m), 1182 (w,br), 1164 (m), 1157 (m), 1107 (s,br), 1104 (m,sh), 1001 (m), 957 (vs), 940 (vs), 915 (vs), 904 (vs), 868 (w), 859 (m), 835 (vs), 828 (m), 757 (vs), 752 (vs), 740 (vs), 723 (s), 711 (vs), 696 (vs), 677 (s), 490 (vs), 424 (s), 414 (s), 345 (s), 341 (w,sh), 312 (m), 309 (m,sh), 286 (vs), 245 (vs).

Raman data ($cm^{-1}$): 1029 (m), 1002 (s), 958 (m), 741 (w), 712 (w), 681 (m), 494 (w), 345 (m), 306 (m,sh), 282 (w), 264 (w).

$^1$H NMR data (400 MHz, d-chloroform, 298K, ppm): 1.362 (d, $^2J(PH)$=9.2Hz, cis-P**Me**$_2$Ph)), 1.760 (t, $^2J(PH)$=4.2Hz, trans-P**Me**(Me)Ph), 1.957 (t, $^2J(PH)$=4.0Hz, trans-P(Me)**Me**Ph), 7.064 (m), 7.169 (m), 7.356 (m), 7.515 (m).

(200 MHz, d-chloroform, 298K, ppm): 1.362 (d, $^2J(PH)$=8.8Hz), 1.762 (t, $^2J(PH)$=4.1Hz), 1958 (t, $^2J(PH)$=4.1Hz), 7.07 (m), 7.17 (m), 7.36 (m), 7.52 (m).

### 7.3.3 $Mo(O)Cl_2(PEt_2Ph)_3$ ν(Mo=O) 938 $cm^{-1}$

This sample was kindly supplied by Subashini Balakvmar of the University of North London, and was prepared by the same route as used to synthesize Enemark blue $Mo(O)Cl_2(PMe_2Ph)_3$ described in section 7.2.4.

Elemental Analysis for $C_{30}H_{45}P_3Cl_2OMo$ F(R): %C, 52.04 (52.87); %H, 6.56 (6.66).

Infrared data (Nujol mull, CsI, $cm^{-1}$): 1572 (w), 1435 (s), 1417 (w), 1330 (vw), 1309 (vw), 1250 (w,br), 1188 (w), 1161 (w), 1101 (m), 1075 (w), 1046 (w), 1031 (m), 1012 (w), 996 (w), 938 (vs), 915 (w), 847 (vw), 801 (vw), 768 (m), 755 (m), 751 (m,sh), 733 (s), 709 (w), 700 (s), 640 (m), 617 (vw), 497 (s), 490 (m,sh), 450 (w), 446 (w,sh), 404 (vw), 321 (vw), 300 (w,sh), 291 (m), 285 (w,sh), 263 (vw), 253 (vw,h), 242 (w).

$^1$H NMR data (400MHz, d-chloroform, 298K, ppm): 0.600 (m, **Me**), 0.954 (m, **Me**), 1.145 (m, $CH_2$), 1.250 (m, **Me**), 1.472 (m, **Me**), 1.637 (br), 2.138 (m, $CH_2$), 2.232 (m, $CH_2$), 2.836 (m, $CH_2$), 4.25 (br), [7.009, 7.082, 7.214, 7.299, 7.434, 7.492 (m), **Ph**], 7.675 (br).

### 7.3.4 $Mo(O)Cl_2(PEt_2Ph)_3$ ν(Mo=O) 940 $cm^{-1}$

This sample was kindly supplied by Subashini Balakvmar of the University of North London, and was prepared by the same route as used to synthesize Enemark blue $Mo(O)Cl_2(PMe_2Ph)_3$ described in section 7.2.4.

Elemental Analysis for $C_{30}H_{45}P_3Cl_2OMo$ F(R): %C, 51.34 (52.87); %H, 6.51 (6.66).

Infrared data (Nujol mull, CsI, $cm^{-1}$): 1571 (vw), 1436 (m), 1415 (w), 1312 (vw), 1250 (w,br), 1192 (vw), 1159 (w), 1131 (vw), 1102 (m), 1075 (w), 1047 (m), 1034 (m), 999 (w), 976 (vw), 940 (vs), 920 (vw), 852 (vw), 770 (m), 757 (m,sh), 752 (m), 745 (m), 731 (s), 712 (m,sh), 703 (m), 698 (m,sh), 673 (vw), 640 (vw), 618 (vw), 523 (vw), 507 (m,sh), 496 (m), 447 (w), 402 (vw), 320 (vw), 291 (w), 283 (vw,sh), 261 (vw,sh), 242 (w).

$^1$H NMR data (400MHz, d-chloroform, 298K, ppm): 0.599 (m, **Me**), 0.952 (m, **Me**), 1.145 (m, $CH_2$), 1.250 (m, **Me**), 1.470 (m, **Me**), 1.680 (br), 2.137

(m, $CH_2$), 2.231 (m, $CH_2$), 2.833 (m, $CH_2$), 4.26 (br), [7.009, 7.082, 7.214, 7.300, 7.434, 7.492 (m), Ph], 7.665 (br).

## 7.4 Experimental Details of Chapter Four

## Synthesis of Niobium Oxyhalides and Bond-Stretch Isomers

### 7.4.1 Synthesis of $Nb(*O)Cl_3$ (* = $^{16}O$, $^{17}O$, $^{18}O$)

4.3ml (20.2mmol) of hexamethyldisiloxane, $((CH_3)_3Si)_2*O$ (* = $^{16}O$, $^{17}O$, $^{18}O$), in 20ml of 1,2-dichloroethane was added dropwise to a stirred yellow suspension of $NbCl_5$ (5.42g, 20.1mmol) in 30ml of 1,2-dichloroethane at room temperature. The mixture was swiftly heated to 80°C with stirring and maintained at this temperature for $4^1/_2$ h. Dissolution of yellow $NbCl_5$ accompanied by the formation of a white granular precipitate. After cooling to room temperature, the pale yellow supernatant solution was filtered off by cannula and the solid washed with n-pentane (2 x 10ml) and dried in vacuo to give a pure white solid (3.60g, 83.4%).

Infrared data for $Nb(^{16}O)Cl_3$ (Nujol, CsI, $cm^{-1}$): 1256 (w), 790 (vs,br), 410 (s,br) and 295 (m,br).

Infrared data for $Nb(^{17}O)Cl_3$ (Nujol, CsI, $cm^{-1}$): 1259 (w), 776 (vs,br), 411 (s,br) and 296 (m,br).

Infrared data for $Nb(^{18}O)Cl_3$ (Nujol, CsI, $cm^{-1}$): 1260 (w), 746 (vs,br), 415 (s,br) and 296 (m,br).

Elemental analysis for $Cl_3ONb$ F(R) %: Nb 35.35 (43.16), Cl 34.09 (49.41).

### 7.4.2 Synthesis of $Nb(O)Br_3$

The synthesis of yellow $Nb(O)Br_3$ is essentially analogous to that of the previously described synthesis of $Nb(O)Cl_3$. Yield 2.32g (94.4%)

Infrared data (Nujol, CsI, $cm^{-1}$): 1255 (w), 758 (s,br), 332 (w) and 295 (w,br).

Elemental analysis for $Br_3ONb$ F(R) %: Nb 22.88 (26.67), Br 65.95 (68.76).

### 7.4.3 Synthesis of $Nb(*O)Cl_3(CH_3CN)_2$ (* = $^{16}O$, $^{18}O$)

10.0ml (46.6mmol) of hexamethyldisiloxane, $(Me_3Si)_2*O$ (* = $^{16}O$, $^{18}O$), in 30ml of acetonitrile was added dropwise, at room temperature, to a yellow suspension of $NbCl_5$ (10.15g, 46.45mmol) in $CH_3CN$ (30ml). The mixture was stirred for 2 h. to give a colourless solution, which was filtered, reduced in volume to ca. 20ml and cooled at -35°C to afford a white crystalline solid. This was isolated and dried in vacuo. Yield 10.26g (91.8%).

Infrared data for $Nb(^{16}O)Cl_3(CH_3CN)_2$ (Nujol, CsI, $cm^{-1}$): 2318 (s), 2303 (s), 2288 (s), 2278 (s), 2250 (m), 2230 (w), 1913 (w), 1367 (s), 1355 (s), 1024 (m), 956 (s), 943 (s), 930 (s), 826 (w), 790 (w,br), 720 (w), 384 (s), 360 (s,br), 330 (s) and 250 (s).

Infrared data for $Nb(^{18}O)Cl_3(CH_3CN)_2$ (Nujol, CsI, $cm^{-1}$): 2313 (s), 2303 (s), 2285 (s), 2277 (s),1405 (w),1366 (s/m), 1354 (w), 1022 (w,br), 957 (s), 944 (m), 930 (w), 926 (w), 908 (vs), 830 (m/s,br), 380 (s), 360 (s), 335 (s) and 245 (w).

### 7.4.4 Synthesis of $Nb(O)Br_3(CH_3CN)_2$

1.10ml (5.1mmol) of hexamethyldisiloxane, $(Me_3Si)_2O$, in 10ml of acetonitrile was added dropwise to a brown suspension of $NbBr_5$ (2.53g, 5.1mmol) in 25ml of acetonitrile. The mixture was stirred for 2 h. to give a red solution which was filtered and reduced in volume to ca. 10ml. On cooling to -20°C an orange crystalline solid was isolated and dried in vacuo (1.13g, 51.1%).

Infrared data (Nujol, CsI, $cm^{-1}$): 2308 (s), 2298 (s), 2280 (s), 2275 (s), 1378 (m), 1364 (m), 1352 (m), 1255 (w), 1022 (m), 952 (vs), 940 (vs), 927 (vs),845 (m,br), 800 (m,br), 418 (w), 405 (w) and 275 (vs,br)

Elemental analysis for $C_4H_6Br_3N_2ONb$ F(R) %: C 11.22 (11.15), N 6.54 (6.51), H 1.46 (1.40), Br 53.97 (55.65).

### 7.4.5 Synthesis of α -$Nb(O)Cl_3(PMe_3)_3$

#### 7.4.5.1 *Reaction of $Nb(O)Cl_3$ with $PMe_3$ in Dichloromethane*

1.20ml (11.61mmol, 5 equivalents) of trimethylphosphine, $P(CH_3)_3$, was condensed onto a frozen mixture of $Nb(*O)Cl_3$ (0.500g, 2.32mmol) and dichloromethane (50ml). The mixture on warming to room temperature turns deep purple, through claret, to a light green coloured solution. After stirring for 24 h. the resulting solution was filtered, reduced in volume and cooled to -78°C to afford pale yellow crystals, which were isolated and dried *in vacuo* . Yield 0.43g (42%).

#### 7.4.5.2 *Reaction of $Nb(*O)Cl_3$ with Neat $PMe_3$ (*=$^{16}O$, $^{18}O$)*

Trimethylphosphine (20ml) was condensed on to frozen $Nb(*O)Cl_3$ (0.500g). The mixture was warmed to room temperature to give a pale white suspension which after 30 mins. stirring had become a pale yellow colour. After stirring for 20 h. the excess $PMe_3$ was removed by vacuum transfer leaving a creamy, yellow solid (73:27 α,β mix). The solid was redissolved in dichloromethane (30ml), filtered and reduced in volume. On cooling to - 78°C pale yellow crystal were formed which were isolated and dried *in vacuo* (0.76g, 73.8%).

*Characterisation of Yellow α-$Nb(O)Cl_3(PMe_3)_3$*

Elemental analysis for α-$C_9H_{27}Cl_3PONb$: refer to section 4.9.

Infrared data for α-$Nb(^{16}O)Cl_3(PMe_3)_3$, (Nujol, CsI, $cm^{-1}$): 1424 (m), 1298 (w), 1284 (m), 1279 (m), 1275 (w), 951 (s,br), 882 (s), 845 (w), 737 (m), 667 (w), 462 (w,br), 355 (m), 300 (s), 285 (m), and 234 (m).

Infrared data for α-$Nb(^{18}O)Cl_3(PMe_3)_3$, (Nujol, CsI, $cm^{-1}$): 1420 (m), 1298 (w), 1278 (m), 951 (s,br), 882 (s), 871 (vw), 854 (m), 834 (s), 822 (w), 737 (s), 667 (w), 352 (m), 334 (w), 293 (s), 277 (s), and 228 (m).

$^1$H NMR data (250MHz, chloroform-d, 298K, ppm): 1.43 (d, $^2$J(PH)=8.6Hz, $PMe_3$).

(400MHz, chloroform-d, 298K, ppm): 1.43 (d, $^2$J(PH)=7.2Hz, $PMe_3$).

(400MHz, dichloromethane-$d_2$, 298K, ppm): 1.442 (d, $^2$J(PH)=7.2Hz, $PMe_3$).

$^{31}$P{$^1$H} NMR (101.26MHz, dichloromethane-$d_2$, 298K, ppm): -5.31 (s, br, $\Delta^1/_2$=1000Hz), -5.31 (s, br, $\Delta^1/_2$=250Hz)

### 7.4.6 Synthesis of β-Nb(*O)$Cl_3(PMe_3)_3$ (*=$^{16}$O, $^{18}$O)

***Reaction of Nb(*O)$Cl_3$ with $PMe_3$ in Dichloromethane***

1.20ml (11.61mmol, 5 equivalents) of trimethylphosphine, $P(CH_3)_3$, was condensed onto a frozen mixture of Nb(*O)$Cl_3$ (0.500g, 2.32mmol) and dichloromethane (50ml). The mixture on warming to room temperature turns deep purple, through claret, to a light green coloured solution. After stirring for a variable duration the solution was filtered and pumped down to dryness affording a pale yellow-green amorphous powder (of variable α,β mix). Yield 1.029g (99.9%). The solid was redissolved in a minimal volume of toluene (ca. 100ml), filtered, reduced in volume and cooled to -20°C forming green crystals, which were isolated and dried *in vacuo* . Yield 0.93g (90.3%).

*Characterisation of Green β-Nb(O)$Cl_3(PMe_3)_3$*

Elemental analysis for β-$C_9H_{27}Cl_3PONb$: refer to section 4.9.

Infrared data for β-Nb($^{16}$O)$Cl_3(PMe_3)_3$, (Nujol, CsI, cm$^{-1}$): 1420 (m), 1294 (w), 1278 (s), 951 (s,br), 915 (w), 871 (s), 842 (w), 739 (m), 722 (w,sh), 693 (w), 667 (w), 364 (w,sh), 350 (w), 298 (s), 275 (m),258 (w,sh) and 230 (m).

Infrared data for β-Nb($^{18}$O)$Cl_3(PMe_3)_3$, (Nujol, CsI, cm$^{-1}$): 1425 (m), 1299 (w), 1284 (m), 1275 (w), 951 (vs,br), 871 (m), 848 (w/m,br), 823 (s), 737 (m), 667 (w), 353 (w), 295 (m), 284 (m) and 236 (w).

$^1$H NMR data (250MHz, chloroform-d, 298K, ppm): 1.43 (d, $^2J(PH)$=8.6Hz, $PMe_3$).

(400MHz, dichloromethane-$d_2$, 298K, ppm): 1.434 ($^2J(PH)$=7.6Hz, $PMe_3$).

$^{31}P\{^1H\}$ NMR (101.26MHz, dichloromethane-$d_2$, 298K, ppm): 3.92 (s, br, $\Delta^1/_2$=2500Hz), -3.95 (s, br, $\Delta^1/_2$=415Hz), -60.44 (s, br, $\Delta^1/_2$=250Hz)

### 7.4.7 Reaction of $Nb(O)Br_3$ with $PMe_3$ in Dichloromethane

*Synthesis of β -$Nb(O)Br_3(PMe_3)_3$*

0.72ml (7.17mmol, 5 equivalents) of trimethylphosphine, $P(CH_3)_3$, was condensed onto a frozen mixture of $Nb(O)Br_3$ (0.500g, 1.43mmol) and dichloromethane (50ml). On warming to room temperature an orange solution is formed. After stirring for 18 h. the solution was filtered and pumped down to dryness to produce a darkish brown amorphous powder (0.825g, 99.7%) with a 10:90 α,β mix. The solid was redissolved in toluene giving rise to a clear orange solution on filtration and reducing in volume. Cooling to -20°C produced brick-red pyramidal crystals, which were isolated and dried *in vacuo* . Yield 0.673g (81.3%).

Infrared data (Nujol, CsI, $cm^{-1}$): 1424 (m), 1296 (w), 1278 (s), 952 (vs,br), 871 (s), 845 (w), 820 (w), 777 (w), 734 (m), 665 (w), 350 (w), 286 (m) and 270 (w).

Elemental analysis for $C_9H_{27}Br_3PONb$, F(R) %: C 18.39 (18.74), H 4.72 (4.79).

$^1$H NMR data (250MHz, benzene-$d_6$, 298K, ppm): 1.14 (s,br, $\Delta^1/_2$ = 18.2Hz, $PMe_3$).

## 7.5 Experimental Details to Chapter Five

## Synthesis of Niobium and Tantalum Sulphidohaldies and Bond-Stretch Isomers

### 7.5.1 Synthesis of $Nb(S)Cl_3$

A chilled (ca. -30°C) carbon disulphide solution (30 ml) of $(Me_3Si)_2S$ (1.70g, 9.5 mmol) was added dropwise over a period of 15 minutes to a stirred suspension of $NbCl_5$ (2.57g, 9.5 mmol) in carbon disulphide (30 ml) cooled in a dry-ice/acetone slush bath. Dissolution of yellow $NbCl_5$ occurred affording a clear yellow solution. The mixture was allowed to warm to room temperature and stirred overnight to give a brown solution. The solution was filtered and the volatiles removed under reduced pressure, leaving a grey amorphous powder which was washed in petroleum ether (2 x 20 ml, b.p. 40-60°C) and dried in vacuo. Yield 2.06g (93%).

Elemental Analysis for $Cl_3SNb$, F(R): %Nb, 39.62 (40.16); %S, 14.11 (13.86); %Cl, 44.01 (45.98).

Infrared data (Nujol, CsI, $cm^{-1}$): 550 (s, sp), 414 (s, sh), 401 (s, sh), 394 (s, br), 355 (m) , 292 (m).

### 7.5.2 Synthesis of $Nb(S)Cl_3(CH_3CN)_2$

A chilled (ca. -30°C) acetonitrile solution (15 ml) of $(Me_3Si)_2S$ (1.70g, 9.5 mmol) was added dropwise to a stirred suspension of $NbCl_5$ (2.57g, 9.5 mmol) in acetonitrile (20 ml) at ca. -30°C. The mixture was allowed to warm to room temperature and stirred overnight to give a yellow solution. Filtration and cooling at -35°C afforded yellow crystals. Yield 2.29g (77%).

Elemental Analysis for $C_4H_6N_2NbS$, F(R): %C, 14.84 (15.32); %H, 1.89 (1.93); %N, 8.62 (8.94).

Infrared Data (Nujol, CsI, $cm^{-1}$): 2310 (s, sp), 2280 (s, sp), 1368 (m), 1358 (m), 1030 (m), 523 (s, sp), 379 (m sh), 370 (m, sh), 354 (s, sp), 334 (s), 316 (s, sp), 280 (m).

$^1$H NMR data (200MHz, $CD_2Cl_2$, 298K, ppm): 2.001 (s, $\Delta^1/_2$=1.2Hz).

### 7.5.3 Reaction of $Nb(S)Cl_3$ with $PMe_3$

*Synthesis of Green $Nb(S)Cl_3(PMe_3)_3$*

Trimethylphosphine (0.67g, 8.79 mmol) was condensed onto a frozen mixture of $Nb(S)Cl_3$ (0.58g, 2.51 mmol) and dichloromethane (50 ml). The mixture was warmed to room temperature and stirred for 12h. to afford a dark green solution. Filtration, followed by concentration and cooling to -78°C affords yellow crystals, which were dried in vacuo. IR spectrum shows the crystals to be an 80:20 (489:455 $cm^{-1}$) isomer mix. Recrystallisation from toluene at -35°C afforded cubic green crystals.

*Characterisation of Green $Nb(S)Cl_3(PMe_3)_3$*

Elemental Analysis for $C_9H_{27}Cl_3NbSP_3$ F(R): %Nb, 24.83 (20.22); %S, 6.93 (6.98); for %C, H, and N refer to section 5.2.7.

Infrared Data (Nujol, CsI, $cm^{-1}$): 1422 (m), 1298 (m), 1277 (s), 950 (s, br), 870 (m), 850 (m), 734 (s), 668 (m), 489 (s, sp), 346 (m, sh), 335 (s), 290 (s, sh), 269 (s, br), 243 (m).

Solution Infrared data ($CH_2Cl_2$, CsI, $cm^{-1}$): 1299 (s), 950 (vs,br), 855 (w,sh), 846 (w), 570 (vw), 484 (s,sp), 453 (w), 337 (w,sh,br), 271 (s,sh).

$^1$H NMR Data (400 MHz, $CD_2Cl_2$, 298 K, ppm): 1.613 (s, br, $\Delta^1/_2$=16 Hz, $PMe_3$).

### 7.5.4 Reaction of $Nb(S)Cl_3(CH_3CN)_2$ with $PMe_3$

*Synthesis of Orange $Nb(S)Cl_3(PMe_3)_3$*

Trimethylphosphine (1.04g, 13.7 mmol) was condensed onto a frozen mixture of $Nb(S)Cl_3(CH_3CN)_2$ (1.22g, 3.89 mmol) and dichloromethane (50 ml). The mixture was warmed to room temperature and stirred for 12h. to afford a dark green

solution. Filtration, followed by concentration and cooling to -78°C affords yellow crystals, which were dried in vacuo. IR spectrum shows the crystals to be an 55:45 (489:455 $cm^{-1}$) isomer mix. Recrystallisation from toluene at -35°C afforded cubic orange crystals.

*Characterisation of Orange $Nb(S)Cl_3(PMe_3)_3$*

Elemental Analysis for $C_9H_{27}Cl_3NbSP_3$ F(R): %Nb, 24.30 (20.22); %S, 7.01 (6.98); for %C, H, and N refer to section 5.2.7.

Infrared Data (Nujol, CsI, $cm^{-1}$): 1423 (m), 1421 (m), 1298 (m), 1286 (s), 950 (s, br), 732 (s), 668 (m), 455 (s, sp), 335 (s), 274 (s).

Solution Infrared data ($CH_2Cl_2$, CsI, $cm^{-1}$): 1299 (s), 950 (vs,br), 846 (w), 484 (m), 453 (s), 336 (s), 320 (s,sh), 310 (m,sh), 274 (s,sh).

$^1$H NMR (400 MHz, $CD_2Cl_2$, 298 K, ppm): 1.601 (s, br, $\Delta^1/_2$=16 Hz, $PMe_3$ ), -3.011 (br, $NbCl_4(PMe_3)_3$

$^{31}P\{^1H\}$ NMR (101.26 MHz, $CD_2Cl_2$, 298 K, ppm): 26.59 (s), 5.19 (s, br, $\Delta^1/_2$=146 Hz), -23.75 (s, br, $\Delta^1/_2$=83 Hz).

*Characterisation of 489:455 $cm^{-1}$ mix $Nb(S)Cl_3(PMe_3)_3$*

Solution Infrared data ($CH_2Cl_2$, CsI, $cm^{-1}$): 1299 (s), 952 (vs,br), 846 (w), 484 (w), 453 (m), 337 (s), 310 (m,sh), 275 (m,sh).

### 7.5.5 Synthesis of $NbCl_4(THF)_2$

$NbCl_5$ (2.40g, 8.88 mmol) was added to a suspension of 80 mg (2.96 mmol) of aluminium powder in 100 ml of acetonitrile. The mixture was stirred for 2 h. and filtered to give a dark orange-brown solution and a yellow-green solid ($AlCl_3$). The acetonitrile solution was removed in vacuo to give a reddish-brown solid. The solid was suspended in 50 ml of THF and vigorously stirred for 3h. Filtration gave a pale yellow solid which was washed in copious amounts of THF. Yield 2.50g (75%).

Infrared Data (Nujol, CsI, $cm^{-1}$): 1360 (w), 1350 (m), 1252 (w), 1170 (w), 1043 (m), 996 (s), 954 (w), 920 (m), 825 (s, br), 685 (w), 342 (s, br), 280 (s), 248 (w).

### 7.5.6 Synthesis of $NbCl_4(PMe_3)_3$

$NbCl_4(THF)_2$ (0.76g, 2.0 mmol) was added slowly with stirring to a solution of $PMe_3$ (0.735g, 11.1 mmol) in 30 ml of toluene. The solution turned dark green and a solid of the same colour was precipitated. Additional product was obtained by cooling the supernatant liquid at -78°C. Yield 0.82g (88%).

Elemental Analysis for $C_9H_{27}Cl_4NbP_3$, F(R): %C, 23.02 (23.35); %H, 6.12 (5.88).

Infrared Data (Nujol, CsI, $cm^{-1}$): 1428 (m), 1422 (m, sh), 1300 (m), 1282 (s), 954 (s,br), 850 (w), 785 (w), 734 (s), 668 (w), 332 (s), 290 (m), 275 (m, br).

Solution Infrared data ($CH_2Cl_2$, CsI, $cm^{-1}$): 1303 (m), 955 (s,br), 310 (s).

$^1$H NMR data (400 MHz, $CD_2Cl_2$, 298K, ppm): -3.011 (s,br, $\Delta^1/_2$=200Hz).

$^{31}P\{^1H\}$ NMR (400 MHz, $CD_2Cl_2$, 298K, ppm): -60.44 (s,br, $\Delta^1/_2$=250Hz).

### 7.5.7 Synthesis of $Ta(S)Cl_3$

A chilled (ca. -30°C) carbon disulphide solution (30 ml) of $(Me_3Si)_2S$ (2.50g, 14.0mmol) was added dropwise over a period of 30 minutes to a stirred suspension of $TaCl_5$ (5.00g, 14.0mmol) in carbon disulphide (30 ml) cooled in a dry-ice/acetone slush bath. Dissolution of white $TaCl_5$ occurred affording a clear yellow solution. The mixture was allowed to warm to room temperature and stirred overnight to give a colourless solution and an orange amorphous solid. The supernatant solution was decanted off the solid, which was washed in petroleum ether (2 x 20 ml, b.p. 40-60°C) and dried *in vacuo*. Yield 3.93g (88%).

Elemental Analysis for $Cl_3STa$, F(R): %Ta, 56.85 (56.66); %S, 11.37 (10.04); %Cl, 31.56 (32.88).

Infrared data (Nujol, CsI, $cm^{-1}$): 459 (s,sp), 413 (m,sh), 377 (s,br), 357 (m,sh), 31? (m), 271 (m).

### 7.5.8 Synthesis of $Ta(S)Cl_3(CH_3CN)_2$

A chilled (ca. -40°C) acetonitrile solution (15 ml) of $(Me_3Si)_2S$ (2.00g, 11.08mmol) was added dropwise to a stirred suspension of $TaCl_5$ (4.00g, 11.08mmol) in acetonitrile (40 ml) at ca. -40°C over a period of 30 minutes. The mixture was allowed to warm to room temperature and stirred overnight to give a deep red solution. Filtration and cooling at -35°C afforded dark green crystals. Yield 3.43g (77%).

Elemental Analysis for $C_4H_6N_2TaS$, F(R): %C, 12.01 (11.97); %H, 1.53 (1.51); %N, 6.75 (6.98).

Infrared data (Nujol, CsI, $cm^{-1}$): 2415 (s,sp), 2410 (m,sh), 2382 (s,sp), 2378 (m,sh), 1367 (m), 1358 (m), 1023 (s), 513 (vs,sp), 451 (w), 410 (w), 328 (vs,vbr).

$^1$H NMR data (200MHz, $CD_2Cl_2$, 298K, ppm): 2.009 (s, $\Delta^1/_2$=1.3Hz).

### 7.5.9 Synthesis of Orange $Ta(S)Cl_3(PMe_3)_3$

#### 7.5.9.1 *Reaction of $Ta(S)Cl_3$ with $PMe_3$*

Trimethylphosphine (0.42g, 5.48mmol) was condensed onto a frozen mixture of $Ta(S)Cl_3$ (0.500g, 1.55mmol) and dichloromethane (40 ml). The mixture was warmed to room temperature and stirred for 12h. to afford a dark green solution. Filtration, followed by concentration and cooling to -78°C affords yellow crystals, which were collected and dried *in vacuo* (0.760g, 88%). IR spectrum shows the crystals to be an 60:40 (470:430 $cm^{-1}$) isomer mix. Recrystallisation from toluene, as a yellow solution, at -35°C afforded cubic orange crystals.

#### 7.5.9.2 *Reaction of $Ta(S)Cl_3(CH_3CN)_2$ with $PMe_3$*

Trimethylphosphine (0.41g, 5.41mmol) was condensed onto a frozen mixture of $Ta(S)Cl_3(CH_3CN)_2$ (0.625g, 1.55mmol) and dichloromethane (50 ml). The mixture

was warmed to room temperature and stirred for 12h. to afford a deep green solution. Filtration, followed by concentration and cooling to -78°C affords yellow crystals, which were collected and dried *in vacuo* (0.65g, 76%). IR spectrum shows the crystals to be a 90:10 (470:430 $cm^{-1}$) isomer mix. Recrystallisation from toluene, as a yellow solution, at -35°C afforded cubic orange crystals.

*Characterisation of Orange $Ta(S)Cl_3(PMe_3)_3$*

Elemental Analysis for $C_9H_{27}Cl_3TaSP_3$: refer to section 5.3.6.

Infrared data (Nujol, CsI, $cm^{-1}$): 1422 (s), 1298 (m), 1278 (s), 950 (vs,br), 852 (m), 730 (vs,sp), 668 (m), 470 (vs,sp), 315 (w,sh), 290 (s), 260 (s,sh), 257 (s).

Raman data ($cm^{-1}$): 735 (m), 671 (m), 466 (s), 285 (w), 197 (m), 187 (m).

Solution Infrared data ($CH_2Cl_2$, CsI, $cm^{-1}$): 1299 (s), 952 (vs,br), 848 (w), 463 (s,sp), 257 (s).

$^1$H NMR data (400 MHz, $CD_2Cl_2$, 298 K, ppm): 1.689 ppm (s, br, Δ = 13.1 Hz, $PMe_3$)

(200 MHz, $CD_2Cl_2$, 298 K, ppm): 1.697 ppm (s, br, Δ = 13.5 Hz, $PMe_3$)

(200 MHz, $CDCl_3$, 298 K, ppm): 1.645 ppm (s, br, Δ = 12.9 Hz, $PMe_3$)

$^{31}P\{^1H\}$ NMR (161.9 MHz, $CD_2Cl_2$, 298 K): 34.402 ppm (s).

*Characterisation of 470:430 $cm^{-1}$ Yellow $Ta(S)Cl_3(PMe_3)_3$*

Elemental Analysis for $C_9H_{27}Cl_3TaSP_3$: refer to section 5.3.6.

Infrared Data (Nujol, CsI, $cm^{-1}$): 1420 (m), 1298 (m), 1279 (s), 954 (vs,br), 852 (m), 734 (s,sp), 668 (w), 470 (m,sp), 430 (w), 312 (s), 282 (m), 248 (m).

Raman data ($cm^{-1}$): 735 (m), 673 (m), 466 (s), 289 (w), 189 (m).

Solution Infrared data ($CH_2Cl_2$, CsI, $cm^{-1}$): 1299 (s), 952 (vs,br), 847 (w), 463 (s,sp), 430 (m), 313 (s), 257 (s).

$^1$H NMR data (200 MHz, $CD_2Cl_2$, 298 K, ppm): 1.686 (s, br, Δ = 13.3 Hz, $PMe_3$), 2.008 (t, $^2J(PH)$= 3.8Hz).

# Appendices

Crystal Data, Colloquia and Lectures.

# Appendix 1

**Appendix 1A: Crystal Data for Yellow α-$Nb(O)Cl_3(PMe_3)_3$ ($\nu$(Nb=O) 882 $cm^{-1}$).**

| | |
|---|---|
| $C_9H_{27}Cl_3NbSP_3$: | 443.41 |
| Crystal System: | Monoclinic |
| Space Group: | $P2_1/c$ |
| Cell Dimensions: | a = 15.250(3) Å |
| | b = 11.131(2) Å |
| | c = 11.673(3) Å |
| | V = 1977.54 $Å^3$ |
| | Z = 4 |
| | $D_c$ = 1.490 g $cm^{-3}$ |
| Final R-value: | 0.0418 (wR = 0.0410) |

**Appendix 1B: Crystal Data for Green β-$Nb(O)Cl_3(PMe_3)_3$ ($\nu$(Nb=O) 871 $cm^{-1}$).**

| | |
|---|---|
| $C_9H_{27}Cl_3NbSP_3$: | 443.41 |
| Crystal System: | Monoclinic |
| Space Group: | $P2_1/c$ |
| Cell Dimensions: | a = 18.809(4) |
| | b = 16.066(3) |
| | c = 14.884(3) |
| | V = 4422.4 $Å^3$ |
| | Z = 4 |
| | $Q_c$ = 2.178 g $cm^{-3}$ |
| Final R-value: | 0.0301 (wR = 0.0329) |

**Appendix 1D: Crystal Data for Orange $Nb(S)Cl_3(PMe_3)_3$ ($\nu$(Nb=S) 455 $cm^{-1}$).**

| | |
|---|---|
| $C_9H_{27}Cl_3NbSP_3$: | 459.56 |
| Crystal System: | Monoclinic |
| Space Group: | $P2_1/c$ |
| Cell Dimensions: | a = 15.190(3) |
| | b = 11.415(3) |
| | c = 11.690(3) |
| | V = 2024.63 $Å^3$ |
| | Z = 4 |
| | $Q_c$ = 1.507 g $cm^{-3}$ |
| Final R-value: | 0.0553 for 2652 reflections |

**Appendix 1E:** **Crystal Data for Green $Nb(S)Cl_3(PMe_3)_3$ ($\nu$(Nb=S) 489 $cm^{-1}$).**

| | |
|---|---|
| $C_9H_{27}Cl_3NbSP_3$: | 459.56 |
| Crystal System: | Monoclinic |
| Space Group: | $P2_1/c$ |
| Cell Dimensions: | a = 15.151(3) |
| | b = 11.565(3) |
| | c = 11.668(3) |
| | V = 2042.78 $Å^3$ |
| | Z = 4 |
| | $Q_c$ = 1.494 g $cm^{-3}$ |
| Final R-value: | 0.0429 for 2888 reflections |

**Appendix 1F:** **Crystal Data for Orange-yellow $Ta(S)Cl_3(PMe_2)_3$ ($\nu$(Ta=S) 470 $cm^{-1}$).**

| | |
|---|---|
| $C_9H_{27}Cl_3TaSP_3$: | 547.61 |
| Crystal System: | Monoclinic |
| Space Group: | $P2_1/C$ |
| Cell Dimensions: | a = 15.131 |
| | b = 11.471 |
| | c = 11.710 |
| | V = 2029.98 $Å^3$ |
| | Z = 4 |
| | $Q_c$ = 1.792 g $cm^{-3}$ |
| Final R-value: | 0.0357 (wR = 0.0378) |

**Appendix 1G:** **Crystal Data for Chatt Blue *cis-mer*-$Mo(O)Cl_2(PMe_2Ph)_3$ ($\nu$(Mo=O) 955 $cm^{-1}$).**

| | |
|---|---|
| $C_9H_{27}Cl_3NbSP_3$: | 597.3 |
| Crystal System: | Orthorhombic |
| Space Group: | Pbca |
| Cell Dimensions: | a = 16.922(3) |
| | b = 16.446(3) |
| | c = 19.262(4) |
| | V = 5360.6 $Å^3$ |
| | Z = 8 |
| | $Q_c$ = 1.480 g $cm^{-3}$ |
| Final R-value: | 0.038 for 4265 reflections |

**Appendix 1H:** **Crystal Data for Enemark Blue *cis-mer*-$Mo(O)Cl_2(PMe_2Ph)_3$ (ν(Mo=O) 941 $cm^{-1}$).**

| | |
|---|---|
| $C_9H_{27}Cl_3NbSP_3$: | 597.3 |
| Crystal System: | Orthorhombic |
| Space Group: | Pbca |
| Cell Dimensions: | a = 11.300(4) |
| | b = 17.636(3) |
| | c = 28,277(6) |
| | V = 5635.2 $Å^3$ |
| | Z = 8 |
| | $Q_c$ = 1.408 g $cm^{-3}$ |
| Final R-value: | 0.0539 for 1914 reflections |

**Appendix 1K:** **Crystal Data for Blue *cis-mer*-$Mo(O)Br_2(PMe_2Ph)_3$ (ν(Mo=O) 956 $cm^{-1}$).**

| | |
|---|---|
| $C_9H_{27}Cl_3NbSP_3$: | 686.2 |
| Crystal System: | Orthorhombic |
| Space Group: | Pbca |
| Cell Dimensions: | a = 17.020(4) |
| | b = 16.797(4) |
| | c = 19.384(5) |
| | V = 5531.3 $Å^3$ |
| | Z = 8 |
| | $Q_c$ = 1.648 g $cm^{-3}$ |
| Final R-value: | 0.0768 for 1869 reflections |

**Appendix 1L:** **Crystal Data for Blue *cis-mer*-$Mo(O)Br_2(PMe_2Ph)_3$ (ν(Mo=O) 942 $cm^{-1}$).**

| | |
|---|---|
| $C_9H_{27}Cl_3NbSP_3$: | 686.2 |
| Crystal System: | Orthorhombic |
| Space Group: | Pbca |
| Cell Dimensions: | a = 11.439(2) |
| | b = 17.660(3) |
| | c = 28.283(6) |
| | V = 5713.5 $Å^3$ |
| | Z = 8 |
| | $Q_c$ = 1.595 g $cm^{-3}$ |
| Final R-value: | 0.0632 for 1953 reflections |

## Appendix 2

### First Year Induction Courses: October 1989

The course consists of a series of one hour lectures on the services available in the department.

1. Departmental Organisation
2. Safety Matters
3. Electrical appliances and infrared spectroscopy
4. Chromatography and Microanalysis
5. Atomic absorption and inorganic analysis
6. Library facilities
7. Mass spectroscopy
8. Nuclear Magnetic Resonance
9. Glass blowing techniques

### Examined Lecture Course: October - November 1989

The course consisted of six 1 hour lectures followed by a written examination.

"Modern NMR Techniques" by Prof. R.K. Harris.

### Research Colloquia, Seminars and Lectures Organised By the Department of Chemistry

* - Indicates Colloquia attended by the author

### During the Period 1989-1990

BADYAL, Dr. J.P.S. (Durham University) 1st November 1989
Breakthroughs in Heterogeneous Catalysis.

BECHER, Dr. J. (Odense University) 13th November 1989
Synthesis of New Macrocyclic Systems using

Heterocyclic Building Blocks.

*BERCAW, Prof. J.E. (California Institute of Technology) 10th November 1989
Synthetic and Mechanistic Approaches to

Ziegler-Natta Polymerisation of Olefins.

BLEASDALE, Dr. C. (Newcastle University) 21st February 1990
The Mode of Action of some Anti-tumour Agents

BOWMAN, Prof. J.M. (Emory University) 23rd March 1990
Fitting Experiment with Theory in Ar-OH

BUTLER, Dr. A. (St. Andrew's University) 7th December 1989
The Discovery of Penicillin: Facts and Fantacies

CHEETHAM, Dr. A.K. (Oxford University) 8th March 1990
Chemistry Zeolites Cages

CLARK, Prof. D.T. (ICI Wilton) 22nd February 1990
Spatially Resolved Chemistry (using Nature's

Paradigm in the Advanced Materials Arena).

*COLE-HAMILTON, Prof. D.J. (St. Andrew's University) 29th November 1989
New Polymer from Homogeneous Catalysis.

CROMBIE, Prof. L. (Nottingham University) 15th February 1990
The Chemistry of Cannabis and Khat.

DYER, Dr. U. (Glaxo) 31st January 1990
Synthesis and Conformation of C-Glycosides.

*FLORIANA, Prof. C. (Lausanne University, Switzerland) 25th October 1989
Molecular Aggregates - A Bridge Between

Homogeneous and Heterogeneous Systems.

GERMAN, Prof. L.S. (USSR Academy of Sciences, Moscow) 9th July 1990

New Syntheses in Fluoroaliphatic Chemistry:

Recent Advances in the Chemistry of Fluorinated Oxiranes.

GRAHAM, Dr. D. (B.P. Research Centre) 4th December 1989
How Proteins Absorb to Interfaces.

*GREENWOOD, Prof. N.N. (University of Leeds) 9th November 1989
Novel Cluster Geometries in Metalloborane Chemistry.

HOLLOWAY, Prof. J.H. (University of Leicester) 1st February 1990
Nobel Gas Chemistry.

HUGHES, Dr. M.N. (King's College, London) 30th November 1989
A Bug's Eye View of the Periodic Table

HUISGEN, Prof. R. (Universität München) 15th December 1989
Recent Mechanistic Studies of [2+2] Additions.

KLINOWSKI, Dr. J. (Cambridge University) 13th December 1989
Solid State NMR Studies of Zeolite Catalysts.

LANCASTER, Rev. R. (Kimbolton Fireworks) 8th February 1990
Fireworks- Principles and Practice.

LUNAZZI, Prof. L. (University of Bologna) 12th February 1990
Application of Dynamic NMR to the Study of
Conformational Enantiomerism.

*PALMER, Dr. F. (Nottingham University) 17th October 1989
Thunder and Lightning.

PARKER, Prof. D. (Durham University) 16th November 1989
Macrocycles, Drugs and Rock'N'Roll.

*PERUTZ, Dr. R.N. (York University) 24th January 1990
Plotting the Course of C-H Activations with
Organometallics.

PLATONOV, Prof. V.E. (USSR Academy of Sciences, Novosibirsk) 9th July 1990
Polyfluoroindanes: Synthesis and Transformation.

POWELL, Dr. R.L. (ICI) 6th December 1989
The Development of CFC Replacements

POWIS, Dr. I. (Nottingham University) 21st March 1990
Spinning off in a Huff: Photodissociation
of Methyl Iodide.

ROZHKOV, Prof. I.N. (USSR Academy of Sciences, Moscow) 9th July 1990
reactivity of Perfluoroalkyl Bromides.

*STODDART, Dr. J.F. (Sheffield University) 1st March 1990
Molecular Lego.

*SUTTON, Prof. D. (Simon Fraser University, Vancouver B.C.) 14th February 1990
Synthesis and applications of Dinitrogen and
Diazo Compounds of Rhenium and Iridium.

THOMAS, Dr. R.K. (Oxford University) 28th February 1990
Neutron Reflectometry from Surfaces.

THOMPSON, Dr. D.P. (Newcastle University) 7th February 1990
The Role of Nitrogen in Extending Silicate Crystal Chemistry.

**During the Period 1990-1991**

ALDER, Dr. B.J. (Lawrence Livermore Labs., California) 15th January 1991
Hydrogen in all its Glory.

BELL, Prof. T. (SUNY, Stoney Brook, U.S.A.) 14th November 1990
Functional Molecular Architecture and Molecular Recognition.

*BOCHMANN, Dr. M. (University of East Anglia) 24th October 1990
Synthesis, Reactions and Catalytic Activity of Cationic
Titanium Alkyls.

BRIMBLE, Dr. M.A. (Massey University, New Zealand) 29th July 1991
Synthetic Studies Towards the Antibiotic Griseusin-A.

*BROOKHART, Prof. M.S. (University of N. Carolina) 20th June 1991
Olefin Polymerisation, Oligomerisation and Dimerisation
Using Electrophilic Late Transition Metal Catalysts.

*BROWN, Dr. J. (Oxford University) 28th February 1991
Can Chemistry Provide Catalysts Superior to Enzymes?

BUSHBY, Dr. R. (Leeds University) 6th February 1991
Biradicals and Organic Magnets.

*COWLEY, Prof. A.H. (Texas University) 13th December 1990
New Organometallic Routes to Electronic Materials.

CROUT, Prof. D. (Warwick University) 29th November 1990
Enzymes in Organic Synthesis.

DOBSON, Dr. C.M. (Oxford University) 6th March 1991
NMR Studies of Dynamics in Molecular Crystals.

GERRARD, Dr. D. (British Petroleum) 7th November 1990
Raman Spectroscopy for Industrial Analysis.

HUDLICKY, Prof. T. (Virginia Polytechnic Institute) 25th April 1991
Biocatalysis and Symmetry Based Approaches to the
Efficient Synthesis of Complex Natural Products.

JACKSON, Dr. R. (Newcastle University) 31st October 1990
New Synthetic Methods: α-Amino Acids and Small Rings.

*KOCOVSKY, Dr. P. (Uppsala University) 6th November 1990
Stereo-Controlled reactions Mediated by Transition

and Non-Transition Metals.

LACEY, Dr. D. (Hull University) 31st January 1991
Liquid Crystals.

LOGAN, Dr. N. (Nottingham University) 1st November 1990
Rocket Propellants.

MACDONALD, Dr. W.A. (ICI Wilton) 11th October 1990
Materials for the Space Age.

MARKAM, Dr. J. (ICI Pharmaceuticals) 7th March 1991
DNA Fingerprinting.

PETTY, Dr. M.C. (Durham University) 14th February 1991
Molecular Electronics.

*PRINGLE, Dr. P.G. (Bristol University) 5th December 1990
Metal Complexes with Functionalised Phosphines.

*PRICHARD, Prof. J. (Queen Mary & Westfield College, 21st November 1990
London University.

Copper Surfaces and Catalysts.

SADLER, Dr. P. (Nottingham University) 17th January 1991
Comet Chemistry.

*SCHROCK, Prof. R.R. (M.I.T.) 24th April 1991
Metal-Ligand Multiple Bonds and Metathesis Initiators.

SCOTT, Dr. S.K. (Leeds University) 8th November 1990
Clocks, Oscillations and Chaos.

*SHAW, Prof. B.L. (Leeds University) 20th February 1991
Synthesis with Coordinated, Unsaturated Phosphine Ligands.

SINN, Prof. E. (Hull University) 30th January 1991
Coupling of Little Electrons in Big Molecules.

Implications for the Active sites of (Metalloproteins

and other) Macromolecules.

*SOULEN, Prof. R. (South Western University, Texas) 26th October 1990
Preparation and Reactions of Bicycloalkenes.

WHITAKER, Dr. B. J. (Leeds University) 28th November 1990
Two-Dimensional Velocity Imaging of State-Selected Reaction Products.

**During the Period 1991-1992**

ANDERSON, Dr. M. (Shell Research) 30th January 1992
Recent Advances in the Safe and Selective Chemical Control of Insect Pests.

*BILLINGHAM, Dr. N.C. (University of Sussex) 5th March 1992
Degradable Plastic - Myth or Magic?

BUTLER, Dr. A.R. (St. Andrew's University) 7th November 1991
Traditional Chinese Herbal Drugs: A Different Way of treating Diseases.

COOPER, Dr. W.D. (Shell Research) 5th December 1991
Colloid Science, Theory and Practice.

*FENTON, Prof. D.E. (Sheffield University) 12th February 1992
Polynuclear Complexes of Molecular Clefts as Models for Copper Biosites.

*FISCHER, Prof. R.D. (University of Hamburg) 17th September 1992
From Organo-f-Element Systems to Organo-Main Group Polymers.

GANI, Prof. D. (St. Andrew's University) 13th November 1991
The Chemistry of PLP Dependant Enzymes.

GEHRET, Dr. J.-C. (Ciba Giegy, Basel) 13th May 1992
Some Aspects of Industrial Agrochemical Research.

*GRIGG, Prof. R. (Leeds University) 4th December 1991
Palladium Catalysed Cyclisation and Ion Capture Processes.

HANN, Dr. R.A. (ICI Imagedata) 12th March 1992
Electronic Photography - An Image of the Future.

HARRIS, Dr. K.D.M. (St. Andrew's University) 22nd January 1992
Understanding the Properties of Solid Inclusion Compounds.

HITCHMAN, Prof. M.L. (Strathclyde University) 26th February 1992
Chemical Vapour Deposition.

HOLMES, Dr. A. (Cambridge University) 29th January 1992
Cycloaddition Reactions in the Service of the Synthesis

of Piperidine and Indolizidine Natural Products.

*JOHNSON, Prof. B.F.G. (Edinburgh University) 6th November 1991
Cluster-Surface Analogies.

KEELEY, Dr. R. (Metropolitan Police Forensic Science) 31st October 1991
Modern Forensic Science.

KNIGHT, Prof. D.M. (Philosophy Department, Durham University) 7th April 1992
Interpreting Experiments: the Beginning of Electrochemistry.

*MARDER, Prof. T. (Newcastle University) 6th May 1992
Metal Catalysed Alkene Hydroboration.

MASKILL, Dr. H. (Newcastle University) 18th March 1992
Concerted or Stepwise Fragmentation in a
Deamination-Type Reaction.

*MORE O'FERRALL, Dr. R. (University College, Dublin) 20th November 1991
Some Acid-Catalysed Rearrangements in Organic Chemistry.

NIXON, Prof. J.F. (University of Sussex) 25th February 1992 The
Tilden Lecture: Phosphaalkynes, New Building Blocks
in Inorganic and Organometallic Chemistry.

SALTHOUSE, Dr. J.A. (University of Manchester) 17th October 1991
Son et Luminere - A Demonstration Lecture.

SAUNDERS, Dr. J. (Glaxo Group Research Ltd.) 13th February 1992
Molecular Modelling in Drug Discovery.

SMITH, Prof. A.L. (ex Unilever) 5th December 1991
Soap, Detergents and Black Puddings.

*THOMAS, Prof. E.J. (Manchester University) 19th February 1992
Applications of Organostannanes to Organic Synthesis.

VOGEL, Prof. E. (University of Cologne) 20th February 1992
The Musgrave Lecture: Porphyrins, Molecules of
Interdisciplinary Interest.

WARD, Prof. I.M. (IRC in Polymer Science, Leeds University) 28th November 1991
The SCI Lecture: The Science and Technology of
Orientated Polymers.

## Conferences and Symposia Attended

1. *"North East Graduate Symospium"*, University of Newcastle-upon-Tyne, 2nd April 1990.

2. *'Symposium in Honour of Profesor Peter L. Pauson - Organometallic Chemistry of the Transition Metals"*, University of Strathclyde, Glasgow, 19th October 1990.

3. *"Waddington Graduate Symposium on Inorganic Chemistry"*, University of Durham, 17th December 1990.

4. *"Autumn Meeting of the Royal Society of Chemistry"*, University of York, 29th September 1991.

5. *"North East Graduate Symposium"*, University of Durham, 3rd April 1992.

## Publications

1. 'The Synthesis and Structure of the Yellow and Green Forms of $[Nb(O)Cl_3(PMe_3)_3]$ and the Orange and Green Forms of $[Nb(S)Cl_3(PMe_3)_3]$; Examples of Perfectly Matched Bond-Stretch Isomers?', *Angew. Chem. Int. Ed. Engl.*, **1991,** 980

2. 'Distortional Isomerism in Oxomolybdenum Systems; the Evidence Re-evaluated', *Angew. Chem. Int. Ed. Engl.*, **1992,** 1607

## Appendix 3

### The Theory of Isotopic Labelling ($^{17}O$ and $^{18}O$)

Isotopic substitution is assumed not to affect the potential function under the influence of which the nuclei move. Thus when the oxygen of M=O in the species $M(O)Cl_3$ (M=Nb) is replaced by $^{17}O$ or $^{18}O$ the M=$^*$O stretching force constant is not changed appreciably. In other words we assume that the effect of such substitutions is purely one of mass change. Furthermore, since the stretching of the metal-oxo bond is essentially a 'localized' vibration (much less 'mixed' with the other coordinates than the other vibrations) it is approximately correct to treat the $M(O)Cl_3$ system as a diatomic molecule X-O (where X=$MCl_3$). The X-O stretching frequency will then be given by equation 1 where k is the force constant of the bond ($Nm^{-1}$) and $\mu$ is the appropriate reduced mass for the vibrating system, and is given by equation 2.

$$\bar{\nu} = \frac{1}{2\pi c}\left(\frac{k}{\mu}\right)^{1/2} \qquad (1)$$

$$\mu = \frac{M_x.M_y}{M_x + M_y} \cdot m_\mu \qquad (2)$$

where $M_x$ and $M_y$ are the masses of the species x and y respectively.

Thus by treating the metal-oxo stretching frequencies as arising from a pseudo-diatomic molecule it is thus possible to calculate predicted metal-oxo stretching frequencies on isotopic substitution and compare them with the experimentally determined values. Using the known effective reduced masses, the force constants for X-$^{16}O$ and the isotopically substituted species can be calculated. Now rearranging equation 1 gives

$$\bar{\nu}^2 = \frac{1}{(2\pi c)^2} \cdot \frac{k}{\mu} \qquad (3)$$

Thus in order to calculate the expected stretching frequency of an isotopically substituted metal-oxo we require:-

$$\frac{\bar{\nu}_o^2}{\bar{\nu}_*^2} = \frac{\mu_*}{\mu_o} = \left(\frac{M_* \cdot M_x}{M_* + M_x}\right) \Big/ \left(\frac{M_o \cdot M_x}{M_o + M_x}\right)$$

$$= \left(\frac{M_*}{M_o}\right) \cdot \left(\frac{M_* + M_x}{M_* + M_x}\right)$$

$$\bar{\nu}_* = \bar{\nu}_o \cdot \left(\frac{\mu_o}{\mu_*}\right)^{1/2} = \bar{\nu}_o \cdot \left[\left(\frac{M_o}{M_*}\right) \cdot \left(\frac{M_* + M_x}{M_o + M_x}\right)\right]^{1/2} \quad (4)$$

where the subscripts $_o$ and $_*$ represent natural abundance and isotopically enriched forms. Tables 3.1 and 3.2 (section 3.6) were drawn up on the basis that the following values were taken:

$M(^{16}O)=15.999$ $M(^{18}O)=17.999$

$M(^{17}O)=16.999$ $M_x=M(NbCl_3)=199.2654$

$M_x=M(NbCl_3(MeCN)_2)=281.3668$

Using the experimental values for the metal-oxo stretching frequencies the experimental value for the force constant in each case can also be calculated, simply by rearranging equation 1 to give:-

$$k = 4\pi^2 c^2 \mu \bar{\nu}^2 \quad (5)$$

The errors in the predicted stretching frequencies for the isotopically labelled species based on that observed experimentally for the naturally occurring O-16 labelled form, can be determined by applying error propagation to equation 4. This gives that:-

$$\sigma^2(\bar{\nu}) = \left(\frac{\partial \bar{\nu}}{\partial \bar{\nu}_o}\right)^2 . \sigma^2(\bar{\nu}_o) \left(\frac{\partial \bar{\nu}}{\partial M_*}\right)^2 . \sigma^2(M_*$$

where $\bar{\nu}_o$ and $M_*$ are considered as the only variables in equation 4. Partial differentiation with respect to the appropriate variable leads to the expression:-

$$\sigma^2(\bar{\nu}) = \left(\frac{M_o}{M_*}\right) \left(\frac{M_* + M_x}{M_o + M_x}\right) . \sigma^2(\nu_o) + \left(\frac{M_*^2}{4M_o.M_x}\right) . \sigma^2(M$$

and, since $\sigma(M_*) = 0.01$ is significantly less than $\sigma(\bar{\nu}) = 2$ cm$^{-1}$, then the expression simplifies to:-

$$\sigma^2(\bar{\nu}) \approx \left(\frac{M_o}{M_*}\right) \left(\frac{M_* + M_x}{M_o + M_x}\right) . \sigma^2(\nu_o \quad (6)$$

Similarly, for the force constant, k, given by equation 5, error propagation leads to:-

$$\sigma^2(k) = \left(\frac{\partial k}{\partial \nu}\right)^2 . \sigma^2(\nu)$$

$$= (8\pi^2 c^2 \mu\nu)^2 . \sigma^2(\nu \quad (7)$$

From table 3.1 (section 3.6) it is seen that in fact the force constant calculated in each case is not constant which is unexpected considering that in the quantum mechanical background it is assumed the model is approximated to a linear diatomic, harmonic oscillator. This implies that on isotopic substitution that the force constants should remain unaltered. Changes of frequency of the bond oscillation are thus assumed to be the result of the change in relative reduced masses on isotopic substitution. One explanation for the inequality of answers is anharmonicity of the vibrations of the metal-oxo bond. That is, the potential energy curve in real molecules is not sufficiently approximated by a simple harmonic oscillator (nor a linear diatomic model). In calculating these values it has been assumed that the motion of the vibrating molecule is approximated by simple harmonics. However, because of anharmonicity

another constant must be introduced. This constant takes into account the deviation from simple harmonic oscillation and instead the Morse potential function is used (figure 1).

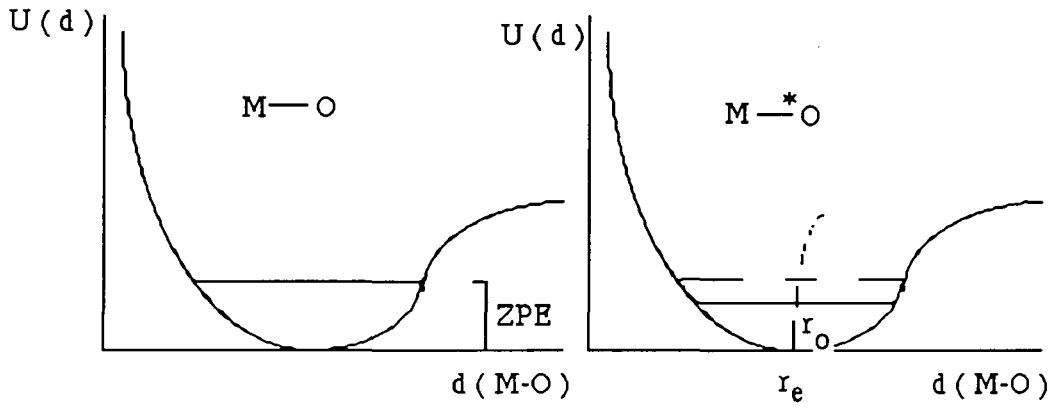


**Figure 1:** Morse potential energy versus bond distance for an anharmonic vibrating diatomic model

The increase in the reduced mass of the isotopically substituted metal-oxo species compared to the form with natural abundance amount and the anharmonic nature of the potential energy curve (which is unaffected by isotopic substitution) causes a reduction in the zero-point energy (ZPE) level in accordance with the square root of the relative reduced mass i.e., $\nu \propto (1/\mu)^{1/2}$. This means that there is a reduction in the bond distance i.e., $r_0(Nb\text{-}^{16}O) > r_0(Nb\text{-}^{*}O)$. The bond length is thus not changed due to a chemical effect but is in fact due to a change in relative reduced masses.

Now $k \propto \partial^2U/\partial x^2$ and thus since the ZPE is different in each case, this expression will give a different value for $k_0$ in each case (the subscript signifies that we are dealing with the lowest vibrational energy level where v=0). Hence, the inequality of experimental values obtained with those calculated. It would of course appear different if the equilibrium value of the force constant , $k_e$, had been calculated since this corresponds to the bottom of the potential U(x) where the value is unchanged. Thus the irregularity arises due to anharmonicity, accounted for by the Morse potential but not by the simple harmonic oscillator model (where isotopic substitution is assumed not to effect bond distances) which is used to carry out the calculations.

## Appendix 4

**Appendix 4A** **Selected Bond Distances (Å) and Angles (°) for Yellow $Nb(O)Cl_3(PMe_3)_3$**

| | | | |
|---|---|---|---|
| Nb - Cl(1) | 2.516(3) | P(2) - Nb - P(1) | 112.7(1) |
| Nb - Cl(2) | 2.533(3) | P(3) - Nb - P(1) | 114.5(1) |
| Nb - Cl(3) | 2.505(3) | P(3) - Nb - P(2) | 116.9(1) |
| | | | |
| Nb - P(1) | 2.642(3) | O - Nb - Cl(1) | 127.8(2) |
| Nb - P(2) | 2.633(3) | O - Nb - Cl(2) | 121.2(2) |
| Nb - P(3) | 2.645(3) | O - Nb - Cl(3) | 126.0(2) |
| | | | |
| | | O - Nb - P(1) | 76.9(2) |
| Nb - O | 1.781(6) | O - Nb - P(2) | 76.4(2) |
| | | O - Nb - P(3) | 76.3(2) |
| P(1) - C(11) | 1.799(9) | | |
| P(1) - C(12) | 1.812(9) | C(11) - P(1) - Nb | 112.1(3) |
| P(1) - C(13) | 1.817(10) | C(12) - P(1) - Nb | 120.3(3) |
| P(2) - C(21) | 1.785(11) | C(13) - P(1) - Nb | 110.8(3) |
| P(2) - C(22) | 1.790(11) | C(21) - P(2) - Nb | 112.7(4) |
| P(2) - C(23) | 1.807(11) | C(22) - P(2) - Nb | 120.0(4) |
| P(3) - C(31) | 1.808(9) | C(23) - P(2) - Nb | 110.8(4) |
| P(3) - C(32) | 1.805(10) | C(31) - P(3) - Nb | 110.9(3) |
| P(3) - C(33) | 1.791(10) | C(32) - P(3) - Nb | 111.6(4) |
| | | C(33) - P(3) - Nb | 119.9(4) |
| Cl(2) - Nb - Cl(1) | 90.9(1) | | |
| Cl(3) - Nb - Cl(1) | 88.0(1) | C(12) - P(1) - C(11) | 103.5(5) |
| Cl(3) - Nb - Cl(2) | 92.3(1) | C(13) - P(1) - C(11) | 103.8(5) |
| | | C(13) - P(1) - C(12) | 104.8(4) |
| P(1) - Nb - Cl(1) | 75.3(1) | C(22) - P(2) - C(21) | 102.3(6) |
| P(1) - Nb - Cl(2) | 161.9(1) | C(23) - P(2) - C(21) | 105.0(5) |
| P(1) - Nb - Cl(3) | 75.8(1) | C(23) - P(2) - C(22) | 104.5(5) |
| P(2) - Nb - Cl(1) | 75.0(1) | C(32) - P(3) - C(31) | 103.5(5) |
| P(2) - Nb - Cl(2) | 73.8(1) | C(33) - P(3) - C(31) | 105.2(5) |
| P(2) - Nb - Cl(3) | 157.6(1) | C(33) - P(3) - C(32) | 104.3(5) |
| P(3) - Nb - Cl(1) | 155.9(1) | | |
| P(3) - Nb - Cl(2) | 74.0(1) | | |
| P(3) - Nb - Cl(3) | 74.3(1) | | |

**Appendix 4B** **Selected Bond Distances (Å) and Angles (°) for Green $Nb(O)Cl_3(PMe_3)_3$**

| | | | |
|---|---|---|---|
| Nb - Cl(1) | 2.487(2) | P(2) - Nb - P(1) | 111.4(1) |
| Nb - Cl(2) | 2.509(2) | P(3) - Nb - P(1) | 114.0(1) |
| Nb - Cl(3) | 2.492(2) | P(3) - Nb - P(2) | 118.2(1) |
| | | | |
| Nb - P(1) | 2.646(2) | O - Nb - Cl(1) | 129.8(1) |
| Nb - P(2) | 2.636(3) | O - Nb - Cl(2) | 119.3(1) |
| Nb - P(3) | 2.644(2) | O - Nb - Cl(3) | 126.4(1) |
| | | | |
| | | O - Nb - P(1) | 77.6(1) |
| Nb - O | 2.087(5) | O - Nb - P(2) | 75.8(1) |
| | | O - Nb - P(3) | 75.5(1) |
| P(1) - C(11) | 1.814(8) | | |
| P(1) - C(12) | 1.807(8) | C(11) - P(1) - Nb | 113.1(3) |
| P(1) - C(13) | 1.801(10) | C(12) - P(1) - Nb | 119.9(3) |
| P(2) - C(21) | 1.815(9) | C(13) - P(1) - Nb | 112.7(3) |
| P(2) - C(22) | 1.807(10) | C(21) - P(2) - Nb | 113.5(3) |
| P(2) - C(23) | 1.795(10) | C(22) - P(2) - Nb | 119.3(3) |
| P(3) - C(31) | 1.805(8) | C(23) - P(2) - Nb | 112.4(4) |
| P(3) - C(32) | 1.821(9) | C(31) - P(3) - Nb | 112.0(3) |
| P(3) - C(33) | 1.804(8) | C(32) - P(3) - Nb | 113.3(3) |
| | | C(33) - P(3) - Nb | 119.5(3) |
| Cl(2) - Nb - Cl(1) | 90.7(1) | | |
| Cl(3) - Nb - Cl(1) | 86.8(1) | C(12) - P(1) - C(11) | 103.2(4) |
| Cl(3) - Nb - Cl(2) | 93.0(1) | C(13) - P(1) - C(11) | 102.3(5) |
| | | C(13) - P(1) - C(12) | 103.5(4) |
| P(1) - Nb - Cl(1) | 76.0(1) | C(22) - P(2) - C(21) | 104.2(5) |
| P(1) - Nb - Cl(2) | 163.1(1) | C(23) - P(2) - C(21) | 102.3(5) |
| P(1) - Nb - Cl(3) | 76.1(1) | C(23) - P(2) - C(22) | 103.2(5) |
| P(2) - Nb - Cl(1) | 75.3(1) | C(32) - P(3) - C(31) | 103.1(4) |
| P(2) - Nb - Cl(2) | 74.3(1) | C(33) - P(3) - C(31) | 103.3(4) |
| P(2) - Nb - Cl(3) | 157.7(1) | C(33) - P(3) - C(32) | 103.9(4) |
| P(3) - Nb - Cl(1) | 154.7(1) | | |
| P(3) - Nb - Cl(2) | 74.3(1) | | |
| P(3) - Nb - Cl(3) | 74.1(1) | | |

Appendix 4C Selected Bond Distances (Å) and Angles (°) for Orange-Yellow $Nb(S)Cl_3(PMe_3)_3$

| | | | |
|---|---|---|---|
| Nb - Cl(1) | 2.490(2) | P(2) - Nb - P(1) | 113.5(1) |
| Nb - Cl(2) | 2.516(2) | P(3) - Nb - P(1) | 116.4(1) |
| Nb - Cl(3) | 2.491(2) | P(3) - Nb - P(2) | 116.5(1) |
| | | | |
| Nb - P(1) | 2.640(2) | S - Nb - Cl(1) | 128.8(1) |
| Nb - P(2) | 2.640(2) | S - Nb - Cl(2) | 123.4(1) |
| Nb - P(3) | 2.636(2) | S - Nb - Cl(3) | 125.7(1) |
| | | | |
| | | S - Nb - P(1) | 77.7(1) |
| Nb - S | 2.194(2) | S - Nb - P(2) | 77.5(1) |
| | | S - Nb - P(3) | 77.5(1) |
| P(1) - C(11) | 1.816(10) | | |
| P(1) - C(12) | 1.827(11) | C(11) - P(1) - Nb | 113.1(3) |
| P(1) - C(13) | 1.807(11) | C(12) - P(1) - Nb | 119.2(4) |
| P(2) - C(21) | 1.824(11) | C(13) - P(1) - Nb | 114.1(6) |
| P(2) - C(22) | 1.835(10) | C(21) - P(2) - Nb | 114.4(4) |
| P(2) - C(23) | 1.824(10) | C(22) - P(2) - Nb | 117.2(4) |
| P(3) - C(31) | 1.821(10) | C(23) - P(2) - Nb | 113.3(4) |
| P(3) - C(32) | 1.808(9) | C(31) - P(3) - Nb | 113.6(4) |
| P(3) - C(33) | 1.812(10) | C(32) - P(3) - Nb | 113.5(4) |
| | | C(33) - P(3) - Nb | 119.3(4) |
| Cl(2) - Nb - Cl(1) | 88.8(1) | | |
| Cl(3) - Nb - Cl(1) | 87.2(1) | C(12) - P(1) - C(11) | 101.5(6) |
| Cl(3) - Nb - Cl(2) | 91.2(1) | C(13) - P(1) - C(11) | 104.3(6) |
| | | C(13) - P(1) - C(12) | 102.8(6) |
| P(1) - Nb - Cl(1) | 74.8(1) | C(22) - P(2) - C(21) | 103.2(5) |
| P(1) - Nb - Cl(2) | 158.9(1) | C(23) - P(2) - C(21) | 102.3(5) |
| P(1) - Nb - Cl(3) | 75.2(1) | C(23) - P(2) - C(22) | 104.8(5) |
| P(2) - Nb - Cl(1) | 75.3(1) | C(32) - P(3) - C(31) | 103.5(5) |
| P(2) - Nb - Cl(2) | 73.7(1) | C(33) - P(3) - C(31) | 103.1(5) |
| P(2) - Nb - Cl(3) | 156.8(1) | C(33) - P(3) - C(32) | 102.0(5) |
| P(3) - Nb - Cl(1) | 153.7(1) | | |
| P(3) - Nb - Cl(2) | 73.7(1) | | |
| P(3) - Nb - Cl(3) | 74.0(1) | | |

**Appendix 4D** Selected Bond Distances (Å) and Angles (°) for Green $Nb(S)Cl_3(PMe_3)_3$

| | | | |
|---|---|---|---|
| Nb - Cl(1) | 2.475(1) | P(2) - Nb - P(1) | 110.4(1) |
| Nb - Cl(2) | 2.501(1) | P(3) - Nb - P(1) | 116.1(1) |
| Nb - Cl(3) | 2.482(1) | P(3) - Nb - P(2) | 117.3(1) |
| | | | |
| Nb - P(1) | 2.647(1) | S - Nb - Cl(1) | 131.2(1) |
| Nb - P(2) | 2.654(1) | S - Nb - Cl(2) | 121.8(1) |
| Nb - P(3) | 2.647(1) | S - Nb - Cl(3) | 124.4(1) |
| | | | |
| | | S - Nb - P(1) | 76.8(1) |
| Nb - S | 2.296(1) | S - Nb - P(2) | 76.4(1) |
| | | S - Nb - P(3) | 75.8(1) |
| | | | |
| P(1) - C(11) | 1.813(6) | | |
| P(1) - C(12) | 1.817(6) | C(11) - P(1) - Nb | 114.4(2) |
| P(1) - C(13) | 1.811(6) | C(12) - P(1) - Nb | 117.8(2) |
| P(2) - C(21) | 1.826(6) | C(13) - P(1) - Nb | 113.5(2) |
| P(2) - C(22) | 1.812(6) | C(21) - P(2) - Nb | 116.2(2) |
| P(2) - C(23) | 1.828(6) | C(22) - P(2) - Nb | 117.0(2) |
| P(3) - C(31) | 1.826(5) | C(23) - P(2) - Nb | 112.7(2) |
| P(3) - C(32) | 1.802(5) | C(31) - P(3) - Nb | 113.2(2) |
| P(3) - C(33) | 1.819(5) | C(32) - P(3) - Nb | 114.2(2) |
| | | C(33) - P(3) - Nb | 117.9(2) |
| Cl(2) - Nb - Cl(1) | 88.2(1) | | |
| Cl(3) - Nb - Cl(1) | 86.6(1) | C(12) - P(1) - C(11) | 103.1(3) |
| Cl(3) - Nb - Cl(2) | 93.1(1) | C(13) - P(1) - C(11) | 103.8(2) |
| | | C(13) - P(1) - C(12) | 102.6(3) |
| P(1) - Nb - Cl(1) | 76.0(1) | C(22) - P(2) - C(21) | 102.9(3) |
| P(1) - Nb - Cl(2) | 161.2(1) | C(23) - P(2) - C(21) | 103.0(3) |
| P(1) - Nb - Cl(3) | 76.1(1) | C(23) - P(2) - C(22) | 103.2(3) |
| P(2) - Nb - Cl(1) | 76.2(1) | C(32) - P(3) - C(31) | 104.4(2) |
| P(2) - Nb - Cl(2) | 74.8(1) | C(33) - P(3) - C(31) | 102.7(2) |
| P(2) - Nb - Cl(3) | 159.0(1) | C(33) - P(3) - C(32) | 103.0(2) |
| P(3) - Nb - Cl(1) | 153.0(1) | | |
| P(3) - Nb - Cl(2) | 74.4(1) | | |
| P(3) - Nb - Cl(3) | 74.2(1) | | |

**Appendix 4E** **Selected Bond Distances (Å) and Angles (°) for Orange $Ta(S)Cl_3(PMe_3)_3$**

| | | | |
|---|---|---|---|
| Ta - Cl(1) | 2.479(2) | P(2) - Ta - P(1) | 113.0(1) |
| Ta - Cl(2) | 2.501(2) | P(3) - Ta - P(1) | 116.3(1) |
| Ta - Cl(3) | 2.479(2) | P(3) - Ta - P(2) | 117.0(1) |
| | | | |
| Ta - P(1) | 2.631(2) | S - Ta - Cl(1) | 129.7(1) |
| Ta - P(2) | 2.639(2) | S - Ta - Cl(2) | 123.4(1) |
| Ta - P(3) | 2.636(2) | S - Ta - Cl(3) | 126.2(1) |
| | | | |
| Ta - S | 2.219(2) | S - Ta - P(1) | 77.8(1) |
| | | S - Ta - P(2) | 77.3(1) |
| P(1) - C(11) | 1.822(9) | S - Ta - P(3) | 77.3(1) |
| P(1) - C(12) | 1.819(8) | | |
| P(1) - C(13) | 1.821(9) | C(11) - P(1) - Ta | 113.0(3) |
| P(2) - C(21) | 1.829(9) | C(12) - P(1) - Ta | 119.0(3) |
| P(2) - C(22) | 1.827(9) | C(13) - P(1) - Ta | 113.3(3) |
| P(2) - C(23) | 1.816(8) | C(21) - P(2) - Ta | 114.4(3) |
| P(3) - C(31) | 1.822(8) | C(22) - P(2) - Ta | 117.7(3) |
| P(3) - C(32) | 1.808(8) | C(23) - P(2) - Ta | 112.3(3) |
| P(3) - C(33) | 1.811(8) | C(31) - P(3) - Ta | 113.6(3) |
| | | C(32) - P(3) - Ta | 113.5(3) |
| Cl(2) - Ta - Cl(1) | 88.0(1) | C(33) - P(3) - Ta | 118.4(3) |
| Cl(3) - Ta - Cl(1) | 86.3(1) | | |
| Cl(3) - Ta - Cl(2) | 90.7(1) | C(12) - P(1) - C(11) | 103.1(5) |
| | | C(13) - P(1) - C(11) | 104.5(5) |
| P(1) - Ta - Cl(1) | 75.2(1) | C(13) - P(1) - C(12) | 102.3(4) |
| P(1) - Ta - Cl(2) | 158.8(1) | C(22) - P(2) - C(21) | 102.7(4) |
| P(1) - Ta - Cl(3) | 75.5(1) | C(23) - P(2) - C(21) | 103.6(5) |
| P(2) - Ta - Cl(1) | 75.4(1) | C(23) - P(2) - C(22) | 104.5(4) |
| P(2) - Ta - Cl(2) | 74.1(1) | C(32) - P(3) - C(31) | 103.1(4) |
| P(2) - Ta - Cl(3) | 156.4(1) | C(33) - P(3) - C(31) | 103.1(4) |
| P(3) - Ta - Cl(1) | 153.0(1) | C(33) - P(3) - C(32) | 103.3(4) |
| P(3) - Ta - Cl(2) | 74.0(1) | | |
| P(3) - Ta - Cl(3) | 74.2(1) | | |

**Appendix 4F** Selected Bond Distances (Å) and Angles (°) for Chatt Blue $Mo(O)Cl_2(PMe_2Ph)_3$

| | | | |
|---|---|---|---|
| Mo - P(1) | 2.491(1) | P(2) - Mo - P(1) | 93.7(1) |
| Mo - P(2) | 2.542(1) | P(3) - Mo - P(1) | 94.5(1) |
| Mo - P(3) | 2.539(1) | P(3) - Mo - P(2) | 171.2(1) |
| | | | |
| Mo - Cl(1) | 2.538(1) | O - Mo - Cl(1) | 169.3(1) |
| Mo - Cl(2) | 2.454(1) | O - Mo - Cl(2) | 105.2(1) |
| | | | |
| Mo - O | 1.663(2) | O - Mo - P(1) | 92.3(1) |
| | | O - Mo - P(2) | 91.6(1) |
| P(1) - C(11) | 1.815(4) | O - Mo - P(3) | 91.2(1) |
| P(1) - C(17) | 1.814(4) | | |
| P(1) - C(18) | 1.818(4) | Cl(1) - Mo - P(1) | 77.0(1) |
| P(2) - C(21) | 1.817(4) | Cl(1) - Mo - P(2) | 89.5(1) |
| P(2) - C(27) | 1.803(5) | Cl(1) - Mo - P(3) | 89.2(1) |
| P(2) - C(28) | 1.808(4) | Cl(2) - Mo - P(1) | 162.4(1) |
| P(3) - C(31) | 1.809(4) | Cl(2) - Mo - P(2) | 85.2(1) |
| P(3) - C(37) | 1.799(4) | Cl(2) - Mo - P(3) | 85.9(1) |
| P(3) - C(38) | 1.815(4) | | |
| | | Cl(2) - Mo - Cl(1) | 85.4(1) |
| C(11) - P(1) - Mo | 114.1(1) | | |
| C(17) - P(1) - Mo | 118.2(1) | C(17) - P(1) - C(11) | 103.6(2) |
| C(18) - P(1) - Mo | 116.0(1) | C(18) - P(1) - C(11) | 103.2(2) |
| C(21) - P(2) - Mo | 117.6(1) | C(18) - P(1) - C(17) | 99.5(2) |
| C(27) - P(2) - Mo | 116.2(2) | C(27) - P(2) - C(21) | 105.7(2) |
| C(28) - P(2) - Mo | 112.3(2) | C(28) - P(2) - C(21) | 100.1(2) |
| C(31) - P(3) - Mo | 115.7(1) | C(28) - P(2) - C(27) | 102.7(2) |
| C(37) - P(3) - Mo | 116.5(1) | C(37) - P(3) - C(31) | 105.4(2) |
| C(38) - P(3) - Mo | 113.3(1) | C(38) - P(3) - C(31) | 101.4(2) |
| | | C(38) - P(3) - C(37) | 102.7(2) |

**Appendix 4G** Selected Bond Distances (Å) and Angles (°) for Enemark Blue $Mo(O)Cl_2(PMe_2Ph)_3$

| | | | |
|---|---|---|---|
| Mo - P(1) | 2.484(3) | P(2) - Mo - P(1) | 95.6(1) |
| Mo - P(2) | 2.519(3) | P(3) - Mo - P(1) | 95.7(1) |
| Mo - P(3) | 2.530(3) | P(3) - Mo - P(2) | 160.4(1) |
| | | | |
| Mo - Cl(1) | 2.523(3) | O - Mo - Cl(1) | 170.0(3) |
| Mo - Cl(2) | 2.478(3) | O - Mo - Cl(2) | 97.6(3) |
| | | | |
| Mo - O | 1.682(7) | O - Mo - P(1) | 84.3(3) |
| | | O - Mo - P(2) | 97.2(3) |
| P(1)-C(11) | 1.817(13) | O - Mo - P(3) | 99.8(3) |
| P(1)-C(17) | 1.810(12) | | |
| P(1)-C(18) | 1.808(12) | Cl(1) - Mo - P(1) | 85.8(1) |
| P(2)-C(21) | 1.819(11) | Cl(1) - Mo - P(2) | 84.8(1) |
| P(2)-C(27) | 1.837(10) | Cl(1) - Mo - P(3) | 80.2(1) |
| P(2)-C(28) | 1.836(11) | Cl(2) - Mo - P(1) | 177.8(1) |
| P(3)-C(31) | 1.832(11) | Cl(2) - Mo - P(2) | 83.0(1) |
| P(3)-C(37) | 1.838(10) | Cl(2) - Mo - P(3) | 85.1(1) |
| P(3)-C(38) | 1.827(9) | | |
| | | Cl(2) - Mo - Cl(1) | 92.4(1) |
| C(11) - P(1) - Mo | 116.1(4) | | |
| C(17) - P(1) - Mo | 119.0(5) | C(17) - P(1) - C(11) | 103.8(6) |
| C(18) - P(1) - Mo | 112.9(4) | C(18) - P(1) - C(11) | 100.3(6) |
| C(21) - P(2) - Mo | 124.0(3) | C(18) - P(1) - C(17) | 102.2(7) |
| C(27) - P(2) - Mo | 109.0(4) | C(27) - P(2) - C(21) | 103.7(5) |
| C(28) - P(2) - Mo | 112.7(4) | C(28) - P(2) - C(21) | 101.7(5) |
| C(31) - P(3) - Mo | 113.8(4) | C(28) - P(2) - C(27) | 103.7(5) |
| C(37) - P(3) - Mo | 113.2(4) | C(37) - P(3) - C(31) | 102.6(5) |
| C(38) - P(3) - Mo | 119.2(4) | C(38) - P(3) - C(31) | 104.7(5) |
| | | C(38) - P(3) - C(37) | 101.4(5) |

**Appendix 4H** Selected Bond Distances (Å) and Angles (°) for Chatt Blue-Green $Mo(O)Cl_2(PMe_2Ph)_3$

| | | | |
|---|---|---|---|
| Mo - P(1) | 2.503(3) | P(2) - Mo - P(1) | 94.3(1) |
| Mo - P(2) | 2.543(3) | P(3) - Mo - P(1) | 94.0(1) |
| Mo - P(3) | 2.557(3) | P(3) - Mo - P(2) | 171.2(1) |
| | | | |
| Mo - Cl(1) | 2.545(2) | O - Mo - Cl(1) | 169.3(2) |
| Mo - Cl(2) | 2.465(3) | O - Mo - Cl(2) | 105.1(2) |
| | | | |
| Mo - O | 1.698(6) | O - Mo - P(1) | 92.3(2) |
| | | O - Mo - P(2) | 91.1(2) |
| P(1) - C(11) | 1.832(9) | O - Mo - P(3) | 91.6(2) |
| P(1) - C(17) | 1.816(9) | | |
| P(1) - C(18) | 1.836(9) | Cl(1) - Mo - P(1) | 77.1(1) |
| P(2) - C(21) | 1.823(10) | Cl(1) - Mo - P(2) | 89.3(1) |
| P(2) - C(27) | 1.816(9) | Cl(1) - Mo - P(3) | 89.6(1) |
| P(2) - C(28) | 1.829(9) | Cl(2) - Mo - P(1) | 162.7(1) |
| P(3) - C(31) | 1.822(9) | Cl(2) - Mo - P(2) | 86.1(1) |
| P(3) - C(37) | 1.807(10) | Cl(2) - Mo - P(3) | 85.1(1) |
| P(3) - C(38) | 1.832(9) | | |
| | | Cl(2) - Mo - Cl(1) | 85.6(1) |
| C(11) - P(1) - Mo | 114.0(3) | | |
| C(17) - P(1) - Mo | 118.2(3) | C(17) - P(1) - C(11) | 104.0(4) |
| C(18) - P(1) - Mo | 116.0(3) | C(18) - P(1) - C(11) | 103.4(4) |
| C(21) - P(2) - Mo | 115.5(3) | C(18) - P(1) - C(17) | 99.1(4) |
| C(27) - P(2) - Mo | 116.5(3) | C(27) - P(2) - C(21) | 105.1(5) |
| C(28) - P(2) - Mo | 112.8(4) | C(28) - P(2) - C(21) | 102.7(5) |
| C(31) - P(3) - Mo | 117.1(3) | C(28) - P(2) - C(27) | 102.5(5) |
| C(37) - P(3) - Mo | 116.7(3) | C(37) - P(3) - C(31) | 105.7(5) |
| C(38) - P(3) - Mo | 112.3(4) | C(38) - P(3) - C(31) | 100.2(5) |
| | | C(38) - P(3) - C(37) | 102.7(5) |

**Appendix 4I** Selected Bond Distances (Å) and Angles (°) for Chatt Green $Mo(O)Cl_2(PMe_2Ph)_3$

| | | | |
|---|---|---|---|
| Mo - P(1) | 2.524(3) | P(2) - Mo - P(1) | 93.7(1) |
| Mo - P(2) | 2.567(4) | P(3) - Mo - P(1) | 95.8(1) |
| Mo - P(3) | 2.531(4) | P(3) - Mo - P(2) | 162.3(1) |
| | | | |
| Mo - Cl(1) | 2.490(3) | Cl(1) - Mo - O | 173.8(2) |
| Mo - Cl(2) | 2.457(3) | Cl(2) - Mo - O | 94.5(2) |
| | | | |
| Mo - O | 2.028(8) | P(1) - Mo - O | 87.9(2) |
| | | P(2) - Mo - O | 102.3(2) |
| P(1) - C(11) | 1.845(13) | P(3) - Mo - O | 93.0(2) |
| P(1) - C(17) | 1.824(15) | | |
| P(1) - C(18) | 1.867(15) | P(1) - Mo - Cl(1) | 86.7(1) |
| P(2) - C(21) | 1.824(12) | P(2) - Mo - Cl(1) | 81.1(1) |
| P(2) - C(27) | 1.868(14) | P(3) - Mo - Cl(1) | 84.6(1) |
| P(2) - C(28) | 1.854(14) | P(1) - Mo - Cl(2) | 177.0(1) |
| P(3) - C(31) | 1.847(13) | P(2) - Mo - Cl(2) | 87.6(1) |
| P(3) - C(37) | 1.834(13) | P(3) - Mo - Cl(2) | 82.2(1) |
| P(3) - C(38) | 1.842(14) | | |
| | | Cl(2) - Mo - Cl(1) | 90.8(1) |
| C(11) - P(1) - Mo | 116.6(4) | | |
| C(17) - P(1) - Mo | 113.1(5) | C(17) - P(1) - C(11) | 100.5(6) |
| C(18) - P(1) - Mo | 117.2(5) | C(18) - P(1) - C(11) | 104.7(6) |
| C(21) - P(2) - Mo | 120.3(4) | C(18) - P(1) - C(17) | 102.6(7) |
| C(27) - P(2) - Mo | 114.4(4) | C(27) - P(2) - C(21) | 102.8(6) |
| C(28) - P(2) - Mo | 111.7(4) | C(28) - P(2) - C(21) | 103.2(6) |
| C(31) - P(3) - Mo | 120.4(4) | C(28) - P(2) - C(27) | 102.3(6) |
| C(37) - P(3) - Mo | 113.6(4) | C(37) - P(3) - C(31) | 101.7(6) |
| C(38) - P(3) - Mo | 111.4(5) | C(38) - P(3) - C(31) | 105.4(6) |
| | | C(38) - P(3) - C(37) | 102.6(6) |

**Appendix 4J** Selected Bond Distances (Å) and Angles (°) for 'Enemark-like' Blue $Mo(O)Br_2(PMe_2Ph)_3$

| | | | |
|---|---|---|---|
| Mo - P(1) | 2.500(5) | P(2) - Mo - P(1) | 94.3(2) |
| Mo - P(2) | 2.527(5) | P(3) - Mo - P(1) | 96.1(2) |
| Mo - P(3) | 2.545(5) | P(3) - Mo - P(2) | 160.4(2) |
| | | | |
| Mo - Br(1) | 2.669(3) | Br(1) - Mo - O | 168.5(3) |
| Mo - Br(2) | 2.618(2) | Br(2) - Mo - O | 97.2(3) |
| | | | |
| Mo - O | 1.672(10) | P(1) - Mo - O | 82.8(4) |
| | | P(2) - Mo - O | 97.9(4) |
| P(1) - C(11) | 1.793(19) | P(3) - Mo - O | 99.8(4) |
| P(1) - C(17) | 1.806(19) | | |
| P(1) - C(18) | 1.796(20) | Br(1) - Mo - P(1) | 85.8(2) |
| P(2) - C(21) | 1.817(17) | Br(1) - Mo - P(2) | 84.4(1) |
| P(2) - C(27) | 1.792(14) | Br(1) - Mo - P(3) | 79.8(1) |
| P(2) - C(28) | 1.845(15) | Br(2) - Mo - P(1) | 178.5(1) |
| P(3) - C(31) | 1.786(16) | Br(2) - Mo - P(2) | 84.2(1) |
| P(3) - C(37) | 1.838(15) | Br(2) - Mo - P(3) | 85.4(1) |
| P(3) - C(38) | 1.805(15) | | |
| | | Br(2) - Mo - Br(1) | 94.3(1) |
| C(11) - P(1) - Mo | 116.0(7) | | |
| C(17) - P(1) - Mo | 110.3(7) | C(17) - P(1) - C(11) | 100.2(8) |
| C(18) - P(1) - Mo | 119.0(7) | C(18) - P(1) - C(11) | 105.0(9) |
| C(21) - P(2) - Mo | 123.9(6) | C(18) - P(1) - C(17) | 104(1) |
| C(27) - P(2) - Mo | 109.0(6) | C(27) - P(2) - C(21) | 103.5(8) |
| C(28) - P(2) - Mo | 114.1(5) | C(28) - P(2) - C(21) | 100.4(8) |
| C(31) - P(3) - Mo | 114.0(6) | C(28) - P(2) - C(27) | 103.8(7) |
| C(37) - P(3) - Mo | 118.0(6) | C(37) - P(3) - C(31) | 106.0(8) |
| C(38) - P(3) - Mo | 113.4(6) | C(38) - P(3) - C(31) | 101.6(8) |
| | | C(38) - P(3) - C(37) | 101.8(8) |